Global ammonia emissions from seabird colonies

Riddick, Stuart

Awarding institution:
King's College London

Global ammonia emissions from seabird colonies

Stuart N Riddick

A thesis submitted to King's College London for the degree of

Doctor of Philosophy

Department of Geography

2012

Declaration:

Table of Contents

Table of Tables 7
Table of Figures 12
Nomenclature 21
Abstract 25
Acknowledgments 26
Chapter 1: Introduction 28
1.1 Overview 28
1.2 Nitrogen 30
1.2.1 Basic chemical properties of nitrogen 30
1.2.2 Evolution of nitrogen 31
1.2.3 Nitrogen and Ammonia 31
1.3 Global distribution of NH_3 emission 32
1.4 NH_3 emissions from seabirds 34
1.4.1 Seabird behavior relevant to NH_3 emission 36
1.4.2 Nitrogen pathways through seabirds 37
1.4.3 Effects of seabird NH_3 39
1.5 NH_3 emission estimates from seabirds 41
1.6 Global Climate Change 43
1.7 Knowledge Gaps 44
1.7.1 Seabird population estimates 45
1.7.2 Nesting Effect on NH_3 emission 46
1.7.3 Effects of Climate 47
1.8 Aims 47
1.8.1 Objectives 48
1.8.2 Thesis Overview 48
Chapter 2 Methodologies 50
2.1 Introduction 50
2.2 Air movement within the planetary boundary layer 50
2.2.1 The atmosphere and its properties 50
2.2.2 Atmospheric stability 52
2.2.3 Wind Speed in neutral conditions 53
2.2.4 Wind Speed in non-neutral conditions 55
2.3 Gas concentration gradients within the PBL 55
2.3.1 Concentration gradient 55

2.3.2 Resistance analogy 56
2.4 Methods for calculating emission fluxes 58
2.4.1 Gaussian plume method 58
2.4.2 Tracer Ratio (TR) method 60
2.4.3 Flux-gradient method 61
2.4.4 Backward Lagrangian Stochastic (BLS) dispersion method 62
2.5 Assessment of NH_3 measurement instrumentation for studying seabird colonies 65
2.5.1 Passive sampling techniques 66
2.5.2 Active sampling techniques 68
2.6 Approaches used in this project 70
2.6.1 Measuring NH_3 concentration 70
2.6.2 Modelling approach 70
Chapter 3 The global distribution of ammonia emissions from seabird colonies 72
3.1 Introduction 72
3.2 Methods and materials 73
3.2.1 Seabird population estimates 73
3.2.2 Bioenergetics model 74
3.2.3 Calculating Annual NH_3 emission 74
3.2.4 Model parameterization 76
3.2.5 Temperature dependence of NH_3 emissions 77
3.3 Results 78
3.3.1 Global distribution of seabird colony populations and N excretion 78
3.3.2 Global distribution of NH_3 emissions and temperature sensitivity 80
3.3.3 Main seabird species contributing to ammonia emissions 84
3.4 Discussion 85
3.4.1 Temperature Dependence of NH_3 Emissions 86
3.4.2 Uncertainty in input data 87
3.4.3 Magnitude of seabird ammonia emissions compared with other sources 88
3.5 Conclusions 90
Chapter 4 Parameterization of avian derived NH_3 emission from seabird colony substrates 91
4.1 Introduction 91
4.2 Methods 94
4.2.1 Seabird guano 95

4.2.2 NH_3 concentration measurements 97
4.3 Results 98
4.3.1 Background concentrations of substrates 98
4.3.2 NH_3 emission from guano on a substrate 99
4.4. Discussion 100
4.4.1 Background concentration of substrates 100
4.4.2 Guano addition to substrates 101
4.4.3 Implications for global seabird NH_3 emissions 102
4.4.4 Revised global NH_3 emission 103
4.4.5 Significance of F_{hab} 103
Chapter 5: Measuring ammonia emissions seabird colonies 105
5.1 Introduction 105
5.2 Methods 107
5.2.1 Study sites 107
5.2.2 Measurements taken 109
5.2.3 Measuring NH_3 concentration - Passive sampling campaigns 110
5.2.4 Measuring NH_3 concentration - Active sampling campaigns 111
5.2.5 Meteorological data 112
5.2.6 Method of Data Analysis 113
5.3 Fieldwork Sites - Methods, Results & Conclusions 114
5.3.1 Michaelmas Cay- Passive Campaign 114
5.3.2 Ascension Island -Passive Campaign 120
5.3.3 Ascension Island -Active Campaign 128
5.3.4 Isle of May-Passive Campaign 133
5.3.5 Isle of May –Active Sampling Campaign 138
5.3.6 Signy Island – Passive Sampling Campaign 143
5.3.7 Bird Island – Active Sampling Campaign 150
5.4 Discussion 156
5.4.1 General observations 157
5.4.2 Comparison of Passive to Active campaigns 158
5.4.3 Summary of NH_3 emissions from seabird colonies 159
5.4.4 Comparison between measured and modelled emissions 160
5.5 Summary and conclusions 161
Chapter 6: High temporal resolution modelling and validation of climate dependant seabird ammonia emissions 163
6.1 Introduction 163

6.2 Methods and Materials 165
6.2.1 Modelling NH_3 production 165
6.2.2 Blackall's GUANO model 166
6.2.3 Changes to the Blackall (2004) GUANO model 169
6.2.4 Meteorological input data 173
6.2.5 Seabird colony data 174
6.2.6 Sensitivity analysis 174
6.2.7 Comparing model output to measurements 175
6.2.8 NH_3 emission and climate 175
6.3 Results and Discussion: Model applied to measurement sites 176
6.3.1 Sensitivity analysis of the GUANO model 176
6.3.2 Improvements to the GUANO model 177
6.3.3 Michaelmas Cay Great Barrier Reef, Common Noddy (passive measurements) 179
6.3.4 Mars Bay, Ascension Island, Sooty Terns (active measurements) 183
6.3.5 Isle of May, Scotland, Atlantic puffins (active measurements) 187
6.3.6 Signy Island, South Atlantic, Chinstrap penguins (passive measurements) 191
6.3.7 Bird Island, South Atlantic, Macaroni Penguins (active measurements) 194
6.4 Global application of the GUANO model 197
6.4.1 Adapting the GUANO model for calculating global emission 197
6.4.2 Comparing GUANO model and measured NH_3 emissions 197
6.4.3 Bird Behaviour 199
6.4.4 Emission factors and NH_3 Emissions 199
6.4.5 F_{hab} and NH_3 Emissions 203
6.5 Summary 203
Chapter 7: Regional and global significance of seabird-mediated nitrogen cycle processes 206
7.1 Introduction 206
7.2 Methods & Materials 206
7.2.1 GUANO Model development 206
7.2.2 Model Input 207
7.2.3 Annual Emission estimate 215
7.2.4 Analysis of climate effects 215
7.2.5 Climate change scenarios 216
7.3 Results and Discussion 217

7.3.1 Global distribution of seabird NH_3 emission 217
7.3.2 NH_3 emission by seabird species and region 220
7.3.3 Analysis of climate effects on NH_3 emissions 222
7.3.4 Prediction of climate change effects on seabird nitrogen pathways 225
7.3.5 Uncertainty in input data 231
8. General discussion 233
8.1 Summary of findings 233
8.1.1 NH_3 emissions at seabird colonies 233
8.1.2 Climate-specific NH_3 emission rates from seabirds 234
8.1.3 Assessment of measurement techniques 235
8.1.4 Assessment of modelling techniques 237
8.2 Implications of the research 239
8.2.1 Comparison of global emissions with other estimates 239
8.2.2 Effects of seabirds on local environment 240
8.2.3 Seabirds as a model for global emissions 241
8.3 Suggestions for future research 244
8.4 Summary 245
References 249
Appendix 1 Bird species data 265

Table of Tables

Table 1.1 Sources of NH_3 (Bouwman et al., 1997) 33

Table 1.2 Global NH_3 emissions from seabirds as estimated by Blackall et al. (2007). 43

Table 2.1 Range of Monin-Obukhov values for stability conditions 53

Table 2.2 Instruments that can be used to measure NH_3 concentration. 71

Table 3.1 Variation in total seabird NH3 emission by region for: Scenario 1: temperature independent emission rates based on mid-latitude measurements; Scenario 2: combination of mid-latitude measurements with thermodynamic temperature dependence of emissions; Scenario 3, limited temperature dependence as mean of Scenarios 1 and 2. 81

Table 4.1 F_{hab} values for rock, vegetation and burrow nesters (Wilson et al., 2004) 92

Table 4.2 Nesting behaviours of seabirds globally 93

Table 4.3 Background NH_3 concentration and range of uncertainty in NH_3 emission between duplicate experiments (expressed as a percentage) from substrates: burrow, nest, rock, sand, soil and vegetation. 98

Table 4.4 NH_3 concentrations from guano on a substrate minus the substrate background concentration after 23 hours. The chamber was constant at 12.5 °C and RH =60 %. NH_3 concentrations are averaged from duplicate experiments for each substrate. 100

Table 4.5 Comparison of old and new re-absorption coefficients (F_{hab})..... 103

Table 5.1 Instruments used to measure meteorological data on the Isle of May, Ascension Island and Bird Island. 113

Table 5.2 Species specific average adult mass of the birds (g) and monthly attendance (individuals) on Michaelmas Cay between September 2009 and January 2010. The bird counts were conducted by the Queensland EPA at the beginning of each month. The counts were conducted by S. Taylor and W. MacFarlane, Queensland EPA (pers. comm.). 116

Table 5.3 NH_3 concentration (mg m^{-3}) of the ALPHA samplers deployed on Michaelmas Cay during November (5/11/2009 to 10/12/2009) & December (10/12/2009 to 6/1/2010). Top ALPHA samplers are 2 m from the ground, Mid ALPHA samplers are 1 m from the ground and Bottom ALPHA samplers are 0.5 m from the ground. The concentrations shown are means of the triplicate samplers deployed. 118

Table 5.4 Meteorological data for Michaelmas Cay Period 1 (5/11/2009 to 10/12/2009) & Period 2 (10/12/2009 to 6/1/2010). [1] denotes (NOAA, 2010) and [2] denotes directly measured 118

Table 5.5 Uncertainty analysis of the NH_3 emission estimate from the seabird colony on Michaelmas Cay..... 120

Table 5.6 Averaged meteorological data from Ascension Island from 20/5/10 to 9/6/10 126

Table 5.7 NH_3 emission estimates from the passive sampling campaign on Ascension Island from 20/5/10 to 9/6/10 127

Table 5.8 Uncertainty analysis of the NH_3 emission estimate from the seabird colony on Ascension Island 128

Table 5.9 Uncertainties associated with the atmospheric dispersion modelling of the Sooty Tern colony in Mars Bay, Ascension Island 132

Table 5.10 Measured NH_3 Concentrations from ALPHA samplers on Isle of May 1/7/09 to 6/9/09. The concentrations are means of the triplicates deployed. [NH_3] indicates NH_3 concentration, Bgnd [NH_3] indicates background NH_3 concentration, *T* indicates temperature, *P* indicates precipitation, *WS* indicates wind speed, *WD* is wind direction and S.D. is the standard deviation. 135

Table 5.11 NH_3 emissions measured during four passive NH_3 sampling campaigns at the Isle of May , Scotland (1/7/09 to 6/9/09). 137

Table 5.12 Uncertainty estimate of NH_3 emissions passive sampling campaign, Isle of May, Scotland, 1/7/09 to 6/9/09..... 138

Table 5.13 Uncertainty analysis of WindTrax data for the NH_3 emission estimates at an Atlantic Puffin colony on the Isle of May, Scotland, in June/July 2009 143

Table 5.14 Location of ALPHA samplers on Signy Island January/February 2009..... 145

Table 5.15 NH_3 Concentrations ($\mu g\ m^{-3}$) from ALPHA samplers on Signy Island January/February 2009. Period 1 10/01/09 - 25/01/09, Period 2 25/01/09 - 08/02/09 and Period 3 08/02/09 - 21/02/09. Top ALPHA samplers are 2 m above the ground and Mid ALPHA samplers are 1 m above the ground. The concentrations are means of the triplicates deployed. 147

Table 5.16 Meteorological data for Laurie Island, South Orkney Islands during the measurement periods. Period 1 10/01/09 - 25/01/09, Period 2 25/01/09 - 08/02/09 and Period 3 08/02/09 - 21/02/09 (NCDC, 2011). *T* indicates temperature, *P* indicates precipitation, *WS* indicates wind speed, *WD* is wind direction and S.D. is the standard deviation. 147

Table 5.17 NH_3 emission estimates calculated by WindTrax for Signy Island January/February 2009..... 149

Table 5.18 Uncertainty analysis on NH_3 emission estimate from Signy Island, 10/01/2009 – 25/01/2009 150

Table 5.19 Uncertainties associated with the atmospheric dispersion modelling of a Macaroni penguin colony on Bird Island. 156

Table 5.20 Comparison of NH_3 emissions estimated by active and passive measurement methods for the Isle of May and Ascension Island. ... 159

Table 5.21 Summary of seabird colony NH_3 emissions estimated from measurement campaigns at five field sites carried out for this thesis 160

Table 5.22 Comparison of NH_3 emission estimates, modelled by the bioenergetics (BE) model (Scenario 1), the temperature adjusted bioenergetics model (TABE, Scenario 2) and the mid-range best estimate (Scenario 2) with the measured emissions scaled up for the entire breeding season at each site, and the equivalent percentage of excreted nitrogen that is volatilized as NH_3. 161

Table 6.1 The re-absorption of NH_3 by the substrate and overlying vegetation, F_{hab}. F_{hab} values describe relative amount of NH_3 released to the atmosphere. 168

Table 6.2 The amount of NH_3 reabsorbed by the substrate and overlying vegetation, F_{hab}..... 173

Table 6.3 The meteorological stations used in the GUANO models for each of the colonies. 174

Table 6.4 Site-specific seabird data input to the GUANO model. 174

Table 6.5 Sensitivity analysis of the refined GUANO model..... 177

Table 6.6 Adaptations made to the GUANO model and resulting effect on total daily NH_3 emission estimate 22nd May and 6th June 2010, Ascension Island 179

Table 6.7 Comparison between the measured NH_3 emissions and modelled NH_3 emissions, using the GUANO model for measurements made on Michaelmas Cay, Great Barrier Reef, Australia during November (5/11/2009 to 10/12/2009) & December (10/12/2009 to 6/1/2010).. 180

Table 6.8 Comparison between the measured NH_3 emissions and modelled NH_3 emissions using the GUANO model for measurements made on Signy Island during Period 1 (10/01/09 - 25/01/09), Period 2 (25/01/09 - 08/02/09) and Period 3 (08/02/09 - 21/02/09). 192

Table 6.9 Comparison between measured NH_3 emissions, NH_3 emission from the GUANO model and the percentage N volatilized (P_v). The average emission was calculated from the total emission and the total time of the measurement period. 198

Table 6.10 Annual percentage of N volatilized (P_v) by the GUANO model and comparison of mean annual climates in fieldwork location. T_g indicates ground temperature, *RH* indicates relative humidity, *WS* indicates wind speed and *P* indicates precipitation. 202

Table 6.11 Changes to P_v as climate variables in the GUANO model are substituted by values measured at the Isle of May. T_g indicates ground temperature, *RH* indicates relative humidity, *WS* indicates wind speed, *I* indicates irradiance and *P* indicates precipitation. 202

Table 7.1 Comparison between average measured ground temperature and ground temperatures modelled with the Parton and Logan (1982) method, using measured average maximum and minimum air temperature data during the measurement period at each of the field sites. 208

Table 7.2 Summary of data available from the National Climatic Data Center (NCDC) Global Surface Summary of the Day (GSOD) (NCDC, 2011) 210

Table 7.3 The name and distance of the GSOD meteorological station geographically closest to the bird colony. 211

Table 7.4 Comparison of measured data to Global Summary Of Day (GSOD) data with data measured at the field sites, for the duration of the field work. T_A is air temperature, RH is the relative humidity, WS is wind speed and P is the total precipitation measured during the period of field work. The gradient of the linear regression is denoted as *m* and R^2 is the coefficient of determination between the measurements and the GSOD database. 213

Table 7.5 Comparison of measured data for the duration of the field work to National Center for Environmental Prediction and the National Center for Atmospheric Research (NCEP/NCAR) data. T_A is air temperature, T_G is ground temperature, RH is the relative humidity, WS is wind speed, R_n is net radiation and P is precipitation. The gradient of the linear regression is denoted as *m* and R^2 is the coefficient of determination between the measurements and the NCEP/NCAR database. 213

Table 7.6 Comparison of the NH_3 emission estimates made by the TABE model (Chapter 3 - Scenario 2) and the GUANO model for the ten species with the largest NH_3 emissions as calculated by the GUANO model. 221

Table 7.7 Regional NH3 emission estimates calculated by the GUANO mode1 (using a modelled ground temperature; Scenario 1) and the thermodynamically dependent bioenergetics model Scenario 2 (TABE) (Chapter 3). 222

Table 7.8 The product mean correlation coefficient (r) is calculated for each of the variables used in the GUANO model. *RH* denotes average relative humidity during the breeding, *WS* is average wind speed during the breeding season, Total *P* is the annual total precipitation and $T_{breeding}$ is the average temperature during the breeding season. 223

Table 7.9 Results of a multiple regression analysis of NH_3 emission versus environmental factors in the GUANO model. *RH* denotes relative

humidity during the breeding season, *WS* is wind speed during the breeding season, Total *P* is the annual total precipitation and $T_{breeding}$ is the average temperature during the breeding season. The range of the variables denotes the variation globally and ΔPv indicates the difference in *Pv* for one unit change in the variable. 224

Table 7.10 Comparison of global NH3 emission from seabirds in 2099 to IPCC climate change scenarios B1, A1B and A2. 226

Table 7.11 Climate change anomalies of IPCC scenario A2 and the predicted change in *Pv* at the largest seabird colonies. ΔPv indicates the change in *Pv* between the 2010 estimate and the predicted value in 2099. *P* indicates the A2 2099 precipitation anomaly, *T* indicates the A2 2099 temperature anomaly, *RH* indicates the A2 2099 relative humidity anomaly, *WS* indicate the A2 2099 wind speed anomaly and ΔP_v indicates the change in P_v between 2010 and 2099. 228

Table 8.1 Average percentage of nitrogen that volatilizes (P_v) for a range of species. 242

Table of Figures

Figure 1.1 Global NH_3 emission on a 1x1 degree grid (g N m^{-2} yr^{-1}; (1 g N m^{-2} yr^{-1}=10 kg N ha^{-2} yr^{-1})) (Bouwman et al. 1997). 33

Figure 1.2 Predicted foraging distribution of seabird species during an average year in the 1990s, expressed in number (N) of individuals per km^2 (Karpouzi et al., 2007) 34

Figure 1.3 a) Locations and relative magnitude of NH_3 emissions from seabird colonies in the UK, from Wilson et al. (2004). b) The local seabird contribution calculated as percentage of the contribution of seabird emissions compared to NH_3 emissions from agriculture and from seabirds summed for each 1 km of coastline or point source (Wilson et al. (2004). 35

Figure 1.4 Total global food consumption by seabirds (modelled from Karpouzi et al., 2007)..... 38

Figure 1.5 Processes governing the emission of NH_3 from uric acid (adapted from Elliott and Collins, 1982) 39

Figure 1.6 Nitrogen pathways in a Macaroni Penguin colony at Kildalkey Bay, Marion Island (Lindeboom, 1984). The box on the left of the diagram shows the composition of the excreted nitrogen. The boxes with the bold text give the fate of this excreted N summed to 100 %. 40

Figure 1.7 The eight types of nest that birds make a) cup, b) dome, c) dome and tube, d) plate, e) bed, f) scrape, g) mound and h) burrow. Figure taken from Hansell (2000). 46

Figure 2.1 Structure of the planetary boundary layer (after Stull, 1988; Garret, 1992, modified). The brown boxes indicate the boundaries between the layers. 51

Figure 2.2 Schematic of a Gaussian plume. Emission is from height h above the ground. Concentrations vary in x, y and z directions (after Seinfeld and Pandis, 1996, modified for this thesis) 60

Figure 2.3 The Lagrangian stochastic (LS) dispersion of air parcels, showing the trajectories of the emissions from the source and background. U denotes the wind speed and C denotes the measured concentration... 63

Figure 2.4 The side view of an ALPHA sampler. Image courtesy of Tang et al. (2001)..... 68

Figure 3.1 Global distribution of seabird colonies, based on number of breeding pairs. Lines delineate regional boundaries: 1. Africa, 2. Antarctica & Southern Ocean, 3. Asia, 4. Atlantic, 5. Australasia, 6. Caribbean & Central America, 7. Europe, 8. Greenland & Svalbard, 9. Indian Ocean, 10. Middle East, 11. North America, 12. Pacific and 13. South America. To show distribution of the colonies clearly, the number of pairs in each 5° grid square have been summed. 79

Figure 3.2 Regional estimates of breeding pairs of seabird and N excretion calculated in this study. 80

Figure 3.3 Latitudinal variation in global NH_3 emissions from seabird colonies based on the temperature independent bioenergetics model (Scenario 1) and thermodynamically adjusted bioenergetics model estimates (Scenario 2). The limited-temperature dependent NH_3 (Scenario 3) emission is the average of Scenario 1 and Scenario 2. 82

Figure 3.4 Estimated global distribution of NH_3 emissions from seabird colonies, using the mid-estimate between the temperature independent bioenergetics model and the thermodynamically adjusted bioenergetics model (Scenario 3). The results incorporate species and colony specific data on population size, birds' energy requirements, colony attendance, breeding success and estimated volatilization rates for guano deposited onto bare rock and vegetation. To show the distribution of the NH_3 emissions clearly, emissions in each 5° grid square have been summed. 83

Figure 3.5 Illustrations of the global database, showing colony NH_3 emissions mapped on 0.1° resolution for a) the south Atlantic and b) NW Europe. 84

Figure 3.6 The graph shows the comparison of temperature functions from ornithogenic soils OS_{DG2} and OS_{DG4} of Zhu et al. (2011), the temperature independent bioenergetics model (Scenario 1), the thermodynamically adjusted bioenergetics model (Scenario 2) and the limited-temperature dependent model (Scenario 3). Temperature functions have been normalised to 10 °C. 87

Figure 4.1 Illustration of NH_3 emission from guano and its possible re-absorption by an overlying canopy. 92

Figure 4.2 Setup of the experimental chamber to measure NH_3 concentrations in air above guano. Air is cleaned by a charcoal scrubber going into the chamber with the relative humidity controlled by a water bubbler and silica gel. Air from the chamber is sampled at 0.5 L min^{-1} by a Nitrolux^{TM} trace gas sampler. Exhaust air is scrubbed by charcoal and passed through a water bubbler with biocide. 95

Figure 4.3 The NH_3 concentration over 17 hours of multiple guano slurry samples of different water quantities (*2ml, 10 ml, 15ml and 50 ml*). 10 g of seabird guano is used in each trial. The relative humidity remained at 60 % and air temperature remained at 15 °C. 96

Figure 4.4 Background NH_3 concentration (ppb) measured for different substrates (rock, sand, soil, vegetation, burrow and nesting materials) with no added guano. Temperature = 18 °C and RH = 60 %. 99

Figure 4.5 The NH_3 concentration (ppb) measured over 22 hours from guano slurry on top of a substrate (rock, sand, soil, vegetation, nesting materials or placed in a burrow). The air temperature is constant at

18 °C and RH = 60 %. In each trial, guano slurry is made from 10 g of dried guano and 15 ml water. 99

Figure 4.6 Total NH_3 emitted in 23 hours from guano on six different test substrates over 17 hours. The air temperature remained constant at 18 °C and RH at 60 %. The guano slurry was 10 g of dried guano and 15 ml water. 102

Figure 5.1 Global map of fieldwork sites where measurements were conducted for this thesis. 108

Figure 5.2 Set-up of the active sampling equipment deployed on the Isle of May (Scotland), Ascension Island (Atlantic Ocean) and Bird Island (South Georgia) 112

Figure 5.3 Michaelmas Cay before the breeding season. ALPHA samplers were attached to the posts in the picture. Image courtesy of W. MacFarlane (Queensland EPA). 115

Figure 5.4 Deployment of the ALPHA samplers in Michaelmas Cay, October 2009 to May 2010. The birds nest on both vegetation and sand. 117

Figure 5.5 Wind roses for Michaelmas Cay (a) Period 1 (5/11/2009 to 10/12/2009) & (b) Period 2 (10/12/2009 to 6/1/2010) 119

Figure 5.6 Map of Ascension Island. Courtesy of Ministry of Defence, United Kingdom 2003 121

Figure 5.7 Sooty tern colony in Mars Bay, Ascension Island. Inset shows Sooty terns nesting on the clinker in Mars Bay (Photo: S. Riddick). 122

Figure 5.8 The blue area indicates the location of the Sooty tern colony in 2010 at Mars Bay, Ascension Island. Image courtesy of J. Hughes (University of Birmingham). (Pink and green areas on the map indicate the locations of breeding terns and deserted eggs for a previous breeding season.) 123

Figure 5.9 Arrangement of ALPHA samplers used to measure the NH_3 concentration at Mars Bay on Ascension Island. The green area indicates the nest site of the Sooty terns. Two arrangements were used (a): Period 1 (20/05/2010 - 27/05/2010) & Period 2 (27/05/2010 - 02/06/2010) and (b) Period 3 (02/06/2010 - 09/06/2010). 124

Figure 5.10 NH_3 concentrations for each of the masts during the three passive sampling measurement periods at Mars Bay, Ascension Island. During Periods 1 & 2, Masts 1 and 2 sampled at three heights (1.5 m, 1 m and 0.5 m) and Mast 3 at 1 m. During Period 3 all masts sampled at 1.5 m. The distances from each mast to the colony along the sampling transect are given in the figure. The concentrations are means of the triplicate ALPHA samplers deployed. 125

Figure 5.11 Wind roses for Ascension Island during the three measurement periods. 126

Figure 5.12 The set up of instruments used to measure the NH_3 concentrations actively from the Sooty Tern colony in Mars Bay. The AiRRmonia instrument was used to measure the NH_3 concentrations. The air inlet was positioned at 2 m above the ground. Instruments were powered by a Honda Eu10i petrol generator. Micrometeorological parameters were measured with a Gill Windmaster Pro sonic anemometer, on top of the mast 2.5m above the ground. Wind speed was recorded at three heights (2m, 1m and 0.5m) and the temperature, relative humidity and solar irradiance were measured at 0.75m above the ground. 128

Figure 5.13 Instrument set up in the tent at Mars Bay, Ascension Island, May and June 2010. This photograph shows how the instruments were initially deployed. The mast was shortened later. 129

Figure 5.14 Time series of NH_3 concentration, wind speed, ground temperature and roughness length measured at Mars Bay, Ascension Island, 22nd May to 10th June 2010. These data were used as input to the WindTrax modelling software for the estimation of NH_3 emissions from the seabird colony, shown at the bottom. 130

Figure 5.15 NH_3 emissions from the Sooty tern colony, Mars Bay, Ascension Island, 4th June to 8th June 2010, as calculated by the WindTrax model. This highlights the diurnal pattern of NH_3 emissions. 131

Figure 5.16 The averaged diurnal pattern in NH_3 emissions derived from WindTrax emission calculations for the Sooty Tern colony at Mars Bay, Ascension Island. This campaign estimated an average daily NH_3 emission between 22nd May and 10th June 2010 of 18.9 $\mu g\ m^{-2}\ s^{-1}$. The error bars show the variability in hourly emissions by representing the maximum and minimum NH_3 emissions for these hours for the duration of the campaign. 132

Figure 5.17 Primary nesting sites for Atlantic puffins, Herring gulls, European shags and Common guillemots on the Isle of May. The locations of the met station, active measurement site and the ALPHA sampler site have been included. 134

Figure 5.18 The triplicate ALPHA sampler above the Atlantic puffin colony, Isle of May, Scotland. 134

Figure 5.19 Weather station *in-situ* on the Isle of May, collecting data on temperature, humidity, solar radiation, rainfall and ground temperature. 135

Figure 5.20 Wind rose for the Isle of May, Scotland, during the four measurement periods. (a) 01/07/2009 - 15/07/2009, (b) 15/07/2009 - 29/07/2009, (c) 29/07/2009 - 15/08/2009 & (d) 15/08/2009 - 06/09/2009. 136

Figure 5.21 Sampling NH_3 concentrations and collecting turbulence data on the Isle of May, Summer 2009. The image shows sampling at three heights. Measurements were taken from the middle inlet (black funnel). 139

Figure 5.22 NH_3 emission estimates from the Atlantic Puffin nesting area on the Isle of May, Scotland, for the period 13th to 15th July 2009. This highlights the diurnal pattern of NH_3 emissions. 140

Figure 5.23 WindTrax input data and calculated NH_3 emission for the active sampling campaign on the Isle of May, Scotland Summer 2009 141

Figure 5.24 The averaged hourly NH_3 emissions derived from WindTrax emission data for the Atlantic Puffin colony on the Isle of May. Active sampling dates from 01/07/2009 - 23/07/2009. The error bars show variability in hourly emission by representing the maximum and minimum NH_3 emissions for these hours. 142

Figure 5.25 Penguin breeding sites on Signy Island, shaded in black. Map courtesy of the British Antarctic Survey. 144

Figure 5.26 Mast 1 (with triplicate ALPHA samplers at three heights) looking west on Gourlay Peninsula, Signy Island, during the penguin breeding season. Image courtesy of Dr. P. Hill, University of Bangor. 145

Figure 5.27 Location of ALPHA samplers on Gourlay peninsula, Signy Island. The dark grey areas on the map indicate penguin nesting sites. Map courtesy of the British Antarctic Survey. 146

Figure 5.28 Wind roses for Orcadas Base, Laurie Island, South Orkney Islands over the three sampling periods relevant to Signy Island, for which they provide proxy wind data. (a) Period 1 10/01/09 - 25/01/09, (b) Period 2 25/01/09 - 08/02/09 and (c) Period 3 08/02/09 - 21/02/09. 148

Figure 5.29 A map of Bird Island, South Georgia, with locations of the British Antarctic Survey (BAS) research station and the NH_3/met monitoring site at Fairy Point marked. Image courtesy of the British Antarctic Survey. 151

Figure 5.30 Meteorological instruments on two masts on the highest land at Fairy Point, Bird Island, with Willis Island in the distance (10 km). Image courtesy of Sim Tang, CEH. 152

Figure 5.31 Data input to WindTrax and resulting NH_3 emission for active sampling campaign on Bird Island, South Georgia, Nov & Dec 2010 154

Figure 5.32 Average hourly NH_3 emissions derived from WindTrax emission data for the Big Mac penguin colony, Bird Island, for the entire monitoring period 18 Nov to 13 Dec 2010. The error bars show variability in hourly emission by representing the maximum and minimum estimated NH_3 emissions for these hours. 155

Figure 6.1 Pathways taken by nitrogen following excretion as uric acid (after Blackall, 2004 modified). The total mass of excreta (M) is made from 0.6 M of water, 0.21 M of uric acid and 0.19 M non-N guano. 165

Figure 6.2 Calculated net solar radiation for consecutive days at Michaelmas Cay on the 9th December 2009 and 10th December 2009 using data

from National Center for Environmental Prediction (NCEP) and the National Center for Atmospheric Research (NCAR) Reanalysis 1 dataset (NCAR, 2011). 172

Figure 6.3 Temperature offset (Toffset) between the average air temperature (Ave T_a) and ground temperature (Ave T_g) for (a) Bird Island and (b) Ascension Island 173

Figure 6.4 Comparison of Blackall (2004) GUANO model with measurements (Section 5.3.6) and the adaptations made to the model for (a) 22nd May on Ascension Island during a period of no rain and (b) 6th June on Ascension Island during a rain event at 0800. 178

Figure 6.5 Comparison between the measured monthly NH_3 emissions (red line), monthly average modelled NH_3 emissions (green line) and modelled hourly NH_3 emissions (blue line) using the GUANO model for measurements made on Michaelmas Cay, Great Barrier Reef, Australia during November (5/11/2009 to 10/12/2009) & December (10/12/2009 to 6/1/2010). Tick marks on the x-axis indicate midnight on each day. 181

Figure 6.6 Modelled NH_3 emission compared to environmental variables representative of climate at the sooty tern colony on Michaelmas Cay, Great Barrier Reef, Australia from 5/11/2009 to 6/1/2010). Tick marks on the x-axis indicate midnight on each day. 182

Figure 6.7 Comparison between measured and modelled NH_3 emissions from the Sooty tern colony at Mars Bay, Ascension Island 22nd May to 10th June 2010. Tick marks on the x-axis indicate midnight on each day. 183

Figure 6.8 Comparison between hourly measured and modelled NH_3 emissions from the Sooty tern colony at Mars Bay, Ascension Island, 22nd May to 10th June 2010. The line on the graph represents the 1:1 line. Individually labelled points indicate Julian date and hour of measurement. 184

Figure 6.9 Modelled NH_3 emission compared to environmental variables representative of climate at the Sooty tern colony at Mars Bay, Ascension Island, 22nd May to 10th June 2010. Tick marks on the x-axis indicate midnight on each day. 186

Figure 6.10 Comparison between the measured NH_3 emissions and modelled NH_3 emissions using the GUANO model for measurements made on the Isle of May between 5th July and 17th July, 2009. The F_{hab} value used in the GUANO model was 0.64. Tick marks on the x-axis indicate midnight on each day. 187

Figure 6.11 Comparison between hourly measured and modelled NH_3 emissions from the puffin colony on the Isle of May between the 29th June and the 23rd July, 2009. The larger outliers are indicated on the figure with the Julian date and the hour of measurement. 189

Figure 6.12 Modelled and measured NH_3 emission compared to environmental variables representative of climate at the Atlantic puffin colony on

the Isle of May between the 7th July and the 17rd July 2009. F_{hab} for adults was set at 0.64. Tick marks on the x-axis indicate midnight on each day. 190

Figure 6.13 Comparison between the measured NH_3 emissions (red line), modelled hourly NH_3 emissions using the GUANO model (blue line) and the average of the modelled emission during each measurement period (green line) on Signy Island during Period 1 (10/01/09 - 25/01/09), Period 2 (25/01/09 - 08/02/09) and Period 3 (08/02/09 - 21/02/09). Tick marks on the x-axis indicate midnight on each day. 191

Figure 6.14 Modelled NH_3 emission compared to environmental variables representative of climate made on Signy Island during 10/01/09 - 21/02/09. Tick marks on the x-axis indicate midnight on each day. 193

Figure 6.15 Comparison between hourly measured and modelled NH_3 emissions from the Big Mac Macaroni penguin colony, Bird Island, South Georgia, from 18/11/2010 to 13/12/2010 (measurements based on AiRRmonia concentration data supplied by Sim Tang, CEH). Tick marks on the x-axis indicate midnight on each day. 194

Figure 6.16 Comparison between hourly measured and modelled NH_3 emissions from the Macaroni penguin colony on Big Mac, Bird Island between 18/11/2010 and 13/12/2010. 195

Figure 6.17 Modelled NH_3 emission compared to environmental variables representative of climate at the Big Mac Macaroni penguin colony on Bird Island from 18/11/2010 to 13/12/2010. Tick marks on the x-axis indicate midnight on each day. 196

Figure 6.18 Comparison between the percentages of nitrogen that volatilizes for measured NH_3 emissions and NH_3 emissions calculated by the GUANO model. 198

Figure 6.19 Collation of correlation coefficients between hourly modelled NH_3 emissions and environmental factors at all fieldwork sites. 200

Figure 6.20 Relationship between percentage N volatilized (P_v) and relative humidity, temperature, wind speed, precipitation and ground temperature for NH_3 emissions simulated by the GUANO model during the measurement period. 201

Figure 6.21 The effect of changing climate variables at each of the field sites. In each case, the climate variable measured at the Isle of May is substituted into the GUANO model. 203

Figure 6.22 Both graphs show the comparison of P_v calculated for the BE (green dashed line) and TABE (Blue solid line) at temperatures from 0°C to 30 °C. Graph a) shows P_v during the measurement period calculated from GUANO model emissions (solid dot - estimated P_v, hollow dot - P_v accounting for habitat) at each measurement site of this study (Michaelmas Cay, Ascension, Isle of May, Big Mac and Signy Island) and Blackall et al (2004) measurements for the Bass Rock and Isle of May. Graph b) shows

annual P_v values calculated from GUANO model emissions (solid dot - estimated P_v, hollow dot - P_v accounting for habitat) at each measurement site of this study (Michaelmas Cay, Ascension, Isle of May, Big Mac and Signy Island) and Blackall et al (2004) measurements for the Bass Rock and Isle of May. 205

Figure 7.1 Comparison of the diurnal variation in average measured ground temperature and ground temperatures modelled with the Parton and Logan (1982) method, using measured average maximum and minimum air temperature data during the measurement period at each of the field sites. 209

Figure 7.2 The temperature offset (T_o, °C), difference between average air temperature and ground temperature, for the three field sites during the measurement period (nesting time at each of the colonies): Solid Line: Isle of May (56 °N), Dashed line: Ascension (8 °S) and Dotted Line: Bird Island (54 °S). 214

Figure 7.3 Climate change anomalies for IPCC climate change scenarios B1, A1B and A2 for precipitation, temperature, relative humidity and wind speed. 216

Figure 7.4 Global NH_3 emissions from seabirds, calculated using the revised GUANO model with ground temperature data. 219

Figure 7.5 Comparison of the total NH_3 emission estimates made by the bioenergetics model (Chapter 3 - Scenario 2) and the GUANO model (using a modelled value for ground temperature). The average temperature and rainfall are also presented. 220

Figure 7.6 The percentage of nitrogen excreted that volatilizes as NH_3 (*Pv*, %) plotted, for all colonies in the global seabird database, against the average daily precipitation (mm m^{-2} day^{-1}), the average wind speed during the breeding season (m s^{-1}), the average relative humidity during the breeding season (%) and the average air temperature during the breeding season (°C). 223

Figure 7.7 Spatial distribution of the percentage of excreted nitrogen that volatilizes (P_v) at seabird colonies, calculated using the revised GUANO model with ground temperature data. 227

Figure 7.8 Changes to percentage of excreted nitrogen that volatilizes (P_v) estimated for 2010 at seabird colonies when b) wind speed anomalies are considered only, c) relative humidity anomalies are considered only, d) precipitation anomalies are considered only and e) temperature anomalies are considered only. Climate anomalies are taken from the IPCC A2 climate change scenario (IPCC DDC, 2011). 230

Figure 7.9 Effects of climate change on *Pv* at the 9 largest seabird colonies, calculated with the GUANO model. Crosses indicate NH_3 emissions for 2010 using Global Summary of Day (GSOD); open circles represent predicted NH_3 emissions by incorporating temperature,

wind speed, relative humidity and precipitation anomalies for 2099 (IPCC Scenario A2, worst case). 231

Figure 8.1 Contribution of seabird NH_3 emissions as estimated here as a percentage of total NH_3 emissions from seabirds and other sources (estimated by the EDGAR database (version 4.1) of EC-JRC, 2010). 234

Nomenclature

Commonly used symbols in this thesis

Symbol	*Description*	*Generally used (SI) units or value of constant*
Latin alphabet		
A	Cross sectional area of ALPHA sampler	3.4636×10^{-4} m^2
A_{eff}	Assimilation efficiency of ingested food	-
B	Sub-layer Stanton number	-
b	Plant specific leaf area index	-
Ch	Chicks	-
CH	Transfer coefficient for heat flux	1×10^{-3}
c_p	Specific heat of air at constant pressure	J kg^{-1} K^{-1}
c_T	Temperature dependent Henry's Law constant	-
d	Zero-plane displacement	m
D	Diffusion coefficient of NH_3 in air	2.09×10^{-5} m^2 s^{-1}
D_A	Density of breeding adults	birds m^{-2}
D_χ	Molecular diffusivity of a gas	m^{2}s^{-1}
e_a	Mean ambient water vapour pressure	kPa
e_s	Saturated water vapour pressure	kPa
$f_{(H2O)}$	Dry mass of guano added as water	%
F_e	Average nitrogen excretion rate	g m^{-2} hr^{-1}
$F_{e\text{-}br}$	Nitrogen excretion rate per breeder	g bird^{-1} day^{-1}
$F_{e\text{-}ch}$	Nitrogen excretion rate per chick	g bird^{-1} yr^{-1}
F_{Ec}	Energy content of food	kJ g^{-1}
F_H	Hourly NH_3 emission rate	g NH_3 m^{-2} hr^{-1}
$F_{H2O(evap)}$	Mass of water evaporated	kg m^{-2} hr^{-1}
$F_{H2O(g)}$	Water added in excreted guano	kg m^{-2} hr^{-1}
$F_{H2O(pptn)}$	Water added during rain events	kg m^{-2} hr^{-1}
$F_{H2O(ro)}$	Water lost as run-off	kg m^{-2} hr^{-1}
F_{hab}	Habitat fractional release parameter	-
F_{Nc}	Nitrogen content of food	g N g^{-1}
F_{Nv}	Fraction of excreted nitrogen that volatilizes	-

f_{pH}	pH factor	-
f_{RH}	Relative humidity factor	-
f_T	Temperature factor	-
F_t	Annual NH_3 emission rate	g NH_3 m^{-2} yr^{-1}
F_{TAN}	TAN converted from the UA	g m^{-2} $hour^{-1}$
f_{tc}	Fraction of time spent at colony	-
F_w	Nitrogen washed off by the rain	g m^{-2} $hour^{-1}$
g	Acceleration due to gravity	m s^{-2}
H	Sensible heat flux	J m^{-2} s^{-1}
h_s	Height of the source	m
I_p	Photosynthetic radiation intensity	W m^{-2}
k	Von Karman constant	0.4
K_z	Vertical eddy diffusivity	m^2 s^{-1}
L	Monin-Obukhov length	m
L_α	Length of the ALPHA diffusion tube	0.006 m
M	Adult mass of bird	g
m	Slope of the saturation vapour pressure curve	kPa K^{-1}
m_b	Mass of NH_3 on a blank (unexposed) sample	µg
$M_{fledging}$	Mass of chick at fledging	g
N	Number of gas particles	-
ND	Nest density	nests m^{-2}
N_e	Nitrogen excreted	g m^{-2}
N_w	Nitrogen washed off by rain	g m^{-2}
$Prec$	Precipitation	mm
P	Atmospheric pressure	kPa
P_{chicks}	Breeding productivity	ch fledge $pair^{-1}$
Q	Rate of emission of gas	g m^{-2} s^{-1}
Q_{H2O}	Water budget	kg m^{-2}
$Q_{NH3}(br)$	Annual NH_3 emission for breeders	g NH_3 $bird^{-1}$ yr^{-1}
$Q_{NH3}(ch)$	Annual NH_3 emission for chicks	g NH_3 ch^{-1} yr^{-1}
$Q_{NH3}(nbr)$	Annual NH_3 emission for non-breeders	g NH_3 $bird^{-1}$ yr^{-1}
Q_s	Emission source strength	g s^{-1}
Q_t	Rate of emission of the tracer	g m^{-2} s^{-1}
Q_{UA}	UA budget	g m^{-2}

$R_a(z\text{-}d)$	Aerodynamic resistance at height (z-d)	s m^{-1}
R_b	Quasi-laminar layer resistance	s m^{-1}
R_c	Residual resistance to emission at the surface	s m^{-1}
Re_*	Turbulence Reynolds number	-
RH	Relative Humidity	%
R_n	Net solar radiation	W m^{-2}
R_s	Resistance of stomatal pathway	s m^{-1}
$R_t(z\text{-}d)$	Total resistance at height (z-d)	s m^{-1}
R_w	Resistance of cuticular pathway	s m^{-1}
Sc	Schmitt Number	-
T	Temperature	K
t	Averaging time	s
T_a	Air temperature	°C
$t_{breeding}$	Length of breeding season	Days
T_g	Ground temperature	°C
u	Wind velocity	ms^{-1}
u_*	Friction velocity	ms^{-1}
v	Volume of the extraction solution	ml
V	Effective volume of air sampled	m^3
ν_a	Viscosity of air	kg m^{-1} s^{-1}
WS	Wind speed	m s^{-1}
z	Height	m
z_0	Roughness length	m

Greek alphabet

Γ	Adiabatic lapse rate	K km^{-1}
γ	Psychrometric constant	kPa $°C^{-1}$
δe	Vapour pressure deficit	kPa
κ	Thermal diffusivity of air	m^2 s^{-1}
λ_v	Latent heat of vaporization	MJ kg^{-1}
ρ	Density of air	kg m^{-3}
σ_y	Lateral concentration distribution	m
σ_z	Vertical concentration distribution	m

τ	Shear stress	N m^{-2}
Φ_H	Correction factor for heat	-
Φ_M	Correction factor for momentum	-
X	Gas concentration	g m^{-3}
X_*	Friction concentration	g m^{-3}
X_α	Average concentration of ALPHA sampler	g m^{-3}
X_a	Gas concentration in air	g m^{-3}
X_b	Background concentration of gas	g m^{-3}
X_c	Canopy surface concentration	g m^{-3}
X_t	Measured concentration of the tracer gas	g m^{-3}
Ψ_H	Stability function for heat	-
Ψ_M	Stability function for momentum	-

Abstract

Seabirds transport significant amounts of nitrogen from the ocean to the land in the form of excreta. The subsequent volatilization of nitrogen may result in significant emissions of atmospheric ammonia (NH_3) in remote coastal systems. Blackall et al., (2007) estimated global seabird NH_3 emissions to be 242 Gg N $year^{-1}$, however their emission estimate was not parameterised for all climate types and is based on old and potentially inaccurate historical population data.

To update the global seabird NH_3 emission estimate, a contemporary seabird database of 261 million breeding seabird pairs was developed. This dataset was used in conjunction with a refined version of an existing seabird NH_3 model (GUANO) to estimate NH_3 emissions from seabirds in a range of climates. The estimate was further refined by using seabird habitat parameters that were validated through laboratory and field measurements. The field measurements, in various climate types, provide a more robust mechanism by which seabird emission factors could be validated for use in the global model. A global seabird NH_3 emission estimate of 82 [37 - 127] Gg NH_3 $year^{-1}$ is presented, with uncertainty as a result of variation in diet composition (± 23 %), non-breeder attendance (± 13 %), ground temperature estimates (± 32 %) and seabird population estimates (± 36 %).

Seabirds in the tropics are more significant emitters than previously thought, whilst emissions from polar regions were less significant than expected. The largest calculated NH_3 emissions were on islands in the Southern Ocean and Pacific Ocean, with a maximum colony emission of 3.9 Gg NH_3 $year^{-1}$ from the Sooty tern colony on Baker Island, Pacific Ocean. These NH_3 emissions are environmentally relevant, as they primarily occur as “hot-spots” in otherwise nutrient-free regions and may play a fundamental ecological and biogeochemical role in these ecosystems.

Acknowledgments

This project was supported by a grant from the NERC CEH Integrating Fund and jointly carried out between the Centre for Ecology & Hydrology and King's College London. Firstly, I would like to thank my CEH supervisor, Dr. U. Dragosits for all her support and enthusiasm throughout the project. Thanks also to other supervisors at CEH, official and un-official, for all their advice, expertise and inspiration, including Professor M. A. Sutton, Dr. F. Daunt, Dr. C. F. Braban and Professor S. Wanless. Thanks also to particular members of staff at CEH for their advice and patience, including Ms. S. Tang for her invaluable contributions in assembling ALPHA samplers before deployment and analysing them on their return, Mr. M. Newell for his continued support throughout the three year data collection period on the Isle of May and for not making too much noise in the morning when he went out to count birds and Dr. A. Gray for his knowledge on the working of Ascension Island. Also thanks to the many members of the Atmospheric Sciences and Seabird groups at CEH for their support.

Many thanks to my KCL supervisor, Dr. T. Blackall, for all his support throughout the project, especially for his contributions during fieldwork on both the Isle of May and Ascension Island. Also, thanks to Professor S. Grimmond and the Environmental Monitoring and Modelling (EMM) Research Group at KCL.

I am grateful to all contributors that provided data for the seabird database: Birdlife International, Eric Woehler (University of Tasmania, Australia), Halvard Strom (Nordic Seabird Group), Yat-tung Yu (Hong Kong Bird Society), Roddy Mavor (JNCC), David Irons (US FWS), Canada's Important Bird Areas, Australian Department for Environment, Graeme Taylor (Department of Conservation, NZ), Pablo Yorio (Centro Nacional Patagónico), Chin Aik Yeap (Malaysian Nature Society), Philip Round (Mahidol Unversity), Aevar Petersen (Icelandic Institute of Natural History), Carsten Egevang (Greenland Institute of Natural Resources), Takashi Yamamoto (Japan National Institute of Polar Research), Tycho Anker-Nilssen (Norwegian Institute for Nature Research), Jaanus Elts (Estonian Ornithological Society), Martti Hario (Finnish Game and Fisheries Research), Yuri Artukhin (Pacific Institute of Geography), Michelle Paleczny (UBC), Robin Allen

(Florida Fish and Wildlife Conservation Commission), Christina Kisiel (NJ Fish and Wildlife, USA), Michelle Gibbons, Daniel Rosenblatt (both Stony Brook University), Sue Cameron (North Carolina Wildlife Resources Commission), Brent Ortego (US FWS Texas), Shawn Stephensen (US FWS Oregon) and Ruth Boettcher (VA Game and Inland Fisheries).

Many thanks to Elena Alcon-Perez, a Leonardo da Vinci scholarship student, who helped conduct the chamber experiments in Chapter 4. I am also grateful to Sarah Robinson of the Royal Zoological Society of Scotland and the keepers in the Penguin enclosure at Edinburgh Zoo for allowing me to collect penguin guano samples.

Data collection during fieldwork was a collective success, with contributions from individuals throughout the world. Thanks to Dr. P. Hill of the University of Bangor for the deployment and collection of ALPHA samplers on Signy Island, and also to Mr. D. Briggs of BAS on Signy for information on the climate and nesting penguins. To Mr. W. MacFarlane and Mr. S. Taylor, of the Department of Environment and Resource Management, Queensland Parks and Wildlife Service, Australia, for deploying and retrieving ALPHA samplers from Michaelmas Cay and their expertise on the birds at Michaelmas during a meteorologically unsettled time on the Great Barrier Reef. Thanks to Mr. S. Stroud, Ms. N. Williams and Ms. O. Renshaw at the Conservation Department on Ascension Island for approving the research permit in Mars Bay and assistance when equipment was held up at customs. The whole seabird team and other researchers on the Isle of May, especially to Professor M. Harris, Ms. T. Alampo and Mr. D. Pickett (both Scottish National Heritage). Special thanks to Mr. A. Easton and Mr. C. Murray for transport to and from the island. Thanks to Ms. S. Tang and Dr. J. Schmale for data collection in appalling conditions on Bird Island.

Finally thanks to my parents- thanks to dad for all the long conversations about instrumentation problems, data collection, data analysis and the difficulties of writing, and thanks to mum for her support (and putting up with us). Most of all, I would like to thank my wife for everything she has done to help me get the project finished.

Chapter 1: Introduction

1.1 Overview

Nitrogen gas (N_2) makes up 78 % of the atmosphere. In this diatomic form it is unreactive and cannot be used directly by plants for growth. To be usable by plants, N_2 needs to be 'fixed' into reactive nitrogen (N_r) compounds, and one of the key forms is ammonia (NH_3). Most NH_3 in the environment is formed by either the microbial decomposition of plant materials or as nitrogen compounds in animal excreta. Waste nitrogen from animals is from the breakdown of proteins and amino acids. NH_3 can be readily used by plants for growth, however excess NH_3 in the environment can result in acidification and eutrophication of ecosystems altering interspecies competition (Sutton et al., 2011). This has important ramifications on the biodiversity and ecology of an ecosystem.

Seabird colonies occur in remote coastal locations, and because of their isolation from anthropogenic N_r sources they play a major role in local nitrogen cycles (Lindeboom, 1984; Mizutani and Wada, 1988; Wilson et al., 2004). Seabirds excrete nitrogenous waste in the form of uric acid (Bryant and Furness, 1995). The rate of uric acid excretion depends on the type of bird and can be locally very large. For example, the nitrogen deposition at a Northern gannet colony on the Bass Rock has been estimated at more than 52 Mg N ha^{-1} yr^{-1} (Blackall et al. 2007). Hydrolysis of uric acid produces NH_3 gas, some of which volatilizes to the atmosphere. As a consequence of high excretal density, seabird colonies are potentially large sources of NH_3 emission (Kildaw et al., 2005). Large colonies, with millions of nesting pairs, can result in NH_3 'hotspots' e.g. Zavodovski Island, South Sandwich ~ 6 Gg NH_3 yr^{-1} (Blackall et al. 2007). The variability of the NH_3 emissions is due to a number of factors including the number and size of birds, nesting type, the climate at the colony, topography of the colony and the vegetation at the colony.

Population size is an important factor when estimating NH_3 emission from a seabird colony. Several global seabird population estimates exist: Brooke (2004) estimated 700 million free-living individual seabirds, whilst Karpouzi (2007) estimated 900 million free-living individuals. The variability in these estimates is indicative of the difficulty when estimating seabird populations. Population fluctuations due to

climatic events, ecosystem and biological events and anthropogenic pressures have been observed at many colonies and indicate the ever-changing nature of these populations (Croxall et al., 2002; Lewis et al. 2001). Once the bird population is known, the amount of guano deposited at the colony can be estimated from the following information: 1) the mass of the bird, 2) the breeding success of the bird, 3) the amount of time that the bird spends at the colony and 4) the length of the breeding season (Wilson et al., 2004).

Studies have shown that NH_3 emission depends on the pathway between the source and the atmosphere and re-absorption of NH_3 by the soil and overlying vegetation (Sutton et al. 1995a). Wilson et al (2004) developed a habitat fractional release parameter (F_{hab}) to describe the net emission of NH_3 from excreted nitrogen deposited onto different substrates. Values of F_{hab} were initially based on unpublished field measurements and then adjusted to fit the model.

The amount of NH_3 emitted by the excreted nitrogen depends on the climate and the environment surrounding the guano because of chemical, changes in pH (Sutton et al., 1993) and physical processes, such as temperature (Zhu et al., 2011). The thermodynamics of NH_3 emission depends on climate and surface conditions, where the rate of NH_3 emission increases with an increase in temperature, according to Henry's law which expresses the equilibrium between NH_3 in the aqueous and gas phases (Nemitz et al., 2001; Sutton et al., 1993). Blackall et al. (2007) suggested that water availability may be an important factor to NH_3 emission, and limited water in tropical conditions may counteract the tendency for increased emissions in warmer conditions.

Estimates of NH_3 emissions from seabirds have been made for both the UK and on the global scale, but at present none adequately address the uncertainty associated with climatic variation. An initial estimate of the annual UK NH_3 emission by seabirds was made by Sutton et al. (1995b) of 0.37 kt $year^{-1}$. This estimate was calculated using emission factors derived in a UK climate for large birds and small birds, and the UK seabird population was separated into these two categories. The re-absorption of NH_3 by vegetation for burrow and vegetation nesters was not accounted for.

Wilson et al. (2004) derived a bioenergetics model to estimate the rate of nitrogen excretion of a bird depending on the metabolic rate and the absorption efficiency of nitrogen during digestion. Measurements made in the UK were used empirically to derive relationships describing both the absorption of NH_3 by vegetation and the effects of climate. That study used detailed population data and accounted for non-breeders and chicks. Wilson et al. (2004) estimated the UK NH_3 emission by seabirds at 2.7 kt NH_3 $year^{-1}$.

The approach of Wilson et al. (2004) was applied by Blackall et al. (2007) to estimate a global NH_3 emission of 242 Gg N $year^{-1}$. That emission estimate did not take account of the effects of a changing temperature and used seabird population estimates mainly for the 1960s to 1970s. The factors used by Blackall et al. (2007) to describe the absorption of NH_3 by vegetation had the same uncertainty as the Wilson et al. (2004) UK study. In order to assess global NH_3 emissions, this study needs to account for variations in climate, seabird population change since the 1970s and uncertainties associated with the F_{hab} factor.

This introductory chapter provides a description of both nitrogen and NH_3 and explains how NH_3 fits into the nitrogen cycle, how NH_3 can be transported through the atmosphere and the effect of NH_3 deposition on an ecosystem. The chapter then focuses on the production of NH_3 by seabirds and explains the environmental importance of these relatively small emissions. The previous seabird NH_3 emission estimates are described and the shortcomings of the methods used to derive them are discussed. This chapter finishes by identifying knowledge gaps and outlining the structure of the thesis.

1.2 Nitrogen

1.2.1 Basic chemical properties of nitrogen

The most abundant compound in the Earth's atmosphere is diatomic nitrogen (N_2) (Visek, 1984). Large amounts of energy are required to split N_2 because of the triple bond between the nitrogen atoms. Although N_2 is relatively unreactive, under specialised physical, chemical or biological conditions it can be converted into more reactive forms, termed reactive nitrogen (N_r) compounds.

Nitrogen is found in many forms. In plants and animals, organic nitrogen molecules include amino acids, proteins and nucleic acids. Biological and chemical processes can break organic N molecules down to smaller organic N compounds, inorganic N compounds or back to atmospheric N_2. Inorganic N molecules include: nitrogen oxides (NO_x), ammonia (NH_3), nitrous oxides (N_2O) and nitrates (NO_3^-).

1.2.2 Evolution of nitrogen

Nitrogen is found in all living cells and is a constituent of proteins and enzymes. Described as a primary nutrient, along with potassium and phosphorus, nitrogen is responsible for the growth and survival of plants. It is also a key component of chlorophyll, which plants use to create energy from sunlight. Animals obtain nitrogen by eating plants or plant-eating animals. Metabolic processes within living tissue produce nitrogenous waste. In most mammals it is excreted in the form of urea, $(NH_2)_2CO$, during urination. In birds and reptiles, nitrogenous waste is formed as uric acid, $C_5H_4N_4O_3$. Both urea and uric acid can convert to NH_3 through enzymatic hydrolysis.

Depending on the environmental conditions, such as soil type or vegetation cover, NH_3 formed from urea or uric acid can stay in the soil or will volatilize to form atmospheric NH_3. NH_3 is found in the atmosphere, soil and water (Galloway et al., 1995). In the atmosphere it is normally found in concentrations between 0.1 and 50 parts per billion (ppb) (Sutton et al., 1993).

1.2.3 Nitrogen and Ammonia

The nitrogen cycle is the process by which N_2 and N_r move through the hydrosphere, geosphere, biosphere and atmosphere. Plants obtain nitrogen from the atmosphere, from the decay of plant and animal matter or from fertilizer. NH_3 emission is a bi-directional flux between the bio-sphere and the atmosphere and NH_3 can be absorbed by vegetation as it volatilizes. NH_3 emission occurs if the surface concentration of NH_3 is larger than the concentration of NH_3 in the air (Asman et al., 1998).

Once in the atmosphere the lifetime of NH_3 is relatively short, between 0.5 hours to 5 days, because it readily converts to ammonium (NH_4^+) containing aerosols (Fowler et al., 1997). The transport range of NH_3 is estimated at between 10 and

100 km (Fowler et al., 1998). All NH_3 emissions eventually return to the surface of the Earth as dry or wet deposition, although NH_4^+ containing aerosols may transfer several thousand kilometres. Dry deposition occurs as a direct reaction or absorption to the surface and is most important for uptake of NH_3 gas with a smaller contribution from NH_4^+ containing aerosols. Wet deposition is the removal by clouds and precipitation scavenging returned to the ground as precipitation, and is most important for removal of NH_4^+ containing aerosols with smaller contribution from direct scavenging of NH_3 gas.

Nitrogen compounds ensure plant growth, especially in agricultural contexts; however, the absorption of excessive amounts of nitrogen compounds by plants has been shown to be harmful. It is suggested that NH_3 is one of the most harmful of all nitrogen compounds present in the atmosphere (Krupa, 2003). Excess NH_3 in the plant can imbalance its nutrients and result in:

- direct damage to leaves
- reduced plant growth and productivity
- intolerance to drought and frost
- reduced resistance to disease and insects (Pearson and Stewart, 1993; Krupa, 2003).

For example, it is reported that common heather (*Calluna vulagris*) near an NH_3 source becomes less resistant to drought, frost, disease and insects (Sheppard et al., 2008). Native plants accustomed to a low nitrogen environment, especially lichens and mosses, are the flora most sensitive to NH_3. Trees in forests are less sensitive, whilst agricultural crops are the least sensitive (Krupa, 2003).

1.3 Global distribution of NH_3 emission

The rate and absolute magnitude of emission depends on climatic variables and the size of the source. Global NH_3 emissions have been estimated at 53.7 Tg N per year (Bouwman et al., 1997). The largest emissions of NH_3 are domestic animals emitting 40 % of the global total, synthetic fertilizers emitting 17 % and the sea emitting 15 % (Bouwman et al., 1997). Wild animals are amongst the smaller emissions providing 0.2 % of the global total (Table 1.2).

Table 1.1 Sources of NH_3 (Bouwman et al., 1997)

Process	Estimated global source (Tg N yr^{-1})
Sources	
Burning Fossil Fuels	0.1
Industrial Processes	0.2
Burning Biomass	5.9
Domestic Animals	21.6
Wild Animals	0.1
Crops	3.6
Human Excrement	2.6
Soil Emission	2.4
Fertilizer	9.0
Oceans	8.2
Sum of Sources	**53.7**

The largest emission occurs in China, India and Northern Europe, where emissions are greater than 3 g N m^{-2} yr^{-1} (Figure 1.2). In Europe the largest emissions occur in the Netherlands, Belgium and Denmark. The average NH_3 emission density for the Netherlands is 5 g N m^{-2} yr^{-1}, and is mainly caused by the dense populations of livestock (Asman et al., 1998).

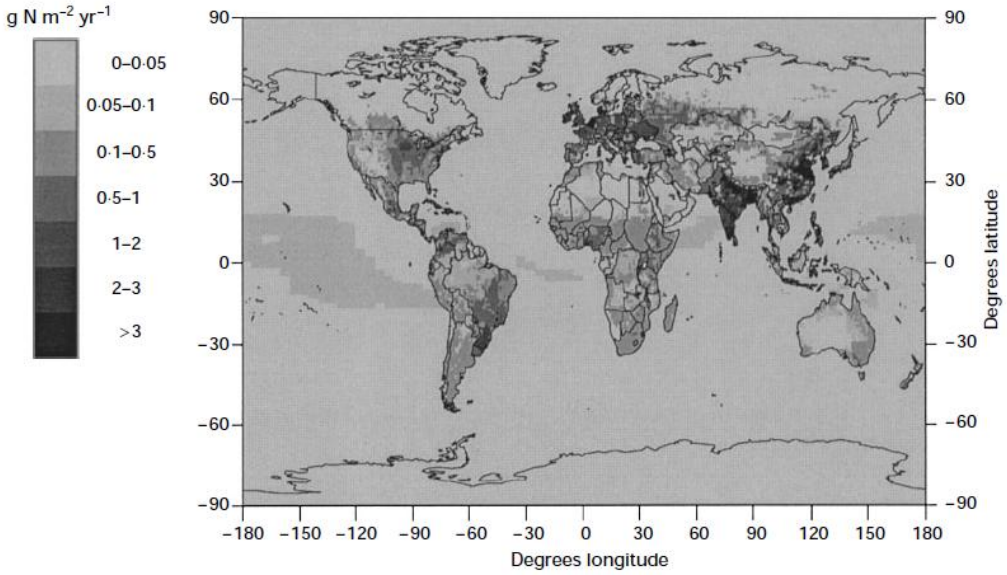

Figure 1.1 Global NH_3 emission on a 1x1 degree grid (g N m^{-2} yr^{-1}; (1 g N m^{-2} yr^{-1}=10 kg N ha^{-2} yr^{-1})) (Bouwman et al. 1997).

Bouwman et al. (1997) estimates that the global NH_3 emission from all wild animals is 0.1 Tg N yr^{-1}. The NH_3 emission estimate was calculated from the land coverage by primary producers. It was assumed that between 3 and 10 % of primary producers are consumed by wild animals, 0.006 g of urea is produced per gram biomass consumed and 10 % of the urea is volatilized as NH_3. Bouwman et al. (1997) makes no direct reference to seabirds, but it is assumed that their 0.1 Tg N yr^{-1} contains the seabirds' contribution to the global NH_3 total.

1.4 NH_3 emissions from seabirds

Until now there are no published data on the spatial distribution of seabirds globally. A map of the foraging distribution of seabird species (Karpouzi et al., 2007) shows that seabirds are densely aggregated around the sub-Antarctic islands of South Georgia, the South Orkneys, Kerguelen Island, Heard Island and Macquarie Island (Figure 1.3). Large numbers of birds also forage around islands in the Pacific Ocean as well as large populations foraging around Svalbard, Greenland and Iceland. This project assumes that only nitrogen excreted on land evolves to form NH_3. Figure 1.2 indicates potential NH_3 emissions from seabirds. By comparing Figures 1.1 and 1.2, there is a strong indication that seabird NH_3 emissions are far removed from other N_r sources, as indicated in Figure 1.1.

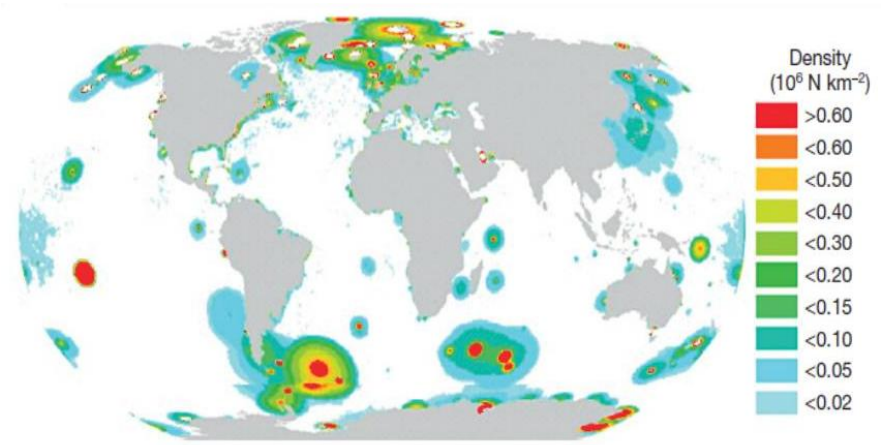

Figure 1.2 Predicted foraging distribution of seabird species during an average year in the 1990s, expressed in number (N) of individuals per km^2 (Karpouzi et al., 2007)

In the UK it is suggested that 366 kt NH_3 is emitted each year (Misselbrook et al., 2000; Sutton et al., 2000), where 72 % of the NH_3 emission comes from domestic animals. An estimated 0.37 Gg NH_3 $year^{-1}$ was emitted from UK seabird colonies

(Sutton et al., 1995b, later refined to 4.2 (1.5 - 8.5) Gg NH_3 $year^{-1}$ (Sutton et al., 2000). The Sutton et al. (2000) UK NH_3 emission estimate from seabirds was based on measurements made at a seabird colony in the UK and the method is critically evaluated in Section 1.4. Despite shortcomings in the calculation method, Sutton et al. (2000) recognised that seabird emission may have importance to local nitrogen cycling due to their isolation from other sources of NH_3.

Wilson et al. (2004) refined the UK NH_3 emission from seabirds to 2.4 Gg NH_3 yr^{-1} by using a species-specific N excretion model and a more detailed seabird population dataset than Sutton et al. (2000). The method of Wilson et al. (2004) is also described and evaluated in Section 1.5. Wilson et al. (2004) found that NH_3 emissions by seabirds total less than 1 % of the UK NH_3 emissions. However, the distribution of seabird colonies indicates the largest emissions are in remote locations with otherwise low NH_3 emissions and may be very important to local N cycling (e.g. colonies in Shetland, Orkney and the Western Isles).

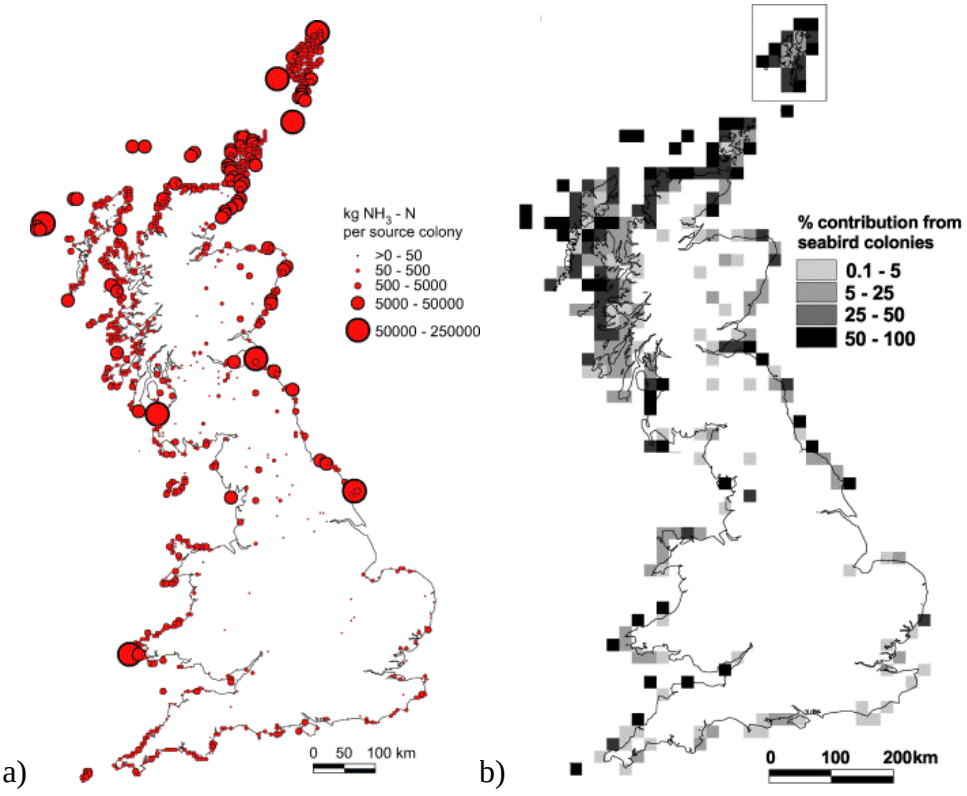

Figure 1.3 a) Locations and relative magnitude of NH_3 emissions from seabird colonies in the UK, from Wilson et al. (2004). b) The local seabird contribution calculated as percentage of the contribution of seabird emissions compared to NH_3 emissions from agriculture and from seabirds summed for each 1 km of coastline or point source (Wilson et al. (2004).

When compared with NH_3 emissions from agriculture, the seabird emission is insignificant in many areas of the country. However, Figure 1.3 shows where seabird colonies create NH_3 hotspots which dominate the local NH_3 emission and should have a substantial impact on the local plant communities (Wilson et al., 2004). In the areas of high seabird density, it is predicted that effects will be similar to emissions near intensive livestock farms. However given that seabird colonies are more remote, the relative influence of seabird NH_3 will be greater (Wilson et al., 2004).

1.4.1 Seabird behavior relevant to NH_3 emission

Seabirds are defined as bird species that obtain their food from the ocean and spend most of their time above or on salt water. Seabirds are classed into four families (Schreiber and Burger, 2001):

- Penguins (Sphenisciformes)
- Albatross, shearwaters, petrels (Procellariiformes)
- Pelicans, boobies, frigatebirds, tropicbirds, cormorants (Pelecaniformes)
- Gulls, terns, guillemots, auks (Charadriiformes - Families: Laridae and Alcidae).

Seabirds are distributed throughout the world but there are distinct differences between the species that inhabit the northern hemisphere and the southern hemisphere. Auk species are found in northern latitudes whilst penguins are limited to the southern hemisphere (Steele, 2010).

The life cycle of seabirds varies between species. Some spend most of the year at the breeding site, such as the Little penguin *Eudyptula minor* which spends up to 320 days a year on land (Gales and Green, 1990; Priddel et al., 2008). Other species only come to land during the breeding season, such as the Snow petrels *Pagodroma nivea* and Cape petrels *Daption capense* which only spend 90 days at the breeding site (Hodum, 2002). The Arctic tern *Sterna paradisaea* journeys from nest sites in the high Arctic to the nutrient rich southern ocean, a round trip distance of 80,000 km (Egevang et al., 2010). Other species, such as the gray-headed albatrosses *Thalassarche chrystostoma*, have been observed to circumnavigate the globe (Croxall et al., 2005).

Around 95 % of seabirds are colonial and annually return to the same nesting site (Schreiber and Burger, 2001). Nesting sites are in remote areas away from predators, usually islands and secluded cliffs. Clutch size depends on species and availability of food (Steele, 2010), as does breeding success. Most species of seabird breed once a year and breeding success varies between 2.4 chicks that fledge per pair for the Guanay Cormorant *Phalacrocorax bougainvillii* (Birdlife International, 2009; Jahncke et al., 2004; Yorio et al., 1999) to 0.1 chicks per pair for the endangered Kermadec Petrel *Pterodroma neglecta* (Birdlife International, 2009; Nunn and Stanley, 2000; Veitch and Harper, 1998). In general, the seabird breeding season has five stages (listed below) and ranges from 60 days to one year, depending on the species (Croxall, 1987):

1. Pre-breeding courtship and nest building activities
2. Egg laying
3. Incubation
4. Chick-rearing
5. Post-fledging.

1.4.2 Nitrogen pathways through seabirds

In general, all of a seabird's food comes from the ocean. The diet is protein-rich with varying nitrogen content depending on the composition of the diet (Phillips et al., 1999; Wilson et al., 2004). Antarctic krill (*Euphausia superb*) are crustaceans eaten by many seabird species in the Southern Ocean, including most penguin species (Karpouzi et al., 2007), and make up almost 40% of the global seabird diet (Figure 1.4). Krill have relatively low nitrogen content (F_{Nc} = 0.023 g N g^{-1} dry mass, Croxall et al. 1984), whereas fish species such as Capelin (*Mallotus villosus*) have higher nitrogen content (F_{Nc} = 0.046 g N g^{-1} dry mass, Bogstad, 1997).

Nitrogen, from the breakdown of amino acids and protein, is excreted in the form of uric acid ($C_5H_4O_3N_4$) (Wright, 1995). Analysis of fresh penguin guano from Marion Island showed that the water content of guano is 80% of the wet mass, and 20 % of the dry mass of guano is nitrogen in the form of uric acid-nitrogen (Lindeboom, 1984).

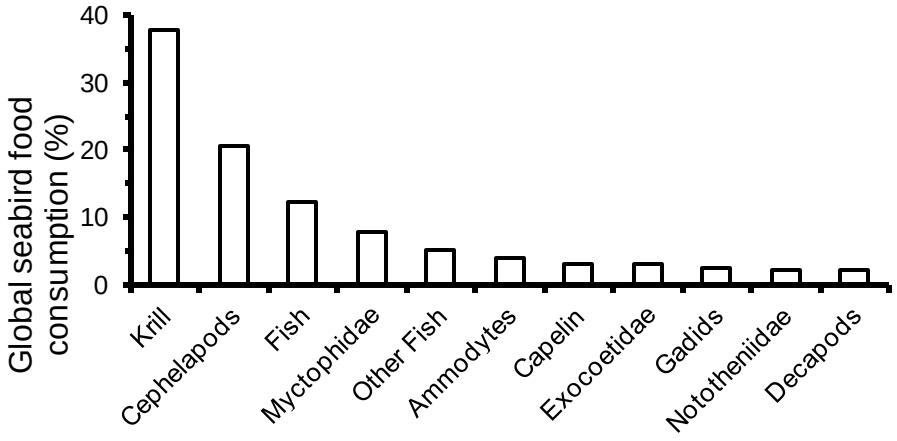

Figure 1.4 Total global food consumption by seabirds (modelled from Karpouzi et al., 2007)

Using the method of Wilson et al. (2004) the amount of nitrogen excreted can be calculated from the adult mass (M, g bird^{-1}), nitrogen content of the food (F_{Nc}, g N g^{-1} wet mass), energy content of the food (F_{Ec}, kJ g^{-1} wet mass) and assimilation efficiency of ingested food (A_{eff} , kJ [energy obtained] kJ^{-1} [energy in food]) (Equation 1.1).

$$N_{excr} = \frac{9.2.M^{0.774}}{F_{Ec}A_{eff}}.F_{Nc} \qquad (1.1)$$

Average values for nitrogen content (F_{Nc} = 0.036 g N g^{-1}) and energy content (F_{Ec}, = 6.5 kJ g^{-1}) (Energy: Nitrogen (E:N) ratio = 180 kJ g^{-1} N) for seabird diet have been use in many studies (Furness, 1991; Wilson et al., 2004; Blackall et al., 2007). Despite the potential wide range of seabird diets (Figure 1.5), the variation in E:N ratio is quite small. For Krill, F_{Ec} = 4.35 kJ g^{-1} (E:N ratio = 189 kJ g^{-1} N) (Croxall and Davis 1990), whereas for Capelin, F_{Ec} = 6.9 kJ g^{-1} (Bogstad, 1997) (E:N ratio = 150 kJ g^{-1} N), demonstrating that irrespective of the composition of the seabird's diet, the E:N ratio varies only by 16%.

The assimilation efficiency of the food is the efficiency in conserving the energy in food when eating it (kJ obtained by the bird per kJ consumed). An average value of A_{Eff} = 0.8 has been used extensively (Furness, 1991; Wilson et al., 2004; Blackall et al., 2007). This value has been estimated to vary a maximum of 21 %, between 0.633 and 0.828 for penguin species (Green et al., 2007).

Excreted uric acid decomposes to form NH_3 through the overall biochemical degradation (Equation 1.2).

$$C_5H_4O_3N_4 + 1.5O_2 + 4H_2O \rightarrow 5CO_2 + 4NH_3 \qquad (1.2)$$

This process requires microbial action working aerobically to decompose the uric acid to form NH_3; water and oxygen are required for the reaction to take place (Koerkamp et al., 1998). The formation of atmospheric NH_3 happens in four steps: 1) bacterial ammonification, 2) gaseous NH3 production, 3) the mass transfer of NH_3 from the ground to the atmosphere and 4) mixing of NH3 in the atmosphere (Elliott and Collins, 1982). Figure 1.5 indicates the changes that happen at each step and the variables that affect the rate of change. The temperature is important in the conversion of uric acid to total ammoniacal nitrogen (TAN), the conversion of TAN to NH_3 in the soil and the transfer of NH_3 in the soil to the atmosphere.

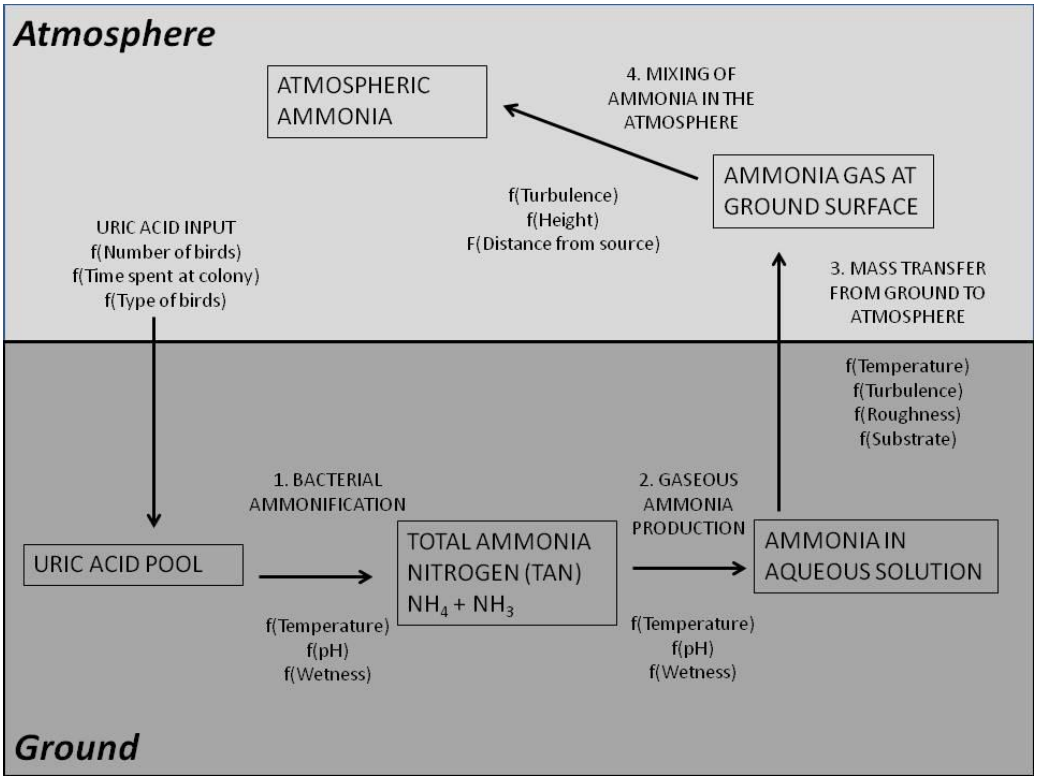

Figure 1.5 Processes governing the emission of NH_3 from uric acid (adapted from Elliott and Collins, 1982)

1.4.3 Effects of seabird NH_3

A study by Lindeboom (1984) estimated that 79 % of excreted nitrogen volatilized to form NH_3 at a Macaroni Penguin colony in Kildalkey Bay, Marion Island. The NH_3 was either blown out to sea (184 kg NH_3 day^{-1}) or deposited on the island (30 kg NH_3 day^{-1}) (Figure 1.6). The subsequent N deposition on the island created an

NH_3 shadow in the nearby vegetation, where the plants were observed to be larger and grow more vigorously than in other parts of the island.

As well as atmospheric NH_3, nitrogen dissolved in runoff has been observed to increase the rate of primary production of plant life at inter-tidal ecosystems (Bosman and Hockey, 1988). Measurements taken from the Maine coastline have shown that NH_3 concentrations in rock pools near gull nesting sites change by several orders of magnitude (Loder et al., 1996). This has been attributed to gull guano being washed into the pools by rainwater. This increase in nutrients has contributed to an increased growth rate in the algae near seabird colonies (Bosman and Hockey, 1988).

Soil acidification has also been observed at seabird colonies. A large gull colony has been observed to induce changes in the soil pH in the Chafarinas Islands (Garcia et al., 2002). Seabird guano was found to mineralize as it entered the soil, and subsequent nitrification of these compounds has led to a significant increase in the acidity of the soil.

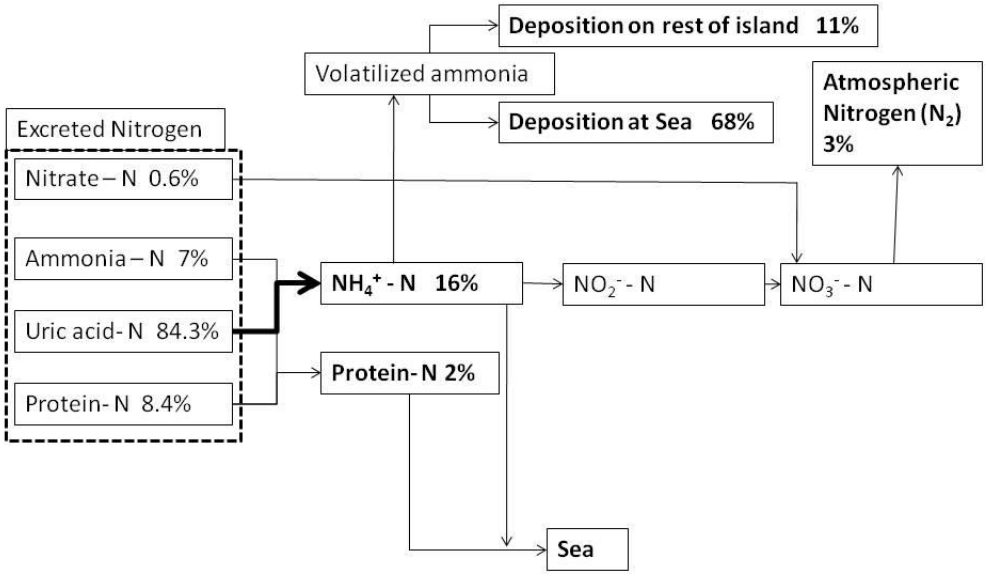

Figure 1.6 Nitrogen pathways in a Macaroni Penguin colony at Kildalkey Bay, Marion Island (Lindeboom, 1984). The box on the left of the diagram shows the composition of the excreted nitrogen. The boxes with the bold text give the fate of this excreted N summed to 100 % .

1.5 NH_3 emission estimates from seabirds

In 1995 a UK NH_3 emission estimate was constructed using literature; this estimate included the contribution from seabirds. The number of seabirds in the UK was estimated at 220,000 breeding pairs of larger seabird (gannet, shag, cormorant) and 2,400,000 breeding pairs of smaller birds (gulls, fulmar, kittiwake, razorbill, guillemot, puffins). An assumption was made that larger birds emit 0.3 kg N $year^{-1}$ $bird^{-1}$ and smaller birds emit 0.1 kg N $year^{-1}$ $bird^{-1}$ giving a UK estimate of 0.37 Gg N $year^{-1}$ from seabirds. The total UK NH_3 emission estimate based on literature values was 450 Gg N $year^{-1}$ in 1995 (Sutton et al., 1995b).

In 2000 the UK NH_3 emission estimate from seabirds was revised following a field study on the Bass Rock in 1998. The Bass Rock is an island in the Firth of Forth, Scotland with 50,000 pairs of Northern Gannet (*Morus bassanus*) nesting on it. The field study used a passive sampling campaign to measure the mean NH_3 concentration on the Bass Rock during the breeding season at 806 µg m^{-3}. The range in emission estimate reported accounted for uncertainty caused by changes in the percentage emission from excreted nitrogen. This was measured to change through the year, and the uncertainty varied from 40 % to 90 %, with a best estimate of 70 %. The NH_3 emission from the colony was then estimated using an atmospheric model. The bird emission estimates were revised to 2.2 (0.95-3.60) kg NH_3-N $year^{-1}$ $bird^{-1}$ for larger seabirds and 0.24(0.07-0.55) kg NH_3-N $year^{-1}$ $bird^{-1}$ for smaller seabirds (Sutton et al., 2000). Large seabirds were defined as gannets, shags and cormorants with a population of 648,000 birds. Other seabirds were defined as gulls, fulmars, kittiwakes, razorbills, guillemots, puffins, terns and skuas with a population of 8,449,000 birds. Overall this led to a UK estimate of NH_3 emission from seabirds of 3.4 (1.24-7.01) Gg NH_3-N $year^{-1}$ (Sutton et al., 2000). There are indications that the uncertainty in emission may be attributable to climate, as the smaller emissions were measured at the end of the breeding season. However, shortcomings of this study were highlighted by Wilson et al. (2004). Sutton et al. (2000) did not account for non-breeders and chicks or for the differences in nesting habitat. It was suggested that guano production may be different depending on the age of the bird and that NH_3 emission may vary depending on the substrate on which guano was deposited.

Wilson et al. (2004) calculated the NH_3 volatilized from seabirds in the UK using a bioenergetics model. The study calculated the nitrogen excreted from a seabird using species specific values of their field metabolic rate (FMR) and the efficiency with which nitrogen can be processed within their body. The emission of NH_3 from the excreted nitrogen was estimated as a function of the birds' nesting behaviour. Values used in this study were 1 for bare rock breeders, 0.2 for nest and vegetation breeders and 0 for burrow breeders. Values were initially based on fieldwork and then tuned to fit the model (Wilson et al., 2004). These coefficients for nest, vegetation and burrow nesters were identified as sources of potential error, but after conducting a sensitivity analysis it was found that changing the nest and vegetation coefficient had little effect on the UK total, as rock breeders contributed the most emission. The habitat correction factor for burrow breeders were based on experimental work conducted by Blackall et al. (unpublished), because NH_3 emissions were undetectable from puffin burrows.

The emission values of Wilson et al. (2004) were corrected for the attendance of non-breeding birds and chicks (Wilson et al., 2004). It was assumed that non-breeders make up 33 % of the colony and spend 50 % less time at the colony than a breeding adult. The attendance of chicks was based on the length of time from hatching to fledging. It was also assumed that only chicks that fledged contributed to NH_3 emission. The total UK NH_3 emission from seabirds using this method was 2.7 [1.78 - 4.48] Gg N $year^{-1}$ (Wilson et al., 2004). The NH_3 emission calculated by this study for the northern gannet was estimated at 2.3 kg N $year^{-1}$ $gannet^{-1}$, the difference between this value and a study by Böttcher (1990) was attributed to a lower value for the fraction of excreted nitrogen (F_{Nv}): The values for F_{Nv} were 0.8 and 0.3 for the Böttcher and Wilson studies respectively and both were calculated from field estimates (Blackall et al., 2004; Böttcher, 1996). The value of F_{Nv} combines all of the effects of climate into one constant. This is a large potential source of uncertainty, but was considered acceptable to use by the authors given the similarities in climate throughout the UK.

The Wilson et al. (2004) bioenergetics model was further applied in a 2007 study to estimate the NH_3 emission from seabirds globally (Blackall et al., 2007). This study estimated the NH_3 emission at 242 Gg N $year^{-1}$ with the highest emissions coming

from the Antarctic region (Table 1.3). Bird population data were collated using a variety of sources. The findings showed that 80 % of the global total was contributed to by only 10 species with penguin species being most responsible for NH_3 emission (48 %) because of their relatively large size and nesting behavior (Blackall et al., 2007).

Table 1.2 Global NH_3 emissions from seabirds as estimated by Blackall et al. (2007).

Region	NH_3 Emission (Gg NH_3 $year^{-1}$)	Contribution to global seabird NH_3 emissions (%)	Dominant Group
Antarctic	129.6	53.6	Penguin
S. America	30.7	12.7	Cormorant
N. America	21.8	9.0	Auk
Europe	18.4	7.6	Auk
Russia	15.6	6.5	Auk
Africa	9.0	3.7	Penguin
Pacific	8.8	3.6	Tern
Greenland	5.4	2.2	Auk
Other Regions	2.3	1.0	Tern

1.6 Global Climate Change

Evidence is growing that strongly suggests the temperature in the lowest 8 km of atmosphere has increased, snow and ice cover over the earth has decreased, the average sea level has risen and the heat content of the oceans has increased (IPCC, 2007). Anthropogenic emissions of greenhouse gases and aerosols have altered the composition of the atmosphere. Emissions of greenhouse gases, such as carbon dioxide (CO_2) and nitrous oxide (N_2O), prevent radiation reflected from the Earth's surface from leaving the atmosphere. Some aerosols increase the Earth's albedo and reduce radiation entering the atmosphere. Changes to natural phenomena, solar radiation and volcanic activity can also act to increase the atmospheric temperature. Evidence shows that these factors have worked together to cause the following trends in climate:

- Precipitation has increased in Northern latitudes (30 °N to 90 °N) and the Tropics (10 °N to 10 °S).

- Precipitation has decreased in the Northern sub-tropics (30 °N to 10 °N).
- No systematic change to precipitation has been observed in the Southern Hemisphere.
- Cloud cover has increased in mid to high latitudes
- A reduction in the frequency of extreme low temperatures
- An increase in the frequency of extreme high temperatures
- An increased frequency in the number of warm episodes of the El Niño-Southern Oscillation (ENSO).
- A small increase in areas experiencing extreme drought or extreme wetness.
- An increase in the frequency of droughts in Africa and Asia.

Given the temperature dependence of NH_3 emission from seabird excreted nitrogen, a changing global climate could impact the magnitude of NH_3 emissions potentially altering delicately balanced ecosystems at seabird colonies. Projections of future climate change scenarios have been calculated using different General Circulation Models (GCM), providing the opportunity to forecast changes in NH_3 emissions from seabird colonies. The outputs of GCMs have calculated average climate anomalies for a range of variables. The four basic climate change scenarios used to calculate climate anomalies are (IPCC, 2007):

- A1 a more integrated world, global surface warming 2.8 °C
- A2 a divided world, global surface warming 3.4 °C
- B1 a world more integrated and more ecologically friendly world, global surface warming 1.8 °C
- B2 a world more divided, but more ecologically friendly, global surface warming 2.4 °C

1.7 Knowledge Gaps

The shortcomings of the Blackall et al. (2007) study are similar to the Wilson et al. (2004) study, in that values used to describe nesting behaviour were based on measurement and subsequent tuning of the Wilson et al. (2004) model. The model also used a temperature-independent calculation to express NH_3 emissions. Studies have shown that temperature is an important driver in the production of NH_3 from uric acid (Elliot & Collins, 1982). However, it has been suggested that the effects of

temperature may be offset by other factors such as water availability, where in hot climates the reduction in available water will slow the NH_3 production (Blackall et al., 2007). Not accounting for temperature results in a major uncertainty in the Blackall et al. (2007) NH_3 emission estimate from seabirds. The second shortcoming of this study is the quality of seabird population data, as the sources used were published in the 1960s and 1970s.

1.7.1 Seabird population estimates

Until now, there has not been a published database listing the size and location of all seabird colonies globally. The remote location and fluctuating numbers of seabirds make it difficult to accurately assess global seabird populations. Recent increases in the documented bird population estimate are a result of improved counting techniques where seabirds can now be counted in the most remote regions. For example, using remote sensing to count Little auks (*Alle alle*) on Northumbria Island, Greenland (Egevang et al., 2003) or using computer based analysis to count Macaroni penguins in colour aerial photographs on bird Island, South Georgia (Trathan, 2004).

Even though the reported number of birds is increasing, the actual numbers of seabirds are subject to change either inter-annually or over longer time frames. Short term changes can be caused by climatic phenomena such as the El Niño-Southern Oscillation, which has a marked effect on seabird populations throughout the world and can cause the collapse of breeding seasons (Jahncke et al., 2004). The El Niño event in 1965 greatly reduced the seabird populations of the northern and central coast of Peru (Duffy, 1994). Long-term changes, such as climate change, affect species which suffer a loss in fitness and decrease in number. For example, Emperor penguins *Aptenodytes forsteri* are known for surviving in the harsh Antarctic climate, but in recent years their populations have been observed to be decreasing (Croxall et al., 2002).

Changes in the seabird colony size are often due to a combination of factors. These can be broadly categorised as: climate change, fisheries interactions, mammal predation, human disturbance and contamination. These factors often act together to affect the seabirds' living conditions, resulting in lower fitness of the entire population. The global seabird population has undergone significant changes since

the 1960s and 1970s and the most accurate and current estimate of the size and location of the global seabird population is required to produce a robust NH_3 emission estimate.

1.7.2 Nesting Effect on NH_3 emission

The amount of NH_3 volatilized depends on the covering of vegetation above the soil (Wilson et al., 2004; Blackall et al., 2007). The flow of NH_3 from the ground to the atmosphere is a bi-directional flow, where gaseous NH_3 can be absorbed by either the substrate or the overlying vegetation.

Birds create nests to provide a place to lay eggs, incubate them and raise the young until they are old enough to fledge. The shape and design of a nest is dependent on the living environment, where the eggs may need protection from predators and weather. Hansell (2000) listed eight possible nest types, described as a) cup, b) dome, c) dome and tube, d) plate, e) bed, f) scrape, g) mound and h) burrow (Figure 1.7).

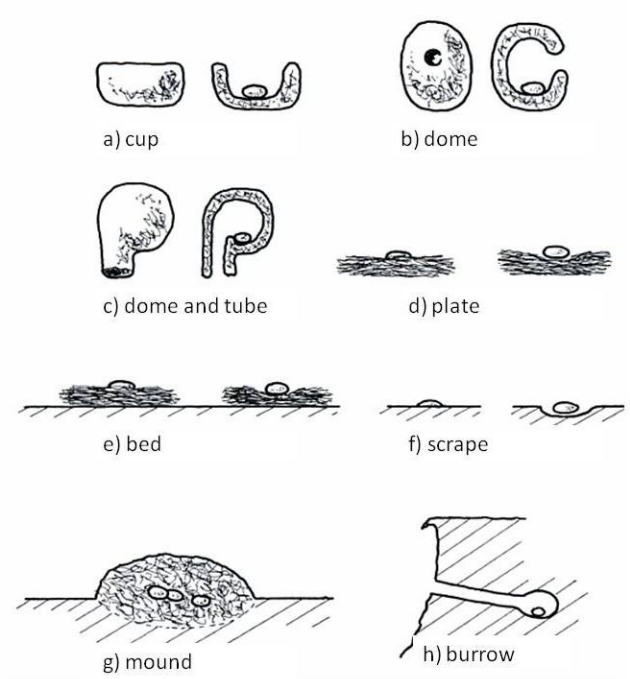

Figure 1.7 The eight types of nest that birds make a) cup, b) dome, c) dome and tube, d) plate, e) bed, f) scrape, g) mound and h) burrow. Figure taken from Hansell (2000).

Seabirds lay their eggs in burrows or on plates, beds and scrapes that can be found on sand, gravel, mud, vegetation and flat ground or ledges on solid rock. Burrows

are made from mud or in small rock crevices. Plates and beds can also be found in trees and other vegetation.

1.7.3 Effects of Climate

Temperature plays a role in the evolution of NH_3 gas from nitrogen in seabird excreta. However, Figure 1.5 shows that other factors are also important when estimating NH_3 emission from a surface. The presence of water is important in two steps: bacterial ammonification of uric acid to form TAN and the formation of aqueous NH_3 from TAN (Elliott and Collins, 1982). Water can either be taken from precipitation events or from the water in the air. Increases in wind speed can increase the rate of emission from the surface as aqueous NH_3 forms NH_3 at the surface then mixes in the atmosphere (Sutton et al., 1992; Sutton et al., 1993; Nemitz et al., 2001). Climate variables are used as input to the process based 'Generation of emissions from Uric Acid Nitrogen Outputs (GUANO)' model created by Blackall (2004) to calculate the rate evolution of NH_3 from nitrogen excreted by seabirds. The GUANO model calculates NH_3 emissions from a single seabird colony using climatic variables (temperature, relative humidity, precipitation and wind speed) and colony specific data (pH, substrate type, N excretion rate). The GUANO model was tested against NH_3 emissions measured from the seabird colony on the Isle of May, UK. This model is described in more detail in Chapter 6.

1.8 Aims

The ultimate aim of this thesis is to create a global seabird NH_3 emission estimate and map. The global NH_3 emission estimate from seabirds will be improved by establishing an updated seabird population database. The database will include colony-specific population counts, spatial data and an estimate of the uncertainty in the population count. This will be the first time that a global seabird population data has been collated. The population data will be used together with the climate-dependent NH_3 emission model to produce a new global NH_3 emission estimate.

This study will use the seabird population dataset with a model based on Henry's Law to estimate the NH_3 emissions from seabird colonies globally. The NH_3 emissions derived from these models will be tested against measurements made in

key climate zones. NH_3 emissions will be measured using techniques in both NH_3 concentration measurements and atmospheric dispersion modelling.

The third section of the project is to use controlled experiments to investigate how overlying vegetation affects NH_3 emission. The last objective of the project is to make projections into how the NH_3 emissions may change over time. Different climate change scenarios will be used to estimate the potential effect of a global changing climate.

1.8.1 Objectives

The objectives necessary to the achievement of the above aims were as follows:

- To prepare a gridded inventory (0.5° x 0.5°) of global seabird emissions
- Exploit new NH_3 measuring techniques and use inverse modeling to quantify NH_3 emissions from Scottish NH_3 sources
- To apply the measurement approach developed above to quantify measured NH_3 emissions under sub-Antarctic and Tropical conditions
- To characterize the temperature dependence of NH_3 emissions from guano, considering different nesting habits and utilizing controlled environment measurements
- To simulate the climatic dependence of seabird NH_3 emissions and incorporate this in the gridded model of global seabird NH_3 emissions, allowing projections to be made to show the effect of future climate change scenarios.

1.8.2 Thesis Overview

Chapter 2 is a review of measurement and modelling techniques used to estimate NH_3 emissions in complex coastal environments. It then reviews previous methods and studies that measure and model the NH_3 concentrations in seabird colonies. This review includes:

- The measurement of NH_3 in the atmosphere – from simple techniques to complex instrumentation
- The modeling of NH_3 - a review of approaches for estimating source strength from measured concentrations.

The chapter ends by making conclusions on which approaches are most suited to measuring and modelling NH_3 emissions at seabird colonies.

Chapter 3 describes the construction of a global seabird population database and maps the seabird distribution, globally and regionally. It then adapts the Wilson et al. (2004) bioenergetics model and produces a preliminary estimate for the thermodynamically adjusted global seabird NH_3 emission using a relationship derived from Henry's Law.

Chapter 4 investigates the measurement of NH_3 emissions from seabird guano in a controlled environment, and in particular, it aims to estimate the 'nesting effect' used in Chapter 3.

Chapter 5 estimates NH_3 emissions from measurements at a range of seabird colonies carried out as part of this research program. The measurement of NH_3 emissions from seabird colonies at different climate regions is compared to modelled emissions in Chapter 3 and is used to validate the modelling approach.

Chapter 6 Blackall's GUANO model is adapted to represent processes under different climates. The refined model is reviewed and a sensitivity analysis is conducted. The emissions modelled are compared to those measured at each of the field sites.

Chapter 7 uses the new climate-dependent model and newly derived values for the nesting effect to map global seabird NH_3 emission.

Chapter 8 is the general discussion. It provides a synthesis of the thesis, sets the results in a broader context and outlines priorities for future research.

Chapter 2 Methodologies

2.1 Introduction

This chapter describes the theoretical basis for the dispersion of a pollutant from a source to the atmosphere, and micrometeorological theory of calculating emissions is reviewed, focussing on pollutant exchange at surfaces. Practical approaches are describes for estimating emission fluxes from measurements of NH_3 concentrations, micrometeorology and meteorology at seabird colonies in key climatic regions (with the ultimate aim to quantify emission fluxes in a global model; see Chapters 5-7). A review of methods to measure atmospheric NH_3 is conducted, with detailed descriptions of instruments chosen to measure NH_3 during experiments undertaken for this thesis. A range of approaches for estimating source strength from measured concentrations are also reviewed. The chapter concludes by describing the approaches most suited to measuring and modelling NH_3 emissions at seabird colonies.

2.2 Air movement within the planetary boundary layer

2.2.1 The atmosphere and its properties

The part of the atmosphere that interacts with the ground is called the planetary boundary layer (PBL). Due to turbulence effects created by the Earth's surface, the air within the PBL air can move vertically and hence mix upwards. Turbulence is the vertical mixing of air caused when airflow encounters an aerodynamic obstruction or changes buoyancy. The height of the PBL varies as a function of surface and meteorological conditions. The layer above the PBL is the free troposphere. The understanding of air movement within the inertial layer of the PBL can be used to infer air/surface exchange fluxes and be used to model how gases move from the surface through the PBL. The behaviour of air movement in the near-surface atmosphere, usually less than 1 km from the surface, is referred to as micrometeorology.

The PBL can be conceptualised as consisting of two main layers: the outer Ekman layer and the Inner Surface layer (with several sub-layers, see Figure 2.1). In the Ekman layer air movements are caused by air pressure changes and the Coriolis force; the shape of the surface and heating effects from the surface have little

influence on the flow of air. By contrast, air movements within the Inner Surface layer are affected by the surface and have little dependence on the Coriolis force (Stull 1988; Garratt, 1992).

The very bottom of the inner surface layer is termed the quasi-laminar (viscous) layer. Due to its immediate proximity to the surface, air does not move in this layer because of frictional forces between air molecules and the ground. The change in momentum between the surface and the atmosphere, called shear stress (τ, N m^{-2}), is zero.

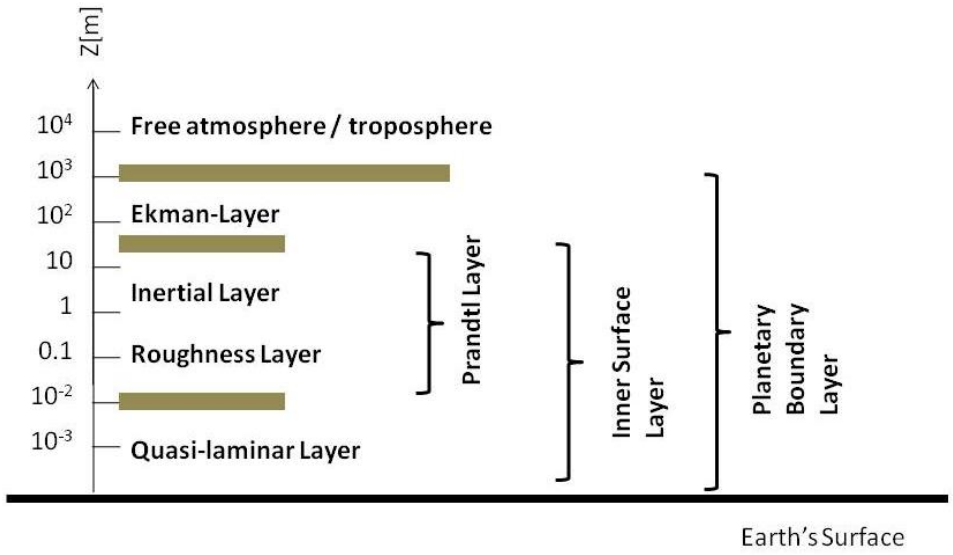

Figure 2.1 Structure of the planetary boundary layer (after Stull, 1988; Garret, 1992, modified). The brown boxes indicate the boundaries between the layers.

The Prandtl layer extends from 10^{-2} m to ~10 m above the surface within the inner surface layer, and within this layer air can move both horizontally and vertically. In the Prandtl layer, τ is non-zero, constant with height and predominately influenced by surface friction. The Prandtl layer can again be separated into two distinct layers: the roughness layer and the inertial layer. The roughness layer is between the quasi-laminar layer and inertial layer, and within the roughness layer, heat and mass are exchanged through molecular diffusion between the surface and the air (Garratt, 1992; Seinfeld and Pandis, 2006). The influence of the surface is most noticeable in the roughness layer, and turbulence is strongly affected by the structure of aerodynamic obstructions.

2.2.2 Atmospheric stability

Atmospheric stability is determined by the direction of the force of buoyancy acting on a gas as it is moved from an equilibrium position. If a gas is displaced vertically and continues to rise, the atmosphere is unstable; if the gas returns to its original position, the atmosphere is described as being stable; and the atmosphere is neutral if the gas remains at a constant height.

The hydrostatic equation states that the vertical speed of a parcel of air will remain constant or at rest unless it is acted upon by and unbalanced force, and can be used to calculate the lapse rate. The adiabatic lapse rate, (Γ, Kkm^{-1}) (Equation 2.1), is a planetary constant and calculated from the change in temperature (T, K) per unit height (z, m). The value of Γ is calculated from the acceleration due to gravity (g, ms^{-2}) and the specific heat of air at constant pressure (c_p, $J\ kg^{-1}\ K^{-1}$) (Equation 2.1).

$$\Gamma = -\frac{dT}{dz} = \frac{g}{c_p} = 9.7Kkm^{-1} \qquad (2.1)$$

Atmospheric stability is defined by the relationship of the adiabatic lapse rate to the atmospheric lapse rate (Γ_A, Kkm^{-1}), where the atmospheric lapse rate is defined as change in temperature of the atmosphere (T_{Atm}, K) with altitude (Equations 2.2 to 2.4).

Unstable atmospheric conditions, where the atmospheric lapse rate is greater than the adiabatic lapse rate (Equation 2.2), are caused by parcels of air being warmer than the surrounding air. The parcel of air moves upwards and is replaced by cooler air, which is then heated and begins to rise. Unstable conditions cause a large amount of vertical mixing and occur on days with large amounts of solar heating and little wind. Stable atmospheric conditions, where the atmospheric lapse rate is less than the adiabatic lapse rate (Equation 2.3), are caused by parcels of air being cooler than the surrounding air. Once the cooler and denser air parcel has been lifted to a height, it returns to its original position because of buoyant forces pushing it downwards. Stable conditions occur when there is no solar heating of the ground and when there is little wind. Stable atmospheric conditions, where the atmospheric lapse rate is less than the adiabatic lapse rate (Equation 2.3), occur when forces of buoyancy do not act upon the air parcel. In neutral conditions the air parcel does not change vertical height and occurs when there is little solar heating and strong winds.

$$-\frac{dT_{Atm}}{dz} > \Gamma \rightarrow Unstable \quad (2.2)$$

$$-\frac{dT_{Atm}}{dz} < \Gamma \rightarrow Stable \quad (2.3)$$

$$\frac{dT_{Atm}}{dz} = \Gamma \rightarrow Neutral \quad (2.4)$$

The Monin-Obukhov length, L, (Equation 2.5) describes the height above the surface at which buoyancy forces dominate the turbulent forces, and is calculated from the density of air (ρ, kg m^{-3}), the specific heat capacity of air at constant pressure ($\widehat{c_p}$, J kg^{-1} K^{-1}), the air temperature at z = 0 (T_0, K), the von Karman constant (k, 0.4), the acceleration due to gravity (g, ms^{-2}) and the sensible heat flux which measures the heat transfer by convection (H, J m^{-2} s^{-1}) (Seinfeld and Pandis, 2006).

$$L = -\frac{\rho \widehat{c_p} T_0 u_*^3}{kgH} \quad (2.5)$$

Table 2.1 gives the stability conditions for given values of L.

Table 2.1 Range of Monin-Obukhov values for stability conditions

Values of L	Stability Conditions
$L < -10^5$m or $L > 10^5$m	Neutral
-10^5m $< L <$ -100m	Unstable
-100m $< L <$ 0	Very Unstable
0 $< L <$ 100m	Very Stable
100m $< L < 10^5$m	Stable

2.2.3 Wind Speed in neutral conditions

Many factors determine how air moves around the surface of the Earth. Horizontal movement of air is caused by pressure gradients, the Earth's rotation and gravity. Vertical movement of air is caused by buoyancy due to pressure gradients, resistances caused by the shape and heating effects of the surface. In neutral conditions only mechanical turbulence causes movement of air. These conditions occur when strong winds cause air to move while the temperature of air throughout

the PBL is constant. Stable conditions occur when the air at the bottom of the PBL is cooler than air at the top, causing little turbulence. Unstable conditions occur when the air at the bottom of the PBL is warmer than the air at the top, resulting in large amounts of convective turbulence.

Under neutral conditions, without frictional forces, air would move parallel to the Earth's surface. The frictional forces which change the direction of air movement are largest at the surface and diminish with altitude, while wind speed increases with altitude. The shear stress in the Prandtl layer, between 10 and 100 m above the surface, is non-zero and constant because of vertical movement of air caused by frictional forces at the surface. The friction velocity, u_*, can be calculated from τ and ρ, the density of air (Equation 2.6), and is a measure of the vertical transport of momentum change and associated with wind speed. u_* is small in light wind because there is little downward transport of momentum from higher in the atmosphere, where the wind is stronger. The friction velocity is large in windy conditions near the surface as horizontal momentum is being carried downward from the upper atmosphere.

$$u_* = \sqrt{\frac{\tau}{\rho}} \tag{2.6}$$

Equation 2.7 describes the wind velocity (u, ms^{-1}) at different altitudes (z, m) in neutral conditions, calculated from the von Karman constant (k = 0.4), the zero-plane displacement (d, m) and the roughness length (z_0, m). The wind velocity increases with height as the effects of mechanical turbulence caused by the surface decrease to zero. The zero-plane displacement is the height above the ground where the momentum of the air due to mechanical turbulence is zero. The roughness length describes the aerodynamic properties of the surface and is derived from wind profile data or using published values from similar surfaces (Stull, 1988; Garratt, 1992; Seinfeld and Pandis, 1996).

$$u(z-d) = \frac{u_*}{k} ln\left(\frac{(z-d)}{z_0}\right) \tag{2.7}$$

2.2.4 Wind Speed in non-neutral conditions

The Monin-Obukhov length (L, m) is used to correct the logarithmic wind profile for non-neutral conditions. Equation 2.8 calculates the wind speed at an altitude incorporating a stability function (Ψ_M) based on the Monin-Obukhov length:

$$u(z-d) = \frac{u_*}{k}\left[ln\left(\frac{(z-d)}{z_0}\right) - \Psi_M\right]. \quad (2.8)$$

The variable Ψ_M is a dimensionless stability function for momentum. Equation 2.9 gives Ψ_M in stable conditions (Paulson, 1970) and Equation 2.10 gives Ψ_M in unstable conditions (Webb, 1970; Businger et al., 1971).

Stable: $$\Psi_M = \frac{-5(z-d)}{L} \quad (2.9)$$

Unstable: $$\Psi_M = 2\ln\left[\frac{(1+x)}{2}\right] + ln\left[\frac{(1+x^2)}{2}\right] - 2arctan(x) + \frac{\pi}{2} \quad (2.10)$$

Where, $$x = \left(1 - 16\left[\frac{(z-d)}{L}\right]^{\frac{1}{4}}\right) \quad (2.11)$$

2.3 Gas concentration gradients within the PBL

2.3.1 Concentration gradient

The transport of a gas from a source on the ground to a height, z, is determined by the dynamics of the air mass as it passes through the tropospheric layers previously described. The following quantitative description of pollutant concentration in the Prandtl Layer has been taken from Seinfeld and Pandis (2006). Similar to the variation of wind speed with height, Equation 2.12 gives the gas concentration (X, μg m^{-3}) at a height (z, m), which can be calculated from the integrated stability corrector for heat (Ψ_H).

$$X(z-d) = \frac{X_*}{K}\left[ln\left(\frac{(z-d)}{z_0}\right) - \Psi_H\right] \quad (2.12)$$

Ψ_H is a dimensionless stability function for heat. Equation 2.13 gives Ψ_H in stable conditions (Paulson, 1970) and Equation 2.14 gives Ψ_H in unstable conditions (Webb, 1970; Businger et al., 1971), where x is defined as in Equation 2.11.

$$\Psi_H = \frac{-5.2(z-d)}{L} \quad (2.13)$$

$$\Psi_H = 2ln\left[\frac{(1+x^2)}{2}\right] \quad (2.14)$$

The instantaneous fluctuation of concentration (X_*, µg m^{-3}) is calculated from the change in concentration (dX, µg m^{-3}) at a given height (dz, m), the von Karman constant, the zero-plane displacement and a correction factor for heat (Φ_H) (Equation 2.15).

$$X_* = \frac{K(z-d)}{\Phi_H}\frac{dX}{dz} \quad (2.15)$$

Equation 2.16 shows the calculation for Φ_H in stable conditions and Equation 2.17 shows the calculation for Φ_H in unstable conditions.

Stable: $$\Phi_H(z-d) = \left\{\frac{1+5.2(z-d)}{L}\right\} \quad (2.16)$$

Unstable: $$\Phi_H(z-d) = \left\{\frac{1-16(z-d)}{L}\right\}^{-0.5} \quad (2.17)$$

2.3.2 Resistance analogy

A gas emitted from a surface experiences forces that resist its passage. The total resistance the gas experiences is a result of resistances of individual layers acting in series. By definition, the total resistance ($R_t(z\text{-}d)$, s m^{-1}) at height (z) to the emission of a gas is the reciprocal of the deposition velocity (V_d, m s^{-1}). The total resistance is the summed values of the resistance to molecular diffusion in the near surface atmosphere ($R_a(z)$, s m^{-1}), the resistance for molecular diffusion through the quasi-laminar layer (R_b, s m^{-1}) and the residual resistance to emission at the surface (R_c, s m^{-1}) (Equation 2.18).

$$R_t(z-d) = R_a(z-d) + R_b + R_c \quad (2.18)$$

Aerodynamic resistance is a function of wind speed, friction velocity and height above the surface. It is also sensitive to advection, and stability functions are used when conditions are non-neutral. Equation 2.19 shows the calculation of $R_a(z)$ from stability functions for heat (Ψ_H; Equations 2.13 and 2.14) and momentum stability functions (Ψ_M; Equations 2.9 and 2.10).

$$R_a(z) = \frac{u(z-d)}{{u_*}^2} - \frac{\Psi_H\left(\frac{z-d}{L}\right) - \Psi_M\left(\frac{z-d}{L}\right)}{k u_*} \quad (2.19)$$

For emissions from low-lying vegetation, R_b can be calculated using the sub-layer Stanton number (B) (Owen & Thompson, 1963) (Equation 2.20).

$$R_b = (Bu^*)^{-1} \quad (2.20)$$

The sub-layer Stanton number is calculated from the friction velocity, roughness length, the turbulent Reynolds number (Re_*) and Schmitt Number (Sc) ($B^{-1} = 1.45{Re_*}^{0.24}Sc^{0.8}$). Reynolds number is a function of the viscosity of air (v_a, kg m^{-1} s^{-1}) ($Re_* = z_0 u^* v_a^{-1}$). The Schmitt Number is a function of molecular diffusivity of NH_3 (D_χ, m^{2}s^{-1}) ($Sc = v_a D_X^{-1}$) (Garland, 1977).

For emissions from very rough vegetation such as forests, the R_b calculated using Equation 2.20 does not agree well with measurements; instead, Equation 2.21 provides a better approximation for R_b (Sutton et al., 1993a), where κ is the thermal diffusivity of air. However, given the empirical nature of Equations 2.20 and 2.21 they should be used with some caution.

$$R_b = 2(ku_*)^{-1}\left(\frac{\kappa}{D}\right)^{0.67} \quad (2.21)$$

The residual resistance to emission at the surface (R_c, s m^{-1}) is easily obtained from measurements because, using Equation 2.22:

$$R_c = R_t(z-d) - R_a(z-d) - R_b = \frac{1}{V_d} - R_a(z-d) - R_b. \quad (2.22)$$

R_c can also be calculated from the resistance of diffusion through cuticular pathway (R_w, s m^{-1}), and the resistance of diffusion through the stomatal pathway (R_s, s m^{-1}) acting in parallel. R_w acts as a sink when NH_3 is absorbed by the leaf surface and can be calculated using the relative humidity (RH, %) (Equation 2.23).

$$R_w = 2.exp\left(\left[\frac{100-RH}{12}\right]\right) \quad (2.23)$$

R_s, is bi-directional flow of NH_3 between the air and plant (Sutton et al., 1993a) and is calculated from the plant-specific minimum value of R_s ($R_{s,min}$, s m^{-1}), the plant specific leaf area index (b) and the photosynthetic radiation intensity (I_p, W m^{-2}).

The values f_e, f_w, f_T and f_s are correction factors for humidity, water stress, temperature and molecular diffusivity, respectively (Hicks et al., 1987):

$$R_s = R_{s,min} \frac{\left\{1+\left(\frac{b}{I_p}\right)\right\}}{(f_e f_w f_T f_s)} \quad (2.24)$$

2.4 Methods for calculating emission fluxes

The aim of the field studies in this project is to calculate the NH_3 emission from seabird colonies in a range of climates. Section 2.2 outlines how a gas moves from the surface to the atmosphere. These mathematical expressions can be used to infer the rate of emission from the surface using concentration and meteorological measurements. Section 2.4 describes some of the approaches currently used.

In most approaches, the instantaneous concentration of NH_3 gas (X, g m^{-3}) downwind of a colony is measured and an inverse dispersion model is used to calculate the rate of emission (Q, g m^{-2} s^{-1}). Deriving the relationship between X and Q is non-trivial and dependent on the rate of diffusion of the gas (Equation 2.25), where u, v and w are the x, y and z components of the wind, respectively.

$$\frac{\partial X}{\partial t} + u.\frac{\partial X}{\partial x} + v.\frac{\partial X}{\partial y} + w.\frac{\partial X}{\partial z} = 0 \quad (2.25)$$

Equation 2.25 can be solved using a mathematical solution, e.g., Gaussian or Lagrangian. The ideal emission surface is a simple homogenous terrain where the velocity of the wind varies with height above the surface according to Equation 2.8. In more complex terrain turbulence caused by aerodynamic obstruction causes larger uncertainties in the calculated value of Q.

Several models have been developed to calculate Q from X measured downwind of a source, and the main types are discussed and compared below. The choice of the most suitable model for this study depended on the constraints of location and practicality.

2.4.1 Gaussian plume method

The Gaussian plume model describes the concentration of a gas as a function of distance downwind from a point source (Seinfeld and Pandis, 2006). As a gas is emitted, it is entrained in the ambient air movements (Figure 2.2) and disperses in the y and z directions with time, forming a cone. The gas is well mixed within the

volume of the cone, and the concentration of the gas depends on the wind speed and the rate of dispersion. The concentration of the gas, *X(x,y,z)* (μg m^{-3}), at any point *x* metres downwind of the source, *y* metres laterally from the centre line of the plume, and *z* metres above ground level can be calculated using the source strength (*Q*, gs^{-1}), the height of the source (h_s, m) and the air stability. The Gaussian plume approach (Equation 2.26) assumes that the vertical eddy diffusivity (K_z), and wind speed (*U*), are constant in the whole domain (Hensen and Scharff, 2001; Hensen et al., 2009).

$$Concentration\ (x,y,z) = \frac{Q}{2\pi\sigma_y\sigma_z} e^{-\frac{y^2}{(2\sigma_y)^2}} \left(e^{-\frac{(z-h_s)^2}{(2\sigma_z)^2}} + e^{-\frac{(z+h_s)^2}{(2\sigma_z)^2}} \right) \quad (2.26)$$

The standard deviation of the lateral (σ_y, m; Equation 2.27) and vertical (σ_z, m; Equation 2.28) concentration distribution are calculated from the roughness length (z_o, m), the averaging time (*T*, s), the instantaneous concentration of NH_3 gas (*X*, g m^{-3}) and values that define the stability class of the air (*a*, *b*, *c* and *d*) taken from tables (Pasquill, 1974).

$$\sigma_y = a\chi^b z_0^{0.2} T^{0.35} \quad (2.27)$$

$$\sigma_z = c\chi^d (10z_0)^{0.53e} \quad (2.28)$$

$$e = (\chi^{-.022}) \quad (2.29)$$

A range of models have been created by various authors using the Gaussian dispersion equation (Equation 2.26) (Hensen et al, 2001; Venkatesan et al., 2002; Pfeffer et al., 2006; Hensen et al., 2009). These models are mathematically simple and have been used extensively to calculate the dispersion of gases from point sources (Pfeffer et al., 2006). Variations of Gaussian plume models have been used to calculate dispersion from a range of sources including methane emissions from landfills (Gaussian plume model; Hensen et al, 2001), NH_3 emissions from farms (Gaussian-3-D plume model; Hensen et al., 2009), radionuclides at a coastal site (GPD model; Venkatesan et al., 2002) and gas emissions from volcanoes (Gaussian dispersion model; Pfeffer et al. 2006). It is reported that Gaussian plume models work best when the pollutant concentration is measured approximately 1 km from the source (Venkatesan et al., 2002).

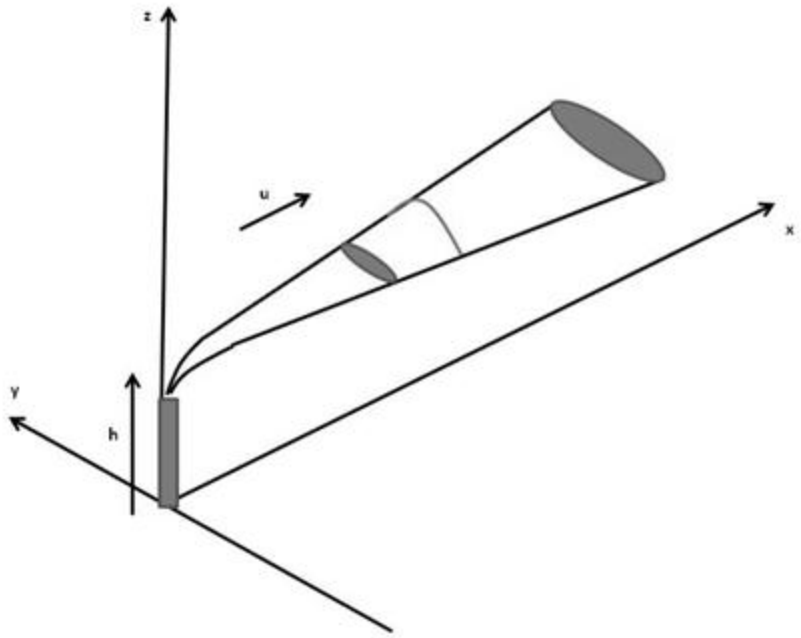

Figure 2.2 Schematic of a Gaussian plume. Emission is from height h above the ground. Concentrations vary in x, y and z directions (after Seinfeld and Pandis, 1996, modified for this thesis)

Blackall et al. (2004) and Blackall et al. (2007) used a Gaussian plume dispersion model to calculate the NH_3 emission from Scottish seabird colonies. Blackall et al. (2007) conducted boat-based campaigns to measure NH_3 concentrations downwind of the seabird colonies on the Isle of May and the Bass Rock, Scotland. They reported that the Gaussian plume based model is suitable for estimating NH_3 emissions from seabird colonies and emissions were used to scale up NH_3 emissions at a regional level. However, there were some uncertainties caused by difficulties parameterising the complex multi-height nature of the emission sources. Also, micrometeorological measurements were difficult to conduct on a moving boat, and therefore land based measurements of wind and stability data were used instead.

2.4.2 Tracer Ratio (TR) method

The Tracer Ratio (TR) uses measurements of concentrations of a pollutant and a tracer gas downwind of a source of unknown strength (Collins et al., 1965). Equation 2.30 shows how the rate of emission of the pollutant gas (Q_p, g m^{-2} s^{-1}) can be calculated if the rate of emission of the tracer gas (Q_t, g m^{-2} s^{-1}), the measured concentration of the tracer gas (X_t, g m^{-3}) and the measured concentration of the pollutant (X_{plume}, g m^{-3}) are known:

$$Q_p = Q_t \cdot \frac{\int_{y_{min}(p)}^{y_{max}(p)} [X_{plume}(p) - X_{bgnd}(p)]\, dy_p}{\int_{y_{min}(t)}^{y_{max}(t)} [X_{plume}(t) - X_{bgnd}(t)]\, dy_t}, \qquad (2.30)$$

where p denotes the pollutant of unknown emission rate, X_{plume} is the measured concentration of the pollutant gas (μg m^{-3}), X_{bgnd} is the measured background concentration of the gas (μg m^{-3}) and y_{max} and y_{min} (both m) represent the crosswind distance between points where X_{plume} equals X_{bgnd}. The main assumption of the TR method is that the tracer gas and the pollutant share dispersion properties, however the advantage is that meteorological data are not required to calculate the emission.

Blackall (2004) and Blackall et al. (2007) used Sulphur hexafluoride (SF_6) as the tracer gas, released from a line source on each island in turn. SF_6 was chosen because of its low background concentration (3 parts per trillion; Ko et al., 1993), stability, inertness (Blackall et al., 2007) and atmospheric persistence (3200 years; Ravishankara et al., 1993). The concentration of both NH_3 and SF_6 were measured downwind from a boat. The TR method was considered robust for estimating NH_3 emission from seabird colonies using boat-based measurements because it did not require meteorological data. Ideally, the use of SF_6 is should be avoided, due to its global warming potential (Ramanathan, 1987; Maiss and Brenninkmeijer, 1998).

In a comparison between the Gaussian plume method and the TR method, Blackall et al., (2004) found these methods to compare favourably. NH_3 emissions from the seabird colony on the Isle of May were measured at 4 and 6 kg NH_3-N h^{-1} for the Gaussian plume and TR methods respectively. NH_3 emissions measured from the Northern Gannet colony on the Bass Rock, Scotland were measured at 21 and 25 kg NH_3-N h^{-1} for the Gaussian plume and TR methods respectively.

2.4.3 Flux-gradient method

Flux-gradient (FG) methods have been used to calculate NH_3 emissions from many surfaces (e.g., Sutton et al. 1993a; 1993b; Nemitz et al. 2001). The FG method uses the friction velocity (u_*) and friction concentration (X_*) to calculate the emission of a gas (Q, g m^{-2} s^{-1}) (Sutton et al. 1993a; 1993b):

$$Q = -u_* X_* \quad (2.31)$$

Equation 2.31 can be simplified to give Equation 2.32, a relationship between K_χ (Equation 2.33) and the integrated stability corrector for heat (Φ_H) (Sutton et al. 1993a).

$$Q = -K_\chi \frac{d\chi}{dz} \quad (2.32)$$

$$K_\chi = \frac{K(z-d)u_*}{\Phi_H} \quad (2.33)$$

Q can be calculated from field measurements. The concentration gradient is measured at heights above the surface, and values from u_* and Φ_H are obtained from sonic anemometer measurements. To calculate a gradient, the gas concentration must be measured at a minimum of two heights.

Various instruments and methods have been used to measure NH_3 concentration profile with height: Sutton et al. (1993a; 1993b) used filter packs sampling over three days, Sutton et al. (2000b) used the Ammonia Measurement by ANnular Denuder sampling with on-line Analysis, (AMANDA) (Wyers et al., 1993). In Sutton et al. (2000b) and Nemitz et al. (2001) the airflow was sampled for two minutes at each height, with a flux calculated for every six minutes of sampling

This method has been used to calculate NH_3 fluxes over a range of ecosystems including moorland, coniferous forest and a variety of arable crops, including oil seed rape and wheat (Nemitz et al., 2001; Milford et al., 2009; Loubet et al., 2011). From a practical perspective, the set up can be relatively simple, with a valve system to sample at three heights, a sonic anemometer and a gas analyser.

2.4.4 Backward Lagrangian Stochastic (BLS) dispersion method

A Lagrangian dispersion model follows air parcels of a pollutant as they move in the atmosphere away from a source (Wilson and Sawford, 1995). Changing horizontal and vertical forces result in the random movement of the pollutant. It is also assumed that the pollutant particles are neutral and do not react in the air (Wilson and Sawford, 1995). A Lagrangian model uses a moving frame of reference as the parcels move from their initial location. The rate of emission can be calculated from pollutant concentration and atmospheric turbulence measurements made at a point

downwind of the source. The motion of the particles is affected by both mechanical and convective turbulence as described in Section 2.1.2.

Lagrangian models can be used to model the movement of parcels either forward or backward in time. Forward modelling follows the parcel of air from a given starting point and predicts how the pollutant disperses downwind. In backward modelling, the resultant position of the parcel of air is known (the measurement point) and the model steps back through each trajectory to infer the rate of emission from the source. Figure 2.3 shows an experimental setup to determine the rate of emission from an area source (shown in light grey), where the concentration of air is measured at a single point downwind of the source. To infer the emission rate of the source using forward modelling requires a vast amount of trajectories to be calculated because most of the emitted pollutant particles will not end up at the measurement point. The number of trajectories required to provide a statistically accurate prediction is computationally challenging (Flesch et al., 1995). Backward Lagrangian models are more computationally efficient, faster and more flexible in calculating emission rate from a source than forward models (Flesch et al., 1995).

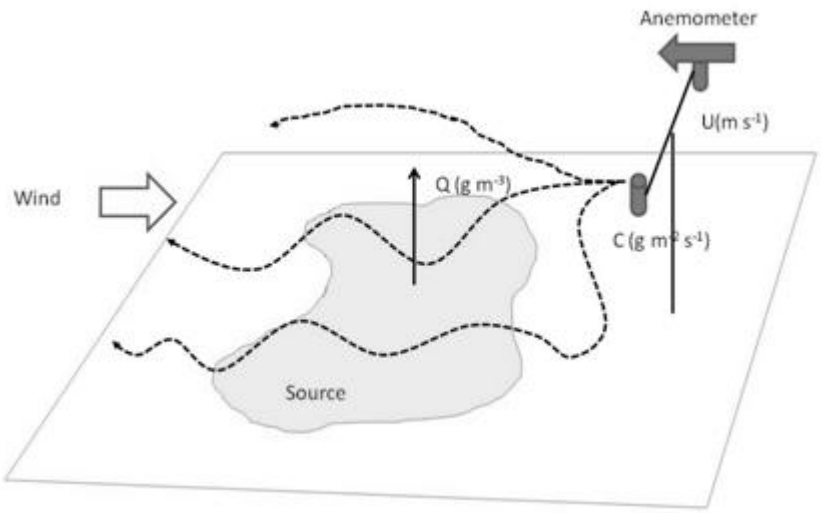

Figure 2.3 The Lagrangian stochastic (LS) dispersion of air parcels, showing the trajectories of the emissions from the source and background. U denotes the wind speed and C denotes the measured concentration.

A backward Lagrangian stochastic (BLS) model infers the rate of emission by simulating the transport of the pollutant from the source to where it is measured and by predicting the ratio of tracer concentration to emission, $(C/Q)_{sim}$ (Flesch et al.,

2004; 2005). The emission rate (Q, g m^{-2} s^{-1}) is then inferred from the measured gas concentration (X_m, g m^{-3}) and the background gas concentration (X_b, g m^{-3}) (Equation 2.34).

$$Q = \frac{X_m - X_b}{\left(\frac{C}{Q}\right)_{sim}} \tag{2.34}$$

The commercial software WindTrax (www.thunderbeachscientific.com) is based on a BLS dispersion model (Flesch et al., 1995; 2004) and was developed to calculate the emission rate of a gas from an area or line source. WindTrax calculates $(C/Q)_{sim}$ by tracing the motion of a number of gas particles (N) from the detector to the source and calculating vertical velocity of the particles at touchdown (w_0, m s^{-1}) (Equation 2.35).

$$\left(\frac{C}{F}\right)_{sim} = \left(\frac{1}{N}\right)\sum\left|\frac{2}{w_0}\right| \tag{2.35}$$

The main advantage of WindTrax is its versatility as it requires only input data from the size of the source, the concentration at the detector, background concentration and wind speed to calculate the emission from a source. The uncertainty associated with the calculated emission rates can also be estimated and represented as the standard deviation of the mean emission. As more data are input, the uncertainty of the emission estimate decreases, e.g. friction velocity and Monin-Obukhov length. If multiple concentration measurement heights are used as input, a linear optimisation algorithm is used in WindTrax to calculate the emission from a surface.

The BLS model working within WindTrax is based on the movement of air in neutral and non-neutral conditions, using the equations for the movement of air detailed in Sections 2.1.3 and 2.1.4. The emission estimates calculated by WindTrax are estimated to be within 10 % for ideal terrain and with concentration sampling periods of between 15 - 120 minutes (Sommer et al., 2005). Ideal terrain is horizontally homogeneous and assumes that the particles move from source to detector over a surface free of obstructions, with a maximum roughness length of 15 cm (Sommer et al., 2005; Flesch et al., 2005; 2009; Laubach and Kelliher, 2005; Laubach et al., 2008). The maximum distance between the source and the detector is 1 km; beyond 1 km uncertainties in the surface layer flow model affect the results (Flesch et al. 2005; 2008). It was identified by Sommer et al. (2005) that the

uncertainty will increase as the length of the measurement period increases and care must be taken when parameterising stability inputs.

The main disadvantages of WindTrax are the inaccuracies in modelling turbulent transport (Denmead et al., 2008) and the assumption that particles are inert, with no chemical reactions in the atmosphere between source and measurement point. Another disadvantage is that WindTrax cannot be used if the roughness height is greater than 15 cm (Flesch et al., 2005; 2008; Laubach et al., 2008). Thus, WindTrax cannot be used for top estimate emissions in a range of environments such as emissions from buildings, in-canopy emissions and emissions from bluff bodies.

In recent years WindTrax has been shown to be a powerful tool in estimating emission from a range of gases, including NH_3 (Flesch et al, 2005; Denmead et al., 2008; McGinn et al., 2008; Bjorneberg et al., 2009; Harper et al., 2009; Harper et al., 2010; Leytem et al., 2010; Turner et al., 2010), CH_4 (Laubach and Kelliher, 2005; Bjorneberg et al., 2009; Gao et al., 2009; Loh et al., 2009; McGinn et al., 2009; Gao et al., 2010; Laubach, 2010), N_2O (Bjorneberg et al., 2009), NO_x (Denmead et al., 2008; Leytem et al., 2010) and CO_2 (Loh et al., 2009; Trottier et al., 2009; Leytem et al., 2010).

2.5 Assessment of NH_3 measurement instrumentation for studying seabird colonies

To measure atmospheric NH_3, active and passive measurement techniques can be used. Passive methods capture gas particles as the pollutant naturally diffuses through the atmosphere. The concentration of the gas is calculated from the amount of pollutant captured and the length of time for which the passive samplers were installed. Active sampling techniques measure the atmospheric concentration of a pollutant by drawing air into an instrument and measuring concentration directly.

Passive samplers are an effective method for providing NH_3 concentration data and have been deployed successfully in remote locations (Blackall et al., 2004; Theobald et al., 2006; Blackall et al., 2007; Schmidt et al., 2010). Whilst passive samplers are an inexpensive, robust and reliable method for collecting NH_3 concentration data, the measured concentrations are time averaged over the deployment period (days –

weeks – months) and data do not indicate how changes in meteorology/climate affect NH_3 emission. Active sampling instruments have a higher time resolution, as they use power to sample air into a sampling device or through a filter membrane at a higher volume. Generally, active sampling instruments have high power requirements and are relatively more expensive. This study measured NH_3 concentrations at seabird colonies using both active and passive sampling techniques. The choice of method depended on the size of the source, the local climate and practicalities such as the accessibility of the colony, frequency of opportunity for access and instrument availability. The following describes the options in methodology and why different methods were chosen for the different study sites.

2.5.1 Passive sampling techniques

Passive sampling techniques have been developed to provide a low-cost solution to sample concentrations of chemical NH_3 in air in remote locations (Blackall et al., 2004; Theobald et al., 2006; Blackall et al., 2008). Types of passive samplers are: (i) open ended diffusion samplers, typical diffusion pathlength of 70 mm (Hargreaves et al., 1987), (ii) diffusion tubes with a membrane to prevent wind incursion (Downing et al., 1994; Tang et al., 2001) and (iii) passive diffusion ‘‘Willems’’ badges, diffusion pathlength after membrane is only 2 mm (Willems and Adema, 1992). An intercomparison of these types of passive sampler has shown that all passive sampler types overestimated concentrations when measuring low NH_3 concentrations (< 3 $\mu g\ m^{-3}$) (Sutton et al., 2001b). Type (ii) samplers were the most precise type of sampler (Sutton et al., 2001b) and were chosen as the most suitable for this study.

Of the type (ii) diffusion tubes, there are two main types of passive sampler generally available: the CEH ALPHA (Adapted Low-cost Passive High Absorption) sampler (Tang et al., 2001; Sutton et al., 2001b) and the Gradko diffusion tube sampler (Gradko, 2011). For this study, the former was chosen due to doubts over the detection limit of the Gradko tubes (Theobald, 2009). ALPHA samplers have been used extensively in the measurement of NH_3 throughout the UK and are routinely deployed in the UK National Ammonia Monitoring Network (NAMN) and comprehensively tested against other systems. ALPHA samplers have a protective

PTFE membrane over the sampling surface and are deployed in an inverted position, which make it very difficult for birds to interfere with the samplers. The samplers are designed to measure ambient NH_3 concentrations and are sensitive to concentrations of less than 0.1 μg m^{-3} NH_3, based on monthly sampling. The extremely high NH_3 concentrations at seabird colonies mean that the ALPHA samplers can be used as detectors for periods as short as a single day (Blackall et al., 2004; 2007)

ALPHA samplers work on the principle that gas diffuses into an absorbing material within a fixed volume. The molecules of the gas to be measured are chemically separated from the air onto the absorbing filter. The passive sampler is left in-situ for a measured time then sealed. Subsequent chemical analysis measures the amount of analyte in its absorbed form (e.g., NH_3 is absorbed as NH_4^+). The average concentration of NH_3 collected by the ALPHA sampler during the measurement time (X_a, g m^{-3}) can then be calculated from the mass of NH_3 on an exposed sample (m_e, μg), the mass of NH_3 on a blank (unexposed) sample (m_b, μg), the liquid volume of the extraction solution (v, ml) and the effective volume of air sampled (V, m^3) (Equation 2.36).

$$X_a = \frac{(m_e - m_b)}{V} \tag{2.36}$$

The effective volume of air sampled (V, m^3) by the sampler is calculated from the diffusion coefficient of NH_3 in air (D, 2.09 x 10^{-5} m^2 s^{-1} at 10°C) (Tang et al., 2001; Sutton et al., 2001b), the tube cross sectional area (A, 3.4636 x 10^{-4} m^2), the sampling duration (T, s) and the length of the diffusion tube (L, 0.006 m) (Equation 2.37).

$$V = \frac{DAt}{L} \tag{2.37}$$

Design of ALPHA Samplers

ALPHA samplers use filter paper coated with citric acid to capture NH_3 from the air (Figure 2.4). ALPHA samplers are attached to a shelter by Velcro at the sampling location. The date and time is noted when the protective cap is removed. After the sampling period, the outer membrane is replaced with a solid cap, and the date and

time are recorded again. A detailed description of the ALPHA sampler can be found in Tang et al. (2001).

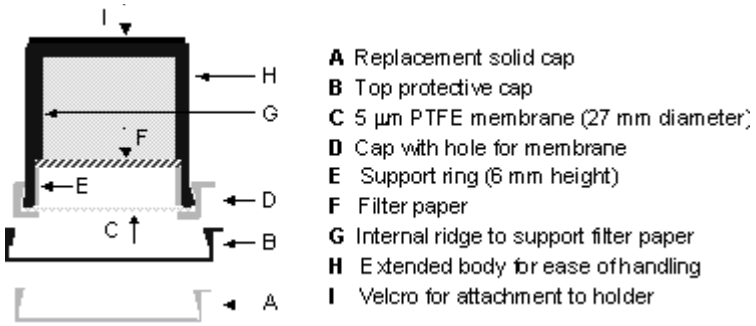

Figure 2.4 The side view of an ALPHA sampler. Image courtesy of Tang et al. (2001)

Chemical analysis of ALPHA samplers is conducted by an instrument called AMFIA (AMmonium Flow Injection Analysis) developed by the Energy Research Foundation of the Netherlands (ECN, Petten, NL). Water is initially added to the exposed filter paper and NH_3 on the filter paper dissolves into the water as NH_4^+. Within the AMFIA, sodium hydroxide is added to the extracted solution, converting the NH_4^+ in solution to gas-phase NH_3. The solution passes a semi permeable gas membrane, where only NH_3 gas passes through the membrane and dissolves into de-ionized water on the other side. The NH_3 is then converted back to NH_4^+ and the concentration is measured using a conductivity block.

2.5.2 Active sampling techniques

The two main measurement principles to measure atmospheric NH_3 concentrations are wet chemical and spectroscopic techniques. Descriptions of the major techniques are given in von Bobrutzki et al., 2010 and Norman et al., 2009.

Three wet-chemistry analyzers could have been used for this project: the Annular rotating batch denuder (RBD), the NH_3 Measurement by ANnular Denuder sampling with online Analysis (AMANDA) and the AiRRmonia. All three instruments were developed by the ECN, Petten, NL. The RBD and the AMANDA instruments (Mechatronics) require large quantities of solutions, and therefore were not suitable for this study. The AiRRmonia was considered suitable as it does not require large volumes of reagent solution and is relatively portable. The AiRRmonia is relatively low power (< 50 W), has a detection limit of 0.04 ppbv, weighs 20 kg and can be deployed using either solar or wind power. The AiRRmonia is calibrated

and filled with reagents every week. The time resolution of the instrument is 10 minutes (ECN, 2003).

An AiRRmonia analyzer was deployed in two of the field experiments carried out (see Chapter 5 for details). The AiRRmonia works by absorbing NH_3 from the air with an acidic solution. The NH_3 forms NH_4^+ in solution, and an alkali is then added to the solution before it passes a semi-permeable membrane. The alkali converts NH_4^+ in solution to gas-phase NH_3. Some of the NH_3 gas passes through the membrane and is dissolved into de-ionized water. The conductivity of this solution is a measure of the NH_3 concentration in air.

Spectroscopic and spectrometric instruments include photoacoustic instruments, infrared absorption spectroscopy instruments (e.g. cavity ring down spectroscopy (CRDS), Open-Path Fourier Transform Infra-Red (OP-FTIR) spectroscopy, tuneable diode laser (TDL) spectrometers and Quantum cascade laser IR spectrometers (QCL IR). The instruments listed in Table 2.2 use these technologies to measure NH_3 concentrations. The ideal attributes of an instrument used to measure NH_3 at remote seabird colonies are: low power consumption, ease of transport, reliability and autonomy. These criteria are generally unfulfilled by the above instruments. The WaSul-Flux has a relatively slow time response (45 min) at low or background concentrations (von Bobrutski et al., 2010). The CRDS has power requirements of around 300 W, which is too high for these field measurements. The DUAL-QCLAS is a sensitive instrument that depends on aligned mirrors and need to be calibrated frequently (von Bobrutski et al., 2010). The TDLAS requires liquid nitrogen cooling (Twigg et al., 2005). Of the available instruments, the Nitrolux and AiRRmonia were considered most suitable for use in this study.

The Nitrolux photoacoustic instrument uses absorption of NH_3 molecules from a line-tunable CO_2 laser to measure concentration. Absorbed radiation is dissipated by the molecules as detectable acoustic waves which indicate the abundance of NH_3 molecules (Cowen et al., 2004). The Nitrolux 1000 is a sensitive instrument (detections limit of 0.1 ppbv), measures from 0 – 2000 ppb, has a relatively quick response time and measures concentrations every 45 s. The response time is a function of temperature and relative humidity. As a spectroscopic instrument, the Nitrolux 1000 requires less than 150 W, and requires little maintenance other than a

six monthly calibration (Cowen et al., 2004) under suitable conditions. However, the instrument weighs 30 kg, has many moving parts and is susceptible to the elements, which made it unsuitable for deployment to remote locations, especially those that required handling by couriers, airport and customs staff.

2.6 Approaches used in this project

2.6.1 Measuring NH_3 concentration

Passive sampling

Passive campaigns are conducted when a non-instrument specialist is travelling to the seabird colony. The CEH ALPHA samplers were selected for passive sampling. Exposed ALPHA samplers are analysed using the AMFIA at CEH Edinburgh.

Active sampling

Active campaigns are conducted by an instrument specialist using either the Nitrolux 1000 or the AiRRmonia gas analyzers. The main attributes that make them suitable are that they use relatively little power and can run unattended for long periods of time. Both instruments can be relatively easily transported to the seabird colony, given careful handling. The AiRRmonia is a weather proofed instrument that has been designed for remote deployment, whereas the Nitrolux 1000 requires shelter, as it was designed for a clean room environment.

2.6.2 Modelling approach

For this study, the BLS technique, and the WindTrax model in particular, is selected to calculate NH_3 emissions from seabird colonies using concentrations measured downwind. The main advantage of the WindTrax model is its versatility, and it has also been described as the best available model for estimating gas emissions in obstacle free terrain (Laubach, 2010). The measurement campaigns in this study are conducted in remote locations and problems with equipment can cause data loss. WindTrax allows emissions to be calculated even when the dataset is incomplete. The fieldwork sites are carefully chosen to ensure that the input data is within the ranges of the model, the distance of NH_3 measurement is less than 1000 m from the colony and the roughness length is less than 15 cm. The topography of the fieldwork sites is described in detail in Chapter 5.

Table 2.2 Instruments that can be used to measure NH_3 concentration.

Instrument	Method	Manufacturer
AiRRmonia	Wet-chemistry	Energy Research Foundation of the Netherlands, Petten, NL (ECN, 2003)
Nitrolux-1000	Photoacoustic spectroscopy	Pranalytica Inc., Santa Monica, CA, USA (Cowen et al., 2004)
WaSul-Flux	Diode laser based photoacoustic spectroscopy	Hi-Lase, H-6720 Szeged, Dóm tér 9. HUNGARY (Pogany et al., 2008)
EnviroSense 1000 Analyzer	Cavity Ring Down Spectroscopy (CRDS)	Picarro Inc., Sunnyvale, CA, USA (Berden et al., 2000)
MIDAC M4401 FTIR spectrometer, Stirling cooled MCT detector module, Infra-red source	Open-path Fourier Transform Infra-Red (OP-FTIR) spectroscopy	MIDAC Corp., Costa Mesa, CA, USA
DUAL-QCLAS	Quantum cascade laser IR spectrometers (QCL IR)	Aerodyne Research Inc., Billerica, MA, USA (Whitehead et al., 2008)
TDLAS	Tuneable diode laser (TDL)	GE Sensing and Inspection Technologies, Billerica, MA, USA (Twigg et al., 2005)

Chapter 3 The global distribution of ammonia emissions from seabird colonies

3.1 Introduction

Seabird colonies are typically found in remote coastal areas. Due to their isolation from anthropogenic N_r sources, colonies are thought to play a major role in the nitrogen cycle within these ecosystems (Lindeboom, 1984). In particular, a significant fraction of the nitrogen is estimated to be lost as ammonia (NH_3) emission to the atmosphere, which will disperse and deposit on local ecosystems (Blackall et al., 2008). The local atmospheric deposition of NH_3 is estimated to have a large impact on plants and soil adjacent to a seabird colony (Anderson and Polis, 1999).

Currently, estimates of NH_3 emissions from seabird colonies at a global scale are extremely uncertain (Blackall et al., 2007). Better quantification of their distribution is necessary to allow for a greater understanding of the biological, physical and biogeochemical effects that seabird colonies have on their immediate environment. Research carried out at UK colonies suggests that emissions are substantial (in some cases more than 100 Mg NH_3 per colony per year) (Blackall et al., 2007). Although these estimates suggest that seabirds contribute only 2 % of the national NH_3 emission in the UK, they dominate local NH_3 emission in the remote areas where they occur (Wilson et al., 2004).

The energetic model approach of Wilson et al. (2004) was extended by Blackall et al. (2007) to calculate the NH_3 emission from seabird colonies at a global scale. Blackall's provisional value suggested an overall emission of 242 Gg NH_3 $year^{-1}$. However, the bird population estimates that underpinned this estimate were predominantly from the 1960s and 1970s and were not spatially referenced. Updated, spatially-referenced population data are now available so there is the opportunity to map global NH_3 emissions using recent data for the first time. The global estimate by Blackall et al. (2007) also took no account of global climate differences, whereas, in principle, NH_3 emissions should be highly temperature sensitive, according to the thermodynamic Henry and dissociation equilibria for NH_3 (Nemitz et al., 2000, Zhu et al., 2011). The consideration of temperature is

important because seabird breeding colonies are distributed across a large range of thermal conditions from the poles to the tropics.

This chapter reports the establishment of an updated seabird population and distribution database coupled with an exploration of the possible consequences of temperature dependence on global NH_3 emissions from seabird colonies, allowing uncertainties to be estimated. By mapping seabird NH_3 emissions at a global scale for the first time, the chapter also quantifies the extent to which these occur in hot spots far from anthropogenic sources. This chapter aims to achieve a better fundamental understanding of the role of natural NH_3 sources, including the sensitivity to environmental conditions relevant for developing a global perspective. In this respect, seabirds represent a "model system" relevant for comparison with other excretal sources of NH_3 emission. Many sources of NH_3, especially agriculture are complicated by different management practices across the globe, whereas seabird emissions are a model system for studying climate dependence.

3.2 Methods and materials

3.2.1 Seabird population estimates

A detailed spatially explicit seabird database was collated from a wide range of sources, incorporating data from 180 countries, comprising 323 species in 33,255 colonies. The author requested access to and use of global seabird population data from government agencies of all countries with a coastline, country-specific conservation organisations and global seabird organisations (e.g. Birdlife International), where available, for the production of global seabird ammonia emission estimates. Data obtained for each colony included: species of bird, population, location, quality of data, method of data collection and the contact details of the collector. These data were collated and checked to ensure that colonies were only represented once.

An indication of the uncertainty of the data collection for each source was incorporated into the database. In the case of penguins, which represent a significant NH_3 source, population uncertainty estimates were taken from the study by Woehler (1993). An attempt was made to consider all seabird NH_3

sources and some data included inland colonies, such as for the UK. However, data for inland seabird colonies outside the UK were not readily available and are not included in the dataset.

3.2.2 Bioenergetics model

The bioenergetics model developed by Wilson et al. (2004) calculated the NH_3 emissions from seabirds using population and bird specific data. Nitrogenous waste excreted by birds is in the form of uric acid ($C_5H_4O_3N_4$), which is relatively insoluble and must undergo bacterial transformation before it can release NH_3. Biochemical degradation of uric acid primarily forms NH_3 (Groot Koerkamp et al. 1998):

$$C_5H_4O_3N_4 + 1.5O_2 + 4H_2O \rightarrow 5CO_2 + 4NH_3. \quad (3.1)$$

3.2.3 Calculating Annual NH_3 emission

Breeding Adults

Using the method of Wilson et al. (2004) the annual NH_3 emission for breeders ($Q_{NH_3}(br)$, g NH_3 $bird^{-1}$ yr^{-1}) can be calculated from the adult mass (M, g $bird^{-1}$), nitrogen content of the food (F_{Nc}, g N g^{-1} wet mass), energy content of the food (F_{Ec}, kJ g^{-1} wet mass), assimilation efficiency of ingested food (A_{eff}, kJ [energy obtained] kJ^{-1} [energy in food]), proportion of excreted nitrogen volatilized as NH_3 (F_{Nv}), length of the breeding season ($t_{breeding}$, days), proportion of time spent at the colony during the breeding season (f_{tc}), a habitat correction factor (F_{hab}) and 17/14 the mass ratio of NH_3 to N. This study aims to estimate the NH_3 emission from seabird guano deposited at the colony and does not attempt to calculate NH_3 emission from seabirds outside the breeding season or out-with the nesting areas.

$$Q_{NH_3}(br) = \frac{9.2.M^{0.774}}{F_{Ec}A_{eff}} F_{Nc}F_{Nv}t_{breeding}f_{tc}F_{hab}\frac{17}{14}. \quad (3.2)$$

F_{Nc} and F_{Ec}, estimated at 0.036 g N g^{-1} and 6.5 kJ g^{-1} (both wet mass), (Energy: Nitrogen (E:N) ratio = 181 kJ g N^{-1}) respectively, have been calculated assuming a high protein, fish only diet (Furness, 1991). A_{eff} is estimated at 0.8 (Furness, 1991). Due to differences in feeding behaviour and food type of seabird species it is recognised that the values of F_{Nc}, F_{Ec} and A_{eff} have associated uncertainty. An uncertainty analysis was conducted on these values, using F_{Nc} and F_{Ec} for

Antarctic krill (*Euphausia superb*), a low nitrogen content food source (F_{Nc} of 0.023 g N g^{-1}, F_{Ec} = 4.35 kJ g^{-1} and E:N ratio of 189 kJ g N^{-1}) (Croxall and Davis 1990). A_{Eff} varies between 0.633 and 0.828 for seabird species (Green et al., 2007).

F_{Nv} was estimated following field campaigns measuring NH_3 emissions from seabird colonies on the Isle of May and the Bass Rock, Scotland (Blackall et al., 2004; 2007). F_{Nv} was estimated at 0.3 and combines the effect of temperature, humidity, wind speed and solar irradiance on volatilization rate for a mid-latitude environment (Wilson et al., 2004). Part of the total guano excretion at the colony will wash to the sea by either rain events or by wave action (Blackall et al., 2008). However, the total amount of N excreted is used as the reference point for the NH_3 emission calculation. The amount of nitrogen lost in run off events would need to be considered in a more detailed dynamic modelling approach, which takes account of local rainfall and run-off.

The term $t_{breeding}$ was calculated by summing species-specific pre-laying (courtship and nest building), incubation and chick-rearing periods. The value for f_{tc} takes into account the loss of excreta whilst the bird is not at the colony, i.e., feeding at sea or during flying. NH_3 emissions in Equation 3.2 are only estimated for guano deposited by seabirds during their attendance at the breeding colony. Previous measurements showed NH_3 emission to occur after the departure of the birds at the end of the breeding season (Blackall et al., 2008) and that NH_3 emission drops to background levels one month after birds have left the colony. It is feasible that NH_3 emissions may last longer in colder and drier locations as suggested by Zhu et al. (2011), however further measurements will be required to test that suggestion.

F_{hab} describes re-absorption of NH_3 by the substrate and overlying vegetation. Wilson et al. (2004) estimated F_{hab} at 1.0 (no re-absorption) for guano excreted on rock, 0.2 for guano excreted on a nest or vegetation and 0 (total re-absorption) for guano excreted in a burrow, which was consistent with the findings of Blackall et al. (2007).

Non-Breeding Adults

Non-breeders are estimated to make up c.33 % of the breeding population of UK seabirds and spend 50 % less time at the colony than breeders, a value that is typical of many seabirds globally (Wilson et al., 2004). The annual NH_3 emission for non-breeders ($Q_{NH_3}(nbr)$, g NH_3 $bird^{-1}$ yr^{-1}) is therefore estimated as:

$$Q_{NH_3}(nbr) = 0.167 Q_{NH_3}(br) . \quad (3.3)$$

Estimates of non-breeder attendance could have spatial and temporal variation. In general, seabirds spend appreciable amounts of time at a colony before recruiting into the breeding population. Variation in non-breeder attendance has been estimated at between 35 and 73 % (Williams and Rodwell, 1992) and an uncertainty estimate is based on these values.

Chicks

Chick attendance is estimated as the length of time between hatching and fledging. The annual NH_3 emission for chicks ($Q_{NH_3}(ch)$, g NH_3 $bird^{-1}$ yr^{-1}) is estimated from the mass of the chick at fledging ($M_{fledging}$, g) and the breeding productivity (P_{chicks}, chicks fledged pair):

$$Q_{NH_3}(ch) = \frac{28.43 M_{fledging}^{1.06}}{F_{Ec} A_{eff}} F_{Nc} F_{Nv} \frac{17}{14} \frac{P_{chicks}}{2} F_{hab} . \quad (3.4)$$

3.2.4 Model parameterization

Species-specific values for input parameters (adult mass, number of days spent at the colony per year, proportion of time at the colony, breeding success, fledging mass of the chick and breeding habitat) were extracted from the literature and are summarised in Appendix 1. Where data were available from multiple colonies and/or years, the mean of colony/year means was used. Of the 318 species of seabird considered, data were available for 311 species (Birdlife International, 2011). Data for the missing species were estimated from similar species identified using information from Birdlife International (2011).

Few data are available for the percentage of time an adult spends at a nest and the same approach as Wilson et al. (2004) was adopted for this study. Seabirds that lay their eggs in open habitat (rock or vegetation) are required to attend the brood continuously until they are large enough to be safe from predators; thus, it was estimated that each adult of these species spends 60 % of their time at the nest.

Burrow nesters do not continuously attend their chicks and each adult was estimated to spend 30 % of their time in the burrow for diurnal species, active during the day, and 10% for nocturnal species that only return to the nest at night.

3.2.5 Temperature dependence of NH_3 emissions

Using the hypothesis that, a temperature corrected value for F_{Nv} instead of a constant derived under Scottish conditions (Wilson et al., 2004; Blackall et al., 2007) could allow for more realistic estimates of NH_3 emission across a temperature gradient. F_{Nv} was therefore investigated in relation to its possible temperature sensitivity. Two estimations are made: Scenario 1: NH_3 emissions independent of temperature, following the method outlined above; Scenario 2: NH_3 emissions calculated on the basis of the combined Henry and dissociation equilibria for NH_3 and ammonium (NH_4^+), following the empirical fit of Nemitz et al. (2000):

$$c_T = \frac{161500}{T} exp\left(\frac{-10378}{T}\right) \qquad (3.5)$$

where c_T is the temperature dependent Henry's Law constant and T is the prevailing temperature (K) (Nemitz et al., 2000). By taking 10 °C as a reference, the proportion of excreted nitrogen that volatilizes, F_{Nv}, at 10 °C is 0.33. In colder climates, where the average temperature during the breeding season is 5 °C, F_{Nv} decreases to 0.09. For colonies where the average temperature is 15 °C F_{Nv} is 0.61. At colonies where the average temperature is greater than 19 °C all of the excreted nitrogen is estimated to volatilize (F_{Nv} = 1).

The local temperature correction factor for NH_3 emission was calculated based on the mid-latitude experimental results of Blackall et al. (2007) from measurements carried out under an average temperature of 283 K. The relationship of Equation 3.5 was used to calculate a temperature correction factor (c_{local}/c_{283}) at all colonies across the globe, using the average air temperature during the breeding season, obtained from the 2010 Global Surface Summary of the Day (GSOD) data set courtesy of the National Climatic Data Center (NCDC, 2011). A geographical information system (GIS) was used to identify the closest measurement sites in the temperature dataset for each of the global seabird colonies. For colonies farther than 1000 km from a measurement site, the temperature was calculated as

the average of the nearest three sites. The decision to use 1000 km as a cut off was taken because it was assumed that for the purposes of this study temperature at sea level would be sufficiently similar to sites with less than this distance. This correction was only necessary for 50 colonies, mostly in the South Pacific.

Other processes can be expected to offset the temperature effect simulated in Scenario 2, such that this can be considered as representing a theoretical maximum temperature dependence. For example, in a cold dry atmosphere the NH_3 emission potential may be smaller, but result in emissions taking place over a longer period of time. Conversely, in warm, dry conditions the rate of urea hydrolysis may be limited, leading to guano accumulation or a higher chance that guano is washed into the sea during intermittent intensive rain events.

Given these uncertainties, the average of Scenarios 1 and 2 ('limited temperature dependence', Scenario 3) is used as the best estimate of NH_3 emission for the purpose of mapping using a GIS. The maps shown in Figures 3.1, 3.4 and 3.5, representing location, size and magnitude of seabird colonies and NH_3 emissions, were produced in a GIS (ArcGIS 9 ESRI inc., 2011). Latitude, longitude, and seabird populations by species for every colony were collected in a detailed spatial database, and NH_3 emissions calculated for each colony. To show the distribution of the NH_3 emissions clearly in Figures 3.1 and 3.4, the contents in each 5 degree grid square have been aggregated and plotted.

3.3 Results

3.3.1 Global distribution of seabird colony populations and N excretion

The global seabird database included a total seabird population of 261 million breeding pairs, with an average date of count being 1992 (and standard deviation of 11 years). Figure 3.1 shows the estimated regional distribution of seabirds globally. Antarctica and the sub-Antarctic islands (69 million pairs) have similar numbers of seabirds to Greenland and Svalbard combined (68 million pairs). Australasia and the Pacific Islands also have large seabird populations.

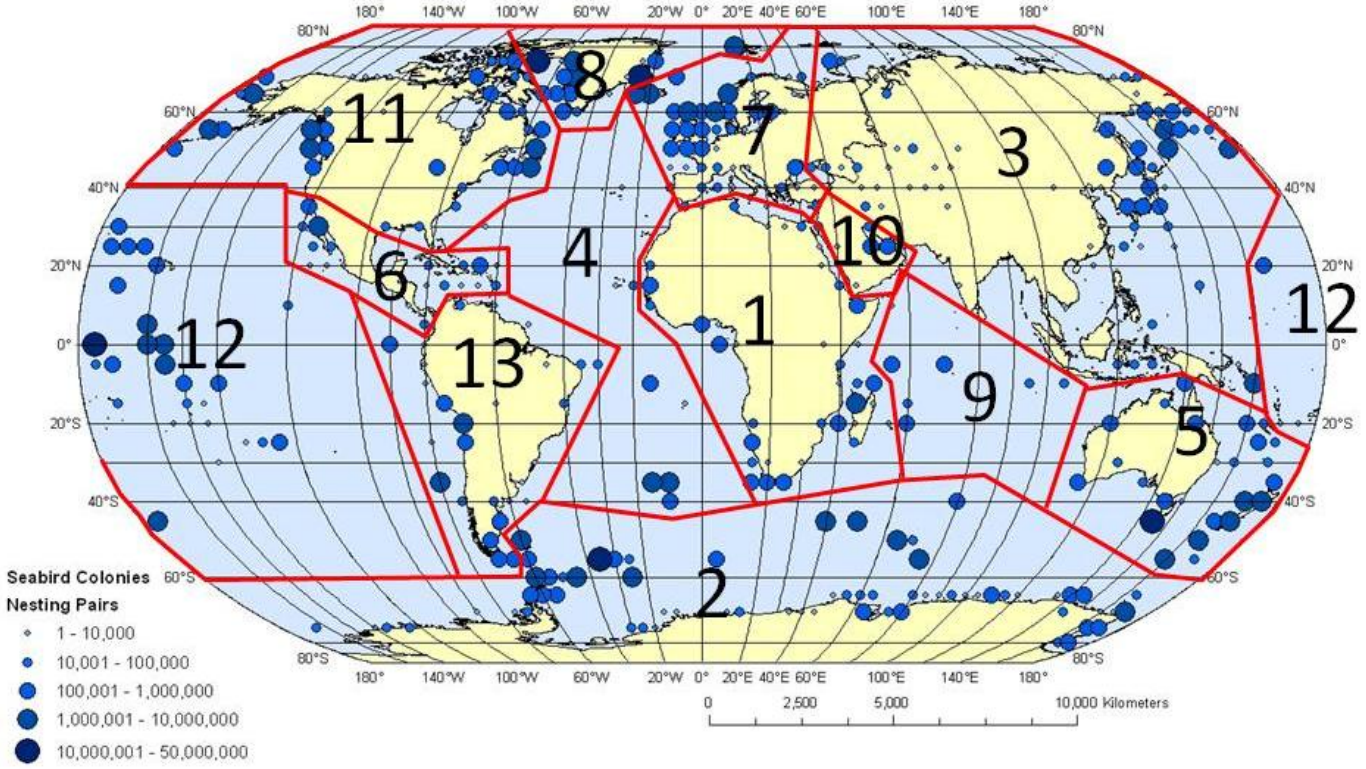

Figure 3.1 Global distribution of seabird colonies, based on number of breeding pairs. Lines delineate regional boundaries: 1. Africa, 2. Antarctica & Southern Ocean, 3. Asia, 4. Atlantic, 5. Australasia, 6. Caribbean & Central America, 7. Europe, 8. Greenland & Svalbard, 9. Indian Ocean, 10. Middle East, 11. North America, 12. Pacific and 13. South America. To show distribution of the colonies clearly, the number of pairs in each 5° grid square have been summed.

However, a large population size does not necessarily correspond to large nitrogen excretion. The differences between species' body masses and length of breeding season are reflected in difference between N excretion on Antarctica and sub-Antarctic islands (858 Gg N year^{-1}) and Greenland and Svalbard (59 Gg N year^{-1}). Total nitrogen from seabird excretion is dominated by Antarctica and Southern Ocean, accounting for 79 % of the total (Figure 3.2).

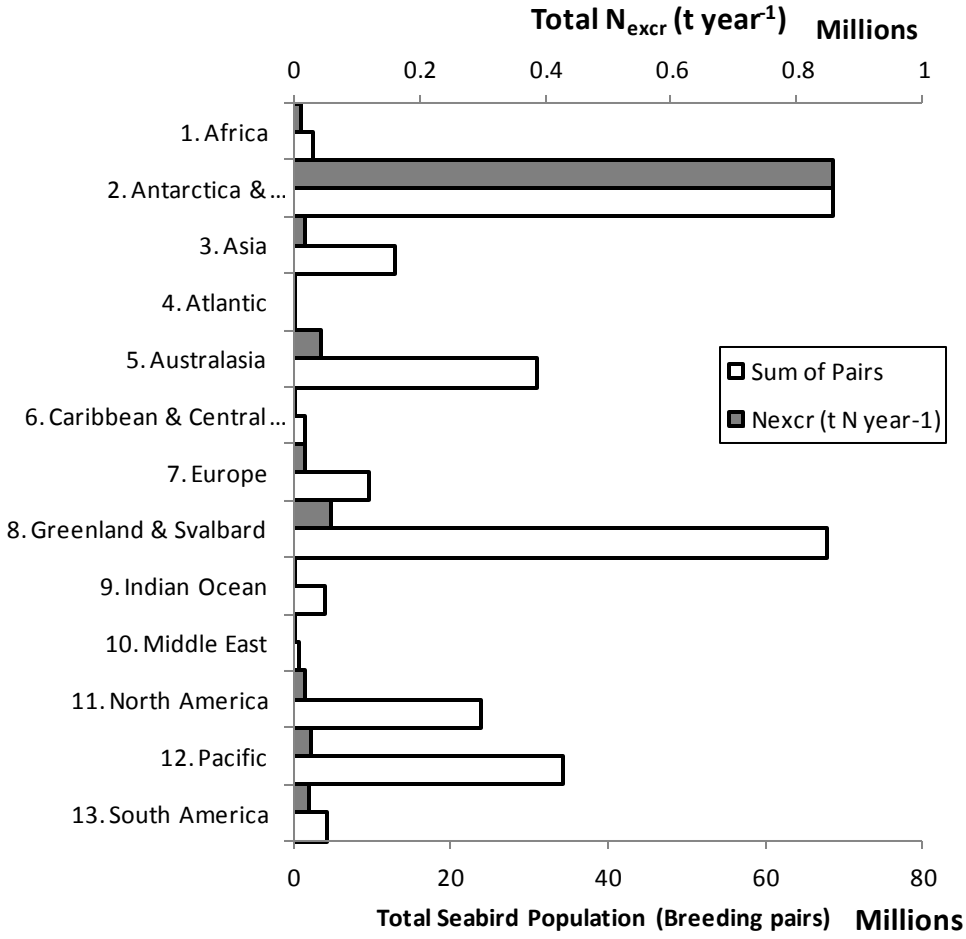

Figure 3.2 Regional estimates of breeding pairs of seabird and N excretion calculated in this study.

3.3.2 Global distribution of NH_3 emissions and temperature sensitivity

Regional estimates of NH_3 emissions are shown in Table 3.1, comparing the Scenarios assuming temperature independent and temperature dependent emissions. The temperature independent global NH_3 emissions are estimated at 404 Gg year^{-1}. When the temperature coefficient based on thermodynamics is

applied, this estimate is reduced to 83.1 Gg year^{-1}, because the major seabird breeding assemblages occur in cool circumpolar conditions, especially Antarctica and Southern Ocean. In these locations, average temperatures in the breeding season are approximately 5-10 °C lower than the UK measurements of Blackall et al. (2007), on which the temperature independent estimates are based. Overall, Antarctica and the Southern Ocean contribute 84% of the total NH_3 emissions in Scenario 1 (similar to the proportion of N excretion noted in Section 3.1), which is reduced to 79% in Scenario 3, and 61% in Scenario 2, as a result of the estimated temperature dependences.

Table 3.1 Variation in total seabird NH3 emission by region for: Scenario 1: temperature independent emission rates based on mid-latitude measurements; Scenario 2: combination of mid-latitude measurements with thermodynamic temperature dependence of emissions; Scenario 3, limited temperature dependence as mean of Scenarios 1 and 2.

	NH_3 Emission (Gg NH_3 Year^{-1})		
Region	Scenario 1	Scenario 2	Scenario 3
1. Africa	3.64	3.43	3.53
2. Antarctica & Southern Ocean	341	52.71	197.24
3. Asia	6.61	1.06	3.83
4. Atlantic	0.01	0.02	0.01
5. Australasia	5.09	3.18	4.14
6. Caribbean & Central America	0.97	2.40	1.69
7. Europe	5.94	2.37	4.16
8. Greenland & Svalbard	23	2.66	12.85
9. Indian Ocean	0.22	0.53	0.37
10. Middle East	0.57	1.41	0.99
11. North America	5.62	1.19	3.40
12. Pacific	2.51	6.01	4.26
13. South America	8.01	6.14	7.08
Total	404	83	244

The extent to which the estimated effect of thermodynamics alters NH_3 emissions with latitude is shown in Figure 3.3. The emissions at higher latitudes are

significantly reduced (Scenario 2) compared with the temperature independent model (Scenario 1).

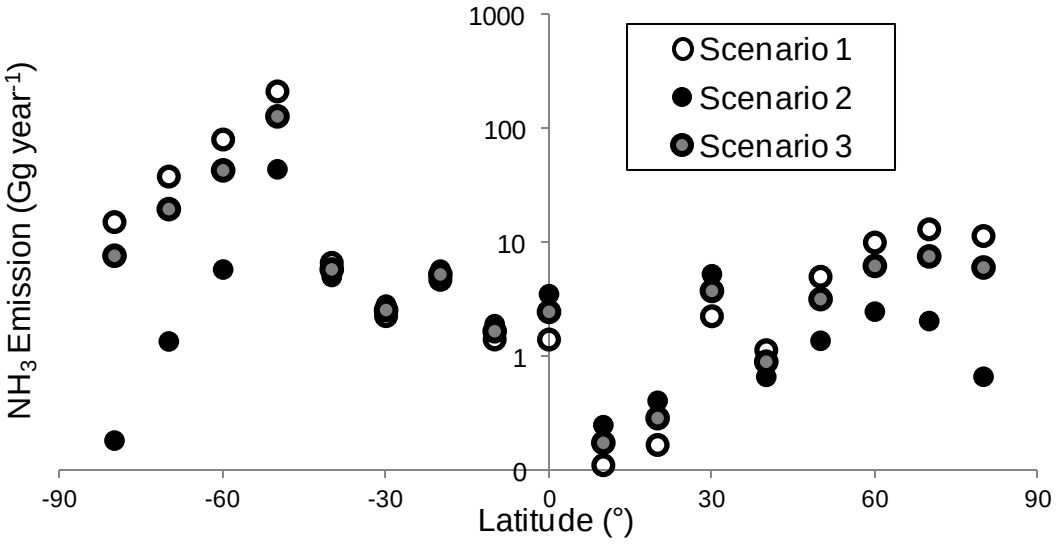

Figure 3.3 Latitudinal variation in global NH_3 emissions from seabird colonies based on the temperature independent bioenergetics model (Scenario 1) and thermodynamically adjusted bioenergetics model estimates (Scenario 2). The limited-temperature dependent NH_3 (Scenario 3) emission is the average of Scenario 1 and Scenario 2.

The emissions between 40 °S and 60 °S contributed 68 % of the overall NH_3 emission from seabird colonies (Scenario 3) and correspond to the large penguin populations on the sub-Antarctic islands. The lowest NH_3 emissions are between 0 °N and 20 °N and contribute 1 % to the global NH_3 emission from seabirds (Scenario 3). Even though these colonies are in a hot climate, the absolute emission values are relatively low, therefore changes to tropical birds emissions have little impact on the global estimate. Many tropical seabird species have a small body mass and nitrogen excreted at these colonies is insignificant when compared to the penguin colonies. Even though the NH_3 emission increases when thermodynamic effects are considered, the NH_3 emission at tropical seabird colonies remains small when compared to the emissions in the Southern Ocean.

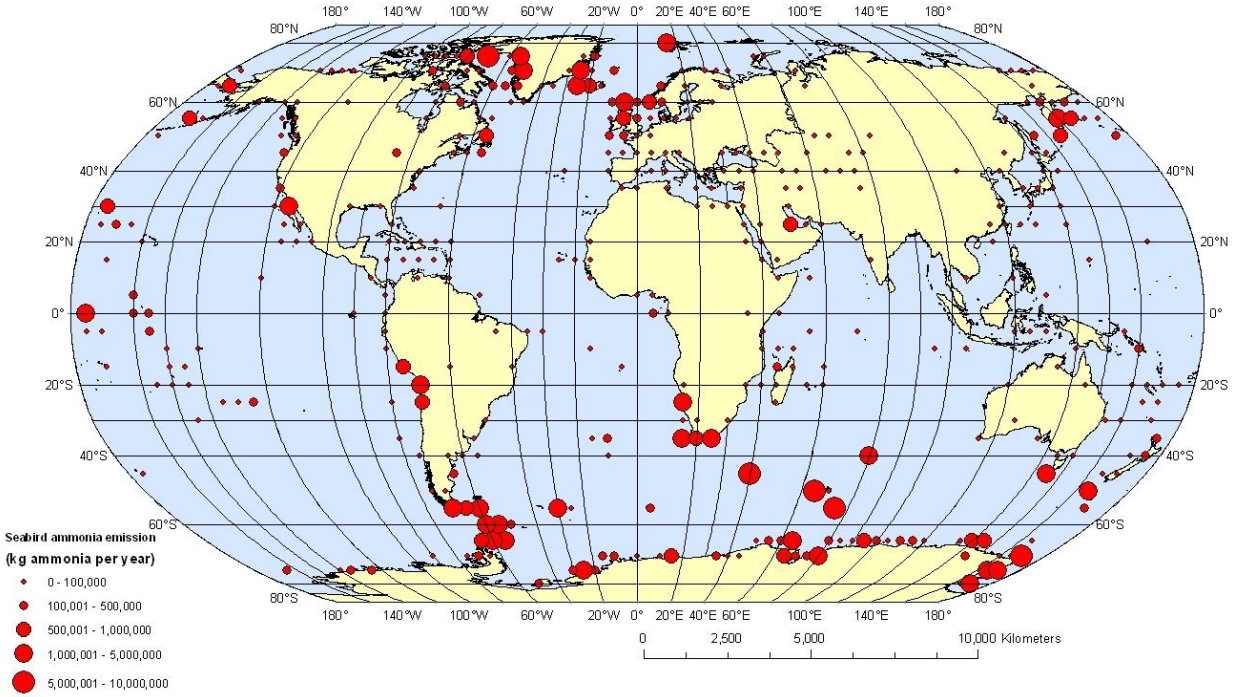

Figure 3.4 Estimated global distribution of NH_3 emissions from seabird colonies, using the mid-estimate between the temperature independent bioenergetics model and the thermodynamically adjusted bioenergetics model (Scenario 3). The results incorporate species and colony specific data on population size, birds' energy requirements, colony attendance, breeding success and estimated volatilization rates for guano deposited onto bare rock and vegetation. To show the distribution of the NH_3 emissions clearly, emissions in each 5° grid square have been summed.

Figure 3.4 shows the estimated global distribution of NH_3 emissions from seabirds using the limited temperature dependent model (Scenario 3), with a total NH_3 emission of 244 Gg NH_3 $year^{-1}$. The resulting emissions database itself is structured with emissions on a colony basis, as illustrated by the maps for the south Atlantic and north-west Europe (Figure 3.5).

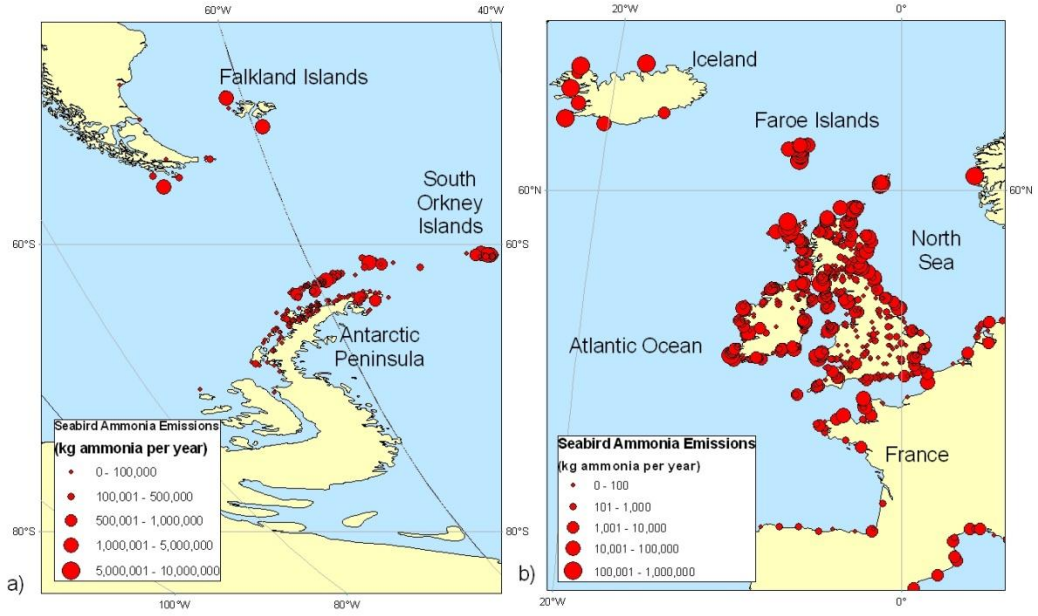

Figure 3.5 Illustrations of the global database, showing colony NH_3 emissions mapped on 0.1° resolution for a) the south Atlantic and b) NW Europe.

3.3.3 Main seabird species contributing to ammonia emissions

By far the largest contribution to NH_3 emission from seabird colonies was provided by a few key species, with 15 of 323 species included in the database accounting for 93.5% of the estimated NH_3 emissions (Scenario 3). Irrespective of the model scenario used, the largest contributors to the global NH_3 emission are the penguins. These birds, which only occur in the Southern Hemisphere, represent the top seven species in terms of NH_3 emission, with the penguin family (comprising a total of 17 species) contributing 80 % of the global NH_3 emission (scenario 3, with range 63-83% for scenarios 1 and 2, respectively). The penguins are numerous, have large body mass, long breeding seasons and many penguin species breed on rocky ground, all of which are characteristics that tend to be associated with high NH_3 emission.

Of the penguins, by far the most important is the Macaroni Penguin (*Eudyptes chrysolophus*), which alone accounts for an estimated 26% of global NH_3 emissions from seabird colonies. The three of the five largest colonies of Macaroni penguins in our database are South Georgia Island, Willis Island and Iles Kerguelen, with estimated annual emissions of 17.4, 16.1 and 6.5 Gg NH_3 $year^{-1}$ (Scenario 3), highlighting their importance as major point sources of NH_3 in the remote marine environment. At these colonies, using Scenario 3, emission densities within colonies range up to 2.7 kg NH_3 m^{-2} yr^{-1} and this refers to the 5.4 million pairs of Macaroni penguin in South Georgia.

3.4 Discussion

This chapter presents the first global map of NH_3 emissions from seabird colonies. It demonstrates substantial spatial heterogeneity, with the largest emissions occurring on the sub-Antarctic Islands throughout the Southern Ocean. The global map allows the location of the largest NH_3 emissions to be identified in relation to seabird contribution to N processes within local ecosystems, as well as a contribution to atmospheric emissions relevant for aerosol balance in remote marine atmospheres.

In an earlier study, Blackall et al. (2007) estimated temperature-independent global emissions from seabird colonies at 242 Gg NH_3 yr^{-1}, which is considerably lower than the temperature independent estimate of 404 Gg NH_3 yr^{-1} (Scenario 1) presented in this chapter. The contrast between the two studies reflects differences in the population estimates, primarily resulting from better data availability since Blackall et al. (2007). Although seabird population changes have also occurred over recent decades and contributed to the differences, such effects are considered secondary compared with the improved quality and coverage of count data.

This study therefore provides an update to previous seabird estimates and indicates a global seabird population of 261 million breeding pairs. Furthermore, the emission estimate noted above is based on breeding birds plus plausible estimates of the non-breeding component and annual chick production. Using Brooke's method, the present study estimates the total number of seabirds to be 1,180 million individuals, updating the previous estimates of 700 million (Brooke, 2004) and 900 million (Karpouzi et al., 2007).

A further difference in the estimate of global seabird colony emission reported here is the larger fraction attributable to penguins. Blackall et al. (2007) estimated that 57% of global ammonia emissions were due to penguin species, as compared with the new estimate from this study of 80% (63-85%), depending on the model scenario used. This larger contribution of penguins can be explained by improved information on population numbers (Trathan et al., 2007).

3.4.1 Temperature Dependence of NH_3 Emissions

Many environmental factors affect the size of NH_3 emission from seabird guano. For example, in Antarctic regions pH of guano, freezing-thawing processes and water amount have all been shown to affect NH_3 emission (Zhu et al. 2011). This study focuses on the global response of NH_3 emission to temperature. The importance of temperature was also shown by Zhu et al. (2011) who observed an exponential relationship between NH_3 emission and temperature (Figure 3.6).

This study used a relationship based on the combined Henry and dissociation equilibria for NH_3 to estimate an upper limit of the temperature dependence of global NH_3 emission by seabirds. According to the thermodynamic relationship, based on temperature alone, the global NH_3 emission from seabirds was estimated at 83 Gg $year^{-1}$ (Scenario 2).

Evidence of climate relationships for NH_3 emissions from animal manure spreading to agricultural land show that responses are not always related to temperature due to confounding interactions, such as altered rates of infiltration and surface run off, as well as of emission duration (Misselbrook et al., 2005). Such relationships are further complicated for avian guano, which is also dependent on water availability for its hydrolysis to produce NH_3. This suggests that, even though temperature may be an important driver in the production of NH_3, it may not be the only climatic variable to affect NH_3 emissions (Zhu et al., 2011). Blackall et al. (2007) suggested that water availability may be an important factor and that limited water in tropical conditions may counteract the temperature effect. To handle these issues, Scenarios 1 and 2 can be considered as limits, with Scenario 3 (limited temperature dependence) providing a best estimate of global NH_3 emission for seabirds at 244 Gg NH_3 $year^{-1}$. The temperature function for Scenario 3 is seen to agree well with the measured NH_3

emissions from ornithogenic soils OS_{DG2} and OS_{DG4} of Zhu et al. (2011) (Figure 3.6). As the temperature changes from 10 °C to 15 °C, the temperature function increases by 115 % in Scenario 2, 46 % in Scenario 3, 42 % for the OS_{DG2} soil and 35 % for the OS_{DG4} soil. Further measurements at colonies in different environments would allow climate factors other than temperature to be incorporated into the model.

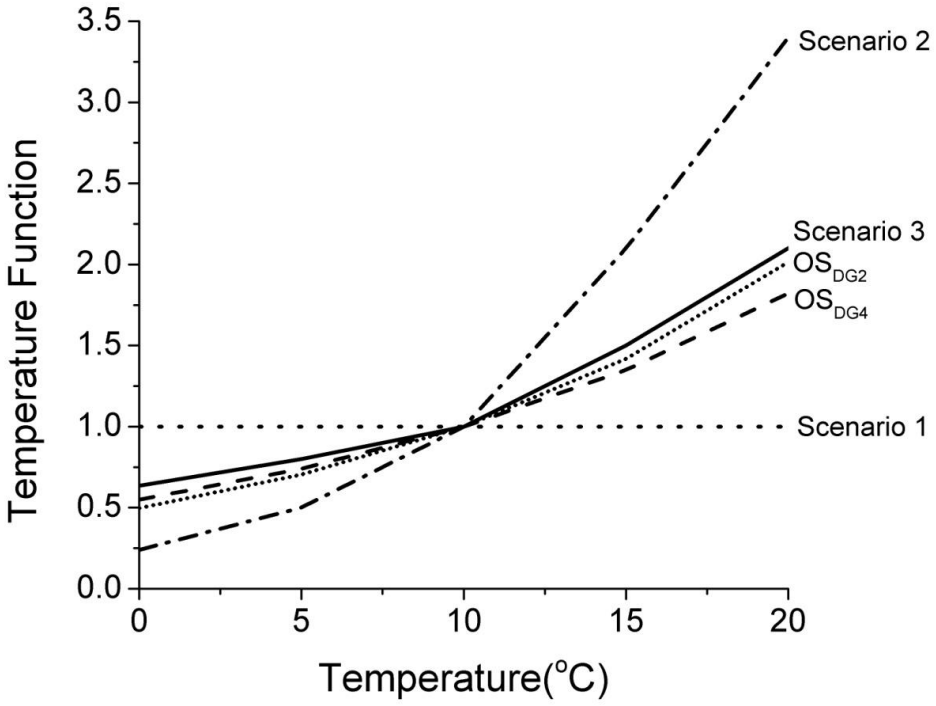

Figure 3.6 The graph shows the comparison of temperature functions from ornithogenic soils OS_{DG2} and OS_{DG4} of Zhu et al. (2011), the temperature independent bioenergetics model (Scenario 1), the thermodynamically adjusted bioenergetics model (Scenario 2) and the limited-temperature dependent model (Scenario 3). Temperature functions have been normalised to 10 °C.

3.4.2 Uncertainty in input data

The input parameters to the bioenergetics model are a source of uncertainty. The values described above will vary within and between years and across species' ranges. For example, breeding success in a given population shows considerable inter-annual variation, and the number of days spent at a colony often varies among populations depending on latitude and/or breeding conditions. Habitat will vary in relation to fine-scale heterogeneity across a colony and through the season, in particular, amongst precocial species, where chicks move away from

the nest soon after hatching. Whilst the importance of this variation across multiple temporal and spatial scales is fully recognized, this approach was to use a representative estimate of each parameter for each species, suitable for input to the global NH_3 emission model.

Bird population data are subject to large uncertainties, and these have a large impact on the estimates of NH_3 emissions. It is difficult to derive a global seabird population uncertainty from colony data because there is no standard method for reporting uncertainty. An attempt has been made at estimating the uncertainty in counts of seabird populations, based on the penguin population uncertainty estimates, since these are responsible for 80 % of the total NH_3 emission from seabirds. The uncertainty in the penguin population is ± 36 % (Woehler, 1993).

An uncertainty analysis was conducted on non-breeder attendance, the values of nitrogen content of the food, the energy content of the food, assimilation efficiency of ingested food and thermodynamic effects. Variation in non-breeder attendance corresponds to an uncertainty in NH_3 emission of ± 13 %. The uncertainty in NH_3 emission caused by E:N ratio of food is ± 5 % and A_{Eff} is ± 15 %. Table 3.1 shows the uncertainty in NH_3 emission associated with thermodynamic effects is ± 49 %. Combining these (using Scenario 3 as the best estimate) suggests that global seabird NH_3 emissions are 244 Gg NH_3 $year^{-1}$ within the range of 88 - 400 Gg NH_3 $year^{-1}$.

3.4.3 Magnitude of seabird ammonia emissions compared with other sources.

On a global scale, the estimated ammonia emissions from seabird colonies amounts to less than 2 % of the 13.8 Tg $year^{-1}$ NH_3 emission from all sources (EC-JRC/PBL, 2010). Seabirds are, nevertheless, relevant sources of NH_3 because they occur as large point sources in remote areas with otherwise low emissions.

The scale of seabird point sources can be gauged by considering colonies of Macaroni penguins. Given the rate of excretion of 6.7 kg N $bird^{-1}$ $year^{-1}$ at the colony, and a colony density of 17,000 individuals ha^{-1} results in colony excretion rates from Macaroni penguins at 114,240 kg N ha^{-1} yr^{-1}. Based on a literature search, this is by far the highest excretal / N input rate ever estimated. The

relatively high N excretion rate of seabirds is highlighted by its comparison with the average N excretion rate of broiler chickens of 0.18 kg N $bird^{-1}$ yr^{-1} (Misselbrook et al., 2000). This demonstrates that seabirds excrete a higher mass of nitrogen, relative to their body mass, than poultry. Prior to this study, the highest published nitrogen excretion rate was reported by Blackall et al. (2007) at 52,200 kg N ha^{-1} yr^{-1} from the Northern gannet *Morus bassanus* colony on the Bass Rock, Scotland. Combined with the large numbers of penguins, these excretion rates translate into extremely high emission rates. For example, on Willis Island, South Georgia, 1 million Macaroni penguins are estimated within an area of 5.9 km^2, providing an estimated emission of 15.6 [4.2 – 26.9] Gg NH_3 $year^{-1}$ from this single source. This is two orders of magnitude larger than the colony source strength of 0.15 Gg NH_3 yr^{-1} estimated by Blackall et al. (2007) for a colony of 100,000 Gannets (Bass Rock) in Scotland.

Such penguin colonies appear to be by far the largest biogenic point sources of NH_3 globally, even including anthropogenic agricultural sources. For example, the largest poultry installation of ~2 million birds emitting NH_3 at 0.1 kg NH_3 $bird^{-1}$ $year^{-1}$ (egg-laying system with infrequent belt cleaning) would provide a total emission of around 0.2 Gg NH_3 $year^{-1}$, which is similar to the emission from a major feedlot of 10,000 cattle emitting ~0.2 kg NH_3 $animal^{-1}$ $year^{-1}$. The only point source of NH_3 that has been estimated to exceed the value of 15.6 Gg $year^{-1}$ given here for Willis Island is the volcano Mount Mijake-jima in Japan, which was calculated to have released 400 Gg NH_3 $year^{-1}$ around the year 2000 (Uematsu et al., 2004, Sutton et al., 2008).

The seabird ammonia database can also be put into context by comparison with the spatial estimates of NH_3 emissions from other sources in the EDGAR database (EC-JRC/PBL, 2010). For the 0.1 x 0.1 degree locations where they occur, seabirds often account for > 99.9 % of NH_3 emissions from all sources and seabird NH_3 emissions are always more than 50 % of the local emissions in each 0.1 x 0.1 degree cell, showing the importance of seabird emission to local ecosystems.

3.5 Conclusions

This study has provided a first mapped estimate of the contribution that seabirds make to global NH_3 emissions. Overall, penguins dominate the global seabird NH_3 emission, accounting for around 80% of the emission, and with Macaroni penguins alone contributing an estimated 26%. The main locations of these emissions are the sub-Antarctic islands and around the Antarctic continent, where high ocean productivity supports a larger seabird biomass than in other areas.

The inclusion of a temperature factor substantially affects the size of the estimated NH_3 emission. However, results from this chapter suggest that temperature is not the sole driver of NH_3 emission (Figure 3.6). Further investigation needs to examine the role of other climatic drivers such as wind speed and precipitation. The main sources of uncertainty are thermodynamic dependence (± 49 %), variation in diet composition (± 23 %), non-breeder attendance (± 13 %) and seabird population (± 36 %). Combining these sources of error provides a global best estimate of NH_3 emission from seabird colonies of 244 [88 to 400] Gg NH_3 $year^{-1}$. Although amounting to less than 2 % of total global emissions, seabird NH_3 emissions are relevant because of their occurrence in remote regions where they are the main NH_3 source, in the form of discrete "hot-spots", leading to intense local impacts on terrestrial ecosystems.

The anticipated temperature dependence of NH_3 emissions also highlights their likely sensitivity to global climatic change. Temperatures are increasing in many parts of the Southern Ocean and the Antarctic Continent (IPCC, 2007). Changes in temperature could result in changes to the nitrogen cycle of sensitive ecosystems, decreased food supplies for the seabirds and resultant population declines. A better understanding of how climate drives NH_3 emission may help to understand some of the challenges that these ecosystems face.

Chapter 4 Parameterization of avian derived NH_3 emission from seabird colony substrates

4.1 Introduction

NH_3 gas can be re-absorbed by either the ground or foliage before becoming part of the atmosphere (Sutton et al., 1995; Misselbrook et al., 2000). As such, it is important to define differences in substrate type when comparing emissions from different locations. Seabirds nest on a range of substrates, and these can be broadly defined as: solid rock, vegetation and burrow (Wilson et al., 2004; Blackall et al., 2007). However, the global seabird database presented in Chapter 3 indicates that seabirds also nest on soil, sand and ice. Wilson et al. (2004) derived a habitat fractional release parameter (F_{hab}) to describe the release of NH_3 from guano excreted onto bare rock, soil and overlying vegetation or inside burrows. However, the estimates for F_{hab} were identified as potential sources of error by Wilson et al. (2004) in their calculation of the UK NH_3 emission from seabirds, especially as they were based on expert judgment and unpublished field measurements.

This chapter uses a controlled environment chamber to investigate the effects of climate and nesting substrate on NH_3 emission. While the focus is on evaluating the habitat fractional release parameters (F_{hab}) derived by Wilson et al. (2004), the chapter is also interested in providing evidence for relationships between climate and NH_3 emission. The following sections detail the current understanding and outline the experimental approach used in this chapter.

4.1.1 Nitrogen excretion

Birds excrete nitrogen in the form of uric acid ($C_5H_4N_3O_3$), which is relatively insoluble and must undergo bacterial transformation to urea and subsequently NH3 before it can potentially volatilise to the atmosphere as gaseous NH_3 (Purves et al., 2003). The rate of NH_3 emission depends on the substrate (e.g. rock, soil, vegetation) onto which the uric acid is excreted (Wilson et al., 2004, Blackall et al., 2007). Once the NH_3 is in gas phase, it can be re-absorbed by either the ground or foliage or dispersed into the atmosphere (Figure 4.1) (Sutton et al., 1995a; Misselbrook et al., 2000).

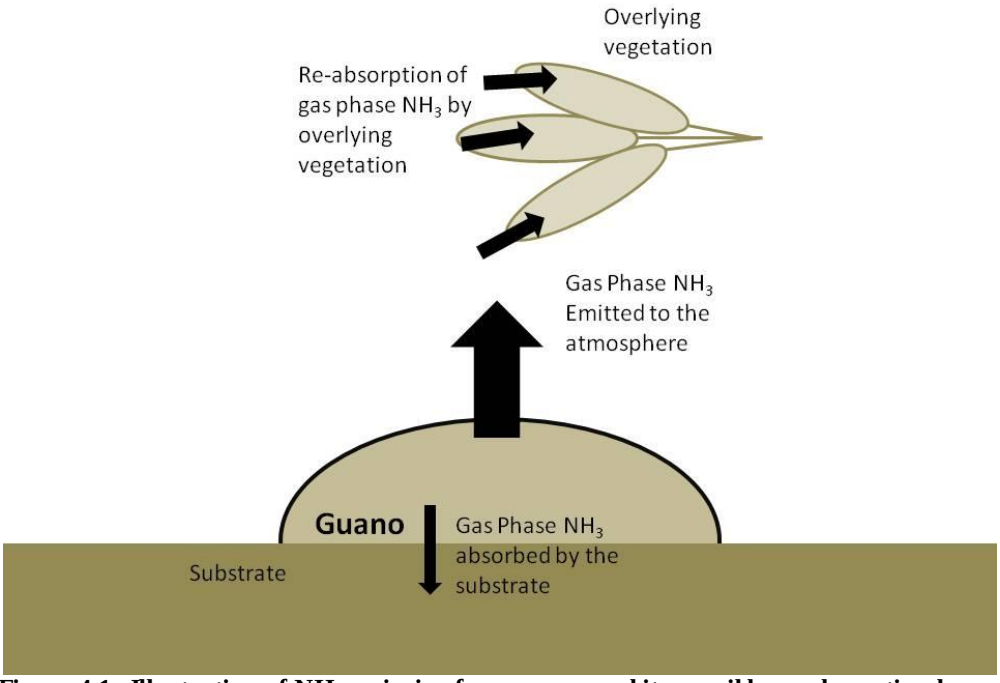

Figure 4.1 Illustration of NH_3 emission from guano and its possible re-absorption by an overlying canopy.

Table 4.1 shows the Wilson et al. (2004) habitat fractional release parameters (F_{hab}) to describe the release of NH_3 from guano excreted onto bare rock/soil, overlying vegetation or inside burrows. All F_{hab} factors are compared to the ideal case, F_{hab} = 1, where all emitted NH_3 is dispersed into the atmosphere and none re-absorbed by either substrate or over-lying vegetation.

Table 4.1 F_{hab} values for rock, vegetation and burrow nesters (Wilson et al., 2004)

Nesting Substrate	Habitat fractional release of NH_3 (F_{hab})
Rock	1.0
Vegetation	0.2
Burrow	0.0

Blackall et al. (2007) incorporated F_{hab} values from Wilson et al. (2004) to estimate the global NH_3 emissions from seabirds to be 242 Gg NH_3 $year^{-1}$. However, the inherent uncertainties in these F_{hab} values potentially introduced significant error in the global seabird NH_3 emissions estimate of Blackall et al. (2007). Also, the range of habitats in the global population is wider than that in the UK, additionally including sand, soil and ice. Global seabird nesting substrates are summarised in Table 4.2, which shows that most birds nest on the

substrates for which values of F_{hab} have been previously estimated by Wilson et al. (2004). However, 15% of birds nest on sand and 3% nest on soil. These birds were assigned F_{hab} values for vegetation, which potentially results in inappropriate F_{hab} values for 47 million pairs of breeding birds. For example, Sooty Terns (*Sterna fuscata*) are the second most abundant species globally, with 35 million pairs, and they nest on sand, but were defined as vegetation nesters by Blackall et al. (2007)..

Table 4.2 Nesting behaviours of seabirds globally

Substrate	Nesting pairs globally (million)	% Global Population
Burrow	1.7	0.6
Ice	0.4	0.2
Rock	157.4	60.4
Sand	40.0	15.4
Soil	8.1	3.1
Vegetation	53.1	20.4

Objectives of this study

In the present study, a homogenous guano source was used to perform a set of controlled laboratory experiments using different substrates. These experiments were carried out to determine the accuracy of the F_{hab} values used in Wilson et al. (2004) and to quantify F_{hab} for other main nesting substrates (sand and soil). All of the main nesting substrates were tested (rock, vegetation, nests made from plant materials, burrow, sand and soil) except for ice, which was impractical because sub-zero temperatures were not achievable in the experimental chamber.

The time-averaged experiments presented in this chapter followed the method of Twigg (2005). The fraction of NH_3 emitted from different substrates was parameterised using a fast response gas phase NH_3 analyser in a controlled environment. The results are used to recalculate the global NH_3 emission from seabirds for new values of F_{hab} in Chapter 6 which allows the modelling of global guano emissions to be better constrained.

4.2 Methods

To study relative NH_3 emissions from guano on different substrates under controlled conditions, experiments were conducted within a small Perspex^{TM} chamber (0.6 m x 0.6 m x 0.6 m). The experimental setup is shown schematically in Figure 4.2 and was previously used to study emissions from liquid manure slurry of cattle (Twigg et al., 2011). Prior to entering the chamber, NH_3 was removed from the ambient air by a charcoal scrubber. The airflow was split to allow the relative humidity (*RH*) of the system to be modified. One air stream was dried through a silica gel pack and the other flow humidified to ~100% *RH* by passing the flow through a bubbler. The airflow rate of each stream was controlled using a needle valve, which was adjusted until the relative humidity sensor gave the relevant reading. Equilibration prior to the acceptance of a settled humidity level took between thirty minutes and 1 hour.

Ambient air was flowed through the chamber at 8 L min^{-1}. The flow was measured by a ball flow meter and the estimated error was 12 %. The guano samples (described in detail below) were placed in the chamber and allowed to equilibrate with the ambient temperature and *RH*. Both temperature and *RH* inside the chamber were measured throughout the experiment, where the thermostatically controlled climate room maintained a constant temperature and was monitored by a Campbell Scientific HMP45C Probe with an accuracy of ± 0.5 °C. The Campbell Scientific HMP45C Probe also measured *RH* between 0.8 to 100 % with an accuracy of ± 1 %. Residence time of the air in the chamber was 27 minutes. The air downstream of the chamber was sampled by a photoacoustic gas phase NH_3 analyser (Nitrolux, Pranalytica Inc., Santa Monica, CA, USA) at 0.5 L min^{-1}. The Nitrolux has a sensitivity of 1 ppb, range of detection from 0 – 2000 ppb and measurement update rate of 45 s. Exhaust air was scrubbed by charcoal and passed through a water bubbler with biocide for health and safety purposes to remove potentially harmful microbes and fungi.

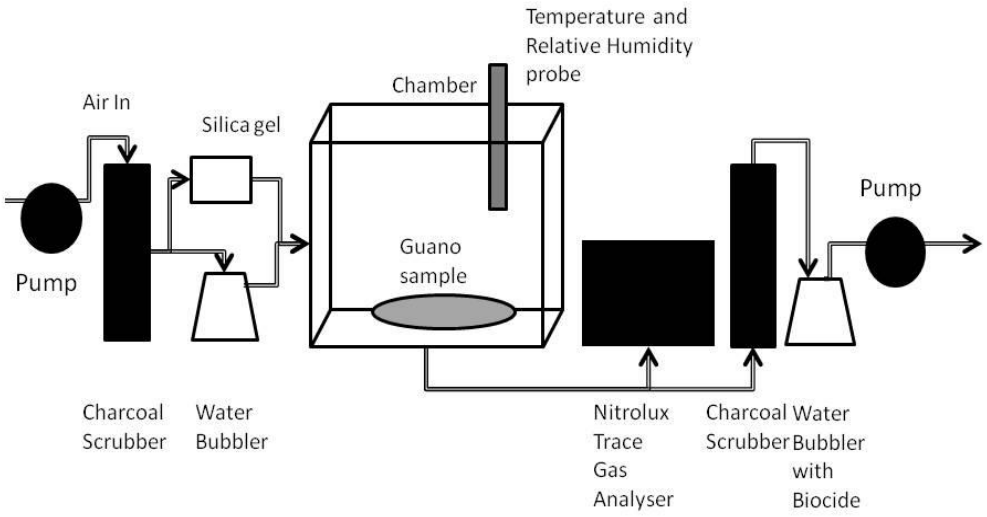

Figure 4.2 Setup of the experimental chamber to measure NH_3 concentrations in air above guano. Air is cleaned by a charcoal scrubber going into the chamber with the relative humidity controlled by a water bubbler and silica gel. Air from the chamber is sampled at 0.5 L min^{-1} by a Nitrolux™ trace gas sampler. Exhaust air is scrubbed by charcoal and passed through a water bubbler with biocide.

4.2.1 Seabird guano

In order to study the emissions from guano, a suitable sample type had to be identified. Several types of guano were considered for use in this study. Fresh guano collected from the penguin enclosure at Edinburgh zoo was initially used. However, logistical difficulties associated with collecting the fresh guano from the penguin enclosure proved to be too problematic and insufficient quantities were obtainable for repeatable experiments to be carried out. Dried seabird guano was therefore purchased. The guano used originates from Peru, and is marketed in the USA as a household fertiliser (Sunleaves Garden Products, Bloomington, IN, USA, www.sunleaves.com). Large colonies of Peruvian boobies (*Sula variegate*), Guanay cormorants (*Phalacrocorax bougainvillii*) and South American brown pelicans (*Pelecanus occidentalis thagus*) are found on islands off Western Peru and South West Chile. In general, these birds feed on Peruvian anchovy (*Engraulis ringens*) and Chilean sardine (*Sardinops sagax*). Guano from these seabird colonies dries naturally, and its nitrogen content is largely conserved in a climate where water is scarce, preventing NH_3 emission in the field.

Preparation of guano slurry

Tests were conducted to ensure the NH_3 from the slurry did not vary during the experiment. Different amounts of water were added to 10 g of guano to make the slurry. Each slurry test sample was placed on a non-absorbent tile in the chamber, and the NH_3 concentrations measured for 17 hours to ensure constancy between guano samples. This allowed the ideal mixture of guano and water to be determined for substrate experiments.

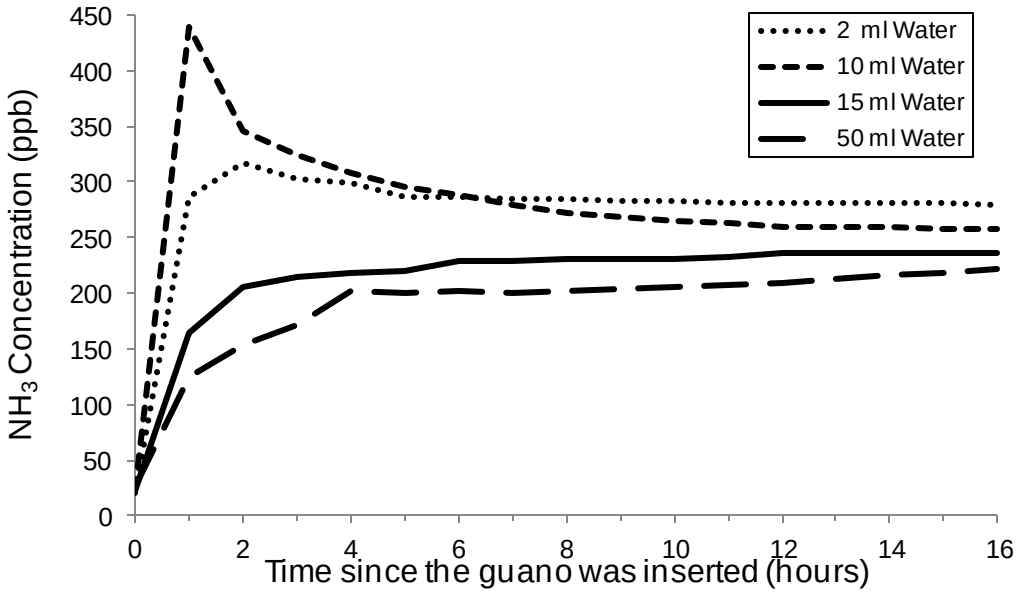

Figure 4.3 The NH_3 concentration over 17 hours of multiple guano slurry samples of different water quantities (*2ml, 10 ml, 15ml* and *50 ml*). 10 g of seabird guano is used in each trial. The relative humidity remained at 60 % and air temperature remained at 15 °C.

The measured concentration within the chamber that changed least was the slurry made from 10 g guano and 15 ml water (Figure 4.4). Following these results, this is the slurry that was added to the test substrate in the following experiments. The slurry samples were made immediately before the experiment to reduce any NH_3 loss after the water was added. For each experiment, the guano slurry was placed on the test substrate (10 cm x 10 cm) in the centre of the chamber. The background NH_3 concentration of the substrate was measured for 24 hours prior to adding guano. During each experiment, the temperature and *RH* were maintained, and the evolution of the NH_3 concentration in the chamber was observed over a period of 24 hours. A steady state NH_3 concentration within the chamber was

taken after the guano had equilibrated with the conditions inside the chamber and the substrate.

4.2.2 NH_3 concentration measurements

Measuring the background NH_3 concentration of the test substrates alone

The concentration measured in this experiment was the background of NH_3 concentration in air plus any NH_3 emitted from the substrate. The NH_3 concentration of air within the chamber was measured in a trial for 24 hours with only the test substrate in the chamber. The average background NH_3 concentration of the air above the test substrate was calculated as the average of duplicate trials and an uncertainty was calculated from the variation in NH_3 concentration measured during steady state.

Measuring NH_3 concentration in the chamber with guano on the test substrate

Guano slurry was used to examine the effects of substrate on the emission rate of NH_3. In all tests, the background NH_3 concentration in the chamber was measured prior to each experiment, as per the trial conditions outlined above, and subtracted from the measured NH_3 concentration. In each experiment, new guano slurry was prepared and experiments were duplicated to find the average NH_3 concentration during steady state emission and associated uncertainty. The temperature and *RH* inside the chamber were kept constant at 18 °C and 60 %, respectively.

The F_{hab} value for each substrate is calculated by comparing the total emission from the guano on the substrate to the total emission of guano on rock. The emission of NH_3 from rock is taken as 100%, based on the assumption that no NH_3 is absorbed by the surface when guano is put onto rock, following the method of Wilson et al. (2004). The NH_3 emission (F, μg m^{-2} s^{-1}) was calculated from the steady state concentration of NH_3 (X_c, μg m^{-3}), the background concentration of substrate (X_{bgnd}, μg m^{-3}), the air flow (V, m^3 s^{-1}) and the sampling area (A, m^2) (Equation 4.1). For this experiment the flow rate was 8 l min^{-1} and the sampling area was 5 cm x 5cm.

$$F = \frac{(X_c - X_{bgnd})V}{A} \qquad (4.1)$$

The test substrates studied were rock, soil, sand, vegetation, burrow and nest. The rock and sand were taken from a nearby beach (Portobello, Scotland, 55.96 °N, 3.12 °W). The rock was washed in fresh water to remove any living organisms or vegetation. The sand was washed and picked through to remove any living or dead organisms or other obvious sources of nitrogen. Unfertilized soil from a garden in Peebles, Scotland was used as the soil substrate. The vegetation substrate was an unfertilized sod of turf (30 x 60 x 20 cm) from the same garden in Peebles, Scotland. The burrows were constructed from turf sod (30 x 60 x 20 cm), also from the garden in Peebles, Scotland, with a 10 cm x 10cm x 10 cm burrow constructed 10 cm below the turf surface. The nesting materials were sticks, twigs and moss gathered on Portobello beach.

4.3 Results

4.3.1 Background concentrations of substrates

Table 4.3 Background NH_3 concentration and range of uncertainty in NH_3 emission between duplicate experiments (expressed as a percentage) from substrates: burrow, nest, rock, sand, soil and vegetation.

Substrate	Background NH_3 concentration after 23 hours (ppb)	Range of uncertainty in NH_3 concentrations between duplicate experiments (%)
Burrow	56.8	26
Nest	74.5	12
Rock	33.9	18
Sand	33.4	12
Soil	29.1	17
Vegetation	29.0	19

After 23 hours, the highest NH_3 background concentration in the chamber was measured for the nest substrate at 75 ppb with a range of ± 2 % between duplicate experiments. The NH_3 concentration in the chamber containing the burrow substrate was lower than the nesting materials substrate, at 57 ppb ± 56 %. However, the variability of NH_3 concentration between burrow substrate experiments was the highest of all test substrates (26 %). The NH_3 concentration of the air inside the chamber containing other substrates (rock, sand, soil and vegetation) was similar (Figure 4.5 and Table 4.3).

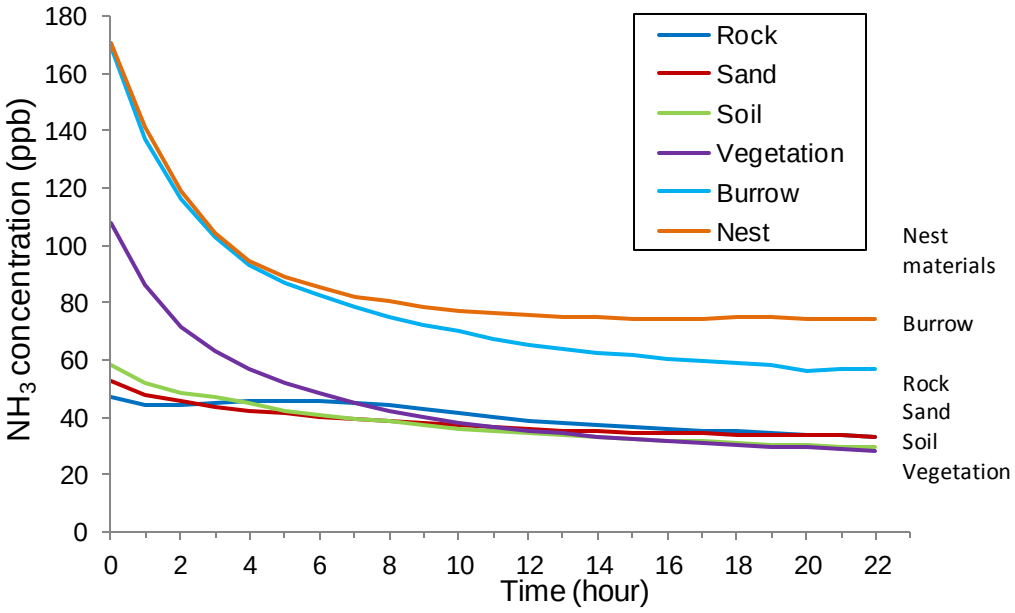

Figure 4.4 Background NH_3 concentration (ppb) measured for different substrates (rock, sand, soil, vegetation, burrow and nesting materials) with no added guano. Temperature = 18 °C and RH = 60 %.

4.3.2 NH_3 emission from guano on a substrate

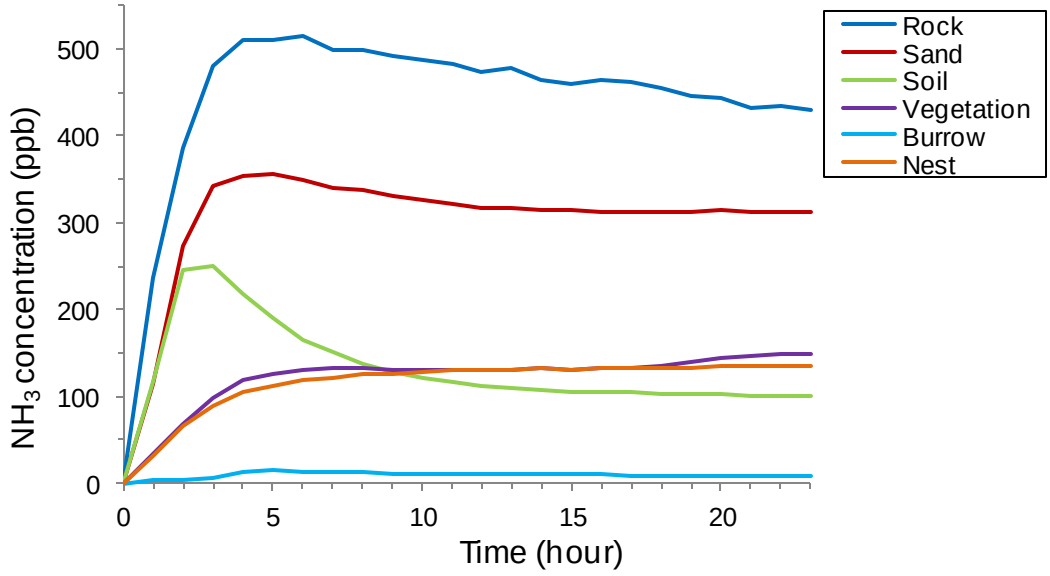

Figure 4.5 The NH_3 concentration (ppb) measured over 22 hours from guano slurry on top of a substrate (rock, sand, soil, vegetation, nesting materials or placed in a burrow). The air temperature is constant at 18 °C and RH = 60 %. In each trial, guano slurry is made from 10 g of dried guano and 15 ml water.

The guano was added on top of nesting substrates (or inside, in the case of the burrow) and the NH_3 concentration was measured over a period of 17 hours

(Figure 4.6). The substrate giving the highest NH_3 concentration in the chamber after 23 hours was the guano on rock, at 430 ppb with a range of ± 17 % between duplicate experiments. The lowest NH_3 concentration in the chamber was measured for the guano inside the burrow at 7 ppb with a range of ± 26 %. After only seven hours, the NH_3 concentration stabilized in the chambers where guano was on the vegetation and nest substrates. For both the rock and the sand substrates, the chamber NH_3 concentration initially peaked and then stabilized after 20 hours. The chamber NH_3 concentration from the guano in the burrow was almost indistinguishable from the background concentration of the substrate.

Table 4.4 NH_3 concentrations from guano on a substrate minus the substrate background concentration after 23 hours. The chamber was constant at 12.5 °C and RH =60 %. NH_3 concentrations are averaged from duplicate experiments for each substrate.

Substrate	NH_3 concentration from guano on a substrate minus background concentration after 23 hours ($mg\ NH_3\ kg^{-1}\ h^{-1}$)	Range of uncertainty in NH_3 concentration between duplicate experiments (%)	Total NH_3 emitted in 23 hours (g)
Burrow	7.6	26	9.49
Nest	135.5	12	6.45
Rock	430.2	17	3.89
Sand	311.7	12	2.56
Soil	100.8	17	0.21
Vegetation	149.6	18	2.55

Of the different substrates tested, the chamber NH_3 concentration was highest for the rock substrate, as expected because there was no re-absorption of NH_3. On the rock, there was an initial peak in NH_3 concentration followed by a decreased rate after 6 hours. The NH_3 concentration of air above sand and soil were initially similar. For the sand, a peak in NH_3 emission occurred after four hours.

4.4. Discussion

4.4.1 Background concentration of substrates

The chamber concentrations of NH_3 from the bare soil and the vegetation (grass/turf) substrates were similar to each other, which was expected because NH_3 emissions from these substrates are caused by decaying matter in the soil

humus (Larsson et al., 1998). The chamber concentration of NH_3 from the burrow substrate was higher than from the vegetation substrate, because of the larger surface area of decaying matter in humus within the soil. The concentration from the nesting materials was also high relative to other substrates and caused by NH_3 emission from decaying leaves and twigs in the nesting material (Sutton et al., 1995).

4.4.2 Guano addition to substrates

The soil has a more marked interaction with the guano as the NH_3 concentration in the chamber decreased sharply three hours after the guano was placed on the soil (Figure 4.6). This may be caused by cation-exchange or other reactions within the soil matrix reducing emission. The effect is similar but much less marked when guano is added to the sand, which may be due to lower levels of potential cation exchange sites.

The difference between total NH_3 emitted from guano on vegetation is only 28 % of that observed for bare rock (Figure 4.7). This may be because vegetation re-absorbs NH_3 that is emitted from guano. NH_3 enters through the stomata in the leaves and is used by the plant for plant growth (Sutton et al., 1995; Stulen et al., 1998). However, the emission uptake from the guano on the artificial nest was similar to the vegetation, which suggests other factors such as physical capture of NH_3 by the materials may be important. The NH_3 emitted from guano in a burrow in the chamber is the lowest of the substrate types tested, with nearly total re-absorption of NH_3 by the soil on the walls and roof of the burrow.

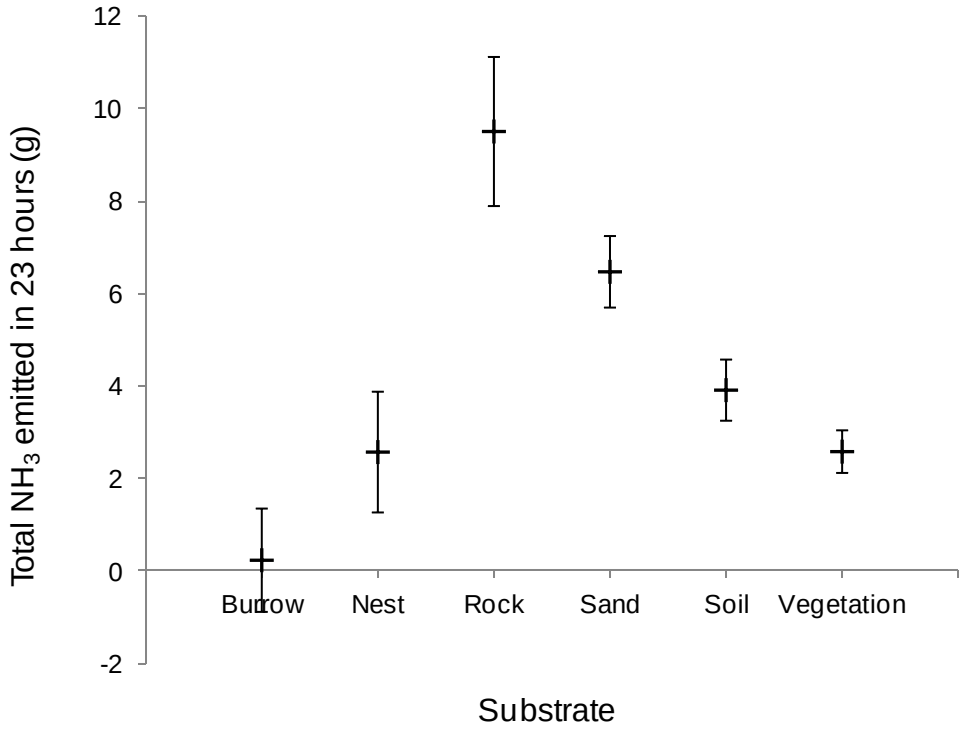

Figure 4.6 Total NH_3 emitted in 23 hours from guano on six different test substrates over 17 hours. The air temperature remained constant at 18 °C and RH at 60 %. The guano slurry was 10 g of dried guano and 15 ml water.

4.4.3 Implications for global seabird NH_3 emissions

The results of this study are used to calculate new values of F_{hab}. Table 4.5 shows that the estimates made by Wilson et al. (2004), based on expert judgment, match very closely to those measured in a controlled environment. F_{hab} for sand and soil are estimated in this study for the first time, as these substrates were not considered by Wilson et al. (2004). The estimates for these additional substrates have an impact on the global NH_3 emission from seabirds, as these were previously grouped as being vegetation nesters. However, the experiments in this study demonstrate the marked difference between NH_3 concentrations measured on sand or soil and vegetation. This study estimates the values for F_{hab} as 0.68 and 0.41 for sand and soil, respectively.

Table 4.5 Comparison of old and new re-absorption coefficients (F_{hab})

Substrate	Wilson et al. (2004) F_{hab}	New F_{hab} (this study)
Rock	1.00	1.00
Sand	-	0.68
Soil	-	0.41
Vegetation	0.20	0.27
Burrow	0.00	0.00
Nest	0.20	0.27

4.4.4 Revised global NH_3 emission

The global NH_3 emission for seabirds, presented in chapter 3, was 244 [88 to 400] Gg NH_3 $year^{-1}$, using F_{hab} values of 1 for rock, 0.2 for vegetation and nests and 0 for burrows. In this estimate, a value of 0.2 is used for sand and soil and the F_{hab} value for ice is taken as 1, as used by Blackall et al. (2007). A recalculation of the NH_3 emission estimates for seabirds globally, using F_{hab} values derived in this study, results in a global NH_3 emission for seabirds of 257 [102 to 412] Gg NH_3 $year^{-1}$, an increase in the total emissions of 5%. Even though the NH_3 emission has only changed by 5%, the impact is more significant when considering the individual colonies.

Changes to F_{hab} have the largest effect on the calculation of the NH_3 emission from the colonies where the adults nest on sand and the chicks are raised in a scrape (e.g. Sooty terns). For example the change of F_{hab} for birds on sand increases the calculated NH_3 emissions from these colonies by 3.4 times compared to the estimate in Chapter 3.

4.4.5 Significance of F_{hab}

The aim of this study was to quantify F_{hab} for the main seabird nesting substrates (rock, sand, soil, vegetation, burrow and nest). Estimated F_{hab} values were a source of uncertainty in previous global seabird NH_3 emission estimates (e.g. Blackall et al., 2007) and in the estimate from Chapter 3 (244 Gg NH_3 yr^{-1}). The F_{hab} values measured in this study are used to recalculate the global NH_3 emission as 257 Gg NH_3 yr^{-1}. This study has shown that the previous F_{hab} estimates were very close to the measured values, and the addition of the soil and sand substrates

does not have a large effect the global seabird NH_3 emission because 60 % of seabirds nest on rock. However, this study shows that the measurement of F_{hab} values has a large impact on the calculation of local NH_3 emissions, where seabirds nesting on sand emit 3.4 times more NH_3 than previously estimated and soil nesters emit twice as much. For example, the NH_3 emission estimates from the Sooty tern colony (population 160,000 pairs) on the Chagos Archipelago in the Indian Ocean changes from 6.3 Gg NH_3 $year^{-1}$ to 21.4 Gg NH_3 $year^{-1}$. Thus, sand and soil nesting seabirds are likely to make a much greater contribution to the magnitude of global seabird NH_3 emissions than previously estimated. This may be may be particularly significant at the local scale and help to identify NH_3 emission hotpots in remote locations.

Chapter 5: Measuring ammonia emissions from seabird colonies

5.1 Introduction

Prior to this study, NH_3 concentrations have been measured at seabird colonies and range from 0.7 to 1330 µg NH_3 m^{-3} (Böttcher, 1996; Blackall et al, 2004, 2007; Schmidt et al., 2010) using both passive (Böttcher, 1996; Blackall et al. 2008; Schmidt et al. 2010) and active techniques (Blackall et al., 2004, 2007). The highest reported NH_3 concentrations at a seabird colony were measured at the Northern gannet colony on the Bass Rock, Scotland, where NH_3 concentrations ranged from 30 to 1330 µg NH_3 m^{-3} (Böttcher, 1996). The smallest reported NH_3 concentrations from a seabird colony were measured over an Atlantic puffin colony on the Isle of May, Scotland (0.4 to 7.5 µg NH_3 m^{-3}) (Blackall et al., 2008). The measurements on the Bass Rock and the Isle of May were both made using passive ALPHA samplers (Tang et al., 2001).

The study by Blackall et al. (2004; 2007) made the first NH_3 emission estimates from a seabird colony using boat-based NH_3 concentration measurements. The NH_3 concentrations were measured by an AMANDA gas analyser (Blackall et al, 2004, 2007) downwind of the colony. Blackall et al. (2007) used NH_3 concentration data and meteorological data as input to an inverse-dispersion model to estimate NH_3 emissions from the Northern gannet colony on the Bass Rock and the Common guillemot colony on the Isle of May. NH_3 emissions were estimated at 26.1 kg NH_3 $hour^{-1}$ (range 6.3 – 88.6 kg NH_3 $hour^{-1}$) for the Bass Rock and 4.5 kg NH_3 $hour^{-1}$ (range 1.0 – 15.5 kg NH_3 $hour^{-1}$) for the Isle of May. The differences show the large variability of NH_3 emission rates. Blackall et al. (2007) postulated that the emission rate depended on the interacting effects of water availability, temperature and wind speed.

Major challenges of the campaign of Blackall et al. (2007) were logistical difficulties presented when making boat-based measurements. NH_3 concentration measurements were made at least 1 km from the colony and sufficient wind was required to blow NH_3 from the source towards the measurement instrument, but not too much wind to make measurement difficult on a small boat. It was observed that waves caused by wind could affect the accuracy of the AMANDA

gas analyser. Suitable days for measurement were few and measurement data were subject to wave-induced uncertainties. As such, it would be beneficial to develop alternative land-based methods.

The approach to make land-based measurements is developed in this chapter. Similar to the boat-based approach, land-based campaigns are conducted by measuring NH_3 concentration, meteorological and micrometeorological data, for calculating NH_3 emissions from seabird colonies. NH_3 concentrations can be measured by active techniques (using ALPHA samplers, see section 2.6.1) or active techniques (using AiRRmonia or Nitrolux instruments, see section 2.6.2). The WindTrax atmospheric dispersion model can then used to calculate the NH_3 emission from the colony (see section 2.4.5). The field sites were chosen to be suitable for atmospheric dispersion modelling, i.e., were required to have relatively flat topography and smooth surfaces (maximum roughness length of 15 cm in WindTrax). The field sites also needed to have sufficiently large seabird derived NH_3 emissions in combination with low background emissions from other possible NH_3 sources. In addition, the sites had to be accessible for setting up and operating the measurement instruments safely, as the instruments are both difficult to move and require attention several times a day.

The chosen field sites were are also selected to represent a typical range of climates where seabird colonies can be found across the globe: tropical, temperate and sub-polar.

In summary, this chapter aims to further develop field-based methods to estimate NH_3 emission from seabird colonies by measuring NH_3 concentration data and meteorological data under a range of climatic conditions, with NH_3 emission estimates generated by inverse-modelling approaches. For the purposes of this thesis, the NH_3 emission estimates measured at each of the seabird colonies are used in Chapter 6 to validate NH_3 emission models, with a view to using the most suitable model as a method for calculating global NH_3 emissions from seabirds (Chapter 7).

5.2 Methods

5.2.1 Study sites

NH_3 emission estimates were made at five seabird colonies in a range climate zones, Michaelmas Cay on the Great Barrier Reef, Signy Island in the South Orkney Islands, the Isle of May in Scotland, Ascension Island in the South Atlantic and Bird Island in South Georgia (Figure 5.1). The following paragraphs give brief descriptions of the field sites. To ensure the information for each field campaign is kept together within the chapter, a detailed description of each site is given in Section 5.3.

Michaelmas Cay

Michaelmas Cay (16.60 °S, 145.97 °E) is a remote seabird colony on the Great Barrier Reef in Australia. It is an uninhabited island 35 km north-east of Cairns and visited daily by tourist boats. The island is relatively flat (maximum elevation 3.5 m) and partially covered by low lying vegetation. During the breeding season it is visited by 20,000 breeding birds (Sooty Terns, Crested terns, Common Noddies and Lesser-crested terns) (W. MacFarlane, EPA Queensland, pers. comm.). The climate is wet and hot, with summer temperatures averaging around 28 °C, an average relative humidity of 85 % and strong prevailing winds (average 6 m s^{-1}) (NOAA, 2010). A passive NH_3 sampling campaign was conducted between November 2009 and May 2010.

Ascension Island

Ascension Island (7.99 °S, 14.39 °W) is a small volcanic island in the Atlantic Ocean. NH_3 concentrations and meteorology were measured at a large Sooty tern colony on the Wideawake Fairs, in Mars Bay (100,000 pairs). The site is relatively easy to access and the climate is dry and hot (average temperature of 27 °C, average humidity of 72 % and average wind speed of 5 m s^{-1}). A measuring campaign using both continuous active and passive instrumentation was carried out between 22nd May 2010 and the 7th July 2010.

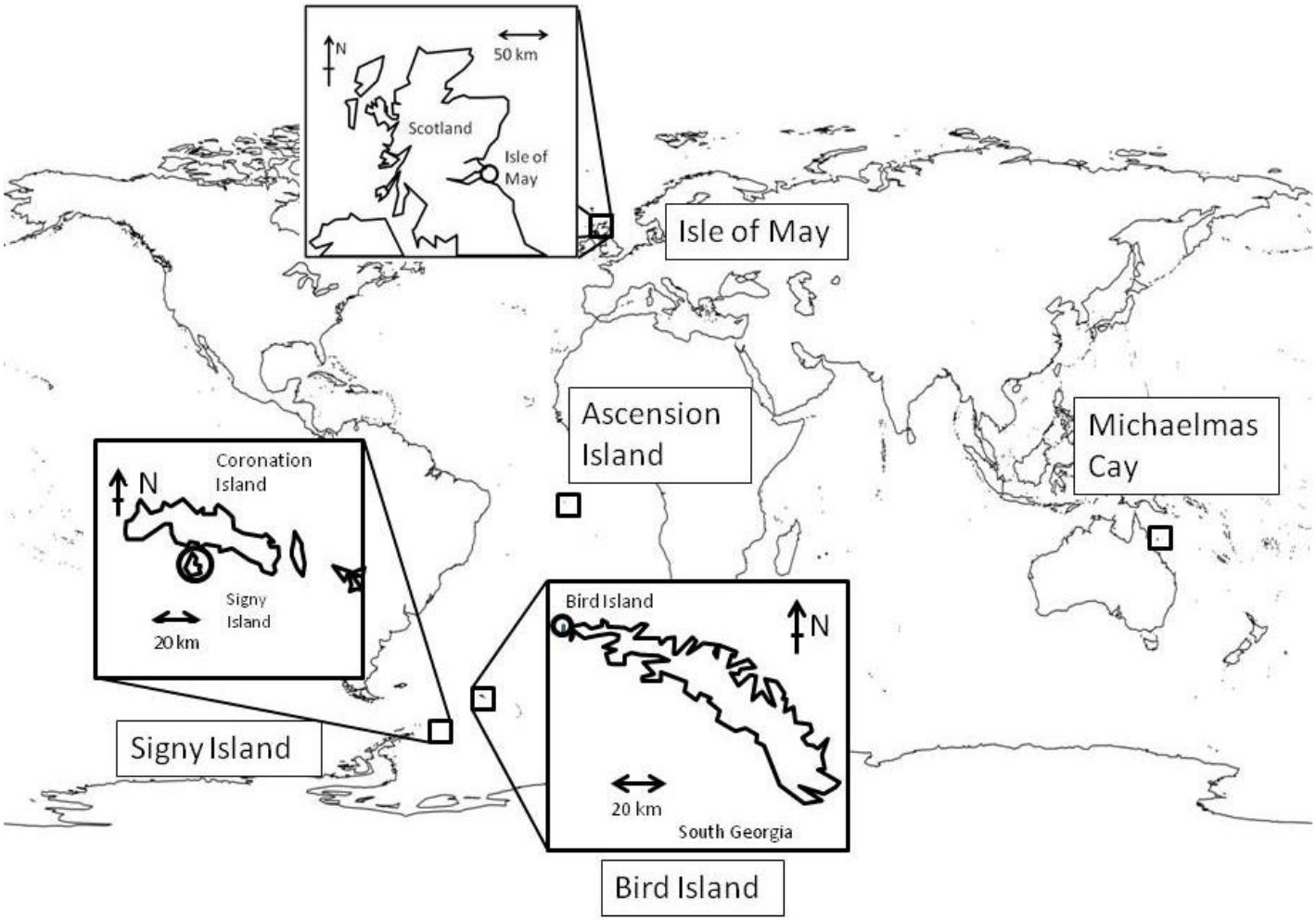

Figure 5.1 Global map of fieldwork sites where measurements were conducted for this thesis.

Isle of May

The Isle of May (56.19 °N, 2.56 °W) is located in the Firth of Forth. The island is a nesting site for many seabird species, including: Common guillemot, European shag, Herring gull and Atlantic puffin. The Isle of May has been a long-term study site for seabird ecology work by CEH since 1973. Measurements of continuous NH_3 concentrations and meteorological variables were made above an Atlantic puffin colony (42,000 pairs). The nest site has a temperate climate (average temperature of 15 °C, average humidity of 80 % and average wind speed of 4 m s^{-1}).

Signy Island

Signy Island (60.72 °S, 45.60 °W) is a small island in the South Orkney Islands in the Southern Ocean. A relatively flat measurement site on the Gourlay Peninsula (10,000 pairs of Adelie penguins and 9,000 pairs of Chinstrap penguins) was used for passive sampling of NH_3 concentrations. This provided an opportunity to measure NH_3 emissions, using passive samplers, from a penguin in sub-polar conditions (average temperature of 2 °C, average humidity of 84 % and average wind speed of 5 ms^{-1}).

Bird Island

Bird Island (54.0° S, 38.05° W) is part of South Georgia, 1000 km south-east of the Falkland Islands and only accessible by boat. The island is the breeding ground for 50,000 pairs of Macaroni penguins, an important species to this study as the third most abundant seabirds (8 % of the global seabird population). In the preliminary global modelling study in Chapter 3, they were estimated to be the largest contributor of seabird NH_3 emissions. Active NH_3 measurement techniques were deployed to derive emission estimates under sub-polar condition at Fairy Point (average temperature of 3 °C, average humidity of 92 % and average wind speed of 5 ms^{-1}).

5.2.2 Measurements taken

At each of the measurement sites NH_3 concentration were measured downwind of the colony, by either passive or active instruments depending on the

circumstances. Meteorological data were measured by a sonic anemometer where available and a suite of traditional meteorological instruments. Details of instrument deployment are given for each site in section 5.3. These data were subsequently used as input to the WindTrax atmospheric dispersion model for calculating the NH_3 emission for each whole colony/site.

5.2.3 Measuring NH_3 concentration - Passive sampling campaigns

In addition to deploying passive ALPHA samplers (Section 2.5.1) in the field, field blanks and laboratory blanks were used to check whether the field samples were contaminated during storage and transport. One field black and one laboratory blank was prepared and analysed for every 10 ALPHA samplers used. Field and laboratory blanks were prepared and sealed at the same time as the samplers that were deployed. The field blanks accompanied the ALPHA samplers used for measurement to the field sites. The laboratory blanks were stored at CEH Edinburgh at 4 °C until analysis, as were the exposed samplers and field blanks upon returning from field work. Analysis of exposed ALPHA samplers was conducted using laboratory facilities at CEH Edinburgh within three months of exposure (The maximum recommended storage period of exposed ALPHA samplers in a cold room is 3 months (Y. S. Tang, pers. comm.). NH_3 was extracted from the ALPHA samplers and analysed using an AMFIA (AMmonia Flow Injection Analysis) system. The AMFIA system is based on selective dialysis of ammonium across a membrane at high pH, with subsequent analysis of conductivity. Calibration standards of 0.1 ppm, 1 ppm and 10 ppm and quality controls (QC's) of concentrations: 0.2 ppm (low QC), 0.9 ppm (high QC), 2 (low QC) and 9 ppm (high QC) were used in the analysis. If extracted samples were outside the calibration range, they were diluted and analysis repeated as necessary.

Calculation of concentration of ammonia in the air

The air concentration of NH_3 (χ, $\mu g\ m^{-3}$) measured by an ALPHA sampler is calculated from the concentration of NH_4 in the extracted sample (X_e, $ng\ ml^{-1}$), the concentration of NH_4 in the extracted sample from the lab blank (X_b, $nh\ ml^{-1}$), the volume of the extracted sample (V_e, ml), the effective volume of air sampled (V_a, m^3) and the conversion of NH_4 to NH_3 (Equation 5.1).

$$\chi = \frac{(X_e - X_b)V_e}{V_a}\frac{17}{18}. \quad (5.1)$$

The effective volume of air sampled is calculated from the time of exposure (t, h), the temperature adjusted diffusion coefficient of the NH_3 (D_T, m^2 s^{-1}), the cross sectional area of the stationary air layer within the sampler (A, 3.4636 x 10^{-4} m^2) and the length of the stationary air layer within the sampler (L, 0.006 m) (Equation 5.2). D_T is corrected for the actual temperature during sampling (T, ºC) using the diffusion coefficient of NH_3 at 10°C (D_{ref}, 2.09 x 10^{-5} m^2 s^{-1}) and the reference temperature (T_{ref}, ºC) of 10 ºC (Equation 5.3) (Hafkenscheid et al., 2009).

$$V = \frac{D_T A t}{L}. \quad (5.2)$$

$$D_T = D_{ref}\left(\frac{273.3T}{273\,T_{ref}}\right)^{1.81} \quad (5.3)$$

5.2.4 Measuring NH_3 concentration - Active sampling campaigns

Active sampling methods were used at sites where it was possible to deploy an instrument specialist to operate the instrumentation for the duration of the campaign (Isle of May, Ascension Island and Bird Island) and electricity was available. Active sampling methods allow NH_3 emissions to be calculated at a much higher time resolution than passive samplers, as described in detail in Section 2.6.2. At each site, a single instrument was used to actively measure NH_3 concentrations at a single height above the ground (Figure 5.2). During the measurement campaigns, NH_3 concentrations were measured using either the Nitrolux-1000 (Isle of May) or the AiRRmonia (Ascension Island and Bird Island). Details of the principle of operation for both instruments are given in Section 2.5.2.

The active NH_3 measurement instrument was deployed downwind of each seabird colony, with the height of the air intake being site-dependent and calculated in advance of the campaigns using a footprint model (Kljun et al., 2004). The footprint modelling was used in conjunction with local judgment to ensure that the instrument intake could be positioned within the NH_3 plume. The footprint size is estimated using: the standard deviation of vertical velocity fluctuations, σ_w (ms^{-1}),

surface friction velocity, u_* (ms^{-1}), measurement height, z (m), Planetary boundary-layer height, h (m) and roughness length, z_0 (m) (Kjlun et al, 2004). The sampling train was set up as follows for all campaigns: Air is drawn through a PTFE membrane filter (1 µm pore size) at the start of the inlet line to remove particles, and then through tubing to the gas analyzer by a Charles-Austin pump (flow rate 8 l min^{-1}). Heating tape and foam insulation were wrapped around the tubing to minimise NH_3 sticking to the tubing. Power was required to run the gas analyzer and the PC collecting the data and was supplied by a Honda Eu10i petrol generator (800W). All of the instruments were housed within a tent to provide protection from wind, precipitation and dust.

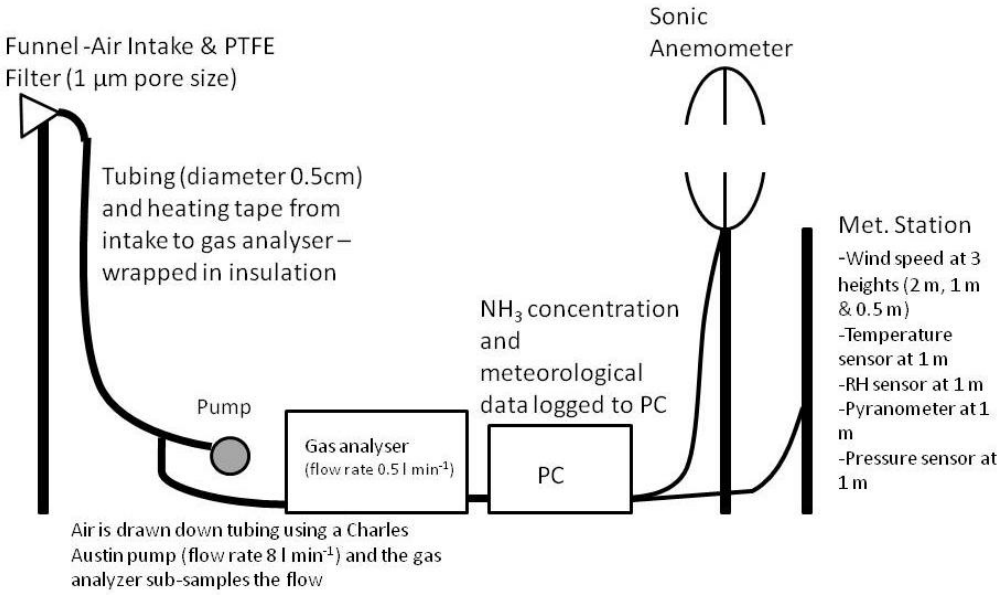

Figure 5.2 Set-up of the active sampling equipment deployed on the Isle of May (Scotland), Ascension Island (Atlantic Ocean) and Bird Island (South Georgia)

5.2.5 Meteorological data

Micrometeorological measurements were taken using a Gill Windmaster Pro sonic anemometer (Gill Instruments, Hampshire, UK). The sonic anemometer measures the u, v and w vector outputs of air movement at 20 Hz. Data collected by the sonic anemometer, 2.5 m above the ground, were used to calculate the roughness height (z_0, m), friction velocity (u_*, m s^{-1}) and Monin-Obukhov length (L, m). The instruments that collect other meteorological data are detailed in

Table 5.1. Wind speed was measured at three heights (1.5 m, 1 m & 0.5 m) on the Isle of May, Ascension Island and Bird Island.

Table 5.1 Instruments used to measure meteorological data on the Isle of May, Ascension Island and Bird Island.

	Sensor	Range	Sensitivity
Air temperature	CS HMP45C Probe	-39.2 - +60 °C	± 0.5 °C
Relative Humidity	CS HMP45C Probe	0.8 - 100 %	± 1 %
Irradiance	Kipp & Zonen SP Lite	0 - 2000 W m^{-2}	± 5 %
Wind Direction	05103 Wind Monitor	0 – 359 °	± 3 °
Wind Speed	05103 Wind Monitor	0 – 50 m s^{-1}	± 0.3 m s^{-1}
Rainfall	SBS500 Tipping Bucket	0 – 500 cm^2	± 0.2 mm
Air Pressure	CS100	600 - 1100 mb	± 2.0 mb
Wind Direction	Gill Windmaster Pro	0 – 359 °	± 0.1 °
Wind Speed	Gill Windmaster Pro	0 – 45 m s^{-1}	± 0.01 m s^{-1}
Sonic Temperature	Gill Windmaster Pro	-40 - +70°C	± 0.01 °C
Speed of Sound	Gill Windmaster Pro	300 – 370 m s^{-1}	± 0.01 m s^{-1}
Ground Temperature	Tinytag Talk 2	-40 - +85 °C	± 0.05 °C
Ground Temperature	CS 107 Probe	-35 - +50 °C	± 1 °C

Ground temperature was measured at Michaelmas Cay, Ascension Island and Bird Island using a Tinytag Talk 2 temperature sensor with data logger (Gemini Data Loggers, UK). The temperature sensor was placed inside a plastic case, to protect it from moisture, and placed onto the surface, with readings logged every 5 minutes. Ground temperature represents a proxy of soil surface temperature, as an estimate of the effective temperature of guano at the seabird colony. The ground temperature on the Isle of May was measured using a CS107 Temperature probe, which was placed on the ground and logged every minute.

5.2.6 Method of Data Analysis

For use in the WindTrax model, NH_3 measurements were corrected for transit time in the tubing and time for the instrument signal to fully respond to changes in concentration. For example, the time taken between the gas entering the sampling tube and the response by the gas analyzer was calculated at 3 minutes 30 seconds for a 4 m length of PTFE tubing (diameter 0.5cm) attached to the AiRRmonia gas analyzer. Transport times for each site, depending on the length of tubing and the instrument used, were determined before deployment.

For each NH_3 concentration dataset, data for periods when air sampled by the analyser had not moved over the seabird colony (i.e., when the colony was not

upwind) was removed. Data were also removed for wind directions that include passage of air over large obstructions. A large obstruction is defined as a building or rock formation that causes turbulence and reduces the accuracy of the emission estimate. Data representing periods of strong stability were also removed, where:

- $u < 0.15$ ms^{-1}
- $u^* < 0.1$ ms^{-1}
- $|L|<2$.

As a further processing step, the NH_3 concentration and meteorological data were averaged over 15 minutes. This reduces the variability caused by turbulence while including variation caused by environmental or atmospheric change (Flesch et al. 2005; 2008; Laubach et al. 2008).

The locations of instruments and NH_3 sources (birds) were determined using a Garmin GPSmap 76S handheld GPS. This consumer-grade GPS receiver has an accuracy of 1.4 m of true position in open sky settings (Wing et al., 2005). The GPS coordinates were then used in WindTrax to describe NH_3 source boundaries and locations of the instruments. Each simulation run in WindTrax uses 50,000 particle projections to back-calculate the NH_3 emission. 15 minute averages of: background NH_3 concentrations (X_b, μg m^{-3}), wind speed (u, m s^{-1}), wind direction (WD, °), temperature (T, °C), and NH_3 concentration at 2m (X, μg m^{-3}), roughness height (z_0, cm) and the Monin-Obukhov length (L, m) were entered into the WindTrax. After the emission estimate has been calculated, an uncertainty analysis was conducted for each site based on the parameters estimated to have the largest associated error.

5.3 Fieldwork Sites - Methods, Results & Conclusions

The author was responsible for planning all field campaigns, the organisation of instruments, the assembly and analysis of ALPHA samplers and all data analysis. The deployment of the ALPHA samplers on Michaelmas Cay was conducted by Wallace MacFarlane and Sascha Taylor of the Department of Environment and Resource Management, Queensland Parks and Wildlife Service, Australia. The Ascension Island and Isle of May campaigns were conducted by the author. The Signy Island ALPHA samplers were deployed by Dr. P. Hill of the University

of Bangor. Measurements on Bird Island were taken by Y. S. Tang of CEH Edinburgh.

5.3.1 Michaelmas Cay- Passive Campaign

Methods

Michaelmas Cay was formed as wave action washed debris to the leeward side of the reef. The island has a covering of low-growing plants, with common species including hairy spinifex (*Spinifex hirsutus*), stalky grass (*Lepturus repens*) and sea purslane (*Sesuvium portulacastrum*) (Figure 5.3).

Figure 5.3 Michaelmas Cay before the breeding season. ALPHA samplers were attached to the posts in the picture. Image courtesy of W. MacFarlane (Queensland EPA).

The birds

The main seabird species present on Michaelmas Cay are Sooty terns (*Sterna fuscata*), Crested terns (*Thalasseus bergii*), Common noddies (*Anous stolidus*) and Lesser-crested terns (*Sterna bengalensis*). On Michaelmas, all bird species are of similar mass and nest in vegetation or in shallow scrapes of sand (Table 5.2). Bird populations are relatively constant through the breeding season (Table 5.2). Compared with prior years, an atypically low attendance of the Sooty Terns during the 2009/2010 breeding season was attributed to unusually severe weather events (Wallace MacFarlane, Queensland, EPA, pers. comm.).

Table 5.2 Species specific average adult mass of the birds (g) and monthly attendance (individuals) on Michaelmas Cay between September 2009 and January 2010. The bird counts were conducted by the Queensland EPA at the beginning of each month. The counts were conducted by S. Taylor and W. MacFarlane, Queensland EPA (pers. comm.).

	Mass (g)	Sept.	Oct.	Nov.	Dec.	Jan.
Common noddy	170	559	5,720	6,726	12,070	8,285
Crested tern	350	28	2	444	572	792
Lesser-crested tern	260	7	64	1,549	2,405	694
Sooty tern	180	9,430	6,530	3,134	1,380	5,455
Total population (individuals)		10,024	12,316	11,853	16,427	15,226

NH_3 concentration – Passive campaign

Due to time, access and financial constraints, an active sampling campaign on Michaelmas Cay was infeasible. W. MacFarlane of the Queensland Environmental Protection Agency agreed to deploy ALPHA passive NH_3 samplers, change them monthly and send the exposed samplers back to the UK. The sampling campaign started when the Sooty terns began nesting on Michaelmas Cay in October 2009 and finished in May 2010.

The initial sampling strategy used four masts holding ALPHA samplers to measure NH_3 concentrations (see Figure 5.4 for a map of the Cay with measurement sites marked). Mast 4 was used to measure a background NH_3 concentration, as it was located in an area with no nesting birds and therefore unlikely to be affected by NH_3 from the prevailing wind away from nesting seabirds. The sampling locations were:

1. North West edge of the vegetation at three heights (0.5, 1 and 2 m).

2. Centre of the vegetation, 50 m from Mast 1, at three heights (0.5, 1 and 2 m).

3. South East of vegetation, 50 m from Mast 2, at three heights (0.5, 1 and 2 m).

4. As far as possible from the birds, but above the high water line (1 m).

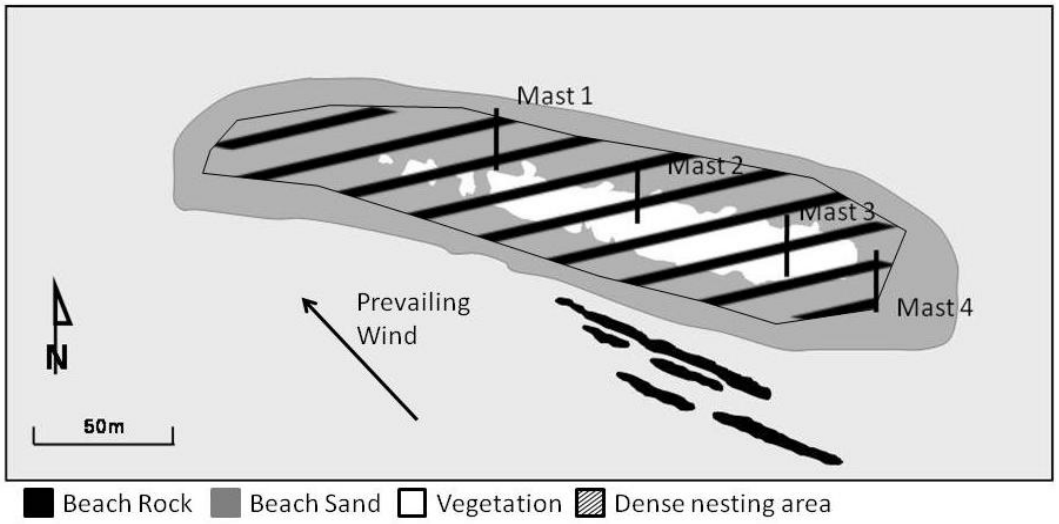

Figure 5.4 Deployment of the ALPHA samplers in Michaelmas Cay, October 2009 to May 2010. The birds nest on both vegetation and sand.

Meteorology

Ground temperature data was measured using a Tiny Talk sensor at a frequency of three hours for a duration of six months. Other meteorological data were obtained from the nearest meteorological station on Green Island, 10 km south of Michaelmas Island (NOAA, 2010). Whilst data measured this far away is not ideal, this represents the best meteorological data available for use in this study, as setting up an (unattended) dedicated met station was discouraged due to the potential for interference by (human) visitors.

Results

Issues during data collection

Weather conditions during the 2009/2010 breeding season meant that the passive sampling campaign on Michaelmas Cay was not as successful as hoped. Extreme heat melted the glue of the Velcro attachments holding the triplicate ALPHA samplers at each site, and caused nearly all samplers to fall from their masts during October. Only 8 samplers of the 30 deployed for this month were recovered. Sampling during November and December was more successful, with 23 ALPHA samplers recovered in both November and December.

Early in 2010 masts 2, 3 and 4 were lost due to very high tides and strong northerly winds. The posts were reinstalled, but only two ALPHA samplers were recovered during each of January, February and March.

NH_3 concentration

Table 5.3 NH_3 concentration (mg m^{-3}) of the ALPHA samplers deployed on Michaelmas Cay during November (5/11/2009 to 10/12/2009) & December (10/12/2009 to 6/1/2010). Top ALPHA samplers are 2 m from the ground, Mid ALPHA samplers are 1 m from the ground and Bottom ALPHA samplers are 0.5 m from the ground. The concentrations shown are means of the triplicate samplers deployed.

	Mast NH_3 concentration (mg m^{-3})									
Period	**Mast 1 2 m**	**Mast 1 1 m**	**Mast 1 0.5 m**	**Mast 2 2 m**	**Mast 2 1 m**	**Mast 2 0.5 m**	**Mast 3 2 m**	**Mast 3 1 m**	**Mast 3 0.5 m**	**4 1 m**
1	18.2	55.3	55.3	53.5	54.7	54.5	23.0	37.7	54.1	1.6
2	10.1	70.0	71.5	49.5	71.7	71.9	8.1	35.4	66.1	3.9

NH_3 concentrations on Michaelmas Cay show great variability for the two measurement periods with good data: Period 1 (5/11/2009 to 10/12/2009) and Period 2 (10/12/2009 to 6/1/2010). The ALPHA samplers nearest the ground measured the highest concentrations (Table 5.3).

Meteorology and micrometeorology

Table 5.4 Meteorological data for Michaelmas Cay Period 1 (5/11/2009 to 10/12/2009) & Period 2 (10/12/2009 to 6/1/2010). [1] denotes (NOAA, 2010) and [2] denotes directly measured

Variable	Period 1	Std Dev	Period 2	Std Dev
Ground Temperature (°C)[2]	29.7	6.9	32.0	7.9
Wind Speed (ms^{-1}) [1]	6.7	2.5	5.3	2.5
Wind Direction (°)[1]	135	28.9	130	64.5
Total Precipitation (mm m^{-2})[1]	155		106	

The air stability was estimated as unstable, at L = -10 m, because of the sun causing large amounts of turbulence during the day. The wind was constant throughout the measurement period and generally came from the south-east throughout the measurement periods (Table 5.4 and Figure 5.5).

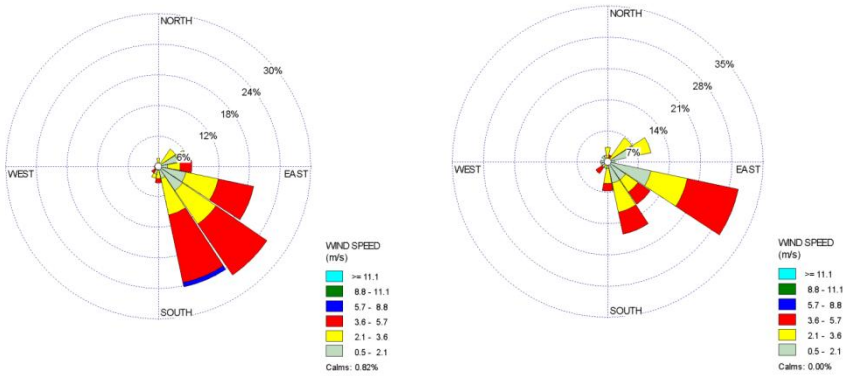

a) b)

Figure 5.5 Wind roses for Michaelmas Cay (a) Period 1 (5/11/2009 to 10/12/2009) & (b) Period 2 (10/12/2009 to 6/1/2010)

Modelled NH_3 emission rate

The NH_3 concentrations, meteorological and micrometeorological data were entered into the WindTrax atmospheric dispersion model. The average estimated NH_3 emission rate for the Sooty tern colony on Michaelmas Cay was 21.3 µg NH_3 m^{-2} s^{-1} during November and 22.2 µg NH_3 m^{-2} s^{-1} during December 2009. The little variation in wind speed and direction suggests that the footprint of the source sampled by each ALPHA sampler was very near to being constant. However, the micrometeorological conditions on Michaelmas can only be estimated relatively crudely from the available data and remain a substantial source of uncertainty.

Discussion

Uncertainty analysis

As shown earlier, the air stability was estimated as unstable, with L = -10 m for the site. Typical stabilities for the weather conditions on Michaelmas range from stable (L = 100 m) to very unstable (L= -5 m). In stable conditions the NH_3 emission calculated by WindTrax decreases because vertical transport of the NH_3 gas decreases. As air becomes less stable the vertical transport of the gas increases and the calculated emission increases.

The background NH_3 concentration at Michaelmas Cay was estimated to be that measured at Mast 4 (November = 1.59 µg m^{-3} and December = 3.9 µg m^{-3}). Tsunogai (1971) estimated that open water background NH_3 concentration for the South Pacific, a location representative of this area, was 0.14 µg m^{-3}.

The NH_3 source area was taken as any part of the island that the birds could have excreted on, with a best estimate of 10,000 m^2. As a maximum, this was taken as the limit of the high water mark. As a minimum this was estimated at 6,000 m^2, calculated from measurements of distribution of nests made by Queensland EPA data (W. MacFarlane, unpublished data).

Table 5.5 Uncertainty analysis of the NH_3 emission estimate from the seabird colony on Michaelmas Cay

Factor	Best estimate	Max Value	Min Value	Uncertainty in NH_3 emission (%)
Roughness Length (cm)	1	15	0.01	15
Monin-Obukhov Length (m)	-10	100	-5	29
Background Conc. ($\mu g\ m^{-3}$)	1.6 - 3.9	3.9	0.14	2
Area of Nest Site (m^2)	10,000	10,000	6,000	13
Total Uncertainty in emission modelling (%)				35

Table 5.5 shows that modelling of NH_3 emissions from the seabird colony on Michaelmas Cay has an uncertainty of ± 35 %. The uncertainty is calculated as the square root of the sum of the individual uncertainties squared.

5.3.2 Ascension Island -Passive Campaign

Methods

On Ascension Island, Sooty terns (*Sterna fuscata*) nest in two large colonies: Waterside and Mars Bay (Figure 5.6). Waterside is the largest colony, with approximately 150,000 pairs, and found at the southern end of the Wideawake airfield. However, this site is relatively inaccessible so was not suitable for this study. The smaller site at Mars Bay is more accessible and located on the south west corner of Ascension Island. Mars Bay is the breeding location for 100,000 pairs of Sooty terns. Strong trade winds blow clean air from the west across the tern colony, thus downwind measurements of atmospheric NH_3 concentrations are unaffected by other NH_3 emission sources (see Figure 5.8).

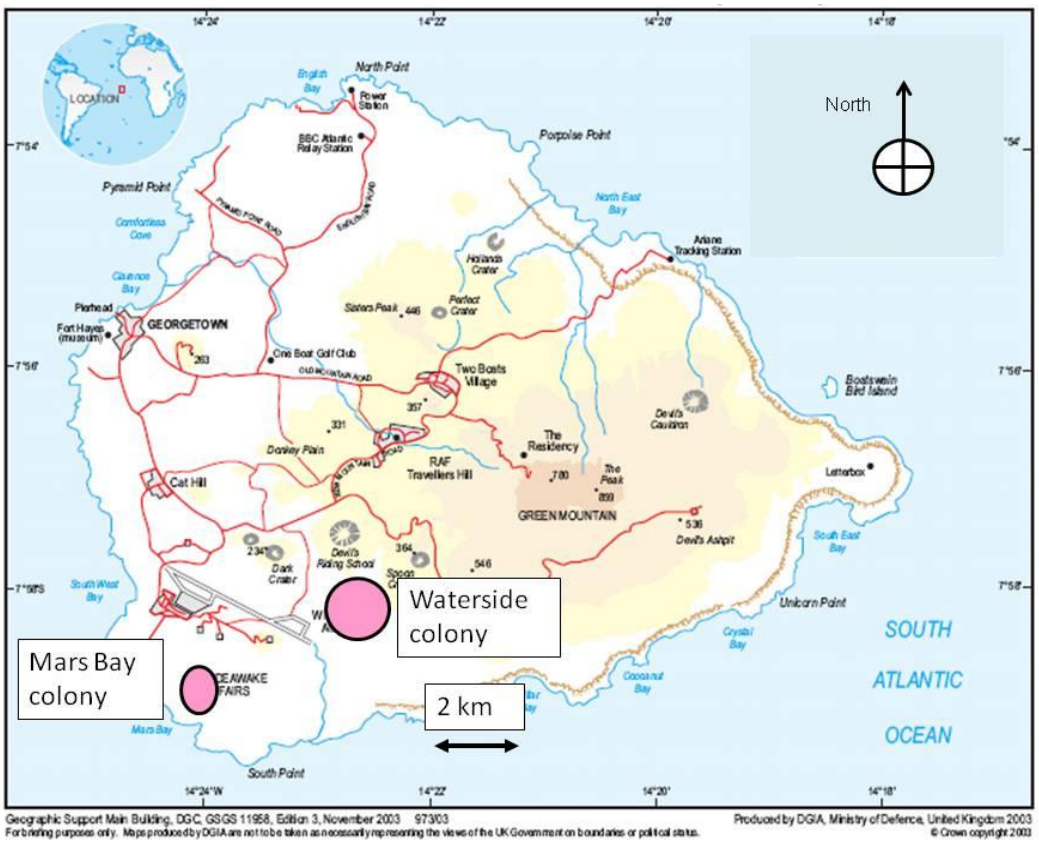

Figure 5.6 Map of Ascension Island. Courtesy of Ministry of Defence, United Kingdom 2003

The study site

At Mars Bay, Sooty terns nest on volcanic clinker on a slightly sloping plain, over a total area of 79,000 m^2. The clinker is made from medium to small rocks (5cm in diameter). Some birds nest on areas of built up clinker, but none more than 1 m tall (Figure 5.7). There is little vegetation within the colony site, only some dried remains of grass and three Mexican Thorn (*Prosopis juliflora*) trees, approx. 1.5 m in height. The perimeter of the colony was mapped at 20 m intervals using GPS on the 25th May 2010.

Figure 5.7 Sooty tern colony in Mars Bay, Ascension Island. Inset shows Sooty terns nesting on the clinker in Mars Bay (Photo: S. Riddick).

The birds

An estimated 200,000 Sooty terns arrived at the Mars Bay Fairs on the 14th April 2010 (S. Stroud, Ascension Island Conservation Department, pers. comm.) and hatching started on the 25th May 2010. The instruments measuring NH_3 concentration, micrometeorology and meteorology were deployed on the 22nd May and sited 150 m from the North-west edge of the colony (Figure 5.8).

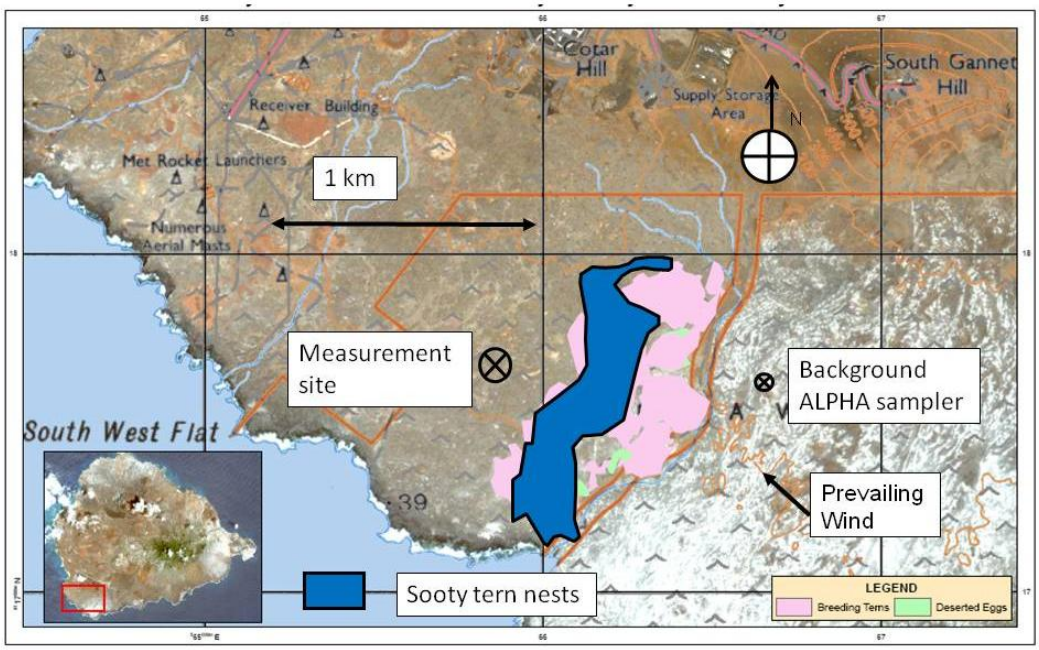

Figure 5.8 The blue area indicates the location of the Sooty tern colony in 2010 at Mars Bay, Ascension Island. Image courtesy of J. Hughes (University of Birmingham). (Pink and green areas on the map indicate the locations of breeding terns and deserted eggs for a previous breeding season.)

NH_3 concentration -Passive Campaign

The ALPHA samplers were exposed for three periods: Period 1 (20/05/2010 - 27/05/2010), Period 2 (27/05/2010 - 02/06/2010) and Period 3 (02/06/2010 - 09/06/2010). The samplers were deployed in two arrangements. Periods 1 and 2: samplers were deployed at 4 locations (Figure 5.9a). Period 3: samplers were deployed along a transect away from the birds in the prevailing wind direction (Figure 5.9b).

Periods 1 and 2. Three sampling stations: Mast 1 sampling at three heights (1.5 m, 1 m and 0.5 m), Mast 2 sampling at three heights (1.5 m, 1 m and 0.5 m) and Mast 3 sampling at one height (1 m).

Period 3. Five sampling stations and all masts sampled at one height (1.5 m).

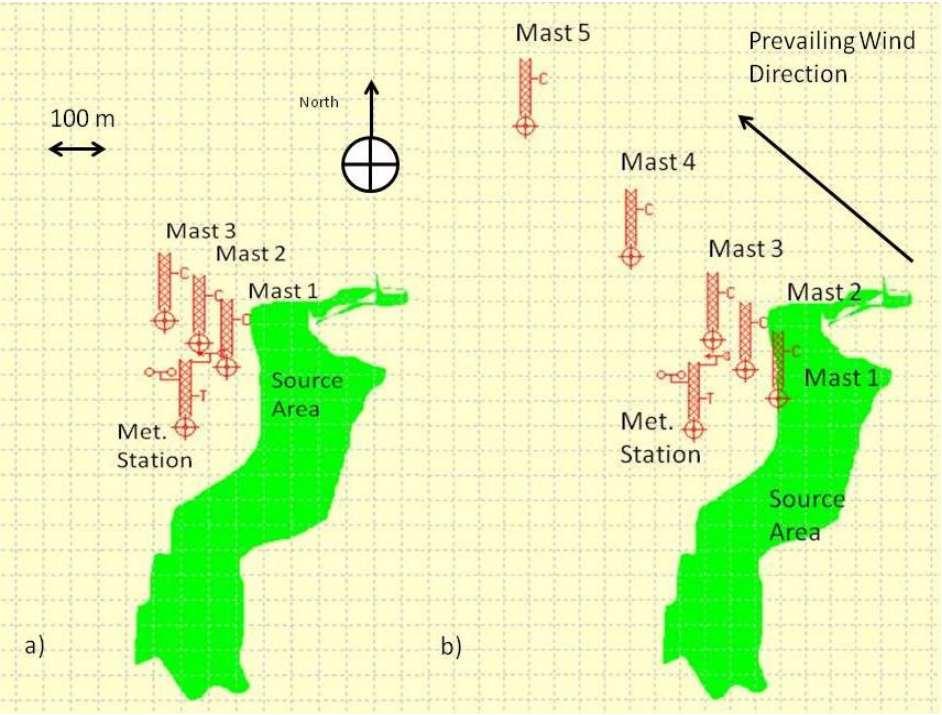

Figure 5.9 Arrangement of ALPHA samplers used to measure the NH_3 concentration at Mars Bay on Ascension Island. The green area indicates the nest site of the Sooty terns. Two arrangements were used (a): Period 1 (20/05/2010 - 27/05/2010) & Period 2 (27/05/2010 - 02/06/2010) and (b) Period 3 (02/06/2010 - 09/06/2010).

Meteorology

The Gill Windmaster Pro sonic anemometer was located on top of the mast, at 2.5m from the ground. Wind speed was recorded at three heights (2 m, 1 m and 0.5 m) and the temperature, relative humidity and solar irradiance were measured at 0.75 m from the ground. The ground temperature was measured using a Tiny Talk data recorder placed on the ground.

Results

NH_3 concentrations

The NH_3 concentrations for each of the masts show that NH_3 concentrations decreased with distance away from the colony (Figure 5.10). The measured background concentrations were 0.1 µg m^{-3} for all three periods.

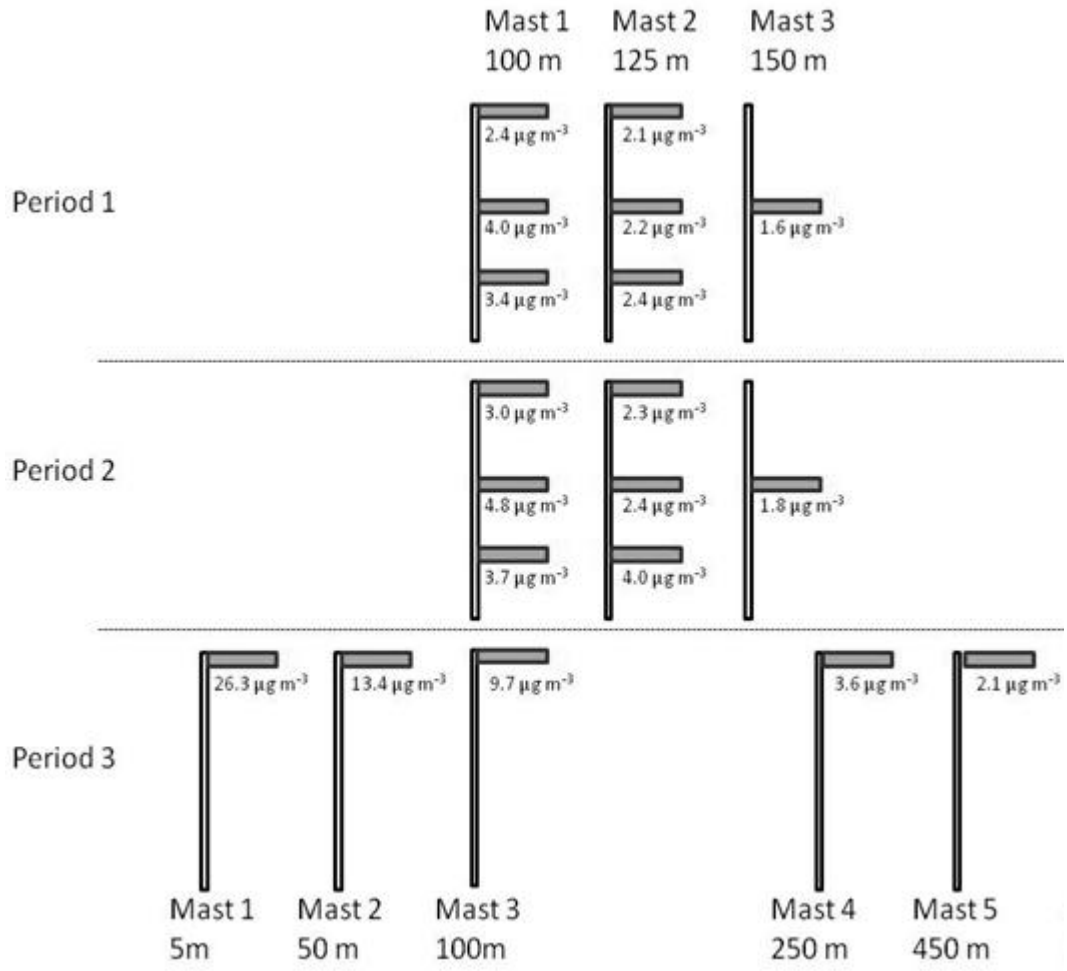

Figure 5.10 NH_3 concentrations for each of the masts during the three passive sampling measurement periods at Mars Bay, Ascension Island. During Periods 1 & 2, Masts 1 and 2 sampled at three heights (1.5 m, 1 m and 0.5 m) and Mast 3 at 1 m. During Period 3 all masts sampled at 1.5 m. The distances from each mast to the colony along the sampling transect are given in the figure. The concentrations are means of the triplicate ALPHA samplers deployed.

Meteorological Data

Average values for roughness length and Monin-Obukhov length were relatively constant throughout the measurement period (Table 5.6). The wind roses for the three measurement periods show constant wind from the south-east (Figure 5.11).

Table 5.6 Averaged meteorological data from Ascension Island from 20/5/10 to 9/6/10

Period	Average u (ms^{-1})	Av z_0 (cm)	Average L (m)	Av T_{ground} (°C)
1	5.1	6.6	-12.7	30.0
2	4.9	6.7	-11.4	30.0
3	4.7	8.4	-21.0	28.8

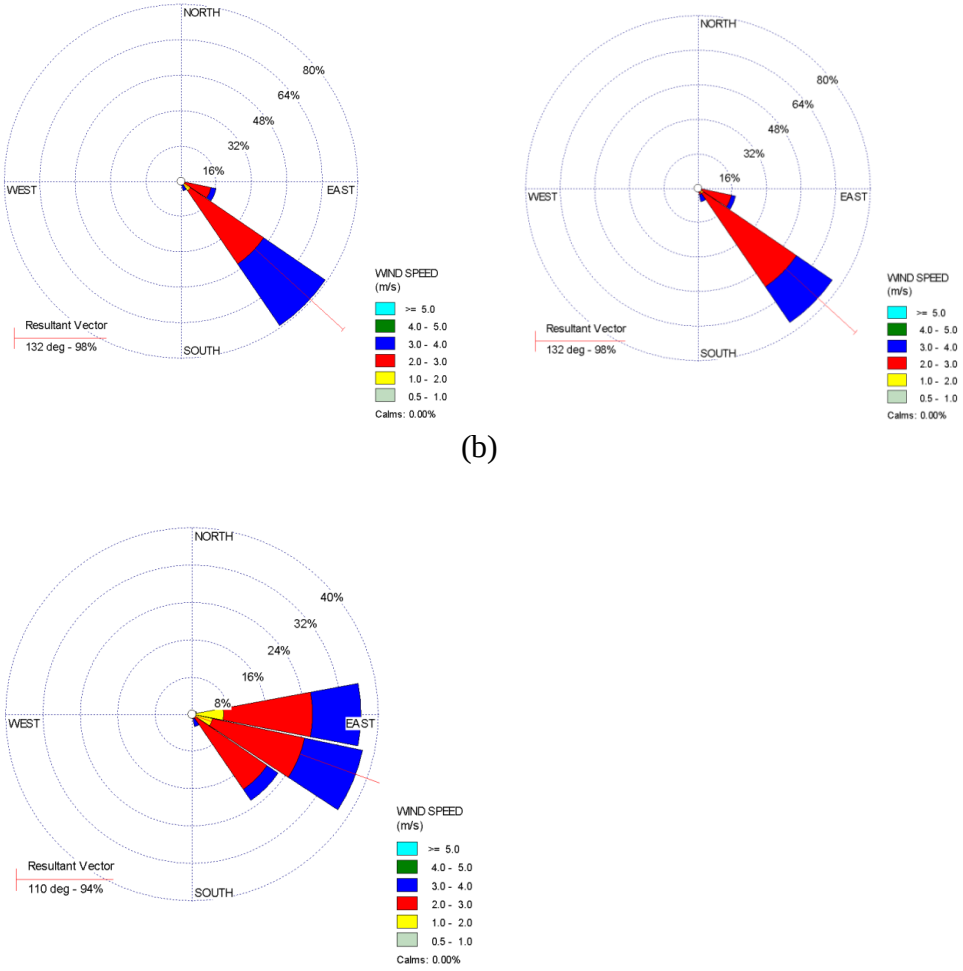

Figure 5.11 Wind roses for Ascension Island during the three measurement periods.

NH_3 emissions

NH_3 emission estimates vary throughout the measurement campaign, with the lowest concentrations measured during the second period and the highest during the third period (Table 5.7). The average NH_3 emission during the campaign was

17.4 μg m^{-2} s^{-1}. The footprint of source sampled by each ALPHA sampler was very near to being constant.

Table 5.7 NH_3 emission estimates from the passive sampling campaign on Ascension Island from 20/5/10 to 9/6/10

Sampling Period	Sampling date	NH_3 emission (μg m^{-2} s^{-1})
1	20/05/2010 - 27/05/2010	18.1
2	27/05/2010 - 02/06/2010	5.0
3	02/06/2010 - 09/06/2010	29.2

Uncertainty Analysis

The average air stability, calculated from measurements made by the sonic anemometer, was classified as unstable (L = -14.8 m). The range of uncertainty of the air stability was taken as the 25 % percentile and 75 % percentile of the average air stability. As the input value of the Monin-Obukhov length becomes less stable, the vertical transport of the gas increases and the calculated emission increases.

The background NH_3 concentrations were measured by ALPHA samplers downwind of the colony in clean air at 0.1 μg m^{-3}. The estimated that the open water background NH_3 concentration for the Atlantic Ocean, a location representative of this area, was between 0.02 μg m^{-3} and 0.44 μg m^{-3} (Johnson, 1994), which fits well with the campaign measurements.

The area encompassing the nests of Sooty terns was measured using a handheld Garmin GPS receiver and estimated to be 79,000 m^2. The NH_3 emission source was taken as any part of the island that the birds could have excreted guano on. From observations, a maximum of this area was taken as 89,000 m^2. As a minimum this was estimated at 69,000 m^2, taken from measurements of distribution of nests.

The overall uncertainty of the Ascension Island passive campaign emission estimates is large (± 24 %) and caused by the uncertainty associated with diurnal variation of the stability of air (Table 5.8).

Table 5.8 Uncertainty analysis of the NH_3 emission estimate from the seabird colony on Ascension Island

Factor	Best Estimate	Max Value	Min Value	Uncertainty (%)
Monin-Obukhov Length (m)	-14.8	29	-7	23
Background Conc. (µg m^{-3})	0.1	0.44	0.02	1
Area of Nest Site (m^2)	79,000	89,000	69,000	7
Total Uncertainty (%)				24

5.3.3 Ascension Island -Active Campaign

Methods

NH_3 concentration -Active Campaign

The AiRRmonia instrument was used to measure NH_3 concentrations actively from the Sooty Tern colony in Mars Bay. The air inlet was positioned at 2 m above the ground (Figure 5.12). Background concentrations were measured using ALPHA samplers (see section 2.6.1 for a description of this approach).

Figure 5.12 The set up of instruments used to measure the NH_3 concentrations actively from the Sooty Tern colony in Mars Bay. The AiRRmonia instrument was used to measure the NH_3 concentrations. The air inlet was positioned at 2 m above the ground. Instruments were powered by a Honda Eu10i petrol generator. Micrometeorological parameters were measured with a Gill Windmaster Pro sonic anemometer, on top of the mast 2.5m above the ground. Wind speed was recorded at three heights (2m, 1m and 0.5m) and the temperature, relative humidity and solar irradiance were measured at 0.75m above the ground.

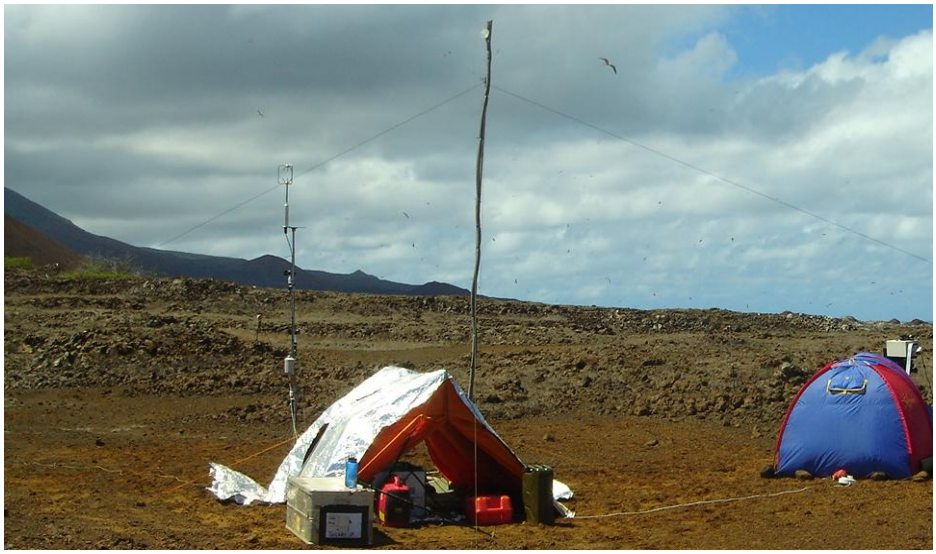

Figure 5.13 Instrument set up in the tent at Mars Bay, Ascension Island, May and June 2010. This photograph shows how the instruments were initially deployed. The mast was shortened later.

Results

NH_3 Concentrations

The NH_3 concentrations measured by the AiRRmonia trace gas analyser were between 0 and 230 $\mu g\ m^{-3}$ (15 minute average values). NH_3 concentrations showed a strong diurnal pattern, with large values during the day and low values at night (Figure 5.14). The large peaks on May 25th 2010 at 0600 hours and June 6th 2010 at 0800 hours correspond to large rain events.

WindTrax Data Input

NH_3 concentration and meteorological data were input to the WindTrax atmospheric dispersion model (Figure 5.14). Ground temperature ranged from 18 to 46 °C with maximum values during the early afternoon. The roughness length on the Ascension Island ranged from 6 to 12.5 cm, well within the useable range of WindTrax.

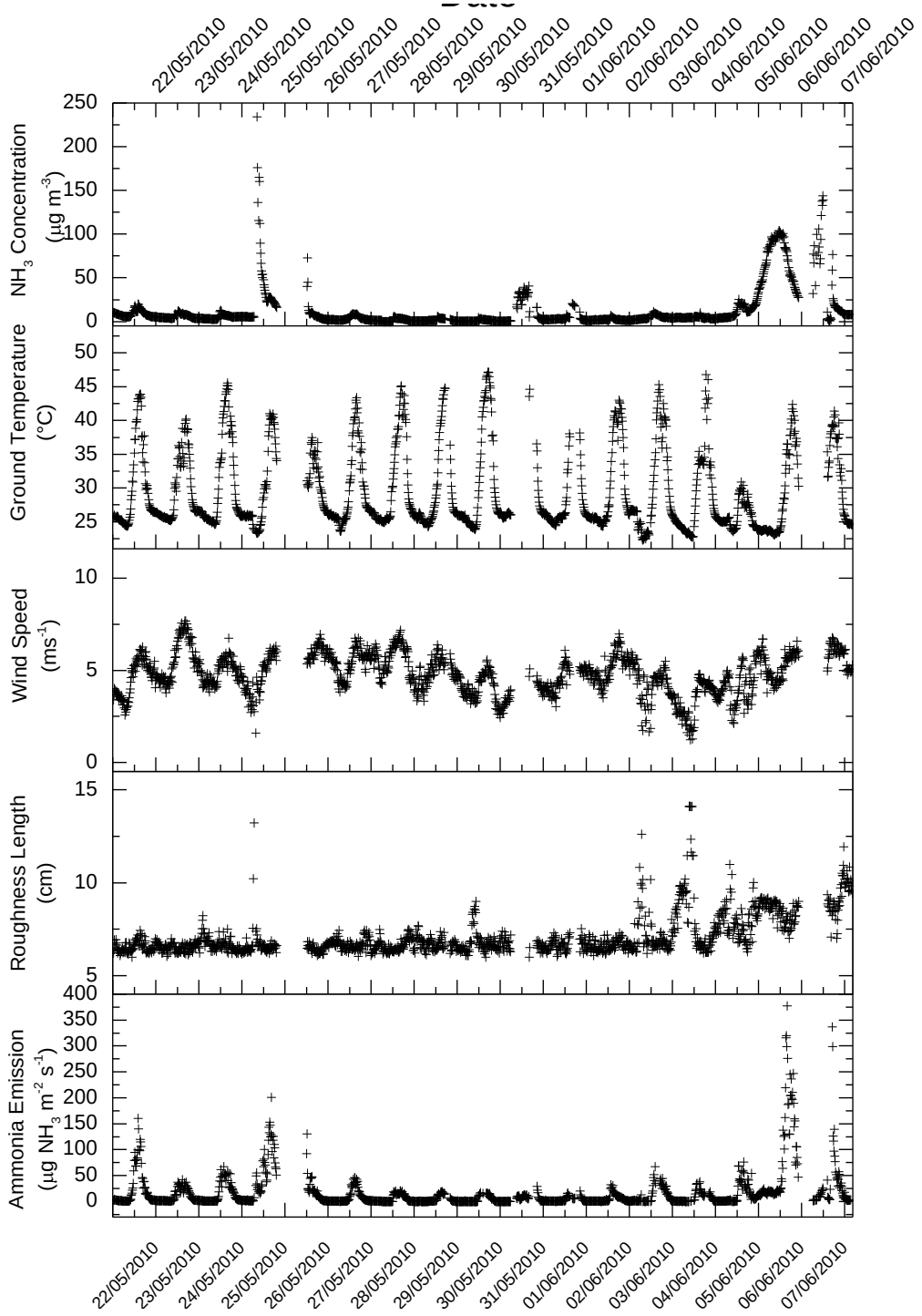

Figure 5.14 Time series of NH_3 concentration, wind speed, ground temperature and roughness length measured at Mars Bay, Ascension Island, 22nd May to 10th June 2010. These data were used as input to the WindTrax modelling software for the estimation of NH_3 emissions from the seabird colony, shown at the bottom.

NH_3 emission

The calculated emissions show a strong diurnal pattern, with NH_3 emissions increasing to a maximum during the hottest part of the day and decreasing to almost zero during the night (Figure 5.15). In periods with no rain NH_3 emissions were relatively small. NH_3 emissions were largest after a rain event on the 6th June, with a maximum emission of 377 µg NH_3 m^2 s^{-1} (Figure 5.15).

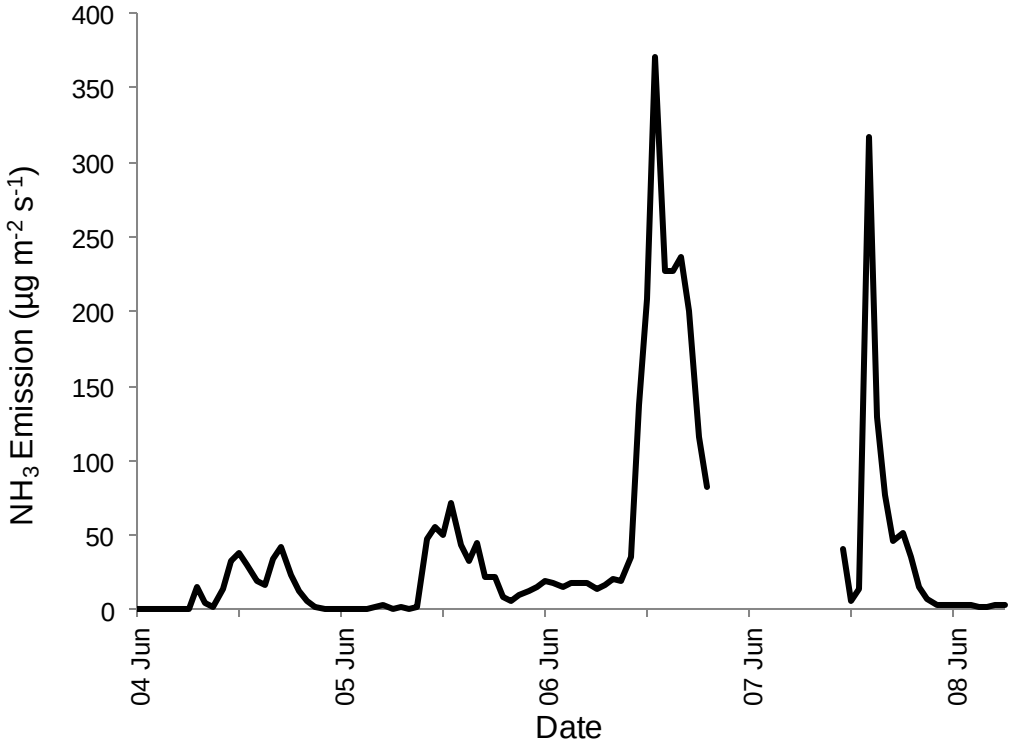

Figure 5.15 NH_3 emissions from the Sooty tern colony, Mars Bay, Ascension Island, 4th June to 8th June 2010, as calculated by the WindTrax model. This highlights the diurnal pattern of NH_3 emissions.

Discussion

Diurnal cycles in NH_3 emissions

NH_3 emissions averaged for each hour of the day show a diurnal pattern (Figure 5.16), with the maximum in the afternoon (between 1400 and 1600 hours) and the minimum during the night (between 0000 and 0600 hours). By integrating the area under the emissions, the daily average NH_3 emission for this campaign was estimated at 1.63 g NH_3 m^{-2} day^{-1} (or 18.9 µg m^{-2} s^{-1}). The error bars show the variability in NH_3 emissions during the measurement period. The largest periods of uncertainty were during the day, while the variability at night was very low.

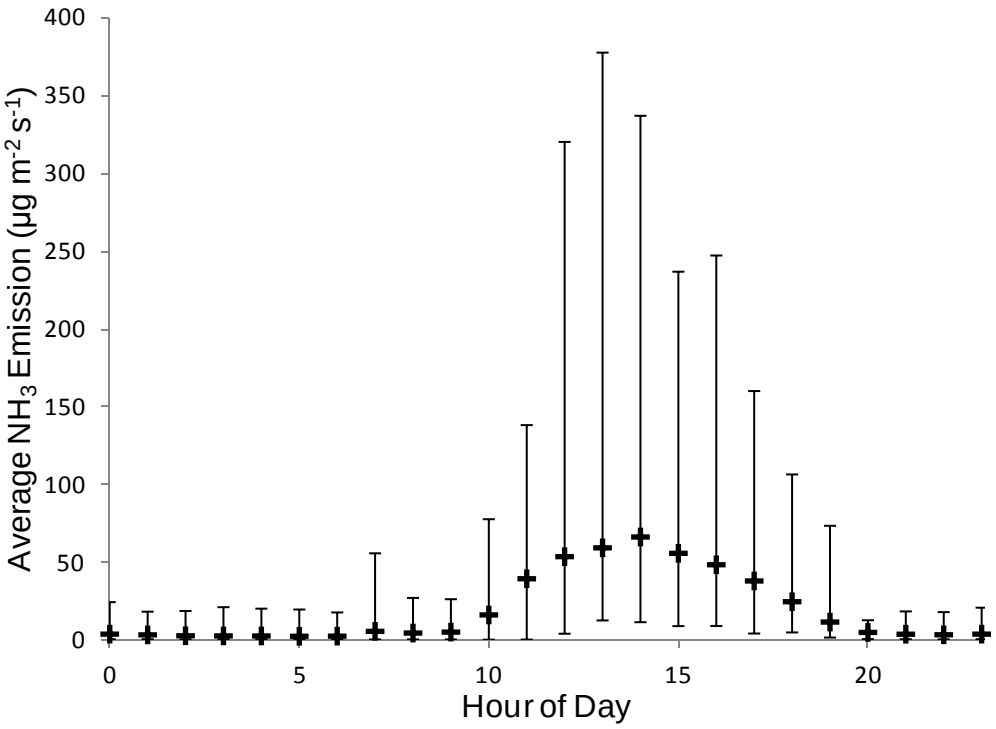

Figure 5.16 The averaged diurnal pattern in NH_3 emissions derived from WindTrax emission calculations for the Sooty Tern colony at Mars Bay, Ascension Island. This campaign estimated an average daily NH_3 emission between 22nd May and 10th June 2010 of 18.9 µg m^{-2} s^{-1}. The error bars show the variability in hourly emissions by representing the maximum and minimum NH_3 emissions for these hours for the duration of the campaign.

Uncertainty analysis

Uncertainties in the background NH_3 concentrations and the size of the nesting area are described in the previous section. The total uncertainty in the modelling of the emission estimate on the Sooty Tern colony in Mars Bay, Ascension is estimated at ± 12 % (Table 5.9).

Table 5.9 Uncertainties associated with the atmospheric dispersion modelling of the Sooty Tern colony in Mars Bay, Ascension Island

Factor	Best Estimate	Max Value	Min Value	Uncertainty (%)
Background Conc. (µg m^{-3})	0.1	0.44	0.02	3
Area of Nest Site (m^2)	79,000	89,000	69,000	9
Total Uncertainty in emission modelling (%)				12

5.3.4 Isle of May-Passive Campaign

Overview

The Isle of May is a National Nature Reserve managed by Scottish Natural Heritage (SNH) and is located in the Firth of Forth, 10 km south-east of Anstruther, Fife. The island is 2 km long and 0.5 km wide and is a popular breeding site for seabirds in the summer months.

The birds

The island hosts a colony of Atlantic puffins (*Fratercula arctica*) and was chosen for this campaign because of its accessibility, suitability for atmospheric modelling and interest in parameterising emissions from burrow nesting birds. The Atlantic puffin is a member of the auk family, with an average adult mass of 420 g. Puffins feed on fish and sand eels and make their nest within a burrow, which may be an existing burrow or freshly excavated by the puffin. An estimated 40,822 pairs of puffins nest on the Isle of May (M. Harris, pers. comm.), and the total area of the puffin colony is 16,000 m^2, measured using GPS. An assumption made was that the site is only inhabited by puffins. However, small numbers of Herring gulls (300 individuals) and Lesser Black-backed gulls (200 individuals) also nest in the area (T. Alampo, SNH, pers. comm.).

Apart from the puffin colony, the Isle of May is also the nesting site for 14000 pairs of Common Guillemot (*Uria aalge*), 5690 pairs of Herring Gull (*Larus argentatus*), 1000 pairs of Arctic Tern (*Sterna paradisaea*), 7000 pairs of Black-legged Kittiwake (*Rissa tridactyla*), 700 pairs of Razorbill (*Alca torda*) and 700 pairs of European Shag (*Phalacrocorax aristotelis*) (Seabird 2000, JNCC). Guillemots and Razorbills primarily nest on cliffs to the west of the island. The largest colonies of Herring gulls are in the north of the island, the Arctic terns nest in the centre of the island and the shags in the south. The largest puffin colonies are on grassy slopes of the east, while smaller pockets of breeding birds exist elsewhere (Figure 5.17).

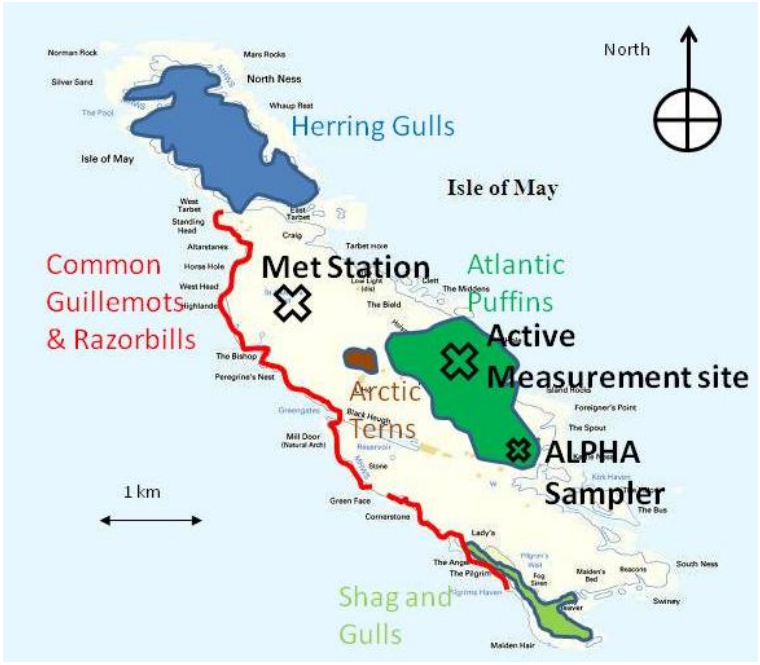

Figure 5.17 Primary nesting sites for Atlantic puffins, Herring gulls, European shags and Common guillemots on the Isle of May. The locations of the met station, active measurement site and the ALPHA sampler site have been included.

NH_3 concentration -Passive Campaign

A triplicate ALPHA sampler was used to measure the NH_3 concentration above the Atlantic puffin colony (56.186 N, 2.555 W), at a height of 1.5 m (Figure 5.17), for periods of 15 days (Table 5.10). Background NH_3 concentrations were measured at the meteorological station with another triplicate ALPHA sampler.

Figure 5.18 The triplicate ALPHA sampler above the Atlantic puffin colony, Isle of May, Scotland.

Meteorology

Meteorological data were collected by a weather station positioned at the highest point of the island (56.186°N, 2.558°W). The weather station (Figure 5.19) was

located to minimise effects on the nesting birds. Micrometeorological parameters were measured with a Gill Windmaster Pro sonic anemometer at 2.5 m until 15th July 2009.

Figure 5.19 Weather station *in-situ* on the Isle of May, collecting data on temperature, humidity, solar radiation, rainfall and ground temperature.

Results

NH_3 concentration

NH_3 concentrations decreased from a maximum during the first period (01/07/2009 - 15/07/2009) to a minimum during the fourth measurement period (Table 5.10). The background NH_3 concentration is 1 µg m^{-3}.

Table 5.10 Measured NH_3 Concentrations from ALPHA samplers on Isle of May 1/7/09 to 6/9/09. The concentrations are means of the triplicates deployed. [NH_3] indicates NH_3 concentration, Bgnd [NH_3] indicates background NH_3 concentration, *T* indicates temperature, *P* indicates precipitation, *WS* indicates wind speed, *WD* is wind direction and S.D. is the standard deviation.

Period	[NH_3] (µg m^{-3})	Bgnd [NH_3] (µg m^{-3})	*T* (°C)	Total *P* (mm)	*WS* (ms^{-1})	Resultant *WD* (°)	S.D. in *WD*
01/07- 15/07	36.1	1.3	15.0	85	3.3	163	86
15/07 - 29/07	16.4	1.1	15.4	29	5.4	278	75
29/07- 15/08	3.3	0.9	14.4	32	4.8	270	57
15/08- 06/09	0.9	0.9	14.8	63	6.6	282	51

Meteorological data

The average temperature for the four measurement periods was similar. The rainfall was largest during the first measurement period and smallest during the second period (Table 5.10). The wind direction during the first measurement period was the most variable, with a resultant direction of 163° to north with a standard deviation of 86°. During the second to fourth measurement periods the wind was mainly constantly from the north-west (Table 5.10 and Figure 5.20).

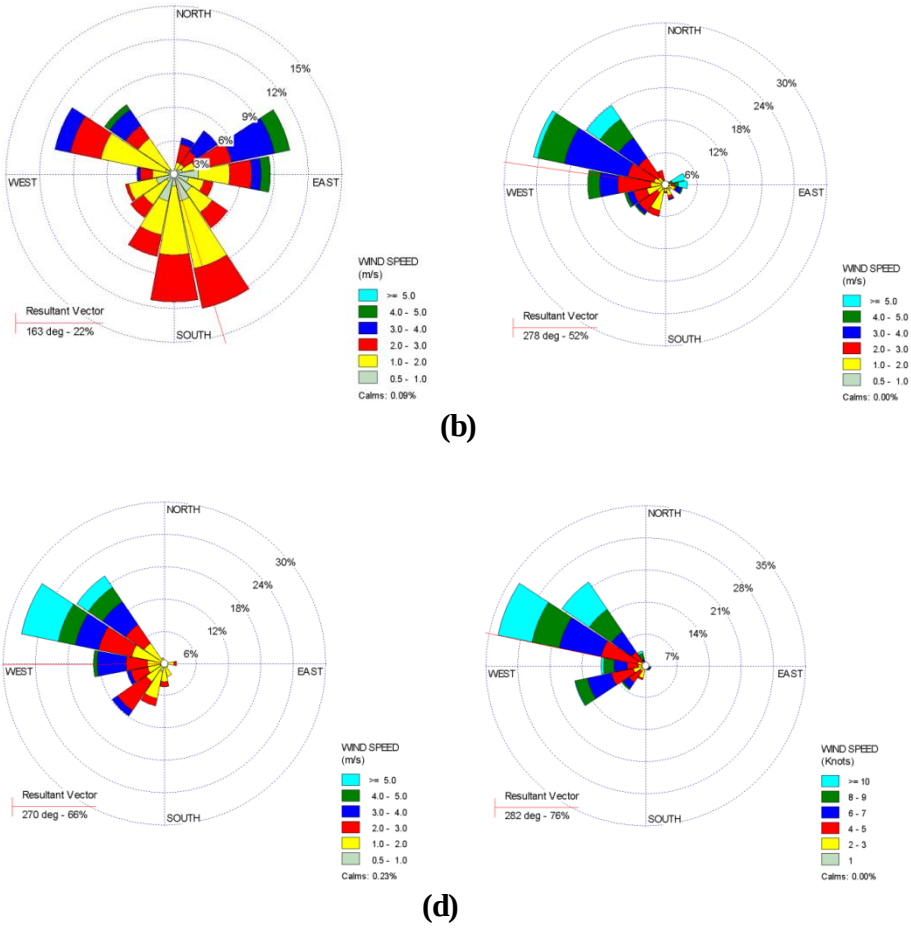

Figure 5.20 Wind rose for the Isle of May, Scotland, during the four measurement periods. (a) 01/07/2009 - 15/07/2009, (b) 15/07/2009 - 29/07/2009, (c) 29/07/2009 - 15/08/2009 & (d) 15/08/2009 - 06/09/2009.

Micrometeorological Data

Average values for roughness length (z_o = 4 cm) and Monin-Obukhov length (L = 25 m) were measured by the sonic anemometer during the active sampling campaign (29/6/09 to 24/7/09). For measurement periods 2, 3 and 4, the stability

was taken as neutral, based on observations of high wind speed and low irradiance. The roughness length was taken 4 cm, the same as for period 1, because this was the best available estimate.

NH_3 emission

The NH_3 concentrations, meteorological and micrometeorological data were entered into the WindTrax atmospheric dispersion model. The NH_3 emission was highest during Period 1(01/07/2009 - 15/07/2009), at 5.09 $\mu g\ m^{-2}\ s^{-1}$ (Table 5.11), which was towards the end of the breeding season. Around the 15th July the birds left the nesting site, NH_3 emission decreased from the maximum to background (0.1 $\mu g\ m^{-2}\ s^{-1}$) over the following two months (Table 5.11).

Table 5.11 NH_3 emissions measured during four passive NH_3 sampling campaigns at the Isle of May , Scotland (1/7/09 to 6/9/09).

Dates	NH_3 Emission from Puffins ($\mu g\ m^{-2}\ s^{-1}$)
01/07/2009 - 15/07/2009	5.09
15/07/2009 - 29/07/2009	1.92
29/07/2009 - 15/08/2009	0.35
15/08/2009 - 06/09/2009	0.10

Discussion

Uncertainty analysis

The roughness length used in WindTrax for the Isle of May was 4 cm. From observations at the site, the minimum that could be estimated for this type of terrain was 1 cm, representing bare soil. The maximum roughness height was estimated at 10 cm. A roughness height of 10 cm corresponds to an object of height similar to 1 m tall grass (Seinfeld and Pandis, 2006). There were no objects taller than 1 m in the vicinity of the colony.

The average Monin-Obukhov length during the first period was 25 m. Active sampling ended on the 15th July and the sonic anemometer was taken off the island. Owing to *L* being estimated measurement periods two to four, the range of uncertainty of the air stability was taken as the 25 % percentile and 75 % percentile of the average air stability.

The estimated open water NH_3 concentration for the southern North Sea is between 0.03 µg m^{-3} and 1.49 µg m^{-3} (Asman et al., 1994).

The area encompassing the burrows of the Atlantic puffins, measured using GPS was 16,000 m^2. The source was taken as any part of the island that the puffins could have excreted on. From observations of nest distribution, the maximum area was 32,000 m^2 and minimum was 8,000 m^2 (M. Harris, CEH, unpublished data).

The overall uncertainty for the model results from the passive campaign on the Isle of May was estimated at ± 38 % (Table 5.12), with the largest uncertainty being the Monin-Obukhov length.

Table 5.12 Uncertainty estimate of NH_3 emissions passive sampling campaign, Isle of May, Scotland, 1/7/09 to 6/9/09

Factor	Best Estimate	Max Value	Min Value	Uncertainty (%)
Roughness Length (cm)	4	10	0.1	12
Monin-Obukhov Length (m)	25	100	-100	28
Background Conc. (µg m^{-3})	1.3 – 0.9	1.49	0.01	8
Area of Nest Site (m^2)	16,000	32,000	8,000	10
Total Uncertainty in modelling (%)				38

5.3.5 Isle of May –Active Sampling Campaign

Method

NH_3 concentration -Active Sampling Campaign

The Isle of May campaign used a Pranalytica Nitrolux trace ammonia analyser to actively measure NH_3 concentrations from the Atlantic puffin colony (Figure 5.17). The Nitrolux was housed in a brick shelter on the Beacon region of the island (56.186 N, 2.555 W). The air inlet was positioned at 1.26 m above the ground (Figure 5.21).

Figure 5.21 Sampling NH_3 concentrations and collecting turbulence data on the Isle of May, Summer 2009. The image shows sampling at three heights. Measurements were taken from the middle inlet (black funnel).

Issues during data collection

The campaign was limited to daylight measurements to reduce disturbance to fledging puffins by the generator. Periods with wind coming from the brick shelter housing the instrument (wind sector 100° to 120°), were removed from the total dataset. To ensure that the NH_3 concentration measurements were representative of air coming from the puffin colony, data were also removed for air coming from other seabird nesting areas (between 135° and 330°).

Results

WindTrax Data Input

The measured NH_3 concentrations ranged from 0 to 215 µg m^{-3} and were lower during the morning and evening than during the day (Figure 5.23). Ground temperature ranged from 12 to 27 °C and peaked during the early afternoon. The roughness length on the Isle of May ranged from 0.1 to 13.8 cm, i.e., within the useable range of WindTrax. A background NH_3 concentration of 0.75 µg m^{-3} (Asman et al., 1994) was used for modelling, because of the direction of the wind for this campaign came from the open ocean.

NH_3 emissions estimated using inverse modelling

NH_3 emissions generally followed a diurnal pattern with low emission early in the morning (<5 µg m^{-2} s^{-1}), building to a peak in the early afternoon (10 to 25 µg m^{-2} s^{-1}), before dropping back to low value (<5 µg m^{-2} s^{-1}) in the evening (Figure 5.22).

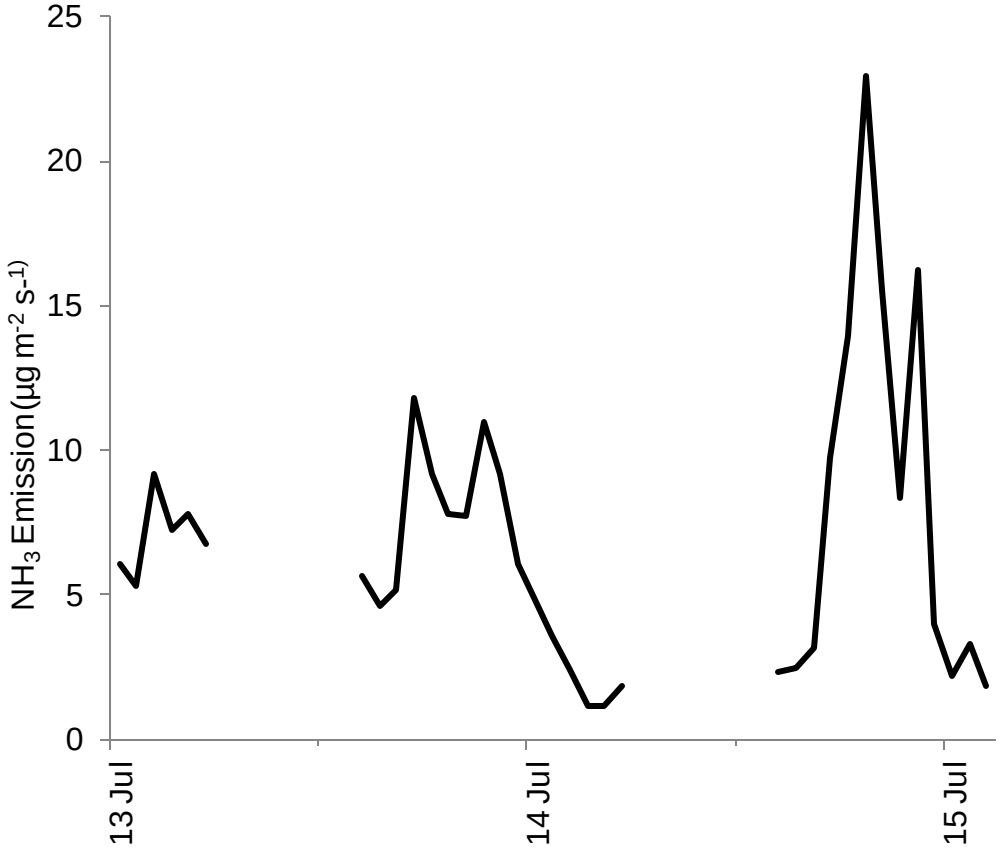

Figure 5.22 NH_3 emission estimates from the Atlantic Puffin nesting area on the Isle of May, Scotland, for the period 13th to 15th July 2009. This highlights the diurnal pattern of NH_3 emissions.

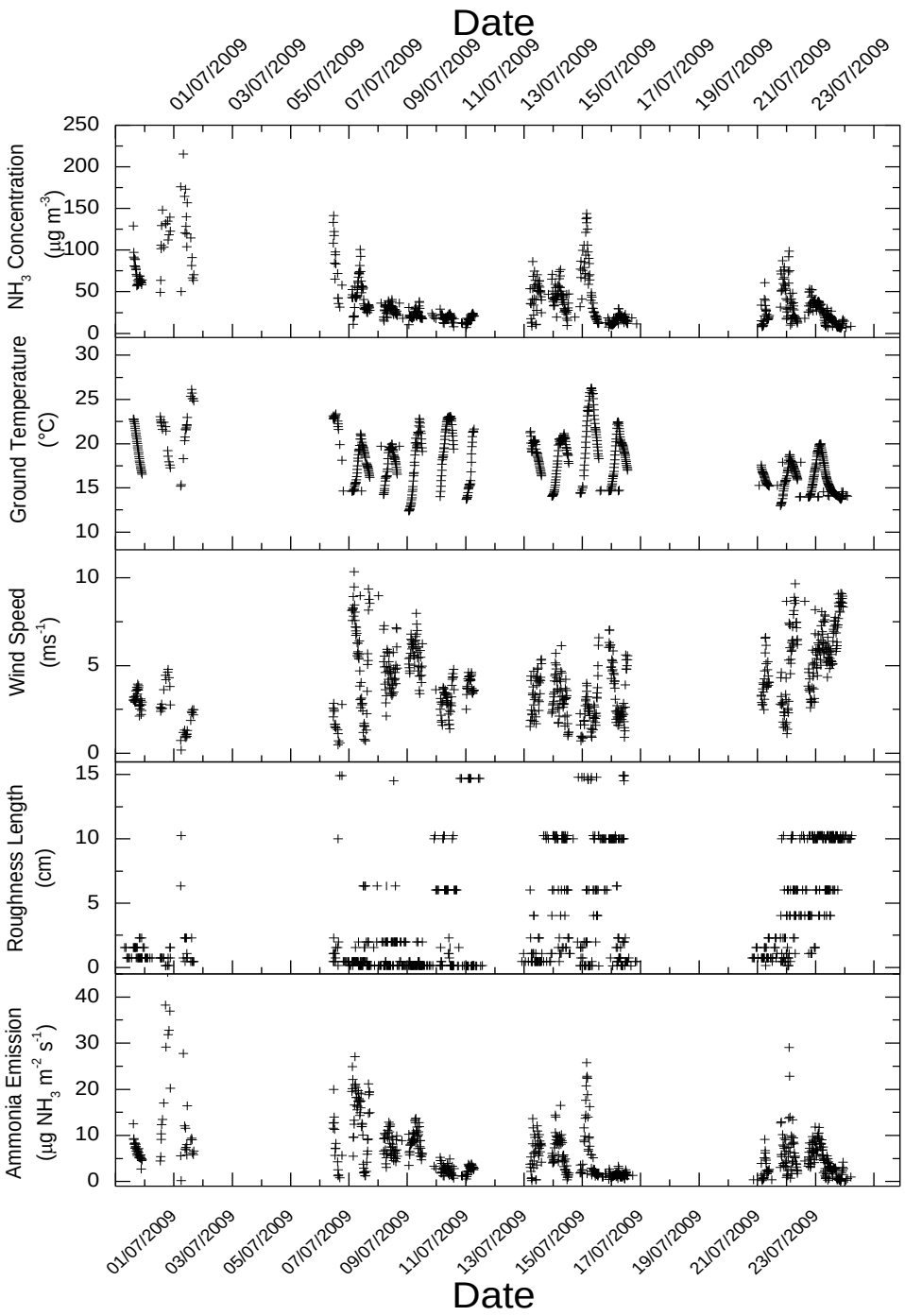

Figure 5.23 WindTrax input data and calculated NH_3 emission for the active sampling campaign on the Isle of May, Scotland Summer 2009

Discussion

While the diurnal pattern described above was common, emissions did not always follow the diurnal peak pattern. For example, NH_3 emissions on 7th July were largest at the start of the day, between 0600 hours and 1000 hours, at 12 - 22 µg m^{-2} s^{-1}. They then decreased to a minimum of 1 µg m^{-2} s^{-1} at 1700, before rising

back to 17 μg m^{-2} s^{-1} at 2200 hours. This pattern may have been caused by a combination of weather and bird behaviour. During the morning, thousands of puffins were sitting on the rocks outside their burrows in the morning sun. In the early afternoon there was a rain event, and during the late afternoon the clouds dispersed and the evening was warm. The processes behind these effects are explored in detail in Chapter 6.

Mean diurnal patterns in NH_3 emissions

On average, NH_3 emissions exhibited a strong diurnal pattern with a maximum in the afternoon (between 1400 and 1600 hours) and a minimum in the early morning (between 0100 and 0400 hours) (Figure 5.24). This study estimated the NH_3 emission at the Atlantic puffin colony on the Isle of May, Scotland, in June and July 2009 to be 0.46 g m^{-2} day^{-1} (5.32 μg m^{-2} s^{-1}).

The uncertainty range shows the variability in daily NH_3 emissions during the measurement period. The largest periods of uncertainty are during the morning and the evening. The near-zero variability at night is an artefact of limited data .

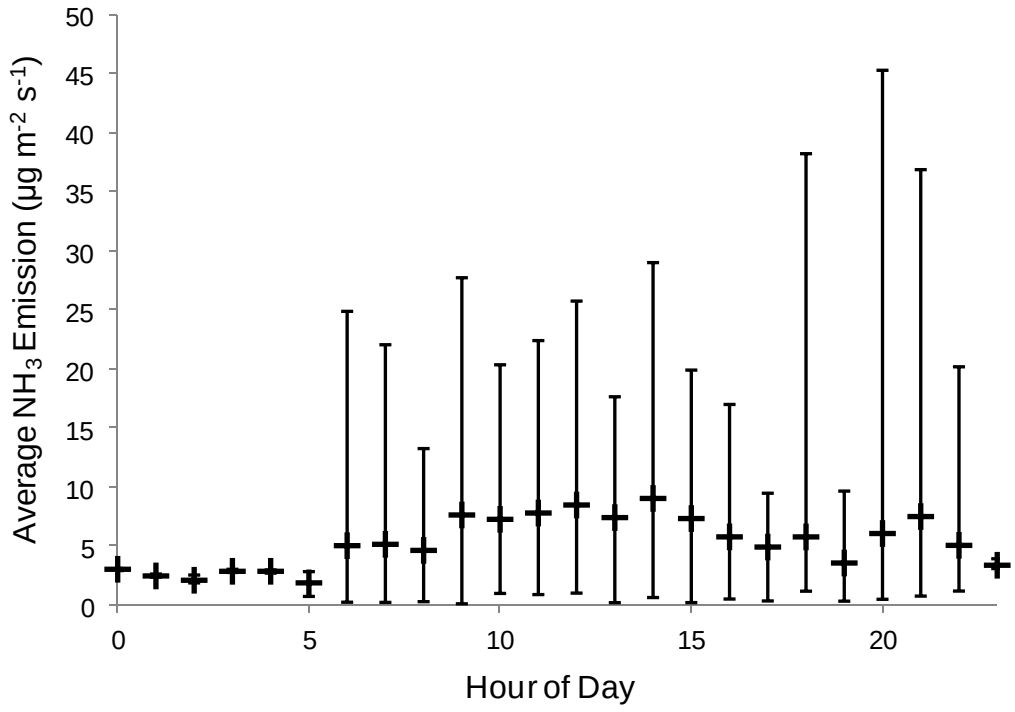

Figure 5.24 The averaged hourly NH_3 emissions derived from WindTrax emission data for the Atlantic Puffin colony on the Isle of May. Active sampling dates from 01/07/2009 - 23/07/2009. The error bars show variability in hourly emission by representing the maximum and minimum NH_3 emissions for these hours.

Uncertainty analysis

Uncertainties in background NH_3 concentrations and the size of the nesting area are described in the previous section. The total uncertainty in the modelling of the emission estimate on the Isle of May is estimated at 12 % (Table 5.13).

Table 5.13 Uncertainty analysis of WindTrax data for the NH_3 emission estimates at an Atlantic Puffin colony on the Isle of May, Scotland, in June/July 2009

Factor	Best estimate	Max Value	Min Value	Uncertainty (%)
Background Concentration (μg m^{-3})	0.75	1.49	0.03	6
Area of Nest Site (m^2)	16,000	32,000	8,000	10
Total Uncertainty in emission modelling (%)				12

5.3.6 Signy Island – Passive Sampling Campaign

Methods

The most accessible penguin nesting colony on Signy Island is found on the Gourlay Peninsula (60.72° S, 45.59° W). This peninsula is a flat, rocky plateau. The campaign to measure NH_3 concentrations on Signy Island was conducted during the austral summer, between the 10th of January and the 21st of February 2009.

The birds

The main penguin species on Signy Island are Adelie and Chinstrap penguins. The colony on the Gourlay Peninsula has an estimated area of 26,560 m^2 (Figure 5.25), with a breeding population of 10,240 pairs of Adelie penguins and 8,748 pairs of Chinstrap penguins. The population data were provided by the British Antarctic Survey (BAS), from the most recent decadal count (11 - 30 December 2009 for Chinstrap penguins, 18th November 2005 for Adelie penguins; D. Briggs, BAS, pers. comm.).

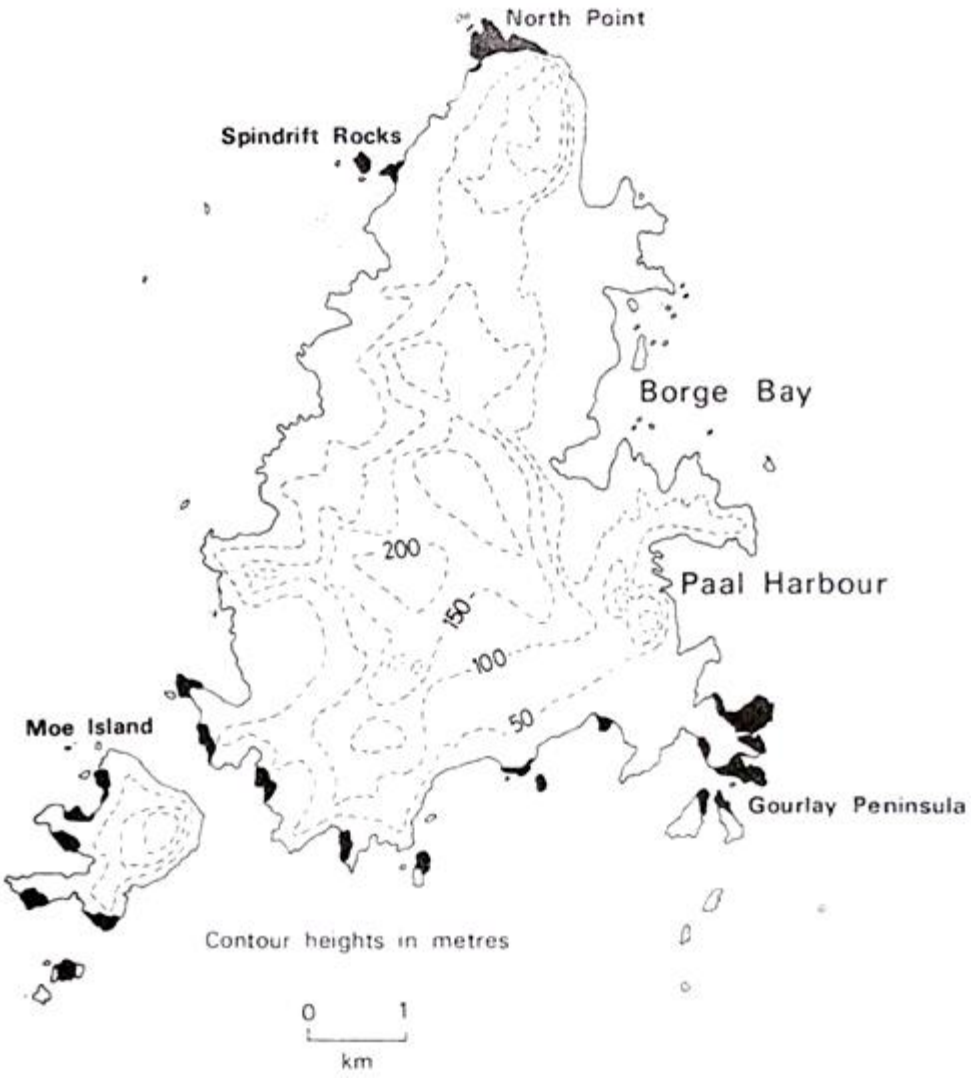

Figure 5.25 Penguin breeding sites on Signy Island, shaded in black. Map courtesy of the British Antarctic Survey.

The Adelie penguins arrived on the Gourlay Peninsula around the 26th September 2009 and the Chinstraps arrived around the 2nd November 2009. The Adelie penguins left the colony around the 25th January 2010, while the Chinstrap penguins were present throughout the study. The nesting site is relatively aerodynamically flat, the main obstacles being some rock formations and the penguins themselves, with both species of penguin around 60 cm tall (Figure 5.26). Nests are formed on bare rock and delineated by small pebbles. The surface roughness was estimated at 2 cm (Seinfeld and Pandis, 2006; P. Hill, University of Bangor, Wales, pers. comm.).

Figure 5.26 Mast 1 (with triplicate ALPHA samplers at three heights) looking west on Gourlay Peninsula, Signy Island, during the penguin breeding season. Image courtesy of Dr. P. Hill, University of Bangor.

Atmospheric NH_3 concentration – Passive sampling campaign

NH_3 concentrations were measured with ALPHA samplers at five locations around the penguin rookery (Figure 5.27) over three separate sampling periods (Table 5.14). The ALPHA samplers were deployed and retrieved by P. Hill of the University of Bangor, with triplicate ALPHA samplers at either one or three heights on each mast (Table 5.14).

Table 5.14 Location of ALPHA samplers on Signy Island January/February 2009

Mast	Location	Heights measured	Details
1	60.726° S, 45.583° W	0.5, 1 & 2 m	In the middle of the flat area in the centre of the Chinstrap penguin rookery.
2	60.727° S, 45.583° W	0.5, 1 & 2 m	Also in the Chinstrap penguin rookery, approximately 200 m South West of Mast 1
3	60.727° S, 45.591° W	1 m	Upwind of close-by penguin or seal area on Gourlay centre, this was clear of the rookery on top of hill.
4	60.725° S, 45.604° W	1 m	Further to the west of Mast 3. There was minimal influence from birds
5	60.713° S, 45.604° W	1 m	As far as possible from any birds, to sample background concentrations, *en route* from Borge Bay to Gourlay

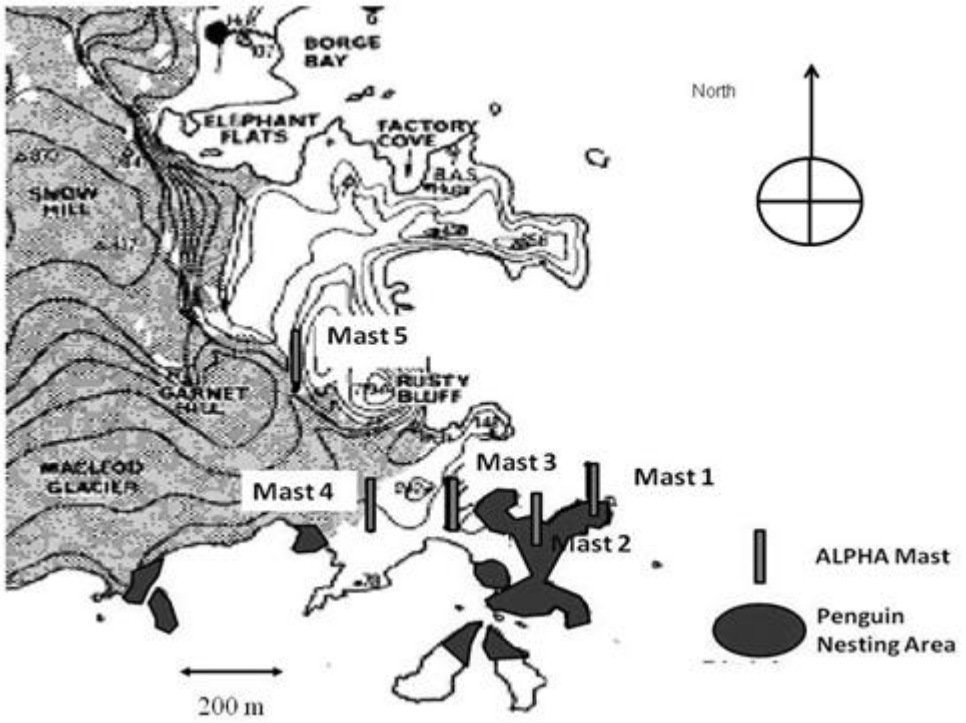

Figure 5.27 Location of ALPHA samplers on Gourlay peninsula, Signy Island. The dark grey areas on the map indicate penguin nesting sites. Map courtesy of the British Antarctic Survey.

Meteorology

Meteorological data for Signy Island were not available. Data were obtained from the US National Climatic Data Center **(**NCDC) Integrated Surface Hourly (ISH) database (NCDC, 2011) from the Argentinian Orcadas Base, located on Laurie Island, South Orkney Islands. The Orcadas base is the closest weather station to Signy Island (50 km).

Problems arising during sampling

During all sampling periods the ALPHA samplers at the lowest height (0.5 m) were interfered with by Snowy Sheathbills (*Chionis alba*). As a result, the ALPHA samplers at 0.5 m were not analysed.

Results

NH_3 concentration

The NH_3 concentrations at Masts 1 and 2, in the middle of the colony, were the highest. The ALPHA samplers lower to the ground also measured higher NH_3

concentration (Table 5.15). NH_3 concentration decreased with distance from the penguin colony to a minimum of 0.9 to 2.1 μg m^{-3} at Mast 5.

Table 5.15 NH_3 Concentrations (μg m^{-3}) from ALPHA samplers on Signy Island January/February 2009. Period 1 10/01/09 - 25/01/09, Period 2 25/01/09 - 08/02/09 and Period 3 08/02/09 - 21/02/09. Top ALPHA samplers are 2 m above the ground and Mid ALPHA samplers are 1 m above the ground. The concentrations are means of the triplicates deployed.

	NH_3 concentration (μg m^{-3})						
Period	Mast 1 2 m	Mast 1 1 m	Mast 2 2 m	Mast 2 1 m	Mast 3 1 m	Mast 4 1 m	Mast 5 1 m
1	157.2	294	326.7	483.3	7.7	2.3	0.9
2	70.6	170.6	92.0	151.5	8.4	1.9	1.4
3	105.6	339.2	154.5	233.8	13.7	5.2	2.1

Meteorology and micrometeorology

Data obtained from the ISH database for Laurie Island show that the wind speed and direction were similar for the three observation periods (Table 5.16 and Figure 5.28). The average daily temperature increased slightly throughout the measurement period, from 0.6 to 1.6 °C (Table 5.16).

Table 5.16 Meteorological data for Laurie Island, South Orkney Islands during the measurement periods. Period 1 10/01/09 - 25/01/09, Period 2 25/01/09 - 08/02/09 and Period 3 08/02/09 - 21/02/09 (NCDC, 2011). *T* indicates temperature, *P* indicates precipitation, *WS* indicates wind speed, *WD* is wind direction and S.D. is the standard deviation.

Period	*WS* (m s^{-1})	S.D. *WS*	*WD* (°)	S.D. *WD*	*T* (°C)	*P* (mm)
1	3.2	1.0	299	59	0.6	70
2	3.3	1.6	299	38	1.0	49
3	3.6	1.2	311	56	1.6	71

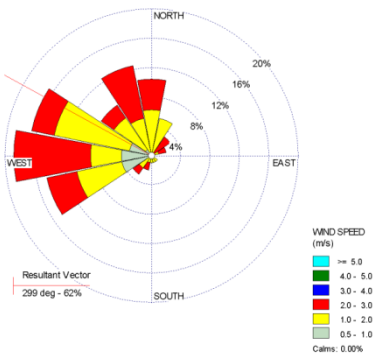

(a)

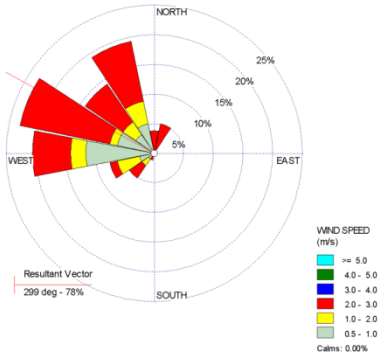

(b)

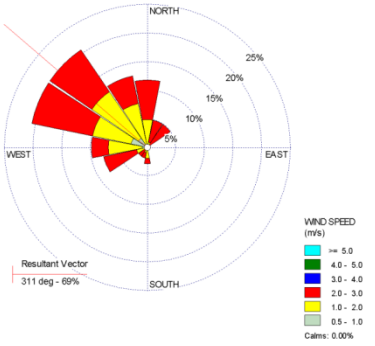

(c)

Figure 5.28 Wind roses for Orcadas Base, Laurie Island, South Orkney Islands over the three sampling periods relevant to Signy Island, for which they provide proxy wind data. (a) Period 1 10/01/09 - 25/01/09, (b) Period 2 25/01/09 - 08/02/09 and (c) Period 3 08/02/09 - 21/02/09.

Stability

The air stability is assumed to be neutral, with $L \rightarrow \infty$ m, owing to overcast skies, constantly strong winds and little difference between ground temperature and air temperature (Seinfeld and Pandis, 2006).

Roughness height

The most obvious causes of aerodynamic roughness were the penguins (average height 60 cm) and rocks (maximum height estimated at 1 m, see Figure 5.26). Therefore, a roughness height of 10 cm, corresponding to an object height of 1 m (Seinfeld and Pandis, 2006), was used for modelling of seabird NH_3 emissions from Signy Island

NH_3 emission rate

NH_3 emission rates for the penguin colony on Signy Island during January and February 2009 ranged from 7.89 to 18.17 µg m^{-2} s^{-1} (Table 5.17). The wind was almost constantly from the north-west (Figure 5.28). This suggests that the footprint of the source sampled by each ALPHA sampler was not a very significant source of variation. The micrometeorological conditions on Signy Island can only be estimated from available data on another island, at 50 km distance and, as such, a large uncertainty is associated with the NH_3 emissions estimated by the modelling method applied.

The difference in the NH_3 emission rates between the two measurement periods may be explained by the birds' behaviour, with colony attendance during the first measurement period high for both Adelie and Chinstrap penguins. The lower emissions during the second and third periods are likely due to the departure of the Adelie penguins.

Table 5.17 NH_3 emission estimates calculated by WindTrax for Signy Island January/February 2009

Measurement periods	Emission Estimate (µg m^{-2} s^{-1})
10/01 - 25/01	18.17
25/01 - 08/02	7.89
08/02 - 21/02	9.02

Uncertainty analysis

The sensitivity analysis was conducted using a minimum roughness length of 1 cm, representing bare soil, and a maximum of 15 cm, representing an object of height 1.5 m (Seinfeld and Pandis, 2006).

The air stability is assumed as constantly neutral, with $L \rightarrow \infty$ m. A range of stabilities typical for the weather conditions was investigated, from stable (L = 100 m) to unstable (L = -100 m). In stable conditions the NH_3 emission calculated by WindTrax decreases because vertical transport of the NH_3 gas decreases. As the input value of the Monin-Obukhov length becomes less stable, the vertical transport of the gas increases and the calculated emission increases.

The concentrations of Mast 5 etc were used as the background for the calculations, at 0.9-2.1 μg m^{-3} for the three measurement periods (Table 5.18). These estimates may be high (and still affected by some bird sources), compared with estimates of 0.01 - 0.31 μg m^{-3} by Gras (1983) for open water background NH_3 concentrations for the Antarctica, a location representative of this area.

The location and size of the area with guano deposited by the penguins has a larger uncertainty associated than for the other field sites where GPS data were collected. Instead, photographs were used to estimate the extent of the area where guano was excreted. Guano deposits were observed up to 10 m from the edge of the area where the penguin nested. The associated uncertainty in area was estimated at ± 20 %.

Table 5.18 shows the overall uncertainty in modelling NH_3 emissions for Signy Island, estimated at ± 34 %, with greatest uncertainty due to the parameterization of the roughness length and the Monin-Obukhov length.

Table 5.18 Uncertainty analysis on NH_3 emission estimate from Signy Island, 10/01/2009 – 25/01/2009

Factor	Best estimate	Max Value	Min Value	Uncertainty (%)
Roughness Length (cm)	10	15	1	26
Monin-Obukhov Length (m)	∞	100	-100	20
Background Conc. (μg m^{-3})	0.9 – 2.1	2.1	0.01	7
Area of Nest Site (m^2)	27,000	31,870	21,250	6
Total Uncertainty in modelling (%)				34

5.3.7 Bird Island – Active Sampling Campaign

Method

Overview

Bird Island (54.0° S, 38.05° W) is part of the archipelago of South Georgia. On the island, rocks and scree, covered in mosses and lichen are found on steep terrain, upland areas are mostly bog meadowland and lower elevations, below 150 m, are covered by tussock grasses (*Poa flabellate*), ranging in height from 30 to 150 cm. The main NH_3 monitoring site was set up to measure emissions from a

Macaroni penguin colony (referred to as "Big Mac") at Fairy Point, on the North-west coast of Bird Island (Figure 5.29).

The birds

Bird Island is the breeding site of 50,000 pairs of Macaroni penguins. 10 km west of Bird Island, Willis Island is one of the largest breeding grounds of this species, with 500,000 pairs of Macaroni Penguins every year (P. Trathan, BAS, pers. comm.). The most accessible penguin colony on Bird Island is the Big Mac colony, where 40,000 pairs of Macaroni penguin breed each year.

Data Collection

All measurements on Bird Island were carried out by Y. S. Tang of CEH Edinburgh. During the campaign, two sampling sites were used: the first site (54.0106 °S, 38.0753 °W) between the 18th and 24th of November 2010 and second (54.0104 °S, 38.0742 °W) between the 8th and 15th of December 2010. The measurement site was relocated to increase the amount of wind coming from Big Mac. The sites were close together and share similar aerodynamic properties.

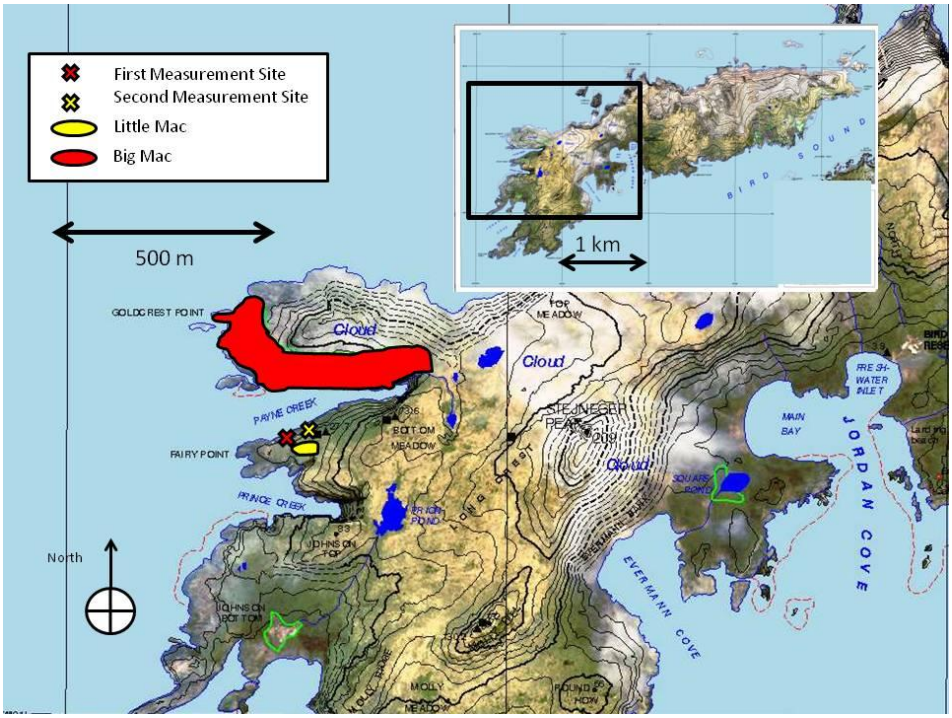

Figure 5.29 A map of Bird Island, South Georgia, with locations of the British Antarctic Survey (BAS) research station and the NH_3/met monitoring site at Fairy Point marked. Image courtesy of the British Antarctic Survey.

NH_3 concentration -Active Sampling Campaign

The AiRRmonia NH_3 analyser was used to actively measure the NH_3 concentrations from Big Mac on a 15 minute basis, with the air inlet positioned at 2 m above the ground. All the instruments were housed within a tent, to provide protection from the wind, precipitation, salt spray and sun.

Meteorology

Micrometeorological parameters were measured using a Gill Windmaster Pro sonic anemometer on a mast 2.5m above the ground. Meteorological data were collected by instruments on two masts on the highest point at Fairy Point (Figure 5.30). Data collected included: air temperature, humidity and solar radiation at 1 m above ground, and wind speed at three heights above ground (0.5 m, 1 m, 2 m). Ground temperature was measured using a Tiny Talk data recorder placed on the ground, as described in section 5.2.5.

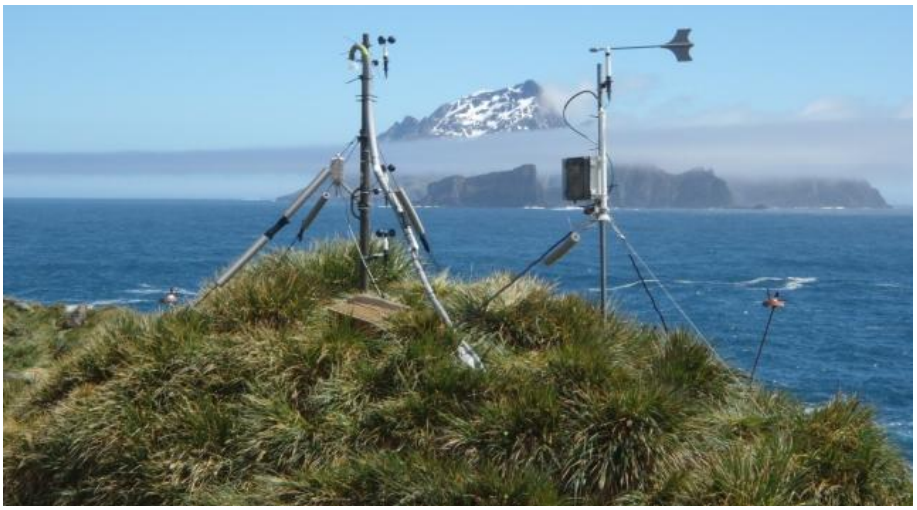

Figure 5.30 Meteorological instruments on two masts on the highest land at Fairy Point, Bird Island, with Willis Island in the distance (10 km). Image courtesy of Sim Tang, CEH.

Issues during data collection

The sonic anemometer was damaged by a bird strike on the 19th November, shortly after deployment. Micrometeorological values were subsequently calculated from the wind profile measurements, using the equations described immediately below.

Micrometeorology

Roughness height (z_0, m), friction velocity (u_*, ms^{-1}) and Monin-Obukhov length (L, m) were calculated from the wind profile at 1.5 m, 1 m and 0.5 m. The friction velocity was calculated from the von Karman constant (k, 0.41), the three heights above ground where wind speed was measured at (z, m) and the respective wind speeds (u, ms^{-1}), where:

$$u^* = k\frac{\Delta ln(z)}{\Delta u}. \quad (5.4)$$

The roughness length was calculated as the exponential of the intercept, with the natural logs of wind measurement heights plotted against wind speeds. The Monin-Obukhov length was calculated using Equation 5.5.

$$L = -\frac{\rho c_p T_0 u_*^3}{KgH} \quad (5.5)$$

Where, ρ is the density of air, c_p is the specific heat capacity of air at constant pressure, T_0 is the absolute temperature of air at z = 0, K is the von Karman constant (≈0.4) and g is the acceleration due to gravity. The sensible heat flux (H, W m^{-2}) was calculated from the density of air, specific heat capacity of air, the air temperature (T_a, K), absolute temperature of air at z = 0 (T_0, K), wind speed (u, m s^{-1}) and the transfer coefficient for sensible heat flux (CH, $1x10^{-3}$) (Pan et al., 2003), where:

$$H = \rho c_p CH(T_a - T_0)u. \quad (5.6)$$

Results

Data Input to WindTrax

The NH_3 concentrations measured by the AiRRmonia trace gas analyser were between 0 and 60 µg m^{-3}, with higher concentrations during the day (Figure 5.31). Ground temperature ranged from 1 to 12 °C, with peaks during the early afternoon. The roughness lengths on the Bird Island ranged from 6 to 12.5 cm and were within the useable range of WindTrax. Gras (1983) estimated open water background NH_3 concentration for the Antarctica, a location representative of this area, at 0.01 - 0.31 µg m^{-3}. The average of these values, 0.15 µg m^{-3}, was used as the background concentration in WindTrax.

NH_3 emission

The maximum and minimum NH_3 emissions from Big Mac during the measurement period were 52.6 µg m^2 s^{-1} and 0.6 µg m^2 s^{-1}, respectively (Figure 5.31). The largest emissions occurred during the day, with smaller emissions at night.

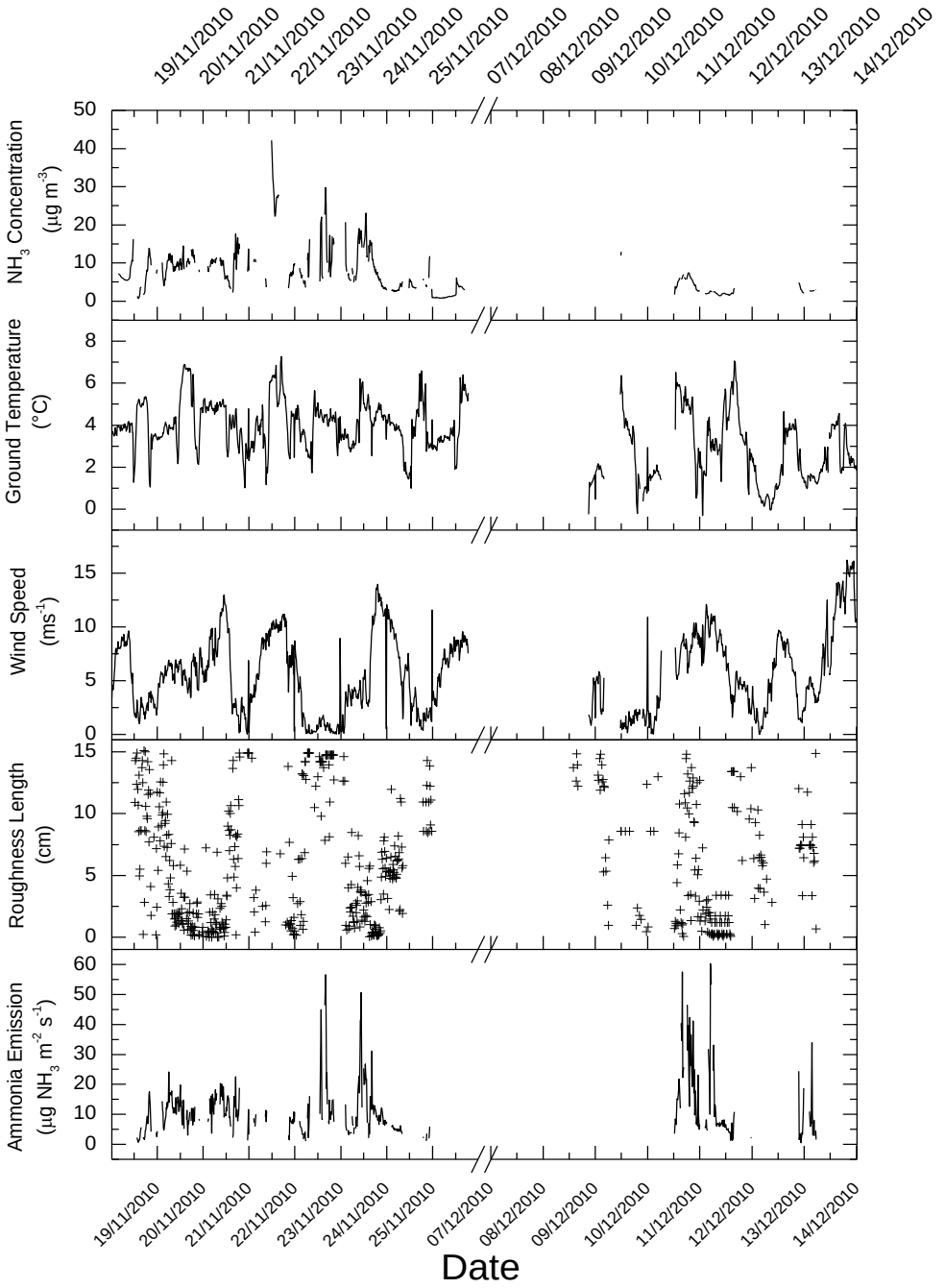

Figure 5.31 Data input to WindTrax and resulting NH_3 emission for active sampling campaign on Bird Island, South Georgia, Nov & Dec 2010

Diurnal variation in NH_3 emissions

NH_3 emissions at Big Mac do not show the strong diurnal pattern calculated for the other colonies. The emissions range from 5 to 10 µg m^{-2} s^{-1} during the night and increase to 20 µg m^{-2} s^{-1} during the day (Figure 5.32). The estimated daily NH_3 emission for the Big Mac colony was 1.02 g NH_3 m^{-2} day^{-1} (average 11.81 µg m^{-2} s^{-1}). The error bars show variability in hourly emission by representing the maximum and minimum NH_3 emissions for these hours during the measurement period.

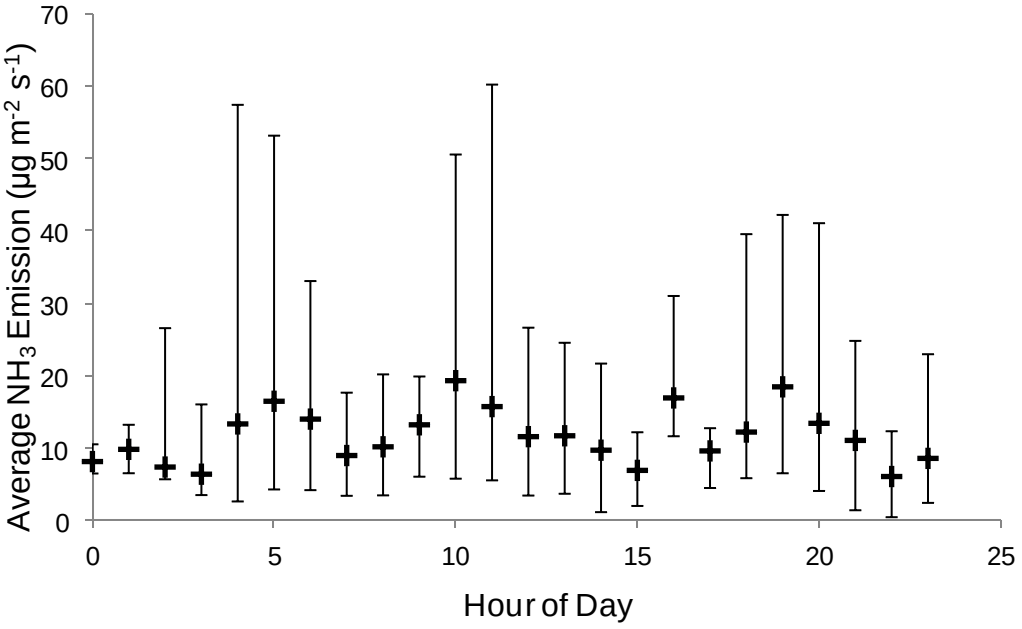

Figure 5.32 Average hourly NH_3 emissions derived from WindTrax emission data for the Big Mac penguin colony, Bird Island, for the entire monitoring period 18 Nov to 13 Dec 2010. The error bars show variability in hourly emission by representing the maximum and minimum estimated NH_3 emissions for these hours.

Uncertainty analysis

The area where the penguins deposit guano has a large uncertainty associated with it, with the footprint area estimated from the position of the nesting area, making the assumption that penguins only excrete guano near their nests. An uncertainty estimate from photographs shows this to be the edge of the area taken up by the nests ± 20 %.

Table 5.19 shows the total uncertainty calculated for the modelled emission estimate from the Big Mac penguin colony at ± 28 %, with the largest uncertainties in emission caused by the estimated size/area of the nest site.

Table 5.19 Uncertainties associated with the atmospheric dispersion modelling of a Macaroni penguin colony on Bird Island.

Factor	Best Estimate	Max Value	Min Value	Uncertainty (%)
Background Concentration (μg m^{-3})	0.15	0.31	0.01	4
Area of Nest Sites (m^2)	30,000	36,000	24,000	27
Total Uncertainty in emission modelling (%)				28

5.4 Discussion

Near-source estimation of NH_3 emissions from seabird colonies using NH_3 concentration data, meteorological data and an atmospheric dispersion model offer a solution to the difficulties presented by boat-based measurements encountered by Blackall et al. (2007). Estimating NH_3 emissions from seabird colonies can be difficult because of near surface air movement caused by complex topography. However, these difficulties can be overcome through the careful selection of suitable colonies. The sites selected for this study were the most topographically and aerodynamically suitable (with a roughness length of less than 15 cm), with adequate ammonia emissions, and relatively accessible, so that heavy instruments can be transported to the sites and set up securely. The findings in this chapter represent the first comprehensive campaign of NH_3 emission estimates from measurements at seabird colonies in a range of climates.

This chapter has introduced two methods that can be used to measure NH_3 emission: passive and active sampling. Measurements were carried out using both methods across five seabird colonies, with NH_3 emissions estimated to range from 5.39 μg m^{-2} s^{-1} at a UK Atlantic puffin colony to 18.40 μg m^{-2} s^{-1} for a Sooty tern colony on Ascension Island.

5.4.1 General observations

NH_3 concentrations measurements were made using both passive and active instruments. The passive campaigns were opportunistic and provided some excellent low-time resolution information on the NH_3 emission from colonies that could not otherwise have been studied. These passive campaigns were planned and organised at CEH Edinburgh, the samplers exposed in the field by a non-specialist and then shipped back for analysis in the laboratory by myself. These campaigns were relatively easy to conduct and were not intrusive to the birds' environment, apart from low levels of disturbance associated with the initial installation/positioning of sampling equipment.

The active sampling methods used to measure NH_3 concentrations at remote sites presented greater logistical challenges because the equipment is large, heavy, noisy and 240 V electricity. The initial active measurement campaign on the Isle of May used the Nitrolux gas analyser. This instrument is not weather proof and has relatively high power consumption (~ 150 W). The high power consumption limited the length of time over which measurements could be taken, as only limited fuel could be taken to the Isle of May in any one trip. Therefore, once all fuel had been used up, it was necessary to return to the mainland for more fuel supplies. Furthermore, the generator used (Honda G200) had a continuous run time of only four hours and needed near constant attention, as it was prone to cutting out, which further reduced the periods of continuous data collection. The generator was turned off at night to avoid distracting puffins from fledging, as advised by the island warden. This meant that only very few data on night time NH_3 concentrations were collected until after the pufflings had fledged.

By the time of the second active measurement campaign on Ascension Island, a year later, many of the challenges encountered on the Isle of May had been overcome. The Nitrolux gas analyser had been replaced by the AiRRmonia, which is lighter and more easily transported to remote field sites. It also uses less power (~ 50 W) and had been weatherproofed, meaning that it was able to run continuously for an extended period of time, and thus data could be collected for both day and night NH_3 concentrations. The AiRRmonia required little attention apart from recalibration every five days, which involved a short interruption to

data collection, for 67 hours out of the total 472 hour long measurement campaign. The generator used on the Isle of May had been replaced with a quieter and more efficient model (Honda EU10i), in combination with an extended fuel tank. A single tank was sufficient for three days, thus necessitating much less regular refuelling.

The third active measurement campaign, at Bird Island, South Georgia, was the most remote and encountered a great deal of problems. The site was distant from the field base (2 hour return trip from the BAS base), and weather conditions were challenging. Heavy and prolonged rain in combination with high winds caused water to permeate into many of the sealed instruments at the exposed Fairy Point site. Water also infiltrated the two generators and the AiRRmonia despite precautions. The fuel tanks required constant attention and the motherboard of the AiRRmonia needed to be replaced. These issues are reflected in the relatively small number of data collected, with 121 hours of data from a 360 hour field campaign.

5.4.2 Comparison of Passive to Active campaigns

One aim of this study was to refine a near-field method to estimate NH_3 emissions from seabird colonies. Of the two methods used, active sampling provides much better time resolution for estimating NH_3 emissions from atmospheric concentration measurements than the passive samplers. The active method also utilises micrometeorological data measured by the sonic anemometer to provide estimates with much less uncertainty. Despite these differences, the NH_3 emission estimates made by the active and passive methods are very similar (Table 5.20).

Table 5.20 Comparison of NH_3 emissions estimated by active and passive measurement methods for the Isle of May and Ascension Island.

Colony and measurement period	Actively Measured NH_3 Emission ($\mu g\ m^{-2}\ s^{-1}$)	Passively Measured NH_3 Emission ($\mu g\ m^{-2}\ s^{-1}$)
Isle of May – Period 1	5.3	5.1
Ascension - Period 1	21.7	18.1
Ascension - Period 2	9.3	5.0
Ascension - Period 3	28.2	29.2

5.4.3 Summary of NH_3 emissions from seabird colonies

Measured NH_3 emissions expressed on a breeding season average basis were largest for tropical seabird colonies and slightly lower for polar colonies (Table 5.21). A commercial poultry installation of ~70,000 birds (0.1 kg NH_3 $bird^{-1}$ yr^{-1}) emits ~19 kg NH_3 day^{-1}, the same as Michaelmas Cay during breeding season. This shows that seabird colonies throughout the world are considerable sources of NH_3 emission. The difference between the colonies in different climates can also be expressed as the percentage of excreted nitrogen that volatilizes (P_v, %). At tropical colonies, such as Michaelmas Cay, 65 % of the excreted nitrogen was estimated to be emitted as NH_3 gas, whereas for Bird Island a P_v of 1.6% was calculated (Table 5.22).

Table 5.21 Summary of seabird colony NH_3 emissions estimated from measurement campaigns at five field sites carried out for this thesis

Colony	Avg. Temp. (°C)	Breeding Pairs of seabirds	Area (m^2)	Measured NH_3 Emission ($\mu g\ m^{-2}\ s^{-1}$)	Uncertainty in modelling (%)
Michaelmas - Passive	27	7,000	10,000	21.8	35
Ascension - Active	28	100,000	79,000	18.9	12
Ascension - Passive	28	100,000	79,000	17.6	24
Isle of May - Active	14	41,000	16,000	5.3	12
Isle of May - Passive	14	41,000	16,000	5.1	38
Signy Island – Passive	2	19,000	27,000	11.7	34
Bird Island - Active	3	40,000	30,000	11.8	28

5.4.4 Comparison between measured and modelled emissions

A further objective of this chapter was to use the measured NH_3 emissions to validate NH_3 emission estimates calculated by the bioenergetics (BE) model (Chapter 3 - Scenario 1), the temperature adjusted bioenergetics (TABE) model (Chapter 3 - Scenario 2) and the mid-range best estimate (Chapter 3 - Scenario 3) (Table 5.23). The measured emissions are scaled up for a complete breeding season by multiplying the average daily NH_3 emission by the number of days the birds spend at the colony.

There is a poor relationship between the BE model (Scenario 1) and the measured emissions (linear regression $R^2 = 0.003$) (Table 5.22). The measured emissions have a better relationship to those calculated by the TABE model (Scenario 2) (Linear regression $R^2 = 0.81$) and the Best Estimate model (Scenario 3) (linear regression $R^2 = 0.71$). The TABE model estimates (Scenario 2) are the best fit, but it overestimates NH_3 emission at all measurement sites, especially in the warmer climates (Michaelmas Cay and Ascension Island). All three models over-estimate the NH_3 emission from Big Mac, which suggests that temperature is not the sole consideration for the proportion of excreted nitrogen that volatilizes as NH_3 in sub-polar Regions. The high level of precipitation at this site is likely to have contributed to the lower emissions.

Table 5.22 Comparison of NH_3 emission estimates, modelled by the bioenergetics (BE) model (Scenario 1), the temperature adjusted bioenergetics model (TABE, Scenario 2) and the mid-range best estimate (Scenario 2) with the measured emissions scaled up for the entire breeding season at each site, and the equivalent percentage of excreted nitrogen that is volatilized as NH_3.

	NH_3 Emission (kg NH_3 $year^{-1}$)				% volatilisation of excreted N			
	Measured	Chapter 3 Scenario			Measured	Chapter 3 Scenario		
		1	2	3		1	2	3
Michaelmas	2.3	1.0	2.4	1.7	65	27	68	48
Signy Island	6.9	45.6	8.9	27.2	3.1	21	4.0	12
Isle of May	1.1	2.3	1.7	2.0	4.7	9.8	7.3	8.5
Ascension	15.3	13.2	32.9	23.1	32	27	68	48
Bird Island	6.5	161.7	36.4	99.1	1.6	40	9	25

5.5 Summary and conclusions

The data presented in this chapter give the first measurement-based NH_3 emission estimates for seabird colonies in a range of climatic conditions. The largest NH_3 emission was found on Michaelmas Cay, where an average emission of 21.78 µg m^{-2} $s^{-1}$was estimated. The smallest emission was calculated for the Isle of May, with an average emission of 5.3 µg m^{-2} s^{-1} for burrow-nesting puffins. This study indicates that seabird colonies are large sources of NH_3 emissions in remote areas, across all climatic regions, from tropical to polar.

This chapter presented a comparison of NH_3 emissions made by passive and active sampling methods. It is recommended that active sampling should be used where possible, because more accurate measurements reduce the overall uncertainty in the estimates. However, if an active campaign is unfeasible (due to challenges caused by finance, time or expertise availability), passive sampling campaigns can produce similar results but will lower the temporal resolution. Care should be taken when parameterising the inputs to the atmospheric dispersion model, as incorrect input can result in large errors in the output.

A comparison of the measurement results with the theoretical model scenarios described in Chapter 3 was carried out, which showed that estimates by the TABE model (temperature adjusted scenario) are in good agreement with

measured emissions ($R^2 = 0.81$). Even though the TABE model has some success at estimating emissions, it overestimates emissions at all field sites. Fieldwork has additionally shown that NH_3 emissions are dependent on factors other than temperature, i.e., precipitation and water availability. These issues are explored in detail in Chapter 6.

Chapter 6: High temporal resolution modelling and validation of climate dependant seabird ammonia emissions

6.1 Introduction

Many empirical studies have reported that environmental factors, such as temperature (Elliot and Collins, 1982; Demmers et al., 1998; Sommer et al., 1991), water availability (Elliot and Collins, 1982; Sommer & Olesen, 2000), pH of the substrate (Stevens et al., 1989; Chantigny et al., 2004; Cortus et al. 2009) and wind speed (Demmers et al., 1998; Sommer et al., 1991; Olesen and Sommer, 1993; Zhang et al., 1994), affect the rate of NH_3 emission from agricultural sources. NH_3 volatilization has been shown to increase in both high temperatures and high wind speeds (Demmers et al., 1998; Sommer et al., 1991), while rain events have caused NH_3 emissions to drop to almost zero (Sommer & Olesen, 2000).

Several studies have reported on modelling NH_3 emissions from agricultural sources. Cortus et al. (2009) used a model to simulate NH_3 emission rates from swine slurries that varied in physical and chemical composition. Pinder et al. (2004) used temperature, precipitation and wind speed to estimate monthly NH_3 emissions from dairy cows. Génermont & Cellier (1997) created a mechanistic model to estimate NH_3 emission from slurry applied to bare soil, based on processes within the soil and dependent on meteorological conditions. The models described above vary in detail, time resolution and complexity, with the Génermont & Cellier (1997) model requiring over 50 input parameters.

Despite differences in complexity, these NH_3 emission models use similar mechanisms to describe the evolution of NH_3: a nitrogen source is deposited on a surface, which is transformed to TAN and then NH_3, with subsequent volatilization of NH_3 to the atmosphere. To varying degrees, climate (e.g. temperature, wind speed, precipitation) and surface properties (e.g. pH, saturation water conductivity and boundary layer resistance) are used to calculate the emission of atmospheric NH_3.

In contrast to agricultural sources, few studies have investigated NH_3 emission from nitrogen excreted by seabirds. Zhu et al. (2011) showed, in laboratory

studies, that the release of NH_3 from nitrogen excreta has strong temperature dependence, where NH_3 emissions increased exponentially with an increase in temperature. NH_3 emissions have also been found to depend on the substrate onto which nitrogen is excreted. When nitrogen excreted on rock, all NH_3 that is volatilized is emitted to the atmosphere, whereas, most NH_3 produced from nitrogen excreted in a burrow is absorbed into the soil and vegetation in the walls and roof of the burrow (Wilson et al., 2004; Blackall et al., 2007; as also shown in Chapter 4).

The first dynamic model to calculate NH_3 emissions from seabird nitrogen excreta is the 'Generation of emissions from Uric Acid Nitrogen Outputs (GUANO)' model developed by Blackall (2004). The GUANO model calculates NH_3 emissions from a single seabird colony using climatic variables (temperature, relative humidity, precipitation and wind speed) and colony specific data (pH, substrate type, N excretion rate). The GUANO model was tested against NH_3 emissions measured from the seabird colony on the Isle of May, UK. The modelled emissions reported by Blackall (2004) using the GUANO model underestimated measured emissions on the Isle of May.

This chapter describes refinements made to the GUANO model so that it can be applied to global seabird populations in varying climates. For example, the refined GUANO model considers water evaporation in hot climates and the difference between air temperature and ground temperature. The NH_3 emissions calculated by the refined model are validated using observations at the five fieldwork sites (Chapter 5). The comparisons of the measured and modelled emissions are used to determine the suitability of the GUANO model in estimating the global NH_3 emissions from seabird colonies.

6.2 Methods and Materials

6.2.1 Modelling NH_3 production

The emission of NH_3 from seabird excreted N can be described in four steps (Figure 6.1):

1. Nitrogen rich guano, in the form of uric acid, is excreted onto the surface by seabirds at the colony. The amount of guano varies depending on the mass and behaviour of the nesting species.
2. A percentage of uric acid is converted to total ammoniacal nitrogen (TAN). The conversion rate depends on climatic conditions and the pH of the surface (Hoff, 1981; Elliot and Collins, 1982, Elzing and Monteny, 1997; Groot Koerkamp et al., 1998).
3. TAN partition between NH_4^+ and NH_3 on the surface. The position of the equilibrium depends on the pH on the surface and the surface temperature (Nemitz et al., 2000).
4. NH_3 on the surface volatilizes to the atmosphere. The rate of volatilization depends on the wind speed, aerodynamic resistance (R_a and R_b) and the amount of NH_3 reabsorbed by the substrate and any overlying vegetation (Sutton et al., 1992; Nemitz et al., 2001).

Guano and TAN may be washed from the surface at any stage when it rains.

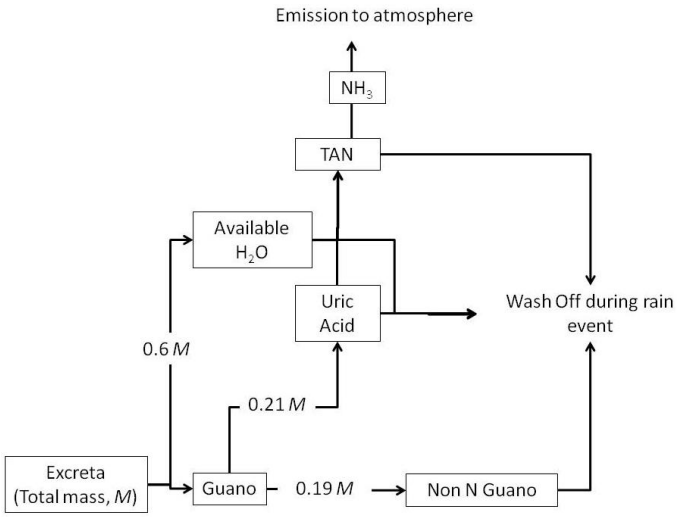

Figure 6.1 Pathways taken by nitrogen following excretion as uric acid (after Blackall, 2004 modified). The total mass of excreta (M) is made from 0.6 M of water, 0.21 M of uric acid and 0.19 M non-N guano.

6.2.2 Blackall's GUANO model

1. Excretion of nitrogen

The rate of excretion by seabirds (described in Section 3.2.2) following the method of Wilson et al. (2004). The amount of nitrogen excreted daily is calculated from the metabolic rate for adults and chicks, the nitrogen content of the food and the efficiency of digestion. Nitrogen excretion of a non-breeding adult at the colony is estimated at 16.7 % of the daily N excreted by a breeding bird at the colony because non-breeders make up 33 % of the breeding population and spend 50 % less time at the colony (Wilson et al., 2004).

The N excretion density at the colony (F_e, g m^{-2} $hour^{-1}$) is calculated from the total time attendance for breeding seabirds (T, days), the proportion of the time spent at the colony during the breeding season (f_{tc}), the number of breeding adults per square metre (D_A), the daily nitrogen excreted per breeding adult ($F_{e\text{-}br}$, g $bird^{-1}$ day^{-1}), the total of nitrogen excreted per chick ($F_{e\text{-}ch}$, g $chick^{-1}$ $year^{-1}$) and the productivity of the species (P, fledged chicks per breeding pair):

$$F_e = \frac{(1.167 T f_{tc} F_{e-br} D_A) + \left(F_{e-ch}\left(\frac{P}{2}\right) D_A\right)}{24T} \qquad (6.1)$$

2. Conversion of Uric acid to Total Ammoniacal Nitrogen

Uric acid (UA) builds up on the surface of the colony until it either undergoes bacterial ammonification to form total ammoniac nitrogen (TAN, g m^{-2}) or is washed away by the rain. It is assumed that all excreted nitrogen is in the form of UA. The processes by which UA is converted to TAN are strongly affected by temperature, pH and moisture (Elliot and Collins, 1982, Elzing and Monteny, 1997; Groot Koerkamp et al., 1998). The GUANO model, which operates on an hourly time-step, calculates the TAN emitted (F_{TAN}, g m^{-2} $hour^{-1}$) from the UA budget (Q_{UA}, g m^{-2}), temperature factor (f_T), relative humidity factor (f_{RH}) and pH factor (f_{pH}) (Equation 6.2).

$$F_{TAN} = f_T f_{RH} f_{pH} Q_{UA} \qquad (6.2)$$

At each time-step (t_N), the UA budget (Q_{UA}, g m^{-2}) is calculated from the total nitrogen excreted (F_e, g m^{-2} $hour^{-1}$), the TAN produced per hour (F_{TAN}, g m^{-2} $hour^{-}$

^{1}) and the nitrogen washed off by the rain (F_w, g m^{-2} hour^{-1}), where N is the hour of the year (Equation 6.3).

$$Q_{UA}(t_{N+1}) = Q_{UA}(t_N) + F_e - F_{TAN} - F_w \quad (6.3)$$

Temperature function (f_T)

The expressions used in the GUANO model to describe the rate of urea hydrolysed to TAN are based on the method of Elliot & Collins (1982) in a poultry litter model. The factors used to describe the conversion of UA to TAN are empirically derived and reach the optimum rate of conversion when the temperature is 35 °C and is expressed as a function of temperature (T, K):

$$f_T = \frac{exp^{(0.165(T+263.15)+1.8)}}{exp^{(0.165(35+263.15)+1.8)}} \quad (6.4)$$

pH function (f_{pH})

The pH function depends on the acidity of the substrate. An assumption made by the GUANO model is that excreted guano adds to existing guano on the ground. Therefore, the pH of substrate is equal to the pH of guano, estimated at 8.5 by Blackall (2004). Taking pH samples was prohibited by the British Antarctic Survey (Signy Island (Section 5.3.2) and Bird Island (Section 5.3.7)) and the Ascension Island Department of Conservation (Section 5.3.6) because sampling could cause undue stress on nesting birds. The empirically derived pH function reaches a maximum at pH 9 (Equation 6.5) (Elliot and Collins, 1982).

$$f_{pH} = \frac{1.34.(pH)-7.2}{1.34.(9)-7.2} \quad (6.5)$$

RH function (f_{RH})

Through experiments with poultry litter, Elliot and Collins (1982) found that the uric acid hydrolysis was rate limited if the moisture coefficient (M_E) of guano is less than 35.5 (Equations 6.6 to 6.8). M_E is empirically derived and dependent on both the relative humidity (RH, %) and T (K) (Equation 6.6).

$$M_E = \left[\frac{-\ln(1-RH)}{0.0000534(T)}\right]^{\frac{1}{1.41}}. \quad (6.6)$$

If $M_E > 35.5$ then $$f_{RH} = 1. \quad (6.7)$$

If $M_E < 35.5$ then $$f_{RH} = 0.0025exp^{0.1676 M_E}. \quad (6.8)$$

3. Conversion of TAN to NH_3

The concentration of TAN on the surface is calculated from total mass of the TAN (Q_{TAN}, g m^{-2}) and the volume of water in the guano:

$$[TAN] = \frac{Q_{TAN}}{Volume\ of\ Water\ in\ the\ Guano\ (ml)} \quad (6.9)$$

A function, Γ, is used to describe the equilibrium of the concentrations of the TAN and hydrogen ions on the surface (Equation 6.22). The formation of NH_3 ions is a reversible reaction dependent on the concentration of H^+ ions.

$$\Gamma = \frac{[TAN]}{[H^+]} \quad (6.10)$$

The temperature dependent Henry's Law constant and solubility equilibrium equation (Nemitz et al., 2000) are used to calculate the canopy surface concentration of NH_3 (X_c, g m^{-3}):

$$X_c = \frac{161500}{T} exp\left(\frac{-10378}{T}\right)\Gamma \quad (6.11)$$

4. Emission of NH_3 to the atmosphere

The amount of NH_3 volatilized is calculated from the NH_3 concentration in the air above the colony (X_a, g m^{-3}), the aerodynamic and boundary layer resistance (R_a and R_b respectively, s m^{-1}), and the amount of NH_3 absorbed by the substrate and overlying vegetation (F_{hab}) (Equation 6.12).

$$NH_3\ emission = \frac{X_c - X_a}{R_a + R_b} F_{hab} \quad (6.12)$$

A habitat correction factor, F_{hab}, is used to parameterise the effect of nesting behaviour of the birds on the emitted NH_3. Blackall (2004) used the values shown in Table 6.1. These values are estimates based on field measurements and consistent with the findings of Blackall et al. (2007).

Table 6.1 The re-absorption of NH_3 by the substrate and overlying vegetation, F_{hab}. F_{hab} values describe relative amount of NH_3 released to the atmosphere.

Substrate	Rock	Veg.	Burrow	Nest
F_{hab}	1.00	0.2	0.0	0.2

The R_a is calculated from the friction velocity (u_*, m s^{-1}) (Seinfeld and Pandis, 2006):

$$R_a = \frac{U}{{u_*}^2} \quad (6.13)$$

The friction velocity is calculated assuming neutral stability from the height that the wind speed is measured (z, m) and the roughness height (z_0, m):

$$u_* = \frac{0.41U}{ln\left(\frac{z}{z_0}\right)} \quad (6.14)$$

R_b depends on diffusivity through the quasi laminar sub-layer, where the entrained transfer is described by the boundary layer Stanton number (B) and is approximately equal to 5 (Sutton et al., 1992; Nemitz et al., 2001):

$$R_b = (Bu_*)^{-1} \quad (6.15)$$

Run-Off

At any stage the model accounts for N (UA or TAN) being washed off the surface. The Blackall (2004) GUANO model parameterizes wash-off as 5 % per mm of rain for all substances. This was based on estimates made by Blackall (2004). The value of percentage wash-off per mm rain is subject to spatial differences where the location, topography and nest substrate could influence N wash-off. For example, excreted N by Common Guillemots on vertical cliffs may be washed off at a greater rate than from the flatter nesting sites of Macaroni penguins. This is very difficult to assay and the current estimate is the best currently available, therefore the spatial variation in run-off is not accounted for in the model.

6.2.3 Changes to the Blackall (2004) GUANO model

Blackall (2004) used the GUANO model to estimate NH_3 emissions in a temperate climate (Isle of May, Scotland), however the NH_3 emissions calculated by the GUANO model were 10 % of the measured emissions. This study has found ways to improve the Blackall (2004) GUANO model by investigating its shortcomings. One of the strengths of the Blackall (2004) model was the parameterisation of climate, thus the meteorological data used as input (hourly values of temperature, relative humidity, wind speed and precipitation) are kept

the same. However, the GUANO model is refined in this study by making the following changes:

a. The first major change is the inclusion of a water budget. The Penman-Monteith equation is included to calculate water evaporation.
b. The relative humidity factor is increased during rain events, representing changes to relative humidity at ground level during rain events.
c. The habitat correction factors (F_{hab}) are based on laboratory experiments of NH_3 emission from seabird excreta in a controlled environment (Chapter 4).
d. The use of ground temperatures instead of air temperatures. The differences between air temperature and ground temperature change with latitude and have a large effect on NH_3 emission.

The following describes the improvements made to the GUANO model in more detail.

a. Water Budget

The water budget (Q_{H2O}, kg m^{-2}) is calculated from the water content of excreted guano ($F_{H2O}(g)$, kg m^{-2} hr^{-1}), rain events ($F_{H2O}(pptn)$, kg m^{-2} hr^{-1}), water run-off ($F_{H2O}(ro)$, kg m^{-2} hr^{-1}) and evaporation ($F_{H2O}(evap)$, kg m^{-2} hr^{-1}).

$$Q_{H2O}(t_{N+1}) = Q_{H2O}(t_N) + F_{H2O}(pptn) - F_{H2O}(evap) - F_{H2O}(ro) + F_{H2O}(g) \quad (6.16)$$

The maximum mass of water evaporated ($F_{H2O}(evap)$, kg m^{-2} hr^{-1}) is calculated using the Shuttleworth adaptation of the Penman equation (Equation 6.16). This is used to calculate the volume of water in guano in Equation 6.9. A detailed explanation of the equation and definitions of all variables are given in Shuttleworth (2007). The Penman equation calculates $F_{H2O}(evap)$using the slope of the saturation vapour pressure curve (m, kPa K^{-1}), net solar radiation (R_n, MJ m^{-2} day^{-1}), psychrometric constant (γ, kPa $°C^{-1}$), wind speed at 2 m (U, m s^{-1}), vapour pressure deficit (δe, kPa) and the latent heat of vaporization (λ_v, MJ kg^{-1}) (Equation 6.17)

$$F_{H2O}(evap) = \frac{m.R_n + \gamma.6.43(1+0.536.U).\delta e}{\lambda_v(m+\gamma)} \quad (6.17)$$

The vapour pressure deficit is the difference between the saturated water vapour pressure (e_s, kPa) and the mean ambient water vapour pressure (e_a, kPa):

$$\delta e = e_s - e_a . \quad (6.17)$$

The saturated water vapour pressure is calculated from the mean air temperature (T, °C) where,

$$e_s = 0.6108.exp\left(\frac{17.27.T}{T+237.3}\right). \quad (6.18)$$

The mean ambient water vapour pressure is calculated from the saturated water vapour pressure and the relative humidity (RH, %) where,

$$e_a = \frac{e_s RH}{100}. \quad (6.19)$$

The slope of the saturated vapour curve is calculated from the saturated water vapour pressure and the mean air temperature, where,

$$m = 4098.\frac{e_s}{(T+237.3)^2}. \quad (6.20)$$

The psychrometric constant is estimated from atmospheric pressure (P, kPa) where,

$$\gamma = 0.000665.P. \quad (6.21)$$

Net solar radiation

Net solar radiation (R_n, W m^{-2}) data were taken from the National Center for Environmental Prediction (NCEP) and the National Center for Atmospheric Research (NCAR) Reanalysis 1 dataset (NCAR, 2011). R_n was derived using an analysis and forecast system, which uses weather observations taken by ships, planes, meteorological station data and satellite observations. Data were available for every six hours on a 2.5 ° x 2.5 ° gridded data set. In the GUANO model, net solar radiation values during the hours of night were set to zero. The hours of night were calculated using the method of Parton and Logan (1981), where the hours of sunrise and sunset were calculated from the latitude and time of year. Net solar radiation during the day is calculated as an average value between consecutive NCEP data points. Figure 6.2 shows the calculated net solar radiation

for consecutive days at Michaelmas Cay (9/12 to 10/12). These are the best available data for net solar radiation.

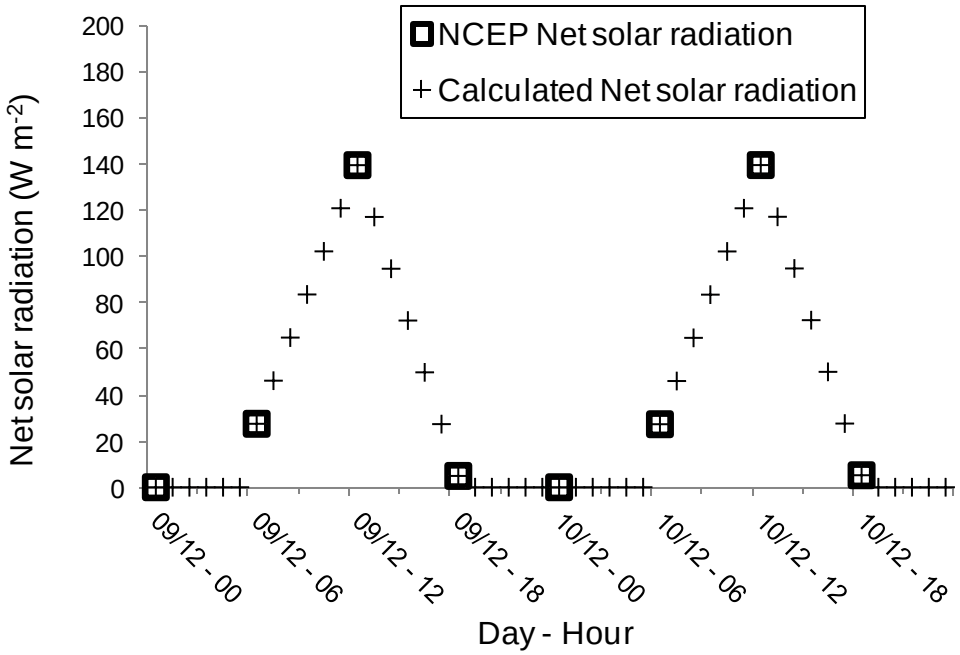

Figure 6.2 Calculated net solar radiation for consecutive days at Michaelmas Cay on the 9th December 2009 and 10th December 2009 using data from National Center for Environmental Prediction (NCEP) and the National Center for Atmospheric Research (NCAR) Reanalysis 1 dataset (NCAR, 2011).

b. Relative humidity factor, f_{RH}

During rain events, f_{RH} is increased to 1, as compared to Blackall (2004), which used f_{RH} values derived using Equation 6.8. Changing f_{RH} to 1 during rain events means that in hot climates, such as on Ascension Island, TAN production increased during rain events.

c. Habitat correction factor, F_{hab}

The F_{hab} values used by Blackall (2004) were adequate for estimating the emissions from colonies within the UK. However, this study also required F_{hab} values for sand and soil. Experiments were conducted under controlled conditions (described in detail in Chapter 4) to determine values of F_{hab} used in this study (Table 6.2).

Table 6.2 The amount of NH_3 reabsorbed by the substrate and overlying vegetation, F_{hab}

Substrate	Rock	Sand	Soil	Veg.	Burrow	Nest
F_{hab}	1.00	0.68	0.41	0.27	0.00	0.27

d. Ground Temperature

Ground temperature (T_g, °C) measurements were taken for the entire breeding season at Michaelmas Cay and on the Isle of May, and these were used directly in the GUANO model. T_g was measured during the fieldwork periods on Ascension Island and Bird Island and an offset was derived to estimate the difference between ground temperature and the air temperature. Figures 6.3 (a) and (b) show the measured offset between the air temperature and ground temperature for Bird Island and Ascension Island, respectively. Despite a distance of 800 km between Bird Island and Signy Island, the T_g measurements on Bird Island provide the best available relationship between ground and air temperatures for Signy Island, as no other nearby T_g data is available for use. Ground temperatures on Signy Island are calculated using the hourly temperature offset measured on Bird Island.

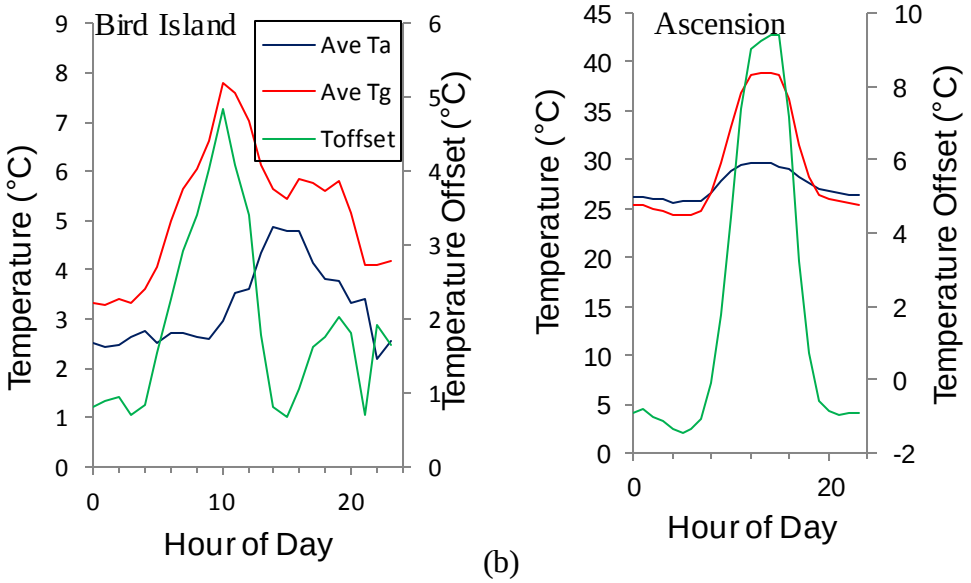

Figure 6.3 Temperature offset (Toffset) between the average air temperature (Ave T_a) and ground temperature (Ave T_g) for (a) Bird Island and (b) Ascension Island

6.2.4 Meteorological input data

To compare the measured NH_3 emissions to the GUANO modelled NH_3 emissions, meteorological data are required for the time the birds arrive at the

colony. This study only measured annual meteorological data for the Isle of May colony. For the other colonies, meteorological data from the nearest station are used. Table 6.3 indicates the nearest meteorological station used for each of the colonies. Data for wind speed, air temperature, relative humidity and rainfall were used.

Table 6.3 The meteorological stations used in the GUANO models for each of the colonies.

Colony	Met Station	Distance from met station to colony (km)
Michaelmas Cay	Green Island	17
Signy Island	Base Orcadas	50
Isle of May	Isle of May	1
Ascension Island	Wideawake airfield	2
Bird Island	Bird Island BAS base	5

6.2.5 Seabird colony data

The GUANO model uses hourly meteorological and environmental data and site-specific seabird data (Table 6.4). The sites are described in detail in Chapter 5.

Table 6.4 Site-specific seabird data input to the GUANO model.

Site	Adult Mass (g)	Nest Density (nests m^{-2})	Bird days at colony	Fraction of time at colony	N excretion rate at colony (g m^{-2} hr^{-1})
Michaelmas	200	1.7	122	0.6	0.20
Signy Is.	4150	0.63	274	0.6	0.79
Signy Is.	5500	0.5	213	0.6	0.81
Isle of May	410	1.27	152	0.3	0.13
Ascension Is.	190	1.26	122	0.6	0.14
Bird Is.	4680	0.85	213	0.6	1.13

6.2.6 Sensitivity analysis

A sensitivity study was performed on the GUANO model to determine the most significant model parameters in relation to the model output. The following model parameters were investigated with a 10 % variation in each input

parameter: surface roughness height (z_0, m), fraction of UA converted to TAN in 24hrs, percentage Nitrogen wash off (% mm^{-1} rain), percentage non-Nitrogen wash-off (% mm^{-1} rain), boundary layer Stanton number (*B*), temperature (*T*, °C), relative humidity (*RH*, %), wind speed (*U*, m s^{-1}), precipitation (*P*, mm m^{-2} hr^{-1}), net solar radiation (*Rn*, Wm^{-2}) and background NH_3 concentration (µg m^{-3}).

6.2.7 Comparing model output to measurements

The refined GUANO model output was compared with measurements from the five fieldwork sites. The sites are ordered by climate, from tropical to temperate to polar. To indicate similarities and differences between measured and modelled NH_3 emissions for the active sampling campaigns, the time series of both are plotted. To assess the fit of the model, the hourly measured emissions (x-axis) are plotted against the hourly modelled NH_3 emissions (y-axis) and the gradient and R^2 of the linear regression calculated.

The average emission for each colony was calculated (in µg m^{-2} s^{-1}) by summing the average NH_3 emission for each hour of the day. The percentage of nitrogen volatilized (P_v) was also calculated from the total nitrogen excreted at the colony during the measurement period and the total nitrogen volatilized as NH_3. The total N excreted is an estimate based on the assumption that seabirds excrete N at a constant rate while at the colony.

6.2.8 NH_3 emission and climate

To identify relationships between climate and NH_3 emission, the time series of NH_3 emission, temperature, wind speed, relative humidity and precipitation events will be plotted for each site.

To investigate whether the effect of each climate variable is long or short term, scenarios were conducted and examined in two ways:

1. The correlation coefficient (R) between NH_3 emission and each climate variable is calculated for observations during the measurement period. Patterns between P_v and climate during the period of the measurement campaign are identified by plotting P_v against each climate variable for each fieldwork site.

2. Patterns between the annual P_v and climate are identified by conducting a sensitivity analysis, where the climate variable measured at the Isle of May is substituted into the GUANO model for each of the fieldwork sites. Isle of May is chosen because it has temperate conditions and is climatically an intermediate between polar and tropical climates.

6.3 Results and Discussion: Model applied to measurement sites

6.3.1 Sensitivity analysis of the GUANO model

A sensitivity analysis of the refined GUANO model is shown in Table 6.5 for the input variable selected. The estimated NH_3 emissions were most sensitive to ground temperature (+59.9 % to -36.8 %). Increases in temperature and wind speed increase NH_3 emission, while increases in relative humidity and precipitation decrease NH_3 emission. Refinements made to the GUANO model in this study have changed the model's sensitivity. For example, Blackall (2004) found that his model was most sensitive to relative humidity, where a change of 10 % *RH* resulted in an increase of 34 % in NH_3 emission. For the refined model, a *RH* change of +10 % results in an NH_3 emission change of 6.7 %. The Blackall (2004) model was less sensitive to temperature than the refined model. In the Blackall (2004) model, an increase in *T* of 25 % resulted in an increase of 24 % in NH_3 emission, whereas a change in *T* by the same amount resulted in a 60 % change in NH_3 emission for the refined GUANO model.

Table 6.5 Sensitivity analysis of the refined GUANO model

Factor		Base value	% Change +10 %	% Change -10 %
Surface roughness height (z_0, m)	Constant	0.1	0.01	-0.02
Fraction of UA converted to TAN in 24 hrs	Constant	0.2	9.30	-9.42
Percentage Nitrogen wash off (% mm^{-1} rain)	Constant	1	-7.12	8.19
Percentage non-Nitrogen Wash off (% mm^{-1} rain)	Constant	0.5%	0.17	-0.15
Boundary layer Stanton number (B)	Constant	5	-0.04	0.04
Temperature (T, °C)	Variable		59.9	-36.8
Relative Humidity (RH, %)	Variable		6.7	-13.0
Wind Speed (U, m s^{-1})	Variable		12.9	-11.0
Precipitation (P, mm m^{-2} hr^{-1})	Variable		-11.8	20.7
Net solar radiation(R_n, Wm^{-2})	Variable		1.2	-2.1
Background NH_3 concentration (μg m^{-3})	Constant	0.1	0.01	-0.02

6.3.2 Improvements to the GUANO model

To highlight the refinements made to the GUANO model, Figure 6.4 shows the cumulative effect that the refinements had on the Blackall (2004) GUANO model estimates of NH_3 emission. The grey dotted line shows the NH_3 emission estimated by the Blackall (2004) GUANO model, using hourly meteorological data (air temperature, relative humidity, wind speed and precipitation) and F_{hab} =1. The grey dashed line shows the effect of changing F_{hab} to 0.67. The black dashed line shows the effect of changing air temperature to ground temperature (with F_{hab} = 0.67). The solid black line shows the effect of including the water budget and the relative humidity factor (including T_g and F_{hab} = 0.67). The black dotted line shows the NH_3 emission measured during fieldwork, using the WindTrax inverse dispersion approach.

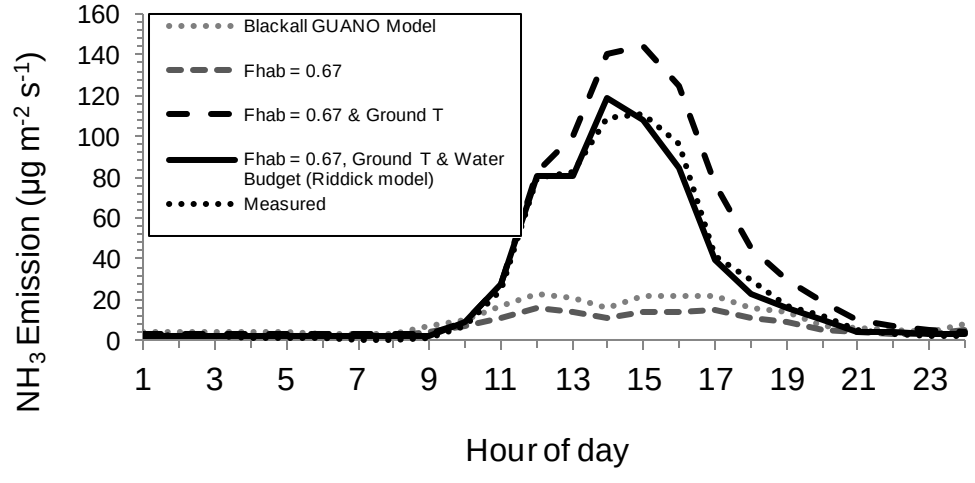

(a)

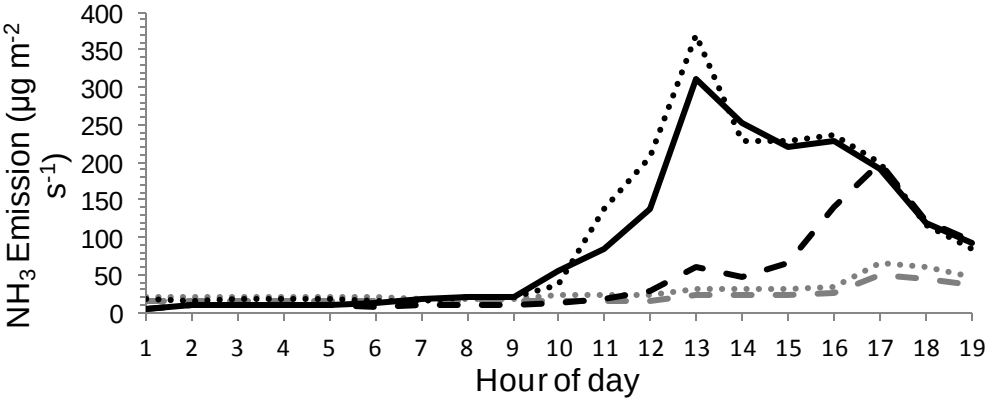

(b)

Figure 6.4 Comparison of Blackall (2004) GUANO model with measurements (Section 5.3.6) and the adaptations made to the model for (a) 22nd May on Ascension Island during a period of no rain and (b) 6th June on Ascension Island during a rain event at 0800.

Refinements to the GUANO model changed the NH_3 emission calculated for 22nd May on Ascension from 0.90 g NH_3 m^{-2} day^{-1} (Blackall GUANO model; grey dotted line, Figure 6.4) to 2.28 g NH_3 m^{-2} day^{-1} (refined GUANO model; solid black line, Figure 6.4). The largest change was caused by use of the ground temperature instead of air temperature.

The inclusion of a water budget and relative humidity factor gave better agreement between modelled and measured emission calculated on the 6th June. The rain event at 0800 increases the rate at which UA evolves to form to TAN and then NH_3 emission, shown as the peak in NH_3 emission at 1300. Including the water budget, where f_{RH} = 1 during the rain event, models this peak well. Changing the value of F_{hab} from 1 to 0.67 reduces the emission estimate by 33 % (Table 6.6).

Table 6.6 Adaptations made to the GUANO model and resulting effect on total daily NH_3 emission estimate 22nd May and 6th June 2010, Ascension Island

Day	Adaptation	% Difference in emission from Blackall GUANO Model
22nd May	Blackall GUANO Model	-
	Change F_{hab} 1 to 0.67	-33
	F_{hab} = 0.67 & T_{ground}	+153
	F_{hab} = 0.67, T_{ground}, H_2O budget & *f(RH)*	+153
	Measured NH_3 Emission	+154
6th June	Blackall GUANO Model	-
	Change F_{hab} 1 to 0.67	-33
	F_{hab} = 0.67 & T_{ground}	+61
	F_{hab} = 0.67, T_{ground}, H_2O budget & *f(RH)*	+238
	Measured NH_3 Emission	+275

6.3.3 Michaelmas Cay Great Barrier Reef, Common Noddy (passive measurements)

Comparison of measured and modelled NH_3 emission

The NH_3 emissions calculated by the refined GUANO model show a strong diurnal pattern, with maximum emissions during the day reaching 500 µg m^{-2} s^{-1} and emission during the night between 1 and 10 µg m^{-2} s^{-1}. The maximum emissions occur when the ground temperature is highest and daytime emissions are lowest when T_g is lower. The average NH_3 emission measured using passive samplers for November and December are very similar to the modelled emissions averaged during the same period (Figure 6.5 and Table 6.7). Discrepancies between measured and modelled emissions may be caused by weather differences between Michaelmas Cay and Green Island, where the meteorological data were obtained. However, it is not expected that there are large differences in rainfall patterns or wind speed between these two sites due to the low lying terrain of these islands and their relative closeness.

NH_3 emission estimates

The average NH_3 emission calculated by the GUANO model is 2.38 g NH_3 m^{-2} day^{-1} (27.52 µg NH_3 m^{-2} s^{-1}) for November and December 2009. The NH_3 emissions measured during the field campaign are 2.24 g NH_3 m^{-2} day^{-1} (25.89 µg NH_3 m^{-2} s^{-1}). Both measured and modelled emission show an increase in NH_3 emission from November to December. The agreement between measured and modelled is better for November than December, with the percentage difference between the measured and modelled emissions as 15 % and 26 %, respectively.

Table 6.7 Comparison between the measured NH_3 emissions and modelled NH_3 emissions, using the GUANO model for measurements made on Michaelmas Cay, Great Barrier Reef, Australia during November (5/11/2009 to 10/12/2009) & December (10/12/2009 to 6/1/2010).

	November 2009	**December 2009**
Measured NH_3 emission estimate (µg NH_3 m^{-2} s^{-1})	21.32	22.23
GUANO Model NH_3 emission (µg NH_3 m^{-2} s^{-1})	25.10	29.94
Difference between measured and modelled (%)	15.0	25.8

NH_3 emissions and emission factors

The largest amounts of NH_3 are emitted when the ground temperature is highest, with a strong correlation between ground temperature and NH_3 emission (R = 0.75). In general, the largest NH_3 emissions each day occur between 1200 and 1400, with exceptions to these midday peaks during rain events. NH_3 emission has a very weak, negative correlation with precipitation (R = -0.1). Wind speed has a weak positive correlation with NH_3 emission, (R = 0.11), whereas relative humidity has a weak negative correlation with NH_3 emission (R = -0.12).

The largest rain events fell on the same days as the lowest modelled NH_3 emissions (11^{th} November and 30^{th} December), but the largest modelled NH_3 emissions happen shortly after these large rain events, usually the following day (Figure 6.6). During rain events, ground temperatures are lower and microbial production of TAN and NH_3 may be reduced. Rain may also wash away available uric acid and TAN. Just after a rain event, there is water available for hydrolysis of uric acid, and during hot days NH_3 is readily volatilized from the surface. These results reinforce the findings of the re-wetting experiments conducted in Chapter 4.

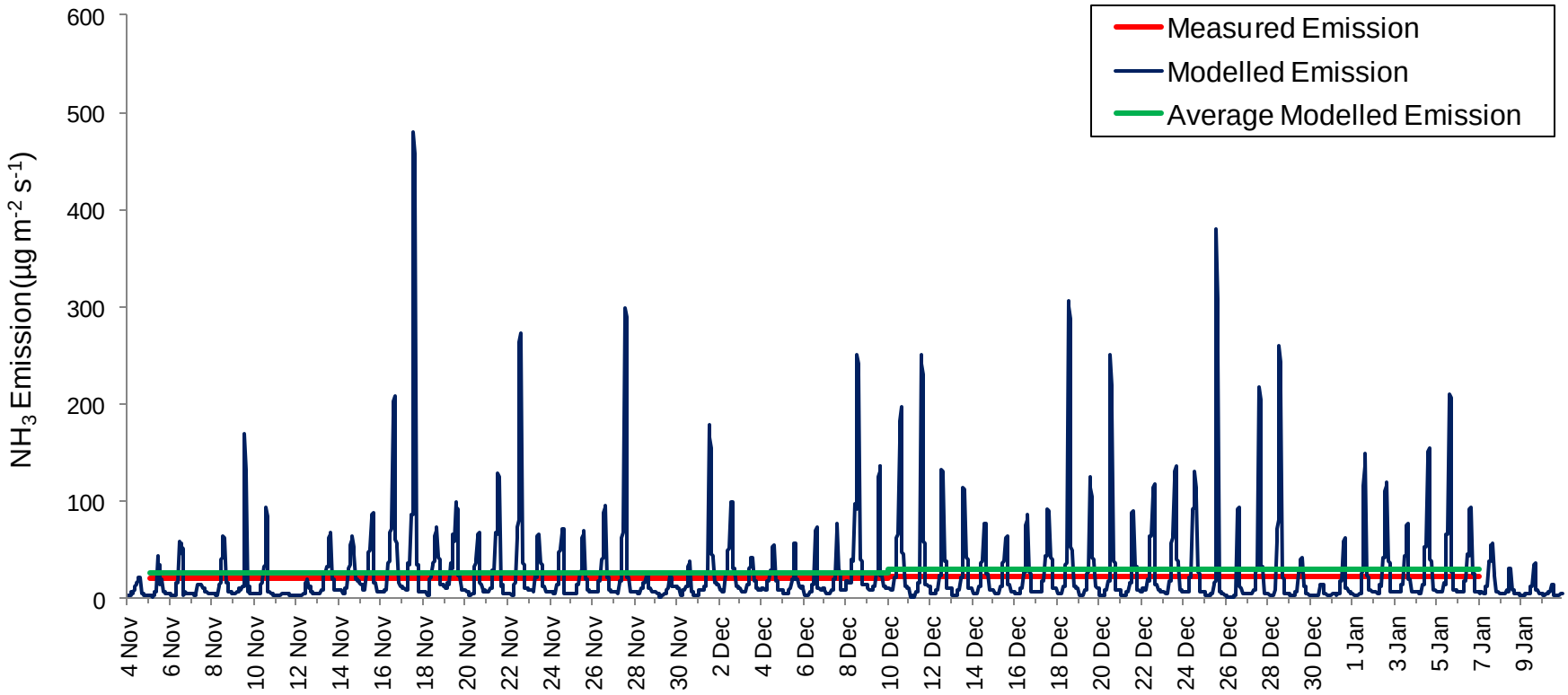

Figure 6.5 Comparison between the measured monthly NH_3 emissions (red line), monthly average modelled NH_3 emissions (green line) and modelled hourly NH_3 emissions (blue line) using the GUANO model for measurements made on Michaelmas Cay, Great Barrier Reef, Australia during November (5/11/2009 to 10/12/2009) & December (10/12/2009 to 6/1/2010). Tick marks on the x-axis indicate midnight on each day.

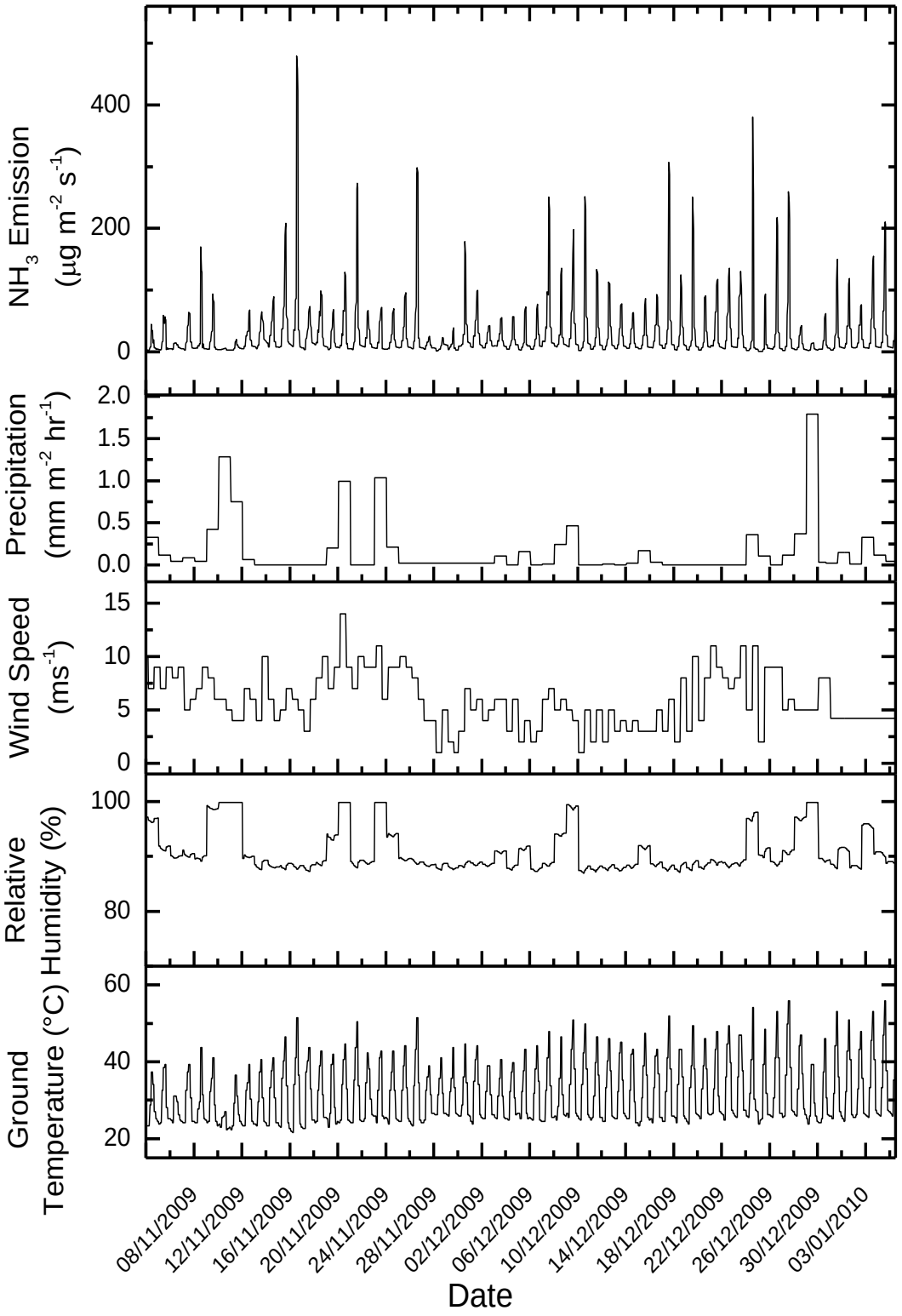

Figure 6.6 Modelled NH_3 emission compared to environmental variables representative of climate at the sooty tern colony on Michaelmas Cay, Great Barrier Reef, Australia from 5/11/2009 to 6/1/2010). Tick marks on the x-axis indicate midnight on each day.

6.3.4 Mars Bay, Ascension Island, Sooty Terns (active measurements)

Comparison of measured and modelled NH_3 emission

Ascension Island has a tropical climate with ground temperatures reaching 35 - 45 °C in the early afternoon (Figure 6.9). The NH_3 emissions calculated by the GUANO model for the Sooty Tern colony at Mars Bay on Ascension Island show a strong diurnal pattern, corresponding to the hottest part of the day. The maximum emission during the measurement period is 370 µg NH_3 m^{-2} s^{-1} (Figure 6.7).

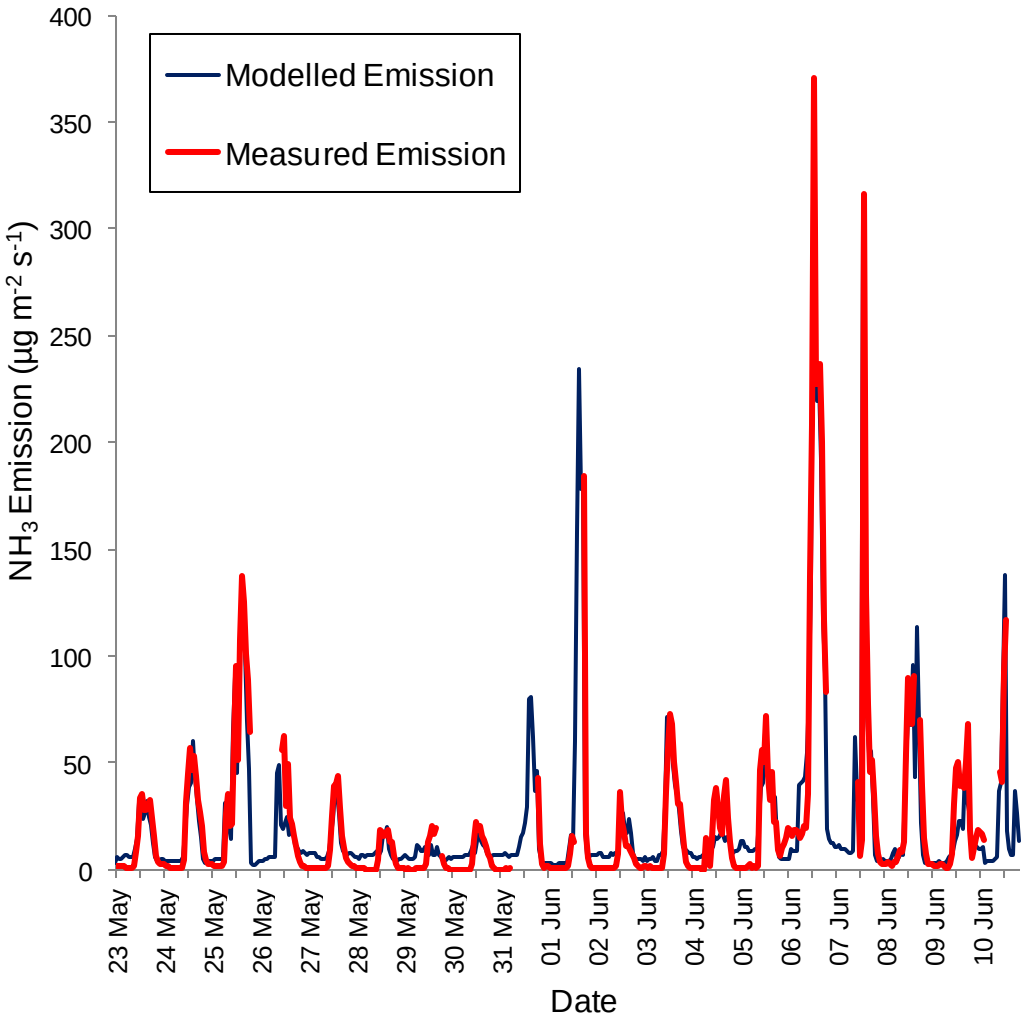

Figure 6.7 Comparison between measured and modelled NH_3 emissions from the Sooty tern colony at Mars Bay, Ascension Island 22nd May to 10th June 2010. Tick marks on the x-axis indicate midnight on each day.

NH_3 emission estimate

The NH_3 emissions calculated by the GUANO model for Ascension Island are very similar to those measured in the field (Figure 6.7). They exhibit good agreement, with a linear regression gradient of 1.08 and $R^2 = 0.67$. Emissions with the poorest agreement are 22nd May (labelled 142 in Figure 6.8) at 1600 and 6th June (labelled 157) between 1100 and 1300. Both represent periods after a rain event, highlighting the difficultly in accurately modelling the timing of uric acid evolution to TAN and then NH_3. The average NH_3 emission using the GUANO model for the Sooty tern colony in Mars Bay is 1.9 g NH_3 m^{-2} day^{-1} (21.5 µg NH_3 m^{-2} s^{-1}).

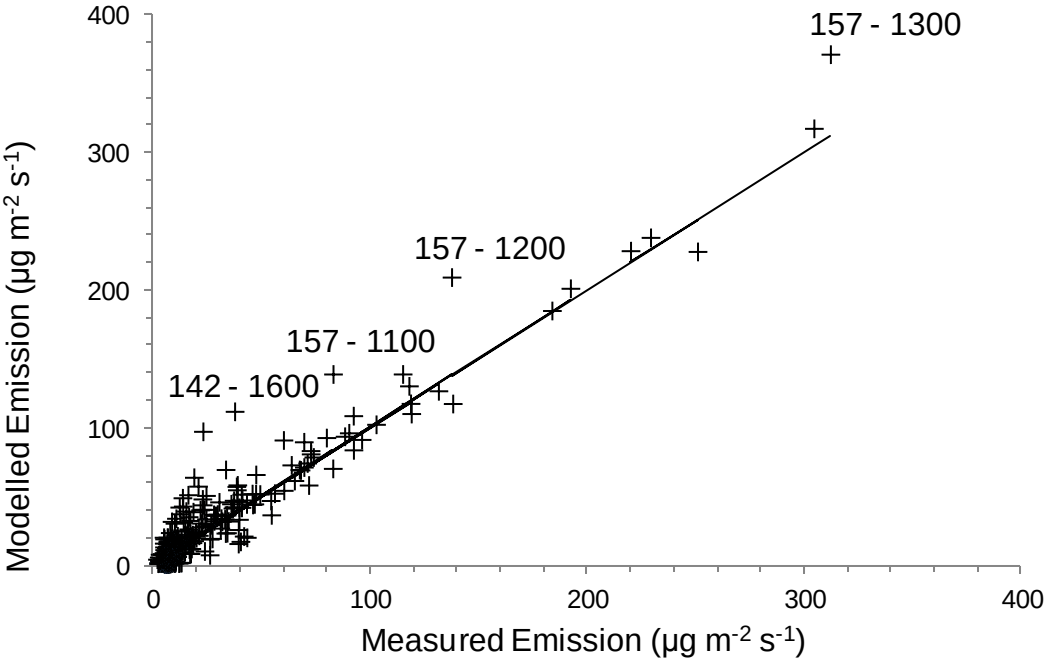

Figure 6.8 Comparison between hourly measured and modelled NH_3 emissions from the Sooty tern colony at Mars Bay, Ascension Island, 22nd May to 10th June 2010. The line on the graph represents the 1:1 line. Individually labelled points indicate Julian date and hour of measurement.

NH_3 emission and environmental factors

On most days, the highest NH_3 emission occurs when the ground temperature is highest, between 1200 and 1600 each day. However, the correlation coefficient between NH_3 emission and ground temperature is relatively small (R = 0.2), indicating this is not the main driver of NH_3 evolution. The correlation between

NH_3 emission and wind speed is also weak (R = 0.1). The correlation coefficient between NH_3 emission and relative humidity and precipitation is much stronger (R = 0.37 and 0.27, respectively).

Unlike Michaelmas Cay, Ascension Island is very dry. The NH_3 emission varies throughout the measurement period and between 26th May and 5th June is very small during the day. These smaller emissions could be caused by high temperature and strong winds evaporating water, and the only available water for uric acid hydrolysis is excreted in seabird guano. NH_3 emission is relatively very high after rain events (25th May and 6th June), when water is available for hydrolysis of UA. Figure 6.9 shows the timing of these large NH_3 emissions after rain events.

GUANO modelled emissions differ from measured emissions during the night (Figure 6.7). The overestimation of the model during the night could have been caused by limitations in the measurements used to calculate the NH_3 emissions in both the GUANO model and input to the atmospheric dispersion model. For the atmospheric dispersion model, the vertical flux of air from the ground to the sonic anemometer is assumed to be constant. However, bird behaviour may increase NH_3 emission in two ways: (1) increase ground temperature (2) increase vertical transport of air by moving around and flapping their wings. Further measurements nearer to the nest site are required to check the validity of these suggestions. These two effects were not measured by either the temperature sensor or the sonic anemometer, as the measurements were made 100 m from the nesting birds.

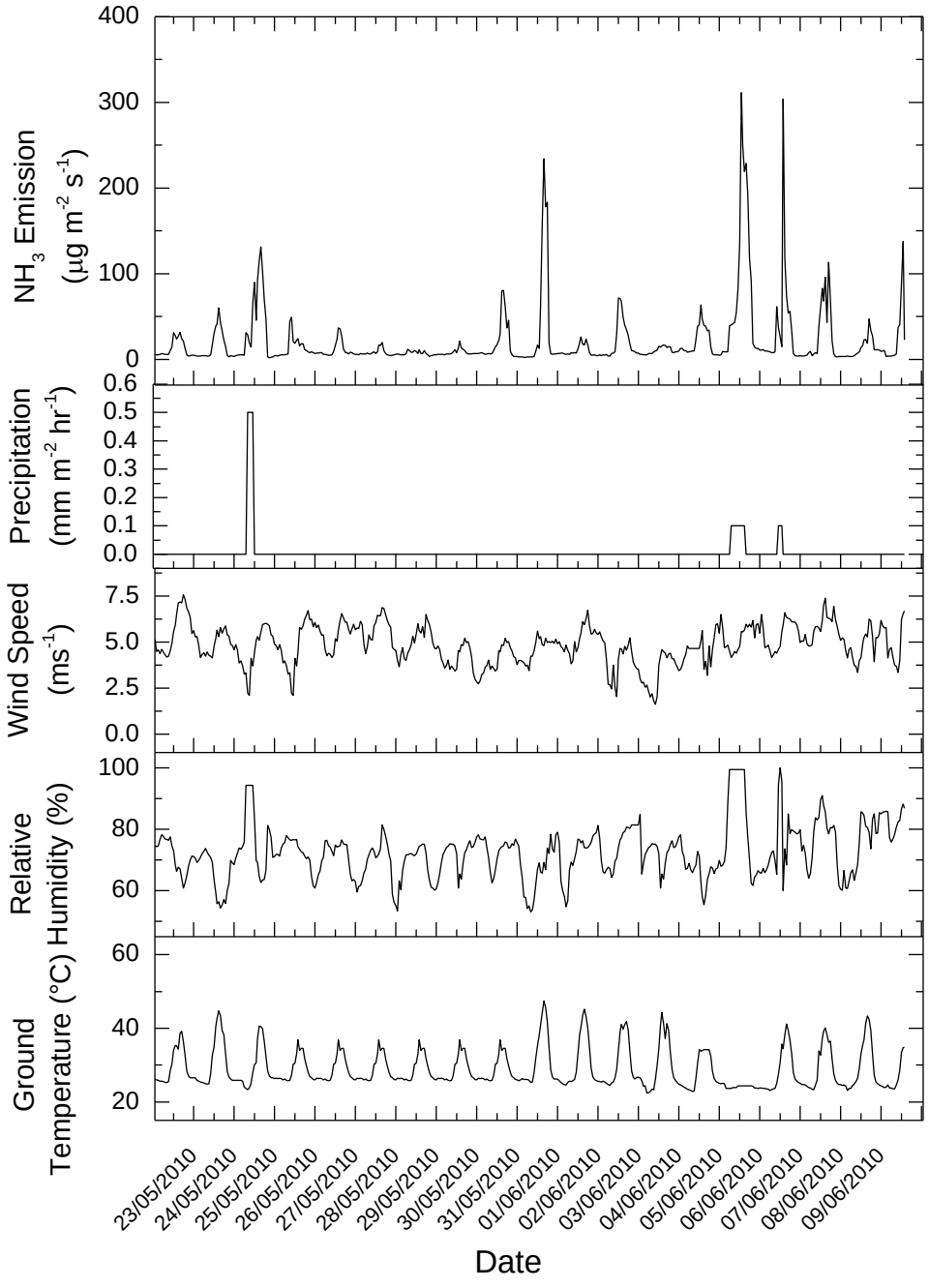

Figure 6.9 Modelled NH_3 emission compared to environmental variables representative of climate at the Sooty tern colony at Mars Bay, Ascension Island, 22nd May to 10th June 2010. Tick marks on the x-axis indicate midnight on each day.

6.3.5 Isle of May, Scotland, Atlantic puffins (active measurements)

Comparison of measured and modelled NH_3 emission

NH_3 emissions calculated by the GUANO model were compared with measured emissions from the 2009 field campaign (see Section 5.3.4). The modelled emissions were lower for the Isle of May puffin colony than Michaelmas and Ascension (both Sooty tern), but did show a similar diurnal pattern. Emissions peaked at a maximum of 25 µg m^{-2} s^{1} and emissions at night dropped to zero. Figure 6.10 compares the measured and the modelled NH_3 emissions.

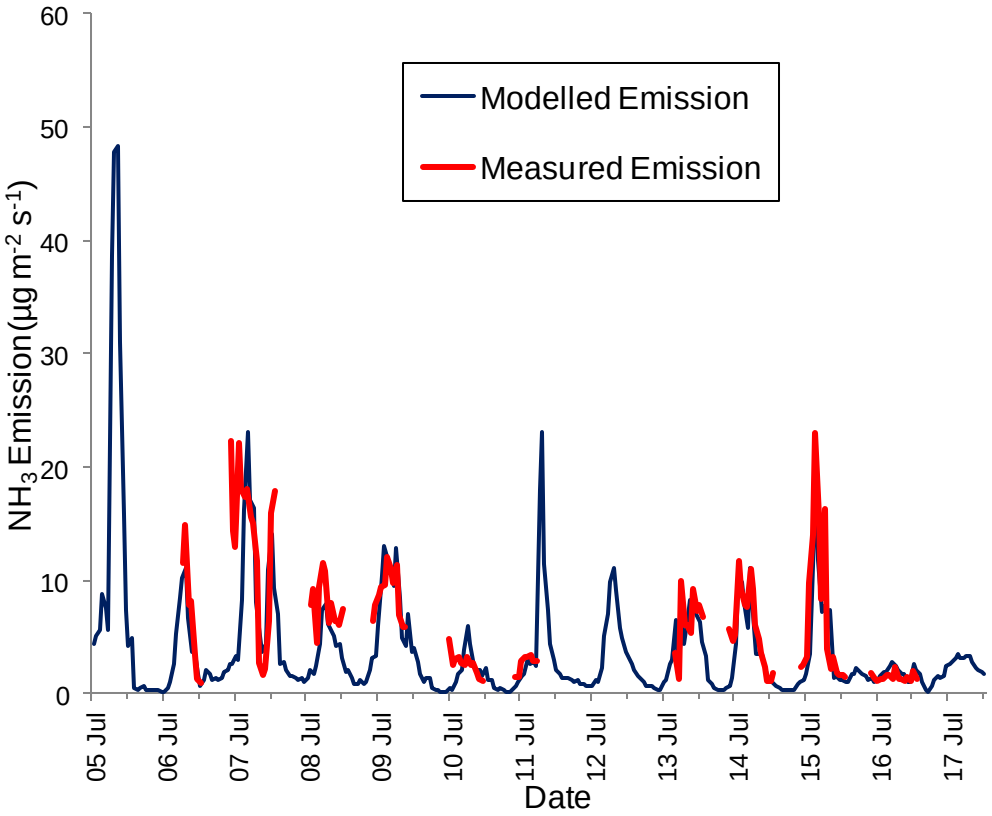

Figure 6.10 Comparison between the measured NH_3 emissions and modelled NH_3 emissions using the GUANO model for measurements made on the Isle of May between 5th July and 17th July, 2009. The F_{hab} value used in the GUANO model was 0.64. Tick marks on the x-axis indicate midnight on each day.

At the beginning of the study, three assumptions were made about the excretory behaviour of puffins: (1) they only excrete outside the nest whilst at the colony, (2) only excrete on vegetation and (3) puffin chicks only excrete in burrows and

leave the colony as soon as they leave the nest. Puffin chicks do not contribute to seabird NH_3 emission at the colony, and chick F_{hab} is set to 0.

Excretory behaviour of puffins varies between individual birds. Assumption (1) varies among individuals: the entrance chamber of most puffin burrows are free from guano, however some adult puffins do excrete in their burrow (M. Newell, pers. comm.). Assumption (2) depends on the time of day and climatic conditions: at dawn and dusk, large numbers of puffins can be seen on exposed rocks across the colony, and this also happens when it is warm and sunny. To accommodate variations in assumption (2), the F_{hab} value for puffins was changed from vegetation only (0.27) to an F_{hab} value between rock and vegetation of 0.64 (average of 1 and 0.27).

Patterns in NH_3 emission

Even though the NH_3 emissions modelled by the GUANO model are similar to the measured emissions on the Isle of May, the GUANO model does not reproduce the measured emission exactly, with a linear regression gradient of 0.59 and R^2 of 0.50. Figures 6.11 shows the hourly measured NH_3 emissions plotted against the hourly modelled emissions. The poorest fitting emissions were measured on day 7th July 2009 (denoted as Julian Date 188 in Figure 6.11). Field notes taken on 6th July 2009 show that many birds were sitting on rocks around the colony on the afternoon and evening of 6th July 2009. Measured emissions were also much larger than those calculated by the GUANO model on the morning of 7th July 2009, possibly because of the smaller lag-time in formation of UA to TAN to NH_3 from N excreted onto the rock, where NH_3 volatilized is not reabsorbed. This highlights the uncertainty in N excretion behaviour of Atlantic Puffins.

The average GUANO model NH_3 emission for the Isle of May is 0.28 g NH_3 m^{-2} day^{-1} (2.41 μg NH_3 m^{-2} s^{-1}), using an F_{hab} value of 0.64. The average hourly NH_3 emission data between 23 and 06 hours should be treated with some caution as only one set of data was used.

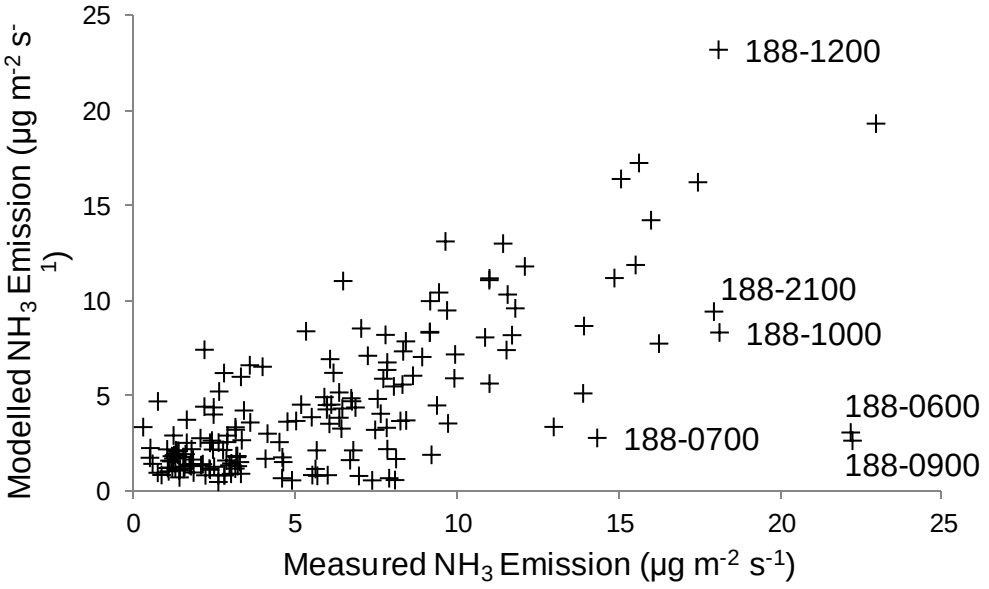

Figure 6.11 Comparison between hourly measured and modelled NH_3 emissions from the puffin colony on the Isle of May between the 29th June and the 23rd July, 2009. The larger outliers are indicated on the figure with the Julian date and the hour of measurement.

NH_3 Emission and environmental factors

NH_3 emissions calculated by the GUANO model were higher when ground temperatures and wind speeds were higher, but NH_3 emissions decrease as relative humidity increases (Figure 6.12). The correlation coefficients between NH_3 emission and ground temperature are very strong and positive (R = 0.7), for wind speed the correlation is medium and positive (R = 0.4) and for relative humidity the correlation is medium and negative (R = -0.3). The correlation between precipitation and NH_3 emission is weak (R < 0.1).

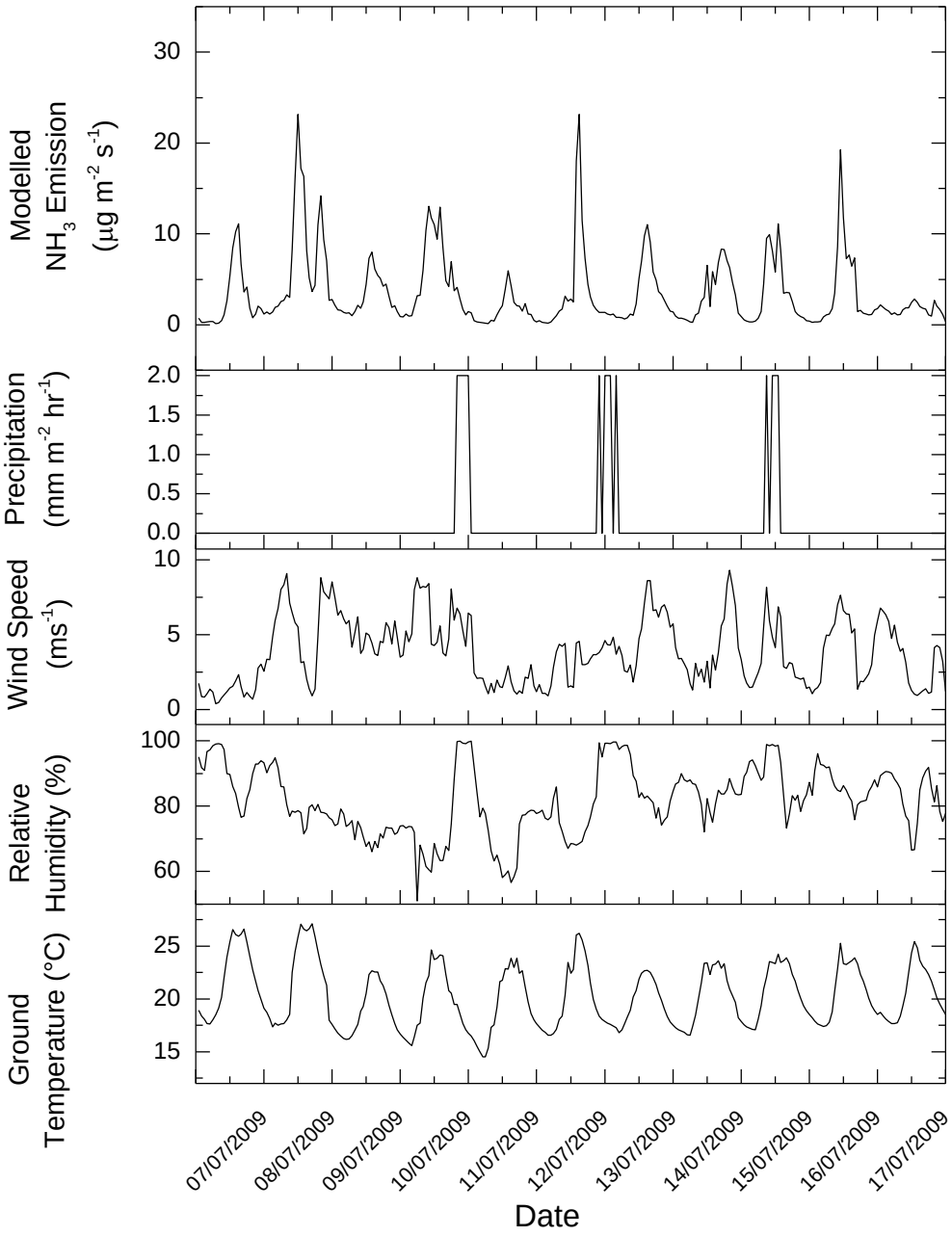

Figure 6.12 Modelled and measured NH_3 emission compared to environmental variables representative of climate at the Atlantic puffin colony on the Isle of May between the 7th July and the 17rd July 2009. F_{hab} for adults was set at 0.64. Tick marks on the x-axis indicate midnight on each day.

6.3.6 Signy Island, South Atlantic, Chinstrap penguins (passive measurements)

Comparison of modelled and measured NH_3 emissions

As with the tropical and temperate regions, modelled NH_3 emissions from this seabird colony in a polar region were strongly diurnal. The Signy Island colony was a mixture of Adelie and Chinstrap penguins for the first measurement period. During the second period, the Adelie penguins began to leave the site and the Chinstrap penguins were alone for the third period. The NH_3 emissions are the highest for the first period, reaching a maximum of 50 µg NH_3 m^{-2} s^{-1}. The first period was also the warmest period, with ground temperatures reaching a maximum of 4.5 °C. Figure 6.13 shows the comparison of the measured NH_3 emissions (red line), modelled hourly NH_3 emissions using the GUANO model (blue line) and the average of the modelled emission during each measurement period (green line). The modelled emission (green line) agrees well with the NH_3 emissions from measurement (red line).

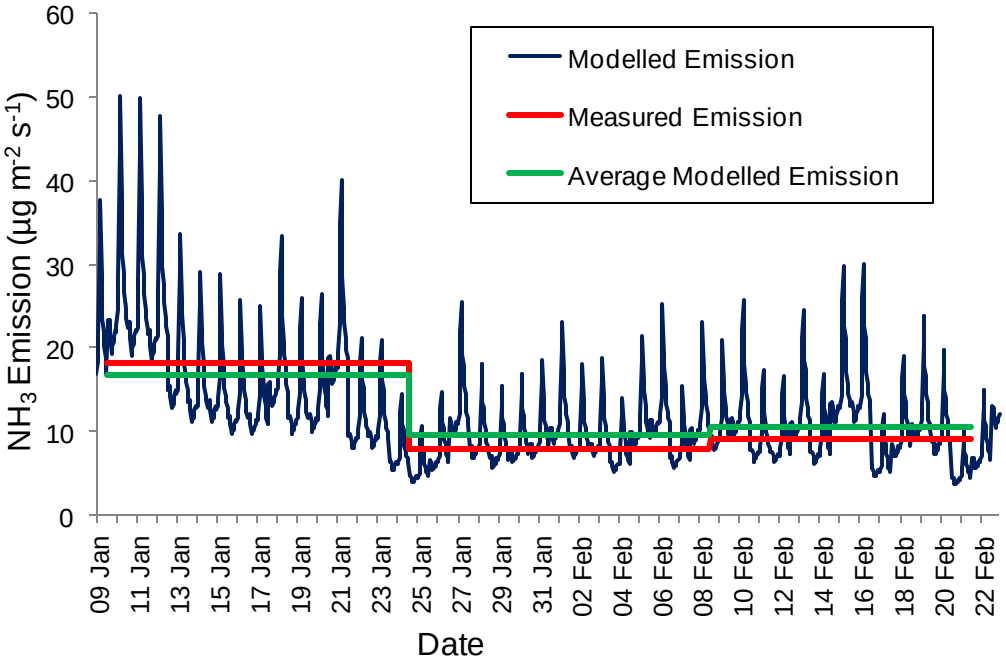

Figure 6.13 Comparison between the measured NH_3 emissions (red line), modelled hourly NH_3 emissions using the GUANO model (blue line) and the average of the modelled emission during each measurement period (green line) on Signy Island during Period 1 (10/01/09 - 25/01/09), Period 2 (25/01/09 - 08/02/09) and Period 3 (08/02/09 - 21/02/09). Tick marks on the x-axis indicate midnight on each day.

NH_3 emission estimates

The average modelled NH_3 emission estimate for Signy Island during February 2009 was 0.92 g NH_3 m^{-2} day^1 (10.68 µg NH_3 m^{-2} s^{-1}). This is similar to the NH_3 emissions measured during the field campaign of 0.78 g NH_3 m^{-2} day^{-1} (9.02 µg NH_3 m^{-2} s^{-1}). The difference between measured and modelled emission was largest for Period 2 (22.9 %) and highlights the uncertainty in parameters used as input in the GUANO model when one species leaves a colony (Table 6.8).

Table 6.8 Comparison between the measured NH_3 emissions and modelled NH_3 emissions using the GUANO model for measurements made on Signy Island during Period 1 (10/01/09 - 25/01/09), Period 2 (25/01/09 - 08/02/09) and Period 3 (08/02/09 - 21/02/09).

	Period 1	Period 2	Period 3
Measured NH_3 emission estimate (µg NH_3 m^{-2} s^{-1})	18.17	7.89	9.02
GUANO Model NH_3 emission estimate (µg NH_3 m^{-2} s^{-1})	16.67	9.70	10.68
Difference between measured and modelled (%)	-8.3	22.9	18.4

Simulated NH_3 emission and environmental

During the measurement period, the maximum modelled NH_3 emissions on Signy Island was 50 µg m^{-2} s^{-1}. NH_3 emissions were larger when the ground temperature increased, and there is a strong correlation between NH_3 emission and ground temperature (R = 0.8) (Figure 6.14). Lower emissions were simulated during rain events, however the correlation between NH_3 emission and precipitation events is weak (R = -0.1). The wind speed was relatively constant throughout the measurement period, and the correlation between NH_3 emission and wind speed is medium (R = 0.4). There is no correlation between NH_3 emission and relative humidity (R < 0.1).

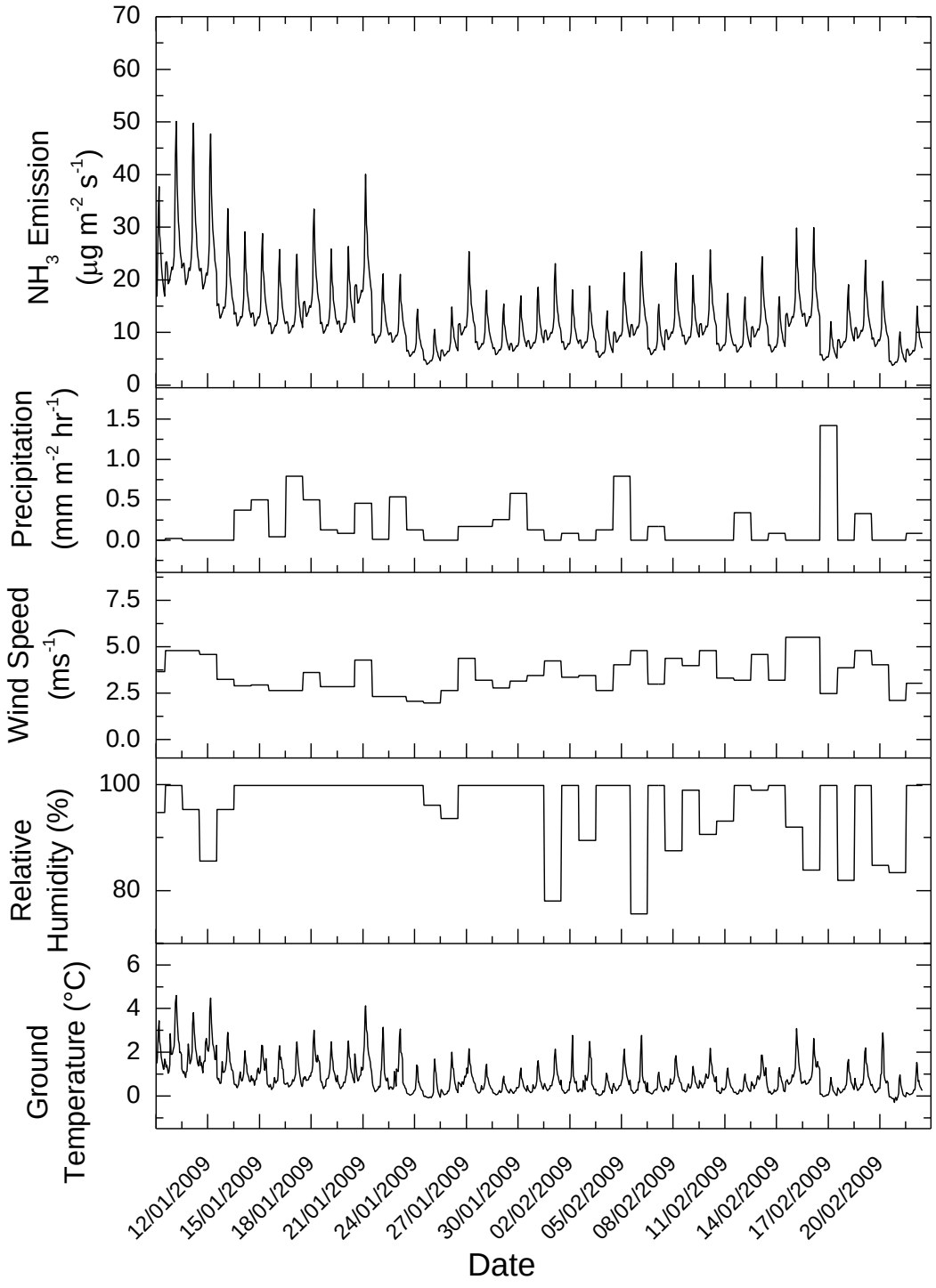

Figure 6.14 Modelled NH_3 emission compared to environmental variables representative of climate made on Signy Island during 10/01/09 - 21/02/09. Tick marks on the x-axis indicate midnight on each day.

6.3.7 Bird Island, South Atlantic, Macaroni Penguins (active measurements)

Comparison of modelled and measured NH_3 emissions

There is no clear diurnal pattern for both measured and modelled NH_3 emissions from the Macaroni penguin colony on Bird Island. Changes in NH_3 emission mainly reflect the variability of wind speed at the measurement site and to some extent temperature. The maximum measured emission at Big Mac on Bird Island was 53 µg NH_3 m^{-2} s^{-1} at 0500 on the 11th December. Most nights, NH_3 emission dropped below 10 µg NH_3 m^{-2} s^{-1}.

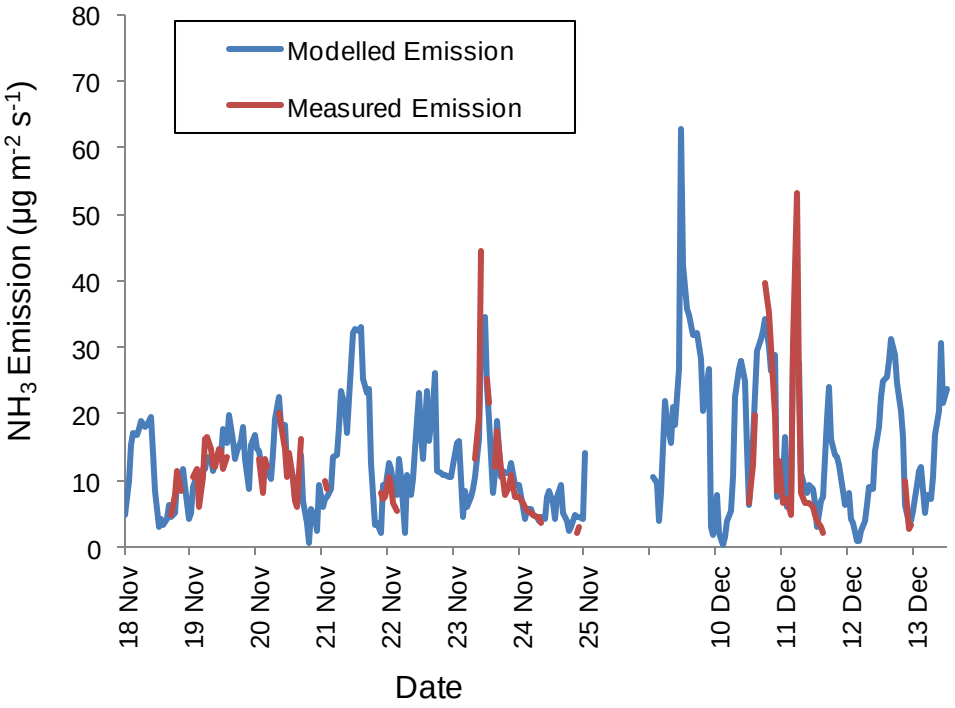

Figure 6.15 Comparison between hourly measured and modelled NH_3 emissions from the Big Mac Macaroni penguin colony, Bird Island, South Georgia, from 18/11/2010 to 13/12/2010 (measurements based on AiRRmonia concentration data supplied by Sim Tang, CEH). Tick marks on the x-axis indicate midnight on each day.

NH_3 emission estimates

Even though the NH_3 emissions change rapidly, the GUANO model replicates the measured NH_3 emissions well, with a linear regression (R^2 = 0.90; Figure 6.16). Most of the modelled emissions at Big Mac are between 0 and 20 µg m^{-2} s^{-1} and similar to those calculated for the Isle of May. This may seem surprising because the difference in N excretion rates at Big Mac and the Isle of May is 1.13 g N m^{-2}

hr^{-1} and 0.13 g N m^{-2} hr^{-1}, respectively, and points to a lower percentage volatilization rate of nitrogen at Bird Island. The average daily modelled emission at Bird Island is 1.10 g NH_3 m^{-2} day^{-1}.

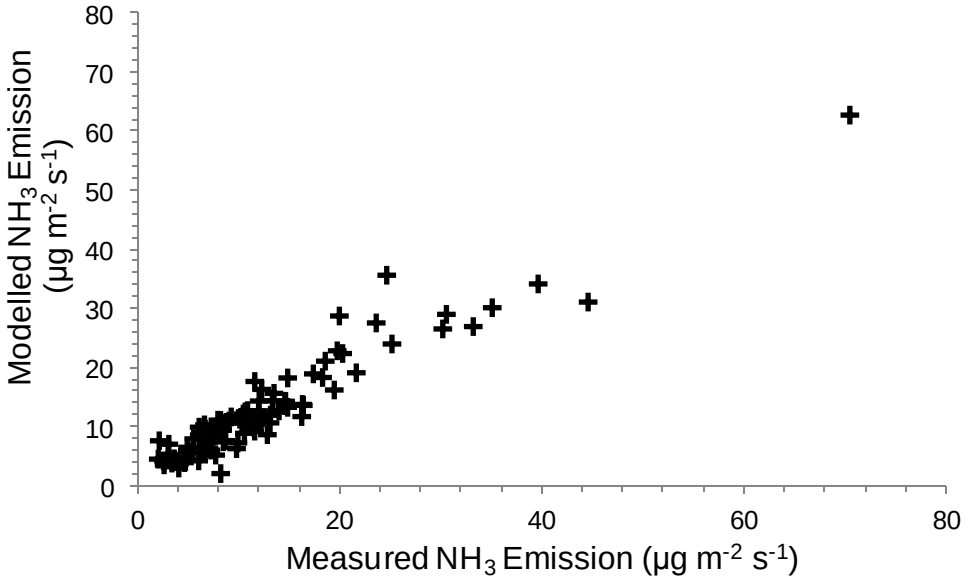

Figure 6.16 Comparison between hourly measured and modelled NH_3 emissions from the Macaroni penguin colony on Big Mac, Bird Island between 18/11/2010 and 13/12/2010.

Modelled NH_3 emission and environmental factors

The modelled NH_3 emissions at Big Mac were a maximum of 53 µg m^{-2} s^{-1}. NH_3 emissions increase as the ground temperature increases, with a strong correlation between NH_3 emission and ground temperature (R = 0.5). Wind speed has the strongest correlation of the climate variables to NH_3 emission (R = 0.9). Lower NH_3 emissions were simulated to happen during rain events, but precipitation events are negatively correlated to NH_3 emission, albeit weakly (R = -0.1). The relative humidity is weakly correlated to NH_3 emission (R = -0.2) (Figure 6.17).

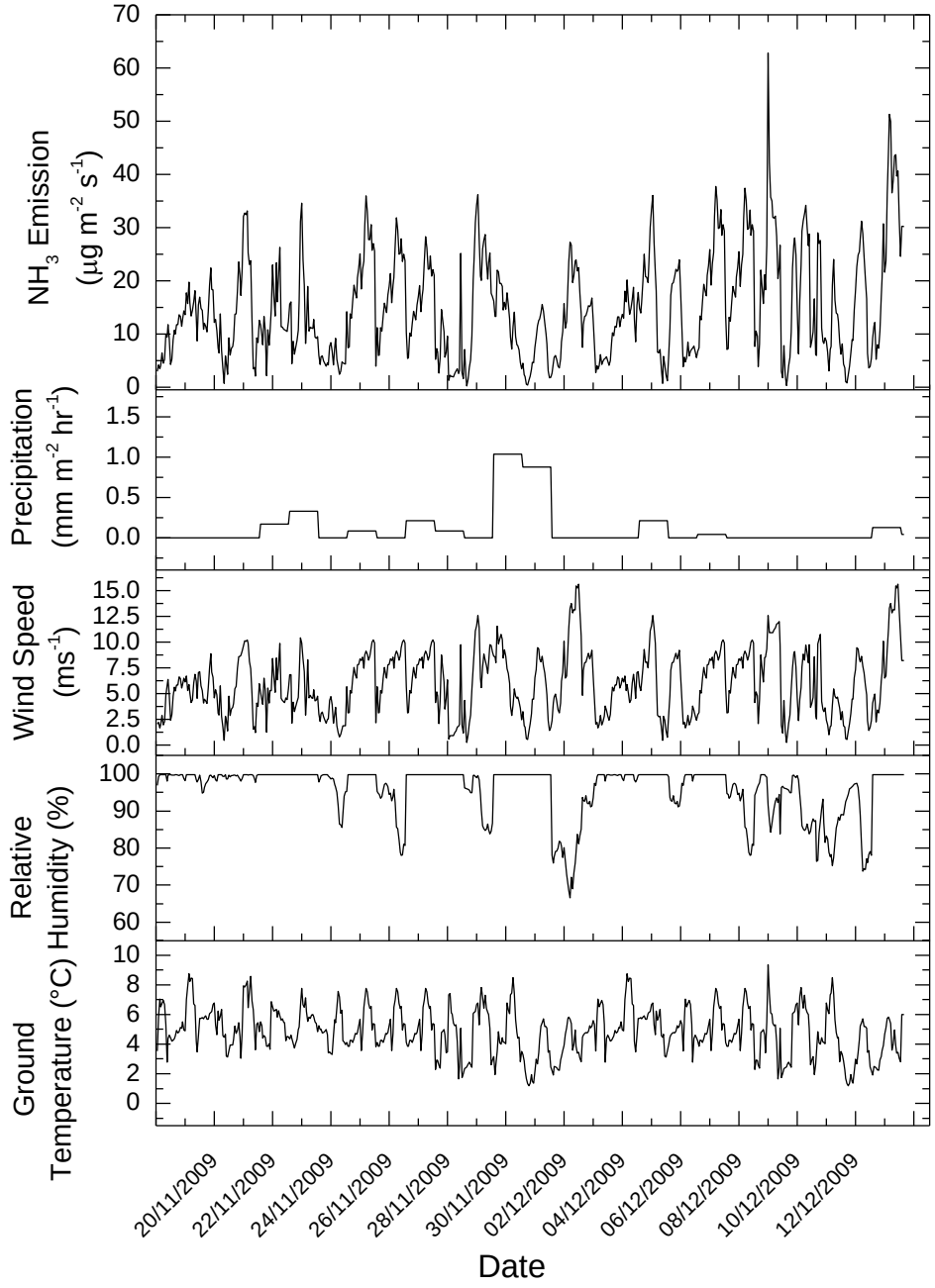

Figure 6.17 Modelled NH_3 emission compared to environmental variables representative of climate at the Big Mac Macaroni penguin colony on Bird Island from 18/11/2010 to 13/12/2010. Tick marks on the x-axis indicate midnight on each day.

6.4 Global application of the GUANO model

6.4.1 Adapting the GUANO model for calculating global emission

The GUANO model was originally designed to calculate NH_3 emissions from seabird colonies in the UK (Blackall, 2004). This study has made several modifications to the original model so that it can be used to calculate NH_3 emissions from colonies throughout the world. The Blackall (2004) GUANO model did not perform well when calculating NH_3 emission in tropical climates, especially when estimating NH_3 emissions on Ascension Island. This study addressed the shortcomings of the Blackall (2004) model by using ground temperature values, incorporating the Penman equation to calculate the water loss by evaporation, increasing TAN production during rain events and updating the values of F_{hab} (based on laboratory experiments).

When the F_{hab} value was changed from 1 to 0.67 for sand nesting birds at Ascension Island, the NH_3 emission was reduced by 33 %. Using ground temperature instead of air temperature in the GUANO model introduced the strong diurnal patterns in NH_3 emission that were observed during field studies, with large peaks during the day and lower emission during the night. Adding a water budget and increasing TAN production during rain events further helped to simulate the large NH_3 emission peaks observed on Ascension (Section 5.3.6).

6.4.2 Comparing GUANO model and measured NH_3 emissions

Section 6.3 of this chapter validates the GUANO model by comparing modelled NH_3 emissions to measured NH_3 emissions from seabird colonies in a range of climatic conditions. The GUANO model uses colony-specific nitrogen excretion rates and representative meteorological data to calculate hourly NH_3 emissions.

The percentage of excreted nitrogen that volatilized (P_v) was calculated, and during the measurement period, P_v is larger for the tropical sites (e.g. Michaelmas (GUANO model P_v = 82.4 %)) and small for the polar sites (e.g. Bird Island (GUANO model P_v = 1.7 %)), showing that climate has a large effect on P_v (Table 6.9). Measured P_v plotted against the adapted GUANO modelled P_v has a linear regression gradient of 1.2 and R^2 of 0.99 (Figure 6.18).

Table 6.9 Comparison between measured NH_3 emissions, NH_3 emission from the GUANO model and the percentage N volatilized (P_v). The average emission was calculated from the total emission and the total time of the measurement period.

	Measured Emission ($\mu g\ m^{-2}\ s^{-1}$)	GUANO Model Emission ($\mu g\ m^{-2}\ s^{-1}$)	P_v Measured (%)	P_v GUANO Model (%)
Michaelmas	22.3	27.5	66.8	82.4
Signy Island	9.0	10.7	2.4	2.9
Isle of May	5.0	3.2	4.7	2.8
Ascension	30.2	21.5	51.9	37.0
Bird Island	12.9	12.7	1.8	1.7

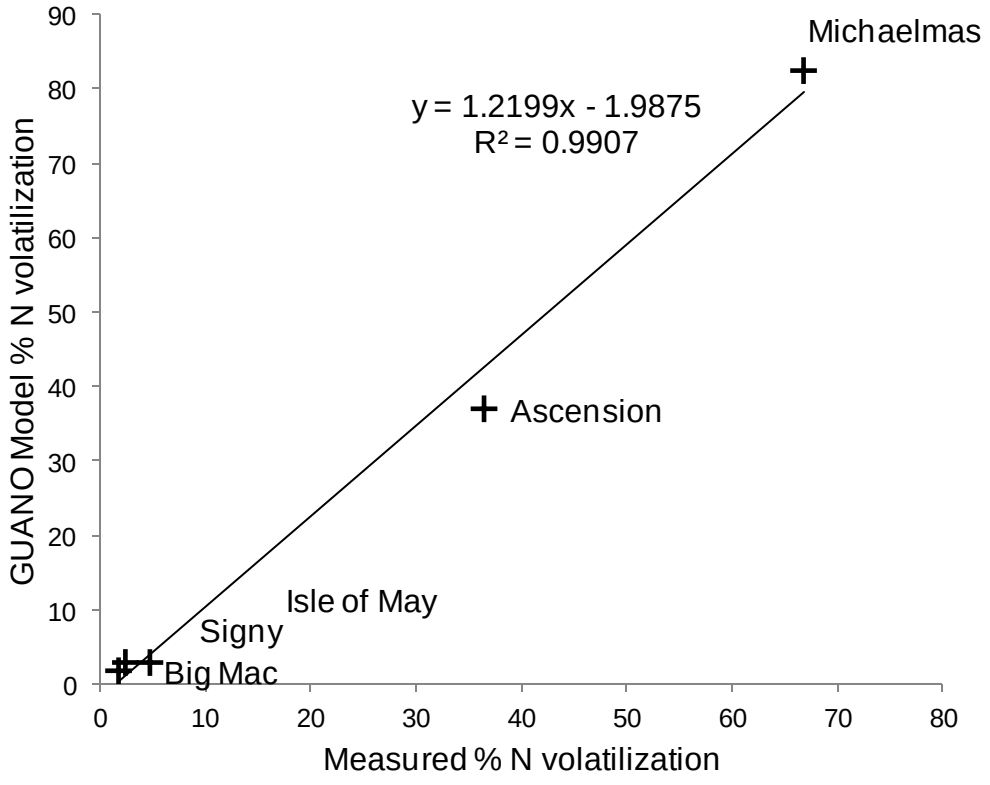

Figure 6.18 Comparison between the percentages of nitrogen that volatilizes for measured NH_3 emissions and NH_3 emissions calculated by the GUANO model.

Even though the GUANO model can be used to calculate NH_3 emissions from a seabird colony in a range of climates, shortcomings of the GUANO model are also identified. Instantaneous (hourly) NH_3 emissions calculated by the GUANO

model do not always capture the measured hourly NH_3 emission. The discrepancy between modelled and measured could be explained by a combination of bird behaviour, the limitations of data collection (e.g. the measurement of vertical flux on Ascension Island (Section 6.3.5)) and parameterization of the lag-time in the evolution of UA to TAN to NH_3 in the GUANO model.

6.4.3 Bird Behaviour

The N excretion rate used in the GUANO model assumes that all birds arrive *en masse* at the colony and deposit guano at a constant rate during the breeding season, and then all birds depart together. These assumptions simplify the complex patterns of bird attendance. The patterns of bird occupation at a colony depend on many factors and are different depending on species, site and climate. Periods of occupation also vary throughout the breeding season because of factors such as food availability and predation from other birds. The model did not account for this variation.

However, these approximations may be considered acceptable where the purpose is to estimate the annual NH_3 emission. The results show good agreement for measured and modelled NH_3 emissions at each fieldwork site (Figure 6.18) and the colony attendance and N excretion rate is suitably parameterized for the purposes of this study. Future improvements to the GUANO model may include changes to the parameterization of attendance, where arrival at the colony reflects a gradual attendance of the birds and attendance may vary throughout the breeding season. This would require a complex ecological study of each species, which is beyond the scope of this study.

6.4.4 Emission factors and NH_3 Emissions

1. Observations in the short-term

Collating the findings from each colony shows that ground temperature is highly correlated to modelled NH_3 emission at most sites, with correlation coefficients for the hourly values ranging from approximately 0.8 (Michaelmas and Signy) to 0.2 (Ascension) (Figure 6.19). The relatively low correlation coefficient between ground temperature and NH_3 emission on Ascension Island indicates that

temperature is not the key driver of NH_3 emission at this site. In contrast, the relatively high correlation between NH_3 emission and relative humidity (R = 0.4) and NH_3 emission and precipitation events (R = 0.3) suggests water availability is more important in estimating NH_3 emissions than temperature in the hot, arid climate on Ascension. In fact, Ascension is the only fieldwork site where there is a positive correlation between NH_3 emission and both relative humidity and precipitation.

Wind speed has a positive correlation at all sites, and the correlation is stronger in the polar climates (Bird Island and Signy Island) and weakest in the tropical climates (Ascension Island and Michaelmas Cay). This may indicate that in colder climates, vertical transport of NH_3 is caused by wind action instead of thermally driven mechanisms present in the tropics. As the wind speed increases, both aerodynamic and boundary layer resistances decrease and, hence, increase NH_3 emission from the surface. Bird Island is the windiest site (2 - 18 m s^{-1}), which may explain its strong effect at this site.

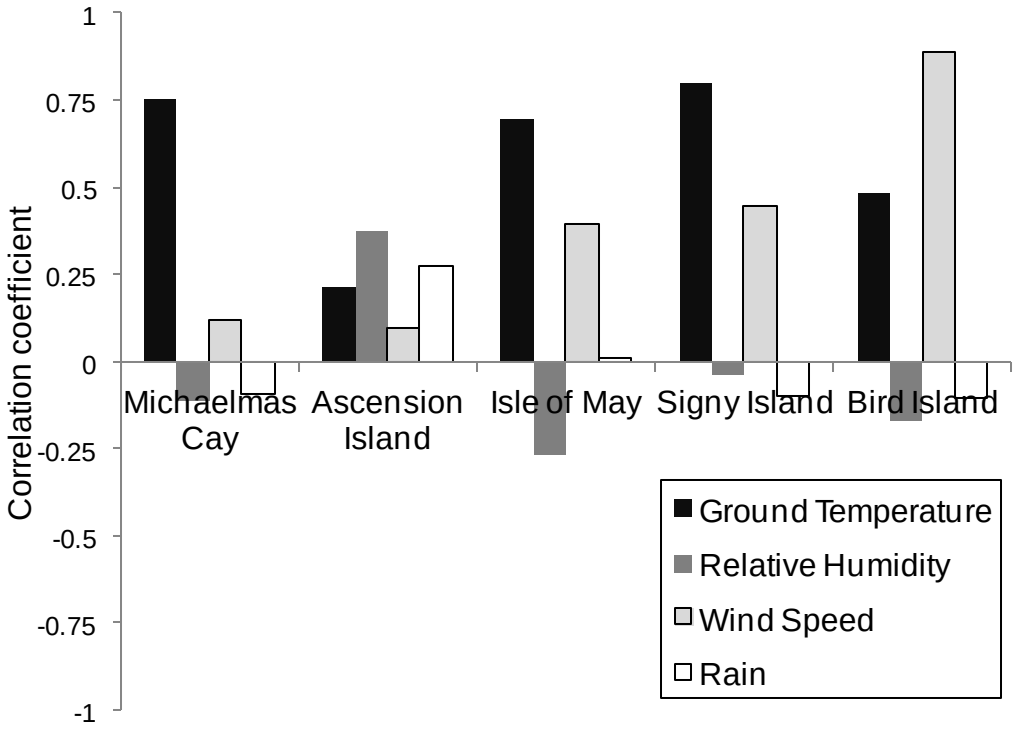

Figure 6.19 Collation of correlation coefficients between hourly modelled NH_3 emissions and environmental factors at all fieldwork sites.

A comparison of average values of these environmental variables to P_v calculated using modelled NH_3 emissions during fieldwork show similar patterns (Figure 6.20). The strongest pattern is the relationship between P_v and ground temperature (R = 0.8), where an increase in ground temperature increases NH_3 emission exponentially. This pattern was also observed by Zhu et al. (2011) and in the chamber experiments in Chapter 3. Wind speed is also strongly correlated with P_v (R = 0.6). As suggested by Figure 6.20, the P_v is weakly, negatively correlated with relative humidity (R = -0.1), but has a stronger negative correlation with precipitation (R = -0.25).

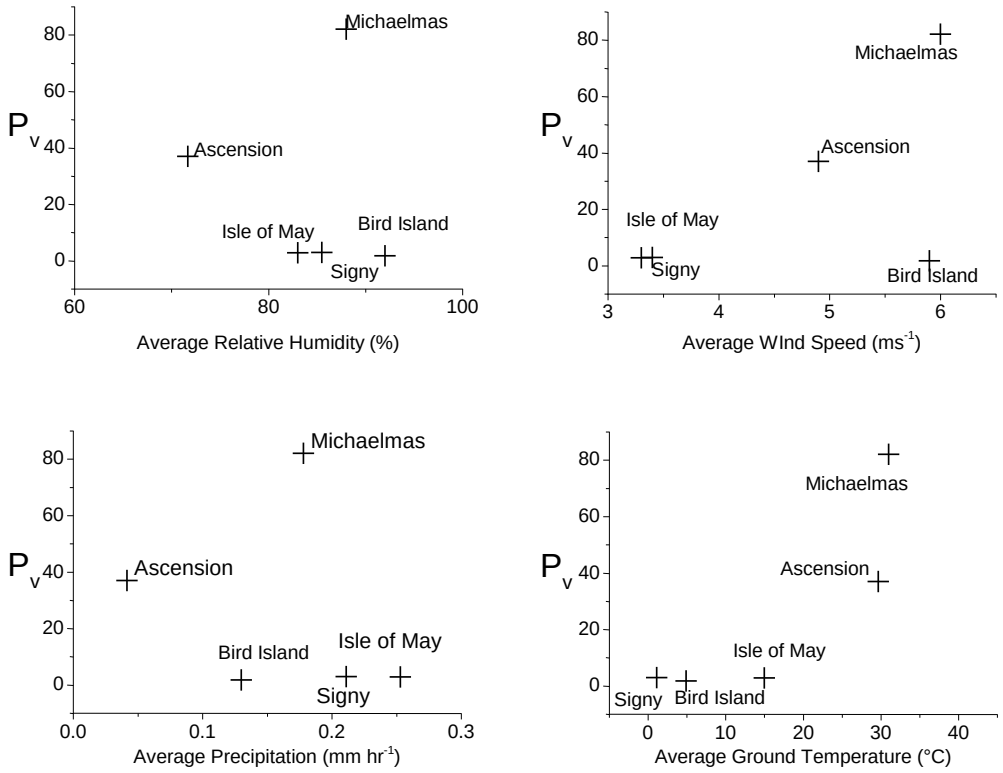

Figure 6.20 Relationship between percentage N volatilized (P_v) and relative humidity, temperature, wind speed, precipitation and ground temperature for NH_3 emissions simulated by the GUANO model during the measurement period.

2. Climate and annual GUANO model NH_3 emissions

Annual modelled P_v values from tropical seabird colonies are larger than the emission from polar colonies. Annual P_v increases in tandem with ground temperature increase (Table 6.10). For these five fieldwork sites, the strongest correlation is between ground temperature and annual P_v (R = 0.98). There is also a strong negative correlation between annual P_v and relative humidity (R = -0.5)

and between annual P_v and precipitation (R = -0.5). Annual P_v values have a very weak correlation with wind speed (R < 0.1)

Table 6.10 Annual percentage of N volatilized (P_v) by the GUANO model and comparison of mean annual climates in fieldwork location. T_g indicates ground temperature, *RH* indicates relative humidity, *WS* indicates wind speed and *P* indicates precipitation.

Colony	Annual P_v (%)	T_g (°C)	*RH* (%)	*WS* (ms^{-1})	*P* ($mm\ hr^{-1}$)
Signy	3.8	0.65	91.11	3.76	0.13
Bird Island	8.2	7.13	89.61	8.45	0.15
Isle of May	22.3	18.06	76.53	5.17	0.10
Ascension	66.7	35.38	72.02	6.93	0.05
Michaelmas	66.6	38.95	88.50	5.26	0.14

As a sensitivity test, each of the environmental variables measured at the Isle of May was substituted into the GUANO model. The results are shown in Table 6.11 and Figure 6.21. The P_v increases by 30 % for the modelled NH_3 emissions on Signy Island when higher temperature values are substituted, whereas P_v decreases by 63 % on Ascension Island when lower temperatures are substituted. Changes to other variables have little or no effect on P_v. This shows that the climate variable with the largest effect on the annual P_v is temperature.

Table 6.11 Changes to P_v as climate variables in the GUANO model are substituted by values measured at the Isle of May. T_g indicates ground temperature, *RH* indicates relative humidity, *WS* indicates wind speed, *I* indicates irradiance and *P* indicates precipitation.

	Change in P_v (%)				
Colony	T_g	*RH*	*WS*	*I*	*P*
Signy Island	+36	-1	+1	+1	1
Bird Island	+21	-1	-1	+1	1
Isle of May	0	0	0	0	0
Ascension Island	-63	-1	-1	0	1
Michaelmas Cay	-64	1	1	0	1

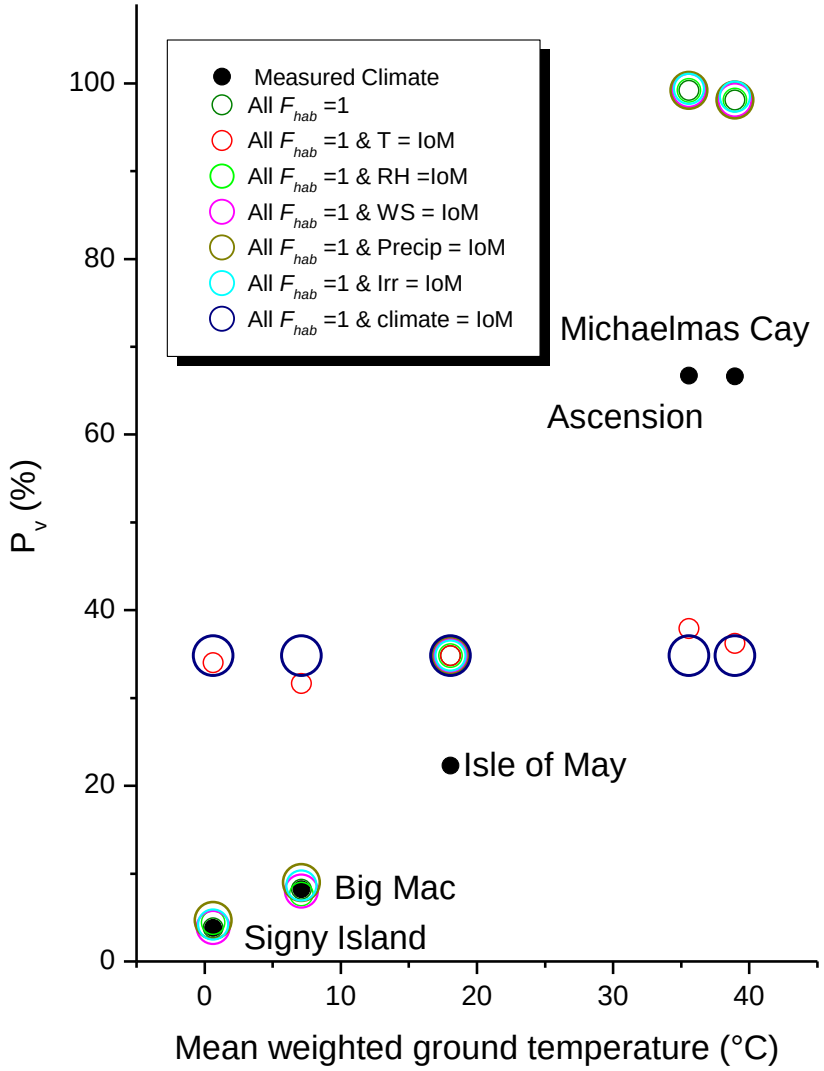

Figure 6.21 The effect of changing climate variables at each of the field sites. In each case, the climate variable measured at the Isle of May is substituted into the GUANO model.

6.4.5 F_{hab} and NH_3 Emissions

Even though climate is essential to calculating NH_3 emission, the nesting habitat is also very important. The annual P_v of the Sooty tern colony on Ascension Island estimated using the GUANO model is 66 % (F_{hab} = 0.67). When F_{hab} in the GUANO model is changed to 1, the P_v for the tern colony change to 99.8 %. This shows the importance of assigning correct values for F_{hab}.

6.5 Summary

This chapter updates the GUANO model of Blackall (2004) and applies it to new experimental sites around the world. The improvements to the model account for new habitat factors, the use of ground temperature and an improved water budget.

The updated model allows NH_3 emissions to be calculated for a broader range of nesting habitats in a variety of climates. The changes to the GUANO model improve the NH_3 emission estimate and provide a better estimate of hourly emission by capturing the strong diurnal features shown by the measurements.

The improved GUANO model uses temperature, relative humidity, wind speed and precipitation to estimate NH_3 emissions. The agreement between measured emissions and the modelled emissions have improved (linear regression $R^2 = 0.02$ (BE Model) and linear regression $R^2 = 0.85$ (TABE model)) (Section 5.5).

When calculating instantaneous NH_3 emission, all climate variables have been shown to have an influence. Increases in NH_3 emission caused by increases in relative humidity and rain events are only observed at the arid Ascension Island fieldwork site. Increases in precipitation decrease NH_3 emission because rain events wash uric acid and TAN from the surface. NH_3 emission increases with wind speed at all sites because as the wind speed increases, both aerodynamic and boundary layer resistances decrease and, hence, increase NH_3 emission from the surface. However, the most obvious relationship is that NH_3 emission increases as ground temperature increases. As ground temperature increases, the conversion of UA to TAN to NH_3 increases, as does the potential for volatilization of NH_3 from the surface.

On an annual time scale, temperature has been shown to be the most influential climate variable, where NH_3 emission rate increases with increased temperature (6.22b). Compared with the conditions of the Isle of May, wind speed or relative humidity did not have a noticeable effect on annual values of P_v. The effects of environmental variables on NH_3 emission will be investigated further in Chapter 7, where colonies that experience much greater precipitation will be used.

This chapter has shown that the GUANO model performs better than the BE (Scenario 1). The GUANO model calculates similar NH_3 emissions to the TABE (Scenario 2) model, however the GUANO model includes a precipitation variable. The GUANO model has been shown to agree well with measurement data and is therefore used to calculate the global NH_3 emission estimates in Chapter 7.

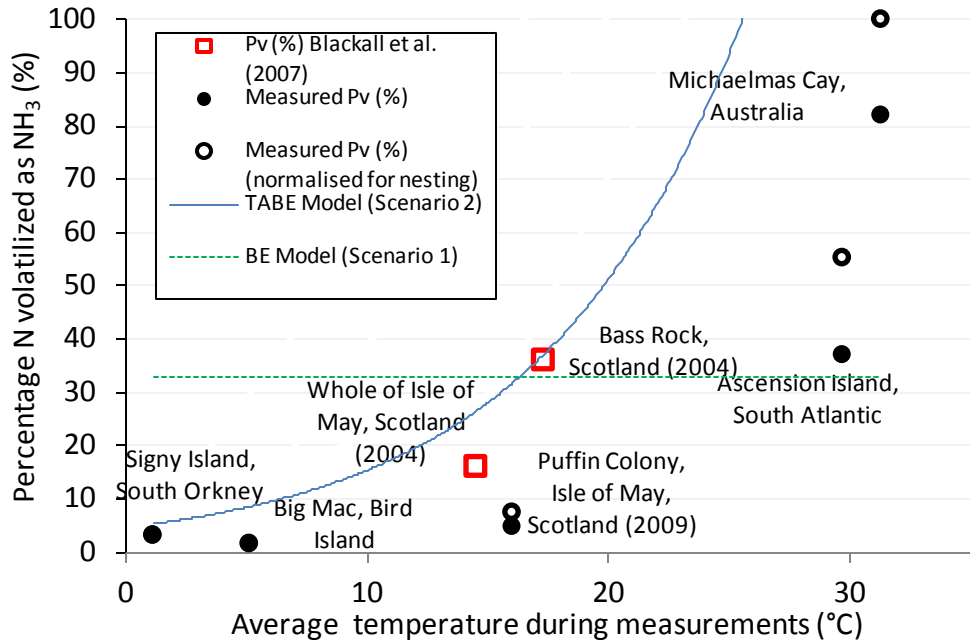

a)

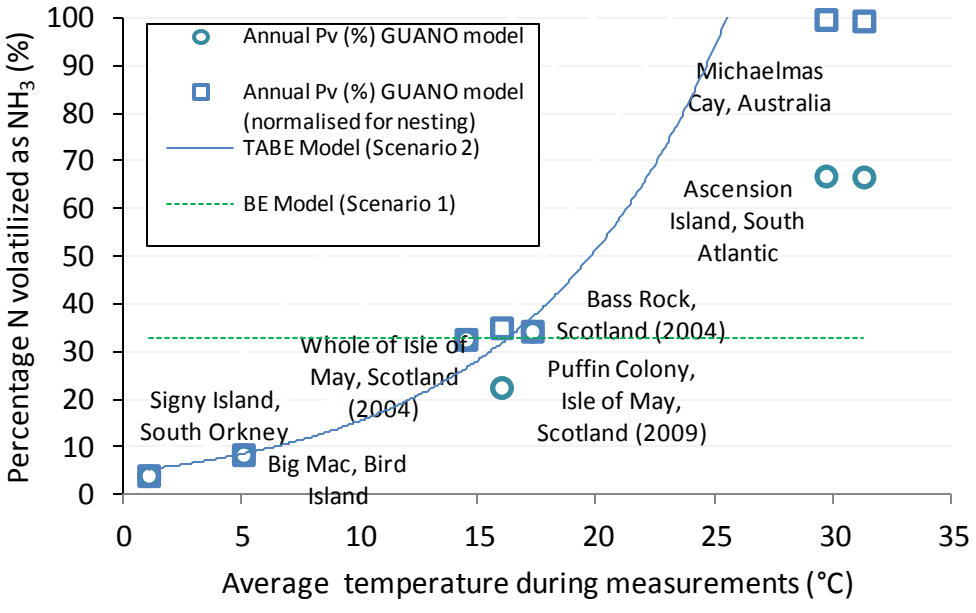

b)

Figure 6.22 Both graphs show the comparison of P_v calculated for the BE (green dashed line) and TABE (Blue solid line) at temperatures from 0°C to 30 °C. Graph a) shows P_v during the measurement period calculated from GUANO model emissions (solid dot - estimated P_v, hollow dot - P_v accounting for habitat) at each measurement site of this study (Michaelmas Cay, Ascension, Isle of May, Big Mac and Signy Island) and Blackall et al (2004) measurements for the Bass Rock and Isle of May. Graph b) shows annual P_v values calculated from GUANO model emissions (solid dot - estimated P_v, hollow dot - P_v accounting for habitat) at each measurement site of this study (Michaelmas Cay, Ascension, Isle of May, Big Mac and Signy Island) and Blackall et al (2004) measurements for the Bass Rock and Isle of May.

Chapter 7: Regional and global significance of seabird-mediated nitrogen cycle processes

7.1 Introduction

Climate has been shown to strongly affect the emission of NH_3 from nitrogen excreted at seabird colonies across a global climate gradient, from the tropics to sub-polar regions (see Chapter 5). The key climatic driver was found to be temperature, with rainfall, relative humidity and wind speed also influencing the percentage of excreted nitrogen that volatilized as NH_3 (P_v).

In this chapter, the revised GUANO model (Chapter 6) is adapted to calculate process-based NH_3 emission estimates for all seabird colonies detailed in the global seabird database (Chapter 3) collated for this thesis. The global model output provides an investigation of the influence of climate drivers on NH_3 emissions from seabirds on a global scale, as well as a comparison with previous, more theoretical modelling efforts with the TABE model (Chapter 3).

In addition to calculating a new best estimate of current global NH_3 emissions from seabirds, predicted changes to seabird NH_3 emissions are also derived, based on selected climate change scenarios (IPCC, 2007). The IPCC suggest that average global surface temperatures will increase by between 1.1 and 6.4 °C by 2100 (IPCC, 2007), and global average rainfall amounts will increase, with regional rainfall amounts changing by as much as ± 20 %. The sensitivity to environmental factors, shown in Chapter 5, suggests these changes will affect NH_3 emissions from seabird colonies throughout the world. As many colonies of penguins and other seabird species occur in delicately balanced, pristine environments with low anthropogenic emissions, these potentially large changes in NH_3 emissions over the next 90 years could have a pronounced environmental impact in these remote regions.

7.2 Methods & Materials

7.2.1 GUANO Model development

The revised GUANO model was converted from the initial Microsoft Excel version to R in order to enable large numbers of colonies to be processed

iteratively at an hourly time resolution. For each seabird colony in the global seabird database (Section 3.2.1), the GUANO model uses climate and bird data and calculates the hourly NH_3 emission (F_H, g NH_3 m^{-2} h^{-1}) for a period of two years. The annual NH_3 emission (F_T, g NH_3 m^{-2} $year^{-1}$) is calculated as the sum of hourly emissions for the second year. The second year is required because it takes into account uric acid from the previous year that has not volatilized or been washed off by rain (Blackall et al., 2008).

7.2.2 Model Input

Bird Attendance

The attendance of seabirds at their breeding colony is calculated from the number of days birds spend at the colony. Bird arrival and departure dates are subject to large spatial heterogeneity. The period of attendance at colonies is listed for each species in Appendix 1.

Nitrogen excretion rates

The average nitrogen excretion rate (F_e, g m^{-2} $hour^{-1}$) for each seabird species in the GUANO model is calculated from the following data (described in detail in Section 6.2.2., see Equation 7.1):

- period of attendance at the colony (T, days),
- proportion of the time spent at the colony during the breeding season (f_{tc}),
- number of breeding adults per square metre (D_A, birds m^{-2}),
- amount of nitrogen excreted per breeding adult ($F_{e\text{-}br}$, g $bird^{-1}$ day^{-1}),
- amount of nitrogen excreted per chick ($F_{e\text{-}ch}$, g $chick^{-1}$ $year^{-1}$) and
- productivity of the species (P, fledged chicks per breeding pair).

$$F_e = \frac{(1.167 T f_{tc} F_{e-br} D_A) + \left(F_{e-ch}\left(\frac{P}{2}\right) D_A\right)}{24T} \qquad (7.1)$$

Species-specific values for input parameters (adult mass, number of days spent at the colony per year, proportion of time at the colony, breeding success, fledging mass of the chick and breeding substrate) were extracted from the literature and are summarised in Appendix 1. Where data were available from multiple colonies

and/or years, the mean of the colony and/or annual mean was used. Of the 318 species of seabird considered, data were available for 311 species (Birdlife International, 2011). Data for the missing species were estimated from similar species identified using Birdlife International (2011).

Parameterization of hourly temperature

To calculate accurate NH_3 emission, the GUANO model requires temperature and net solar radiation data every hour. As global hourly temperature data were unavailable, this study used a model based on Parton and Logan (1982) that calculated the diurnal changes in air temperature given a maximum and minimum value. This temperature model calculates the air temperature at 2 m above the surface for each hour day (H) from the day of year (D), latitude (L, °), maximum temperature (T_{max}, °C) and minimum temperature (T_{min}, °C), using a sinusoidal relationship (Parton and Logan, 1982).

Figure 7.1 shows the diurnal variation in air temperature according to the Parton and Logan (1982) model plotted against the measured air temperature data at 2 m for Ascension Island, the Isle of May and Bird Island. A linear regression shows good agreement between the modelled and measured values for the field sites. The coefficient of determination for each site is shown in Table 7.1.

Table 7.1 Comparison between average measured ground temperature and ground temperatures modelled with the Parton and Logan (1982) method, using measured average maximum and minimum air temperature data during the measurement period at each of the field sites.

Field site	Gradient	R^2
Isle of May	0.90	0.89
Mars Bay, Ascension	0.88	0.84
Big Mac, Bird Island	0.84	0.79

Although the temperatures calculated by the Parton and Logan (1982) model are serially correlated, the model describes the hourly values of the temperature well in temperate, tropical and polar regions during the seabird breeding season (Figure 7.1). However, it should be noted that the Parton and Logan (1982) model

overestimates temperatures as the temperature increases (dawn) and as it decreases (dusk).

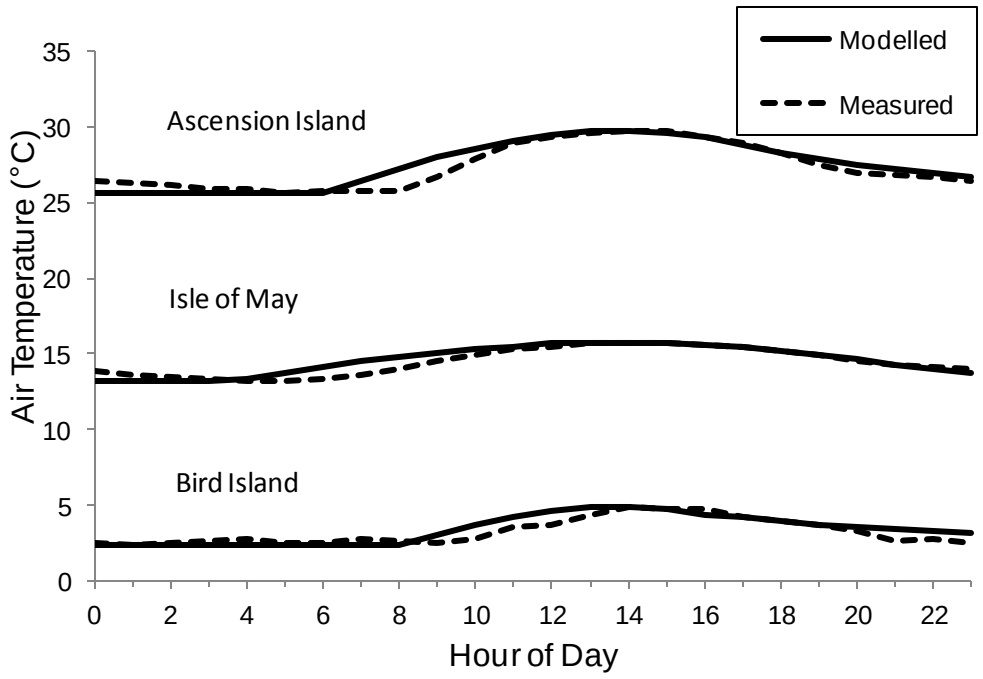

Figure 7.1 Comparison of the diurnal variation in average measured ground temperature and ground temperatures modelled with the Parton and Logan (1982) method, using measured average maximum and minimum air temperature data during the measurement period at each of the field sites.

Meteorological data

The GUANO model requires hourly input data for ground temperature, relative humidity, wind speed, precipitation and net solar radiation. Several global meteorological stations are available that report several of these variables. To determine the most suitable meteorological dataset for use in the global GUANO model, the detailed meteorological data measured from each field work site were compared with two available global meteorological datasets:

(i) National Climatic Data Center (NCDC) Global Surface Summary of the Day (GSOD) data (NCDC, 2011) and

(ii) The National Center for Environmental Prediction and the National Center for Atmospheric Research (NCEP/NCAR) reanalysis data set (NCEP, 2011).

The NCDC GSOD data were available as daily data (Integrated Surface Hourly (ISH) dataset), collated by the USAF Climatology Center. The dataset includes observed data from over 9000 meteorological stations globally. A minimum of four observations is used to derive the daily summary data. Due to unit conversions to the metric system, slight rounding errors may occur. Data reports are based on Greenwich Mean Time (GMT). The available data are summarised in Table 7.2 below:

Table 7.2 Summary of data available from the National Climatic Data Center (NCDC) Global Surface Summary of the Day (GSOD) (NCDC, 2011)

Variable	Unit	Accuracy
Mean temperature	Fahrenheit	0.1
Mean dew point	Fahrenheit	0.1
Mean visibility	Miles	0.1
Mean Wind Speed	Knots	0.1
Maximum sustained wind speed	Knots	0.1
Maximum wind gust	Knots	0.1
Maximum temperature	Fahrenheit	0.1
Minimum temperature	Fahrenheit	0.1
Precipitation amount	Inches	0.01
Snow depth	Inches	0.1

The NCEP/NCAR data are derived using an analysis/forecast system, which uses weather observations taken by: ships, planes, station data and satellite observations. The data are available in a 4 times daily (i.e., 6-hourly) format or as daily averages at a 2.5 ° x 2.5 ° grid resolution, and include: air temperature at the surface (°C), relative humidity (%), precipitation rate (kg m^{-2} s^{-1}), wind speed (m s^{-1}), net solar radiation (W m^{-2}) and ground temperature (°C). The largest uncertainty is associated with the air temperature at the surface (or "skin temperature"), which is determined diagnostically as the temperature to balance the fluxes at the surface. The method used to calculate the skin temperature is acknowledged to fail in conditions with low wind speeds and when the thermal exchange coefficient is close to zero (NCEP, 2011). The net solar radiation data are empirically based and take into account cloud cover.

To evaluate the two global datasets for their suitability for estimating global ammonia emissions, meteorological data for the field sites on Ascension, the Isle of May and Bird Island were obtained from both the GSOD and NCEP/NCAR datasets and compared with measured data collected during the field work carried out for this thesis. The NCEP/NCAR data were taken from the grid cell that contained the bird colony, whereas the GSOD data were taken from the meteorological station geographically closest to the bird colony (see Table 7.3 for details).

Table 7.3 The name and distance of the GSOD meteorological station geographically closest to the bird colony.

Field site	Met station name (NCDC ID #)	Distance between field site and met station (km)
Isle of May	Leuchars Airbase, Fife (31710)	30
Mars Bay, Ascension	Wideawake airhead, Ascension Island (619020)	1
Big Mac, Bird Island	Base Orcadas, Laurie Island, South Orkney Islands (889680)	850

Hourly values of air temperature, relative humidity, wind speed and precipitation were calculated from the GSOD data. Hourly air temperature was calculated using daily maximum and minimum values in the Parton and Logan (1982) method. Hourly values of relative humidity data were taken as the daily average, as were the values for wind speed. The hourly value of precipitation was simply the total daily value divided by 24.

To make a direct comparison between the data sets, hourly values of NCEP/NCAR climate data are calculated in the same way as for the GSOD data. The NCEP/NCAR dataset also included ground temperature and net solar radiation data. Hourly ground temperatures are calculated the same way as hourly air temperatures, using the Parton and Logan (1982) model. Net solar radiation during the hours of night was set at zero, where the hours of night was calculated using the method of Parton and Logan (1982). The hourly solar radiation during the day was calculated as the daily average value during the hours of daylight.

To identify which dataset best represents the actual climate at the colony, the two sets of hourly data (GSOD and NCEP/NCAR) were compared with the hourly

values of meteorological data measured in this study at the three field sites. The quality of fit is determined by calculating the gradient (m) and coefficient of determination (R^2) of the linear regression between measured and GSOD or NCEP/NCAR values for each climate variable.

GSOD data accord more closely to meteorological data measured at Bird Island, the Isle of May and Ascension Island than NCEP/NCAR data (Tables 7.4; 7.5). However, the fit of the GSOD data depends on the proximity of the meteorological station to the seabird colony and also the local conditions (e.g., influence of topography on wind speed/direction). These issues are particularly noticeable by the poor correlation between the GSOD meteorological data measured at Base Orcadas and that measured on Bird Island in the field ($R^2 = 0.10 - 0.13$), which may be caused by the distance between Base Orcadas and Bird Island (850 km). Despite these differences, the GSOD data are still a better fit to measured data than the NCEP data. The GSOD and NCEP/NCAR precipitation both agree well with measured precipitation data, but the GSOD agrees better with the higher rainfall measured on the Isle of May. The GSOD data for air temperature, relative humidity, wind speed and precipitation are the best available meteorological data, while the NCEP/NCAR provides the best net solar radiation data available. The NCEP/NCAR ground temperature data do not fit well to measured values. The poor fit is due to the large area covered by the 2.5 ° x 2.5 ° grid cells. Each of the three islands occupies only a very small proportion of the respective grid cell, thus the data is more representative of the sea surface temperature rather than the land surface temperature of the grid cell. Therefore, the NCEP/NCAR ground temperature data are not suitable for use in the emission model.

Table 7.4 Comparison of measured data to Global Summary Of Day (GSOD) data with data measured at the field sites, for the duration of the field work. T_A is air temperature, RH is the relative humidity, WS is wind speed and P is the total precipitation measured during the period of field work. The gradient of the linear regression is denoted as m and R^2 is the coefficient of determination between the measurements and the GSOD database.

	Hourly T_A		Hourly RH		Hourly WS		Total P	
	R^2	m	R^2	m	R^2	m	Measured (mm)	GSOD (mm)
Isle of May	0.57	1.3	0.58	0.81	0.40	0.35	110	76
Ascension	0.64	0.80	0.20	0.50	0.10	0.19	6	11
Bird Island	0.10	0.25	0.10	0.22	0.13	0.20	98	76

Table 7.5 Comparison of measured data for the duration of the field work to National Center for Environmental Prediction and the National Center for Atmospheric Research (NCEP/NCAR) data. T_A is air temperature, T_G is ground temperature, RH is the relative humidity, WS is wind speed, R_n is net radiation and P is precipitation. The gradient of the linear regression is denoted as m and R^2 is the coefficient of determination between the measurements and the NCEP/NCAR database.

	Hourly T_A		Hourly T_G		Hourly RH		Hourly WS		Hourly Ir		Total P
	R^2	m	R^2	m	R^2	m	R^2	m	R^2	m	NCEP/ NCAR (mm)
Isle of May	0.50	0.64	0.01	0.02	0.12	0.47	0.30	0.32	0.45	0.56	62
Ascension	0.06	0.12	0.01	0.01	0.02	0.05	0.02	0.18	0.52	0.60	12
Bird Island	0.03	0.17	0.01	0.02	0.18	0.02	0.03	0.01	0.34	0.40	79

Ground Temperature Modelling

Ground temperature is different from air temperature measured at 2 m and has a large influence on NH_3 emission calculations in the GUANO model. Ground temperature is very rarely measured, and as shown above the available NCEP/NCAR dataset had a very poor fit with measured ground temperatures (Table 7.5). GSOD data provides air temperature in reasonable agreement with measured values (Table 7.4) and a method for estimating hourly ground temperature values using air temperatures

Measured ground temperature data for the Isle of May, Ascension Island and Bird Island were used to derive a relationship between ground temperature, air temperature, latitude and time of day. Figure 7.2 shows the average temperature

difference between the air and ground for each hour of the day at the three field sites (Isle of May (56 °N), Ascension (8 °S) and Bird Island (54 °S)) calculated as the mean each hour during the measurement period.

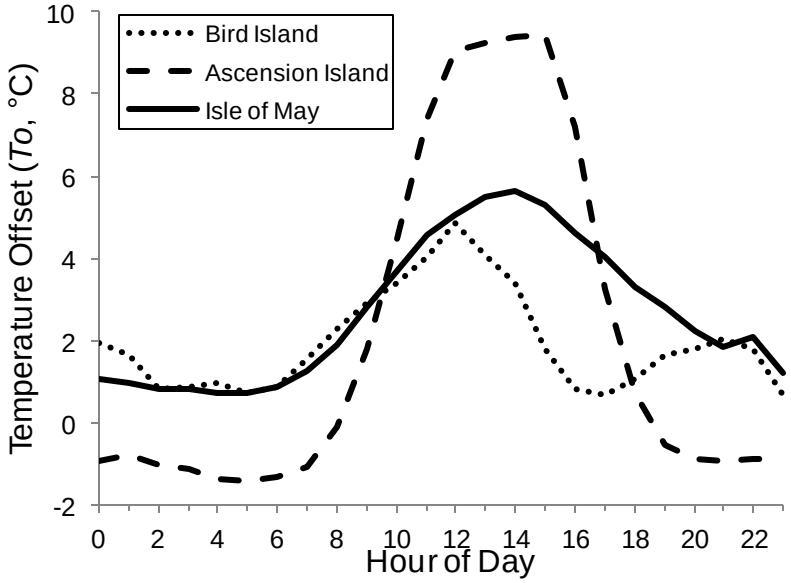

Figure 7.2 The temperature offset (T_o, °C), difference between average air temperature and ground temperature, for the three field sites during the measurement period (nesting time at each of the colonies): Solid Line: Isle of May (56 °N), Dashed line: Ascension (8 °S) and Dotted Line: Bird Island (54 °S).

Diurnal variation in temperature difference is very similar between the Isle of May and Bird Island, 56 °N and 54 °S, respectively, where the ground is warmer than the air throughout the day and night, with a peak during the middle of the day. The diurnal variation in temperature difference between the air and ground on Ascension is different, with the ground colder than the air during the night and much hotter than the air during the day. Although annual variations occur, the focus here is to provide mean profiles during the bird breeding/nesting seasons.

In the absence of measured global surface temperature data, these were derived from the air temperature for each colony, using measured surface and air temperature data from the three field work sites to parameterize a temperature offset (T_o) function. T_o was set at the measured values: equator = T_o (Ascension), 55 °N = T_o (Isle of May) and 55 °S = T_o (Bird Island). Using these fixed points, T_o was derived for each hour at any given latitude based on linear interpolation

between latitudes for these hourly values. For site farther north of the Isle of May and farther south of Bird Island values for these sites were used as limits.

Due to the relatively simple derivation method and the limited number of measurement sites, there is substantial uncertainty associated with the estimated surface temperature. Based on ground temperature daily variations at the three measurement sites, a best estimate of uncertainty in derived ground temperatures at these sites is ± 1 °C. However, the global interpretation of these values must be acknowledged to be more uncertain, and probably ± 2 °C as a best estimate.

Assigning meteorological stations to seabird colonies

The geographically closest meteorological data for each seabird colony were extracted using a GIS. These data are used in the GUANO model to calculate NH_3 emissions for the year 2010. For colonies farther than 1000 km from a measurement site, the climate data were calculated as the average of the nearest three sites. 1000 km was used as the cut off because it was assumed that for our purposes, climate at sea level would be sufficiently similar to sites within this distance. This correction was only necessary for 50 colonies, mostly in the South Pacific and Antarctica.

7.2.3 Annual Emission estimate

The total annual NH_3 emission (F_T, g NH_3 yr^{-1}) from each colony is calculated from the sum of the hourly NH_3 emissions (F_H, g NH_3 $hour^{-1}$), the nest density (*ND*) and the population size (*P*) (Equation 7.2).

$$F_T = \left(\sum_{1^{st}\ January}^{31^{st}\ December} F_H\right) ND \frac{P}{2}. \qquad (7.2)$$

7.2.4 Analysis of climate effects

Correlations were calculated between NH_3 emissions and the hourly climate data for each variable (either GSOD or NCEP/NCAR) by calculating the product moment correlation coefficient (*r*). To identify the relative effects of climate on NH_3 emission, climate variables were fit with a multiple regression model.

7.2.5 Climate change scenarios

Data from the Intergovernmental Panel on Climate Change Special Report on Emissions Scenarios (IPCC, 2007) were used to simulate potential future changes in ammonia emissions from seabirds for different scenarios. The specific scenarios used for the emission calculations were: the best case scenario (B1), the middle scenario (A1B) and the worst case scenario (A2) (Mann & Kump, 2008). They are available from the IPCC data distribution centre (IPCC DDC, 2011), and specifically from the Institut Pierre Simon Laplace (IPSL), France, who used the IPSL-CM4 model (Denvil, 2005). This particular model was chosen because it provided anomaly data on the temperature, northward and eastward wind components, precipitation and humidity for the twenty year average between 2080 and 2099 on a 2.5 °by 3.75 ° grid. The temperature, relative humidity, wind speed and precipitation anomalies summarized for steps of 10 ° latitude are presented in Figure 7.3. These were represented by incorporating the predicted changes in temperature, wind speed, relative humidity and precipitation (anomalies) with the detailed global climate dataset, described in the previous sections (7.2.2).

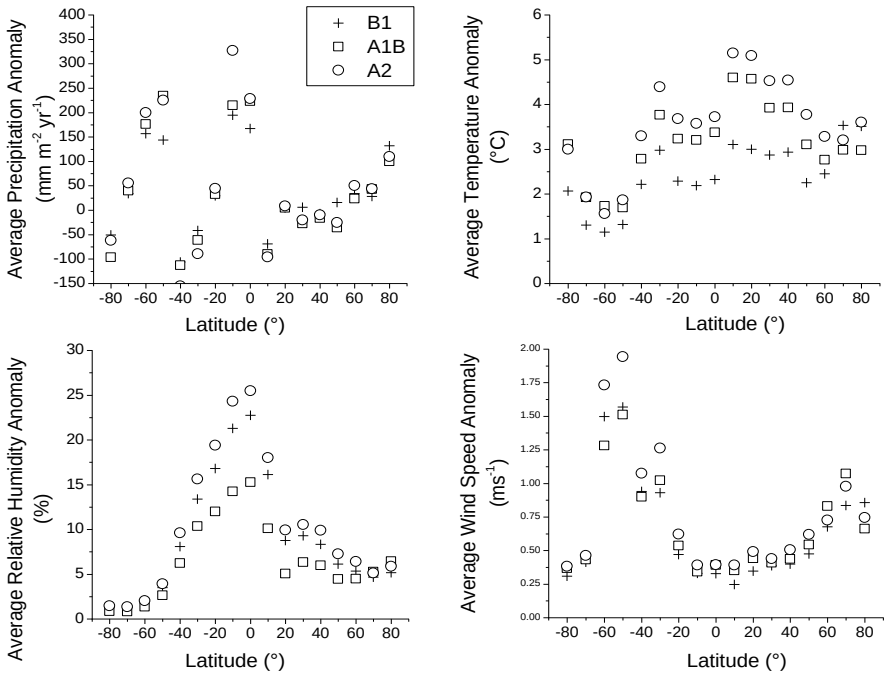

Figure 7.3 Climate change anomalies for IPCC climate change scenarios B1, A1B and A2 for precipitation, temperature, relative humidity and wind speed.

The geographically closest anomaly data for each seabird colony were extracted using a GIS and added to the detailed global climate data, as described in the previous sections (7.2.2), for use in the GUANO model for the year 2099. It should be noted that no account was taken of potential effects of climate change on seabird populations due to changes in food availability or physical changes to breeding sites (e.g., due to sea level rise or increased storm frequency). However, these issues are discussed in Chapter 8.

In summary, the global temperature and wind speed are predicted to increase across the globe, whereas precipitation shows more complex patterns, with some areas predicted to experience increases of 200-350 mm, whereas others may receive up to 150 mm less precipitation per year, on average. Relative humidity increases on average across latitude bands, but there are areas where RH is predicted to decrease, e.g. Antarctica.

7.3 Results and Discussion

7.3.1 Global distribution of seabird NH_3 emission

The total NH_3 emission estimate calculated by the GUANO model is 81.8 Gg NH_3 $year^{-1}$, using modelled ground temperature data (Figure 7.4). Chapter 3 describes the three scenarios of temperature independence (Scenario 1), theoretical temperature dependence (Scenario 2) and a mid-estimate between Scenario 1 and Scenario 2 that accounts for non-linear interactions with water availability and surface infiltration (Scenario 3). Scenario 3 was thought to be the best estimate at 244 Gg NH_3 $year^{-1}$, however the TABE model (Chapter 3 - Scenario 2) gives the closest NH_3 emission estimate of 83.1 Gg NH_3 $year^{-1}$. The Scenario 1 emission estimate is 404 Gg NH_3 $year^{-1}$.

The main differences between the GUANO model and the TABE model are the emissions from colonies between 45 °S and 55 °S, where the TABE model emissions are twice as large as the GUANO model emissions (Figure 7.5). These are the penguin colonies in the Southern Ocean, where temperatures are relatively low and rainfall is high. The pronounced difference between 45 °S and 55 °S may be caused by the slow evolution of uric acid to NH_3 gas at these temperatures simulated in the GUANO model. Additionally, as the unvolatilized nitrogen

remains on the ground longer, there is also a higher probability that it will be washed away by rain rather than emitted to the air.

Between 15 °N and 25 °S, NH_3 emissions calculated by the GUANO model are higher than those calculated by the TABE model (Figure 7.5). Both the models have an exponential relationship between temperature and emission. However, the larger emissions in the tropics may be caused by the use of hourly ground temperature values in the GUANO model instead of an average value for the breeding season. The peaks during the day result in exponentially larger emissions which are reflected in the annual emissions.

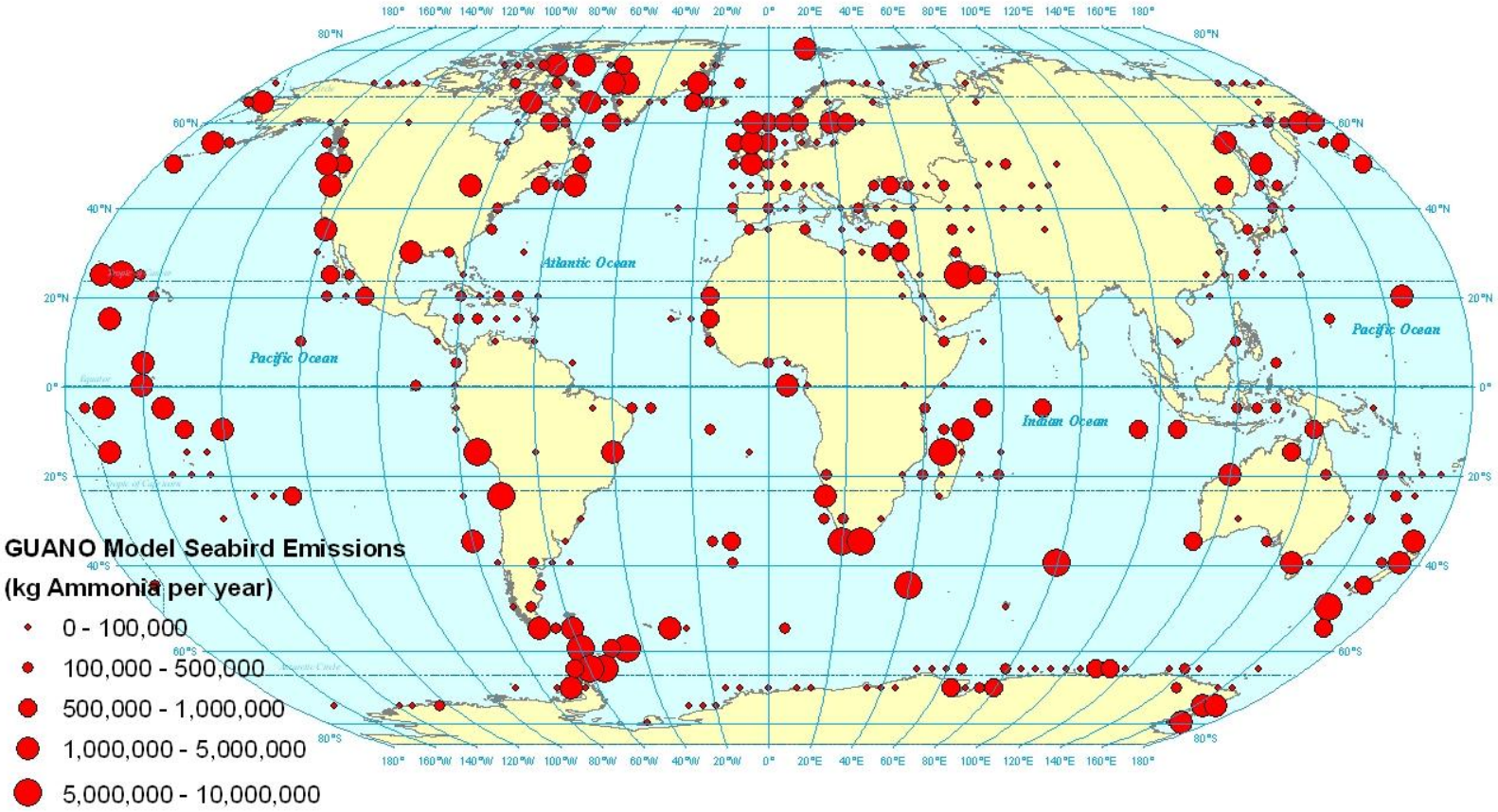

Figure 7.4 Global NH_3 emissions from seabirds, calculated using the revised GUANO model with ground temperature data.

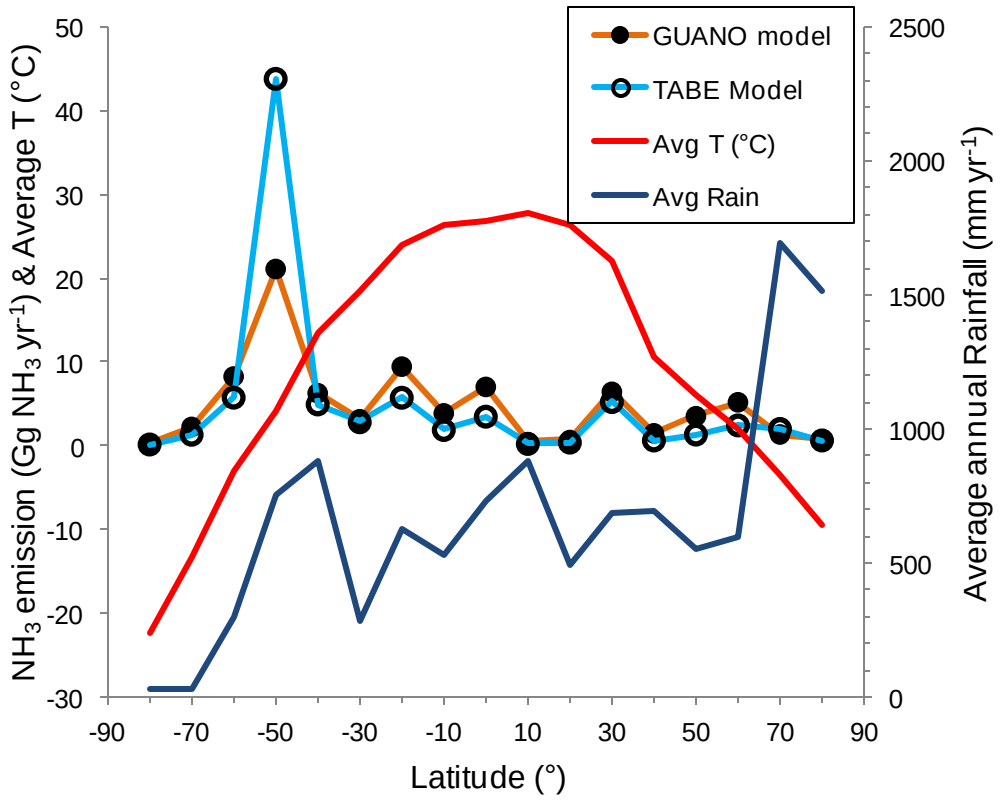

Figure 7.5 Comparison of the total NH_3 emission estimates made by the bioenergetics model (Chapter 3 - Scenario 2) and the GUANO model (using a modelled value for ground temperature). The average temperature and rainfall are also presented.

7.3.2 NH_3 emission by seabird species and region

There are significant differences in emissions for different seabird species. Table 7.6 shows a comparison of the 10 species with the largest emission (as calculated by the revised GUANO model) with the emissions from the TABE model (Chapter 3 - Scenario 2).

NH_3 emissions calculated by the GUANO model are lower than emissions from the TABE model for the highest emitting penguin species. As noted above, this is may be caused by the GUANO model taking into account nitrogen wash-off from the colony during rain events. However, NH_3 emissions calculated by the GUANO model are higher than emissions from the TABE model for species found in the tropics, e.g. Sooty tern, Laysan albatross, as these birds are found in hotter climates. As explained above, the exponential relationship between

temperature and NH_3 emission in the GUANO model uses hourly values of temperature resulting in exponentially larger emissions.

Table 7.6 Comparison of the NH_3 emission estimates made by the TABE model (Chapter 3 - Scenario 2) and the GUANO model for the ten species with the largest NH_3 emissions as calculated by the GUANO model.

Species	Model Emission (Gg NH_3 yr^{-1})		Difference in emission
	GUANO	TABE	(%)
Macaroni Penguin	11.6	17.5	-34
Sooty Tern	10.5	4.6	128
Guanay Cormorant	8.6	4.9	76
Chinstrap Penguin	7.0	4.2	67
Rockhopper Penguin	6.7	13.0	-48
Adelie Penguin	3.3	1.8	83
King Penguin	2.9	10.9	-73
Laysan Albatross	2.8	1.2	133
Short-tailed Shearwater	2.2	1.2	83
Common Guillemot	2.0	1.3	54
Other Penguins	1.2	6.7	-82
Other Species	11.2	15.8	29
Total	81.8	83.1	
NH_3 emission Penguins	42%	65%	

A comparison of the estimates by the revised GUANO and TABE models for 13 regions of the world (see Section 3.3 for a map) is given in Table 7.7. Some regions extend over several climate zones and the relationships between climate drivers and emission are more complex. For example, European NH_3 emissions calculated by the GUANO model from colonies in the south are larger because of the effects of parameterising temperature hourly. However, these are tempered by the effects of precipitation in colonies to the north. These effects result in a difference in emission between the GUANO model and TABE model of -32 %. To further explain the climate drivers of NH_3, emissions are analysed in more detail in Section 7.3.3.

Table 7.7 Regional NH3 emission estimates calculated by the GUANO mode1 (using a modelled ground temperature; Scenario 1) and the thermodynamically dependent bioenergetics model Scenario 2 (TABE) (Chapter 3).

Region	GUANO Model ($Gg\ NH_3\ Year^{-1}$)	TABE ($Gg\ NH_3\ Year^{-1}$)	Change in emission (%)
1. Africa	2.59	3.43	-24
2. Antarctica & Southern Ocean	34.20	52.71	-35
3. Asia	6.15	1.06	482
4. Atlantic	0.05	0.02	151
5. Australasia	5.46	3.18	72
6. Caribbean & Central America	1.99	2.40	-17
7. Europe	1.62	2.37	-32
8. Greenland & Svalbard	1.46	2.66	-45
9. Indian Ocean	1.14	0.53	117
10. Middle East	1.19	1.41	-16
11. North America	3.39	1.19	186
12. Pacific	13.04	6.01	117
13. South America	9.55	6.14	55
Total	81.83	83.11	-2

7.3.3 Analysis of climate effects on NH_3 emissions

In this section, the global GUANO model output is analysed and the influence of the different climate variables across all global seabird colonies is investigated in more detail.

The relationship of the modelled percentage volatilization rate (P_v) with temperature, relative humidity, wind speed and precipitation was calculated for the breeding season at all 9,500 colonies in the global database (see Figure 7.6). The volatilization rate shows a strong positive relationship with temperature and a negative relationship with precipitation. From Figure 7.6, the relationship

between P_v and relative humidity is unclear, as is the relationship between P_v and wind speed.

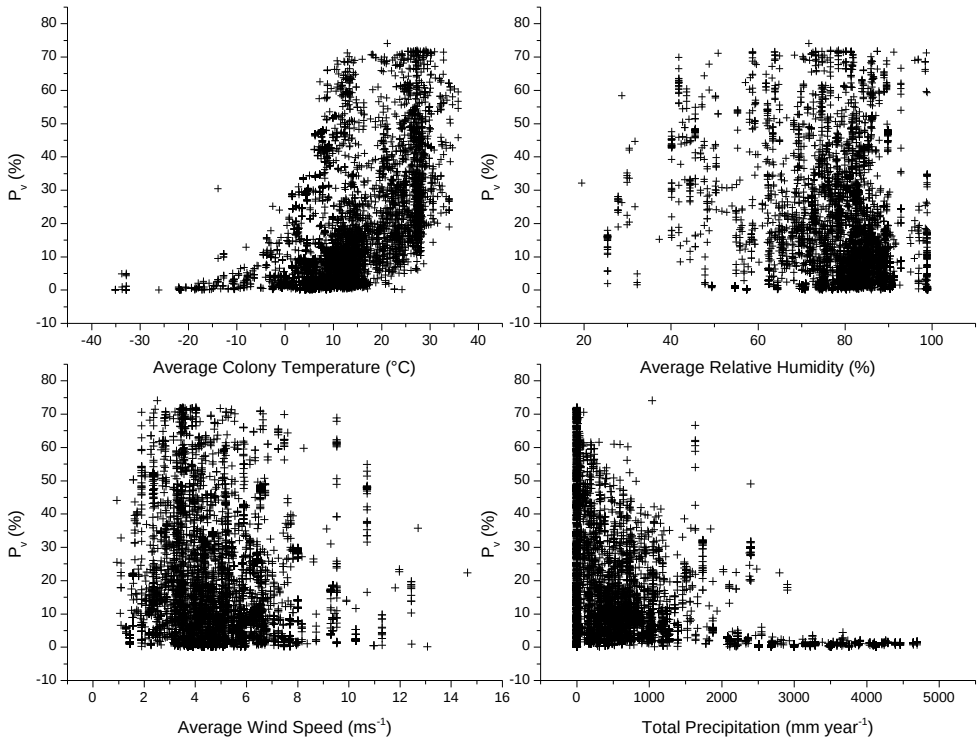

Figure 7.6 The percentage of nitrogen excreted that volatilizes as NH_3 (*Pv*, %) plotted, for all colonies in the global seabird database, against the average daily precipitation (mm m^{-2} day^{-1}), the average wind speed during the breeding season (m s^{-1}), the average relative humidity during the breeding season (%) and the average air temperature during the breeding season (°C).

Given that there is no strong correlation between the climate variables (Table 7.8), they are fitted in a multiple regression model to establish their relative importance to P_v.

Table 7.8 The product mean correlation coefficient (r) is calculated for each of the variables used in the GUANO model. *RH* denotes average relative humidity during the breeding, *WS* is average wind speed during the breeding season, Total *P* is the annual total precipitation and $T_{breeding}$ is the average temperature during the breeding season.

	RH (%)	*WS* (m s^{-1})	P (mm yr^{-1})
Average $T_{breeding}$	-0.29	-0.08	-0.01
Average *RH*		0.17	-0.10
Average *WS*			-0.02

The multiple regression model indicates that modelled across the sites P_v is most sensitive to temperature and precipitation (Table 7.9). Temperature has a strong positive relationship with modelled P_v and precipitation has a negative relationship with P_v. Relative humidity also has a significant, positive relationship with P_v. Wind speed has the least effect on P_v, however the relationship is positive and affected measured emissions at some sites, especially Bird Island (Section 5.3.7).

Table 7.9 Results of a multiple regression analysis of NH_3 emission versus environmental factors in the GUANO model. *RH* denotes relative humidity during the breeding season, *WS* is wind speed during the breeding season, Total *P* is the annual total precipitation and $T_{breeding}$ is the average temperature during the breeding season. The range of the variables denotes the variation globally and ΔPv indicates the difference in *Pv* for one unit change in the variable.

	Average $T_{breeding}$ (°C)	Average *RH* (%)	Average *WS* (ms^{-1})	Total *P* ($mm\ yr^{-1}$)
Maximum	36	100	11	4700
Minimum	-35	40	1	103
Average	11	89	5	845
ΔP_v per 1 unit of variable (%)	0.97	0.10	0.22	-0.006
p-value	$< 2 \times 10^{-16}$	2.2×10^{-13}	0.003	$< 2 \times 10^{-16}$

The relationships between climate variables and P_v can be explained by considering how uric acid evolves to form NH_3. NH_3 emission increases with temperature because of decreased solubility of NH_3 on the surface described by Henry's Law. However, the GUANO model uses hourly values of ground temperature, compared with the seasonal average temperature used in the TABE model. The TABE model does not take into account uric acid, TAN and non-volatilized NH_3 washed away during precipitation events. It is difficult to parameterize N run-off because of differences in how easily N is washed from different nest habitats. Like temperature, increases in *RH* increase the amount of uric acid that converts to TAN because of increased hydrolysis, which would explain the significant relationship between *RH* and NH_3 emission. Wind speed is shown (Figure 7.6) to have a much lesser influence on NH_3 emission. In strong

winds, both aerodynamic and boundary-layer resistances are reduced and the rate of emission increases. However, wind speed only limits the rate of transport of NH_3 from the ground and the magnitude of wind speed has no effect on the rate of NH_3 production.

The effects of climate on P_v can explain why the global seabird NH_3 emission calculated using the GUANO model is lower than previous estimates. The TABE model (Chapter 3 - Scenario 2) estimates that 65 % of global NH_3 emissions are due to penguin species, compared with 42% according to the GUANO model. This smaller contribution by penguins can be explained by temperature reducing the amount of NH_3 evolved from uric acid at these sites. Due to the penguin colonies' location on cold and wet Sub-Antarctic islands, TAN is formed slowly from uric acid, resulting in low NH_3 emission rates. Coupled with this, precipitation events reduce the presence of uric acid, TAN and NH_3 at the surface due to run-off, thereby decreasing the overall percentage of excreted nitrogen that is available for volatilization.

The largest populations of seabirds are found in Antarctica and the Southern Ocean, and because of their relatively large mass, these are also the species excreting the most N (see Figure 3.2 and Appendix 1). On a global scale, seabird N excretion is dominated by Antarctica and the Southern Ocean, which account for 79 % of the total. However, the climate (low temperatures and high rainfall) at these colonies reduces emissions to relatively small values, thus only 34.2 Gg NH_3 $year^{-1}$ are emitted from the 858.2 Gg N $year^{-1}$ excreted in Antarctica and the Southern Ocean (P_v = 4 %) (Figure 7.7). By contrast, NH_3 emissions from the tropics are relatively high compared with the total amount of N excreted, mainly due to hot temperatures. For example, seabird colonies on the Pacific islands emit 13.0 Gg NH_3 $year^{-1}$ from the 29.7 Gg N $year^{-1}$ excreted (P_v = 44 %) (Figure 7.7).

7.3.4 Prediction of climate change effects on seabird nitrogen pathways

The application of the GUANO model to climate change, by incorporating predicted anomalies into the detailed climate dataset, shows that NH_3 emissions could increase substantially through the influence of climate on P_v alone. This is assuming no change in populations and breeding success, etc. Using nitrogen

excretion rates of 2010, increases in NH_3 emission can be predicted in the region of 22-32 Gg NH_3 $year^{-1}$ for the IPCC Scenarios B1, A1B and A2 (Table 7.10).

Table 7.10 Comparison of global NH3 emission from seabirds in 2099 to IPCC climate change scenarios B1, A1B and A2.

	2010	B1 2099	A1B 2099	A2 2099
Total emission (Gg NH_3 $year^{-1}$)	81.8	103.7	111.6	113.8
Change from 2010 emission estimate (%)		26.8	36.4	39.1

The spatial distribution of increases and decreases to the 2010 estimated values of P_v, based on the worst case (A2) climate change anomaly dataset, are calculated using individual climate variables and presented in Figure 7.8. The addition of wind speed anomalies to the GSOD wind dataset shows that wind speed changes in 2099 have little effect on modelled NH_3 emission globally (Figure 7.8b). When the A2 anomalies for *RH* are added to the GSOD dataset, the effect of changes to *RH* on P_v are much larger. The largest estimated increases in P_v are in the currently driest regions of the world, with P_v increasing at seabird colonies on the West Coast of Peru and islands in the Indian and Pacific Oceans (Figure 7.8c). These are regions where guano mining has been conducted, and increases in moisture (*RH*) to these areas may result in an increase in NH_3 loss at these sites.

The consideration of precipitation anomalies can act to either increase or decrease P_v. By adding the precipitation anomalies to the GSOD precipitation data, P_v increases by up to 20 % at colony sites where precipitation decreases, such as the Atlantic provinces of Canada (Figure 7.3 and Figure 7.8d). Increases between 1 and 10 % are estimated throughout Europe, the Caribbean and the Pacific. P_v decreases are estimated for most of the regions with colder climates, including Sub-Antarctic Island and the Arctic.

P_v increases are more moderate when the A2 temperature anomalies are added to the GSOD temperature data (Figure 7.8e). There is little or no increase to P_v in the coldest regions (Sub-Antarctic and Arctic). The regions with the largest increases (7.5 - 10 %) are mainly on islands throughout the Indian and Pacific Oceans.

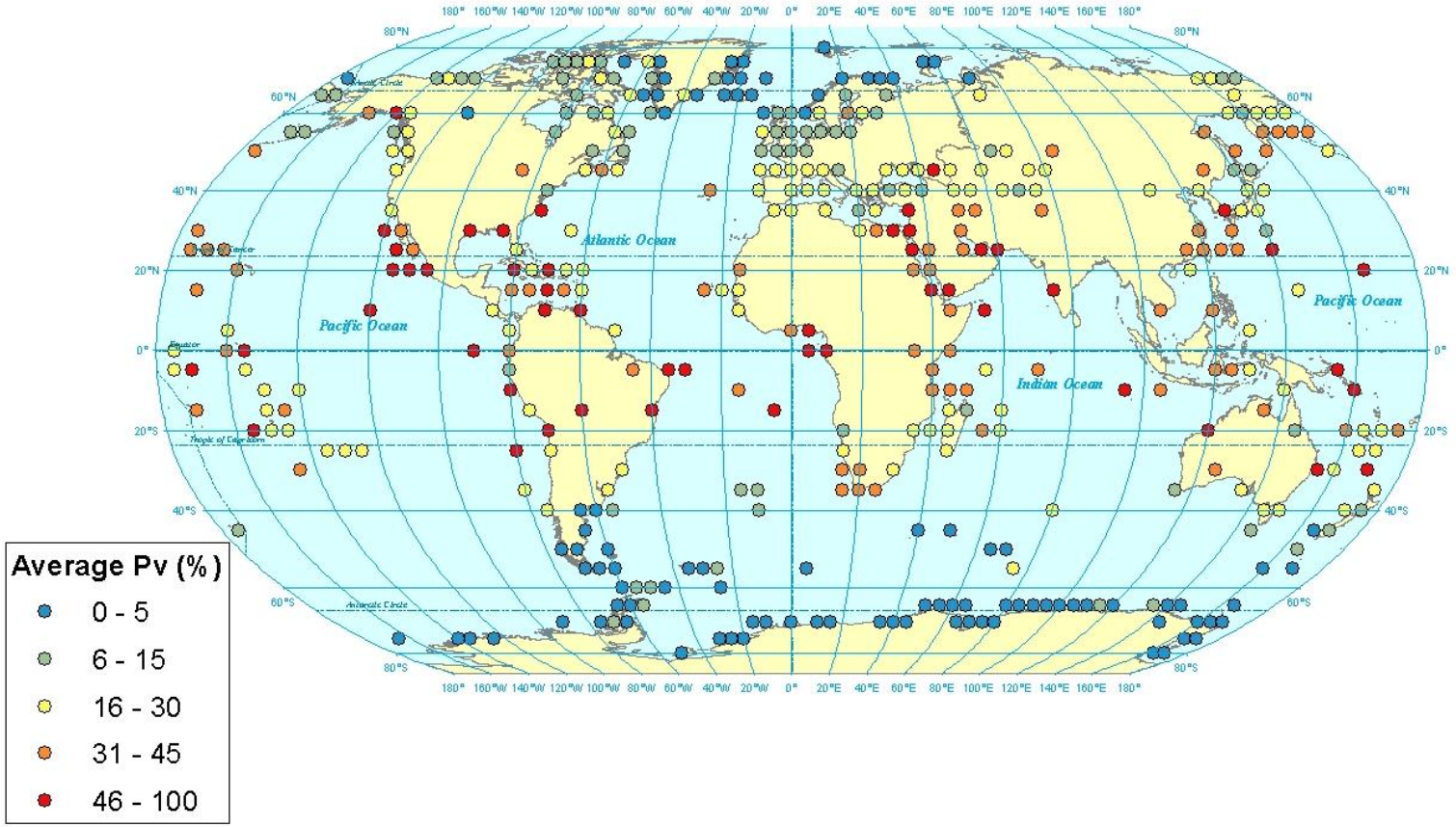

Figure 7.7 Spatial distribution of the percentage of excreted nitrogen that volatilizes (P_v) at seabird colonies, calculated using the revised GUANO model with ground temperature data.

When all the A2 climate anomalies are added to the GSOD dataset, the largest changes to P_v are in the hottest climates, including the Pacific Islands, Indian Ocean islands, Australia and the Mediterranean (Figure 7.8a). The large increases in P_v are caused by the amplifying effect of temperature and water availability from *RH* and precipitation. P_v does not change substantially in the colder climates of the Sub-Antarctic Islands and around the Antarctic peninsula. P_v remain almost constant because of relatively negligible increases in temperature (Figure 7.3) and reduced P_v caused by increases in precipitation.

Table 7.11 Climate change anomalies of IPCC scenario A2 and the predicted change in *Pv* at the largest seabird colonies. Δ*Pv* indicates the change in *Pv* between the 2010 estimate and the predicted value in 2099. *P* indicates the A2 2099 precipitation anomaly, *T* indicates the A2 2099 temperature anomaly, *RH* indicates the A2 2099 relative humidity anomaly, *WS* indicate the A2 2099 wind speed anomaly and ΔP_v indicates the change in P_v between 2010 and 2099.

Colony	Latitude	A2 *P* ($mm\ yr^{-1}$)	A2 *T* (°)	A2 *WS* (ms^{-1})	A2 *RH* (%)	ΔP_v (%)
Tristan da Cunha	-37	-122.2	3.8	1.9	11.4	32.5
Midway Atoll	28	1.3	5.5	0.4	6.8	26.1
Tasmania	-44	-93.5	2.1	1.5	5.1	11.2
Peru	-20	-39.8	4.1	0.2	19.7	3.9
Isles Kerguelen	-49	247.4	1.5	2.2	3.0	0.4
Willis Island	-54	278.8	1.4	2.4	2.5	0.2
South Sandwich Is.	-58	258.3	1.4	2.4	2.3	-1.7
McDonald Islands	-53	282.7	1.2	2.8	2.3	-11.3
Solomon Islands	-8	595.7	3.3	0.6	24.4	-19.0

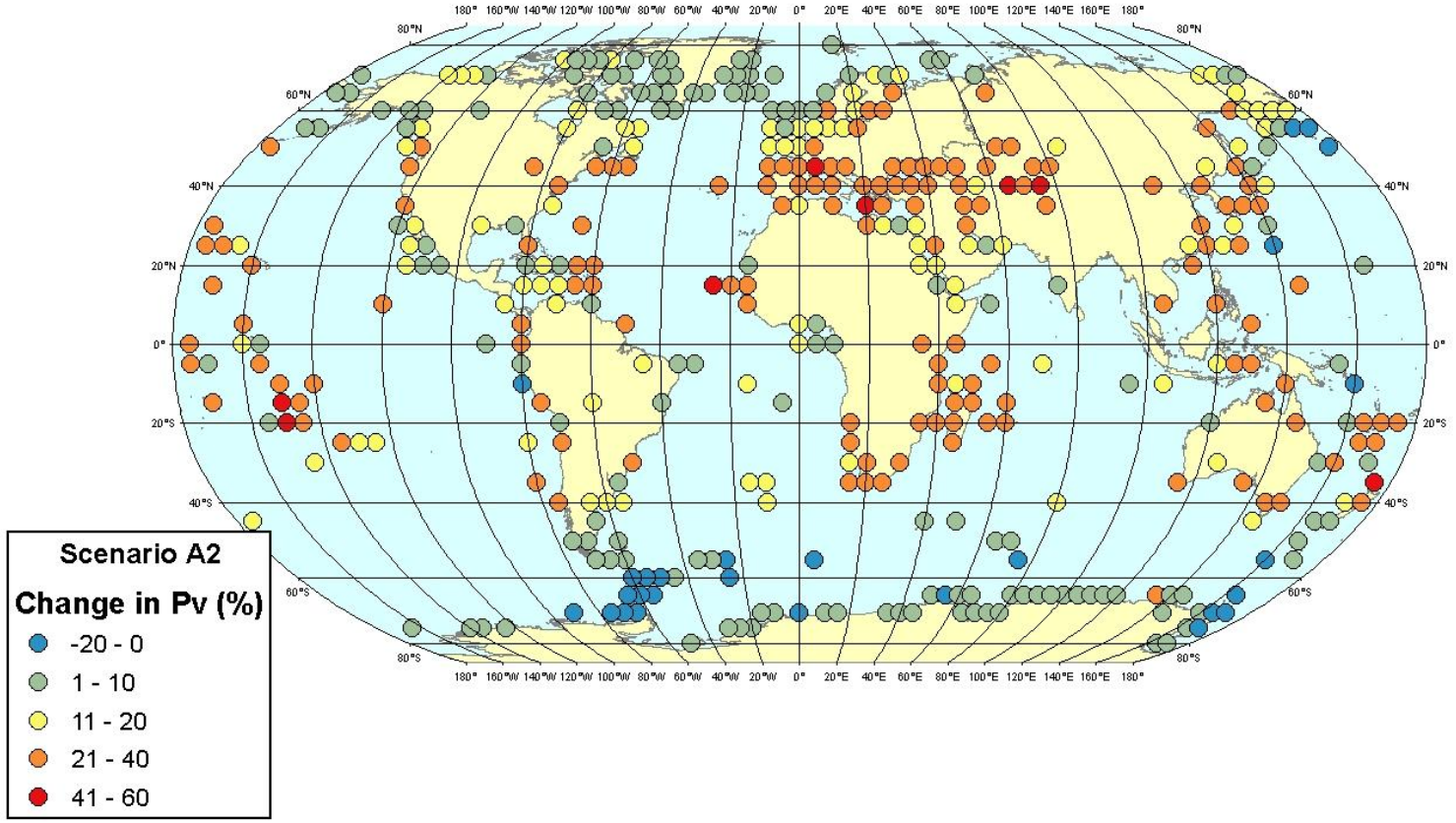

a)

Figure 7.8 a) Changes to percentage of excreted nitrogen that volatilizes (P_v) estimated for 2099 at seabird colonies when all climate anomalies are considered, using the IPCC A2 Scenario

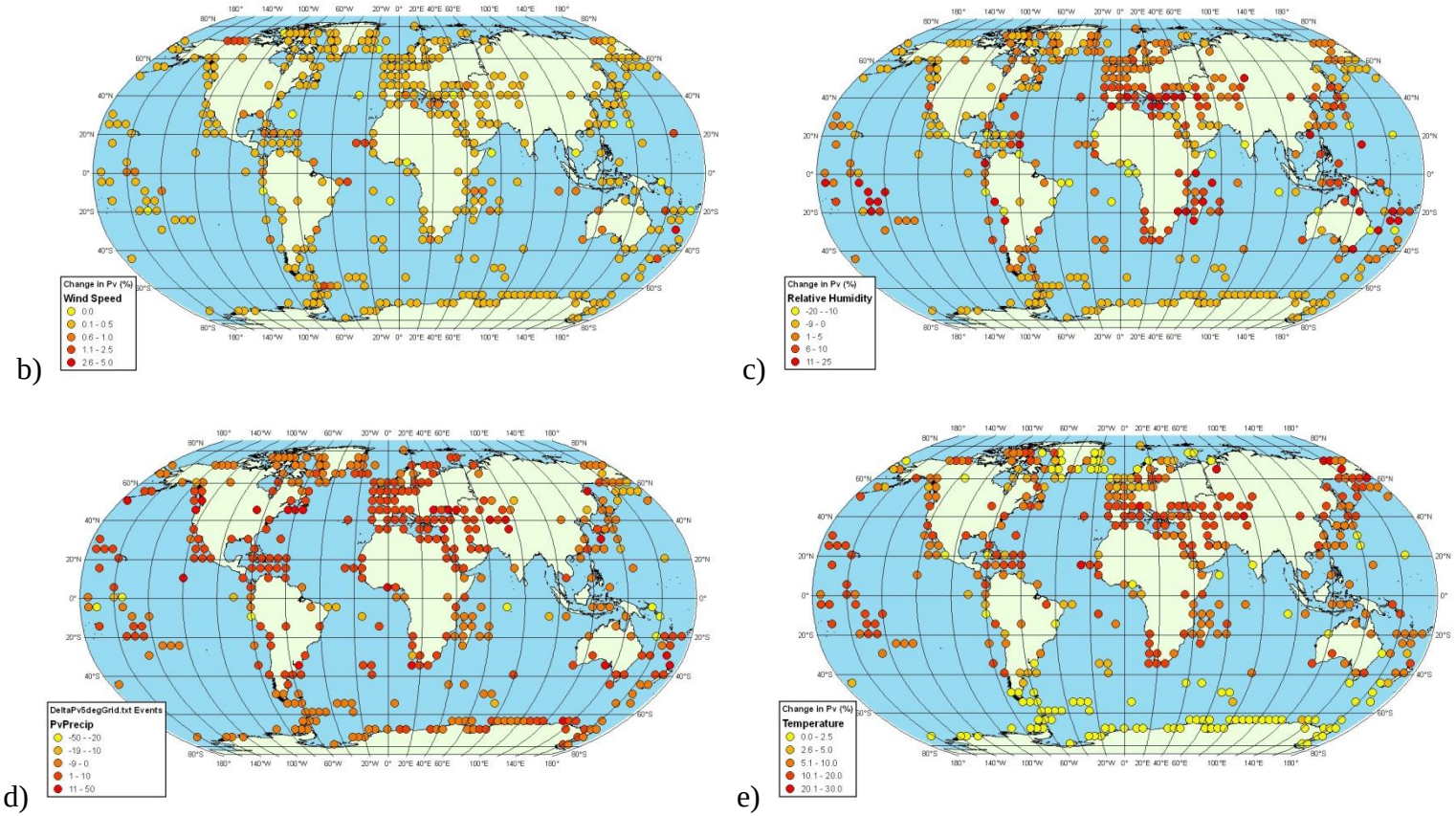

Figure 7.8 Changes to percentage of excreted nitrogen that volatilizes (P_v) estimated for 2010 at seabird colonies when b) wind speed anomalies are considered only, c) relative humidity anomalies are considered only, d) precipitation anomalies are considered only and e) temperature anomalies are considered only. Climate anomalies are taken from the IPCC A2 climate change scenario (IPCC DDC, 2011).

The effects of climate change on P_v at the nine largest seabird colonies are shown in Table 7.11 and Figure 7.9. NH_3 emissions from the penguin colonies on the Isles Kerguelen, South Sandwich Islands and Willis Island are predicted to be largely unaffected by climate change, even in the worst case scenario (A2). This is due to increased rainfall balancing out increased temperatures, as discussed above. At colonies with a large increase in precipitation (e.g. the Sooty tern colony in the Solomon Islands), the NH_3 emissions decrease because the increased precipitation washes excreted nitrogen from the colony before it can be emitted as NH_3. Colonies with predicted temperature increases and precipitation decreases (e.g. the Rockhopper penguin colony on Tristan da Cunha), show the largest increase in NH_3 emissions, due to the coupled effect of a decrease in uric acid wash-off because of decreased precipitation and the increased surface NH_3 concentration.

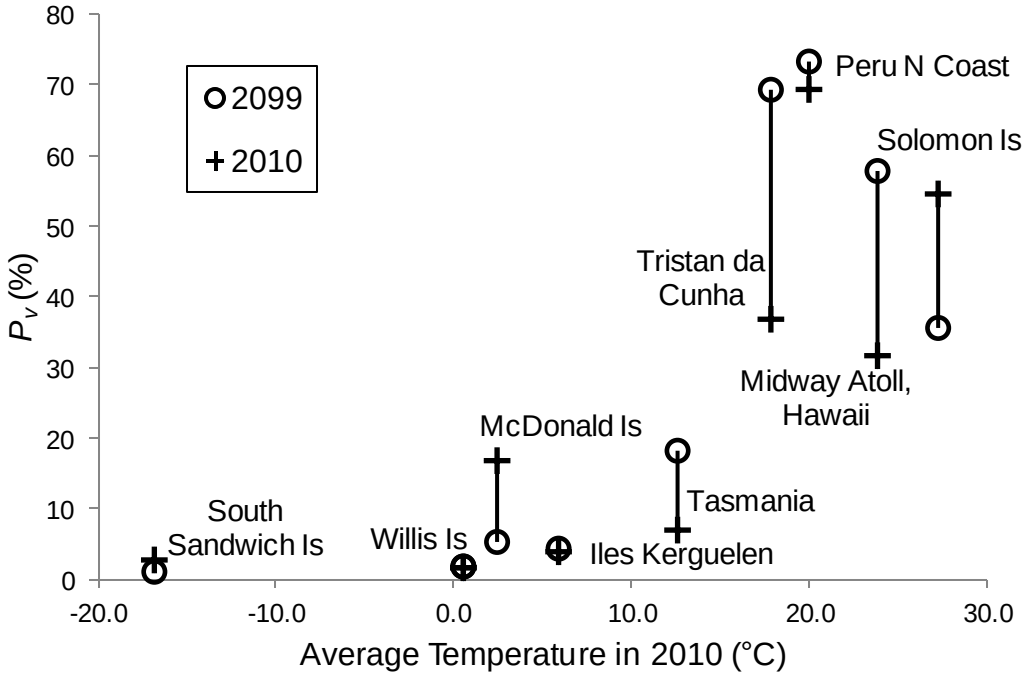

Figure 7.9 Effects of climate change on *Pv* at the 9 largest seabird colonies, calculated with the GUANO model. Crosses indicate NH_3 emissions for 2010 using Global Summary of Day (GSOD); open circles represent predicted NH_3 emissions by incorporating temperature, wind speed, relative humidity and precipitation anomalies for 2099 (IPCC Scenario A2, worst case).

7.3.5 Uncertainty in input data

The climate parameters used as input to the GUANO model are a source of uncertainty, in addition to those already discussed in Section 3.2.2. (e.g. seabird

population estimates, nitrogen content of food). The calculation method for ground temperature was highlighted as an important source of uncertainty. As described in Section 7.2.2, the estimated ground temperature used in the GUANO model is based on average ground temperature variations at the three field measurement sites. An uncertainty estimate of ± 2 °C was estimated. This results in an NH_3 emission uncertainty of ± 32 % at best.

The largest uncertainty in global NH_3 emission is for the seabird population estimate (± 36 %) (Section 3.4.2). New techniques have increased the numbers of seabirds counted in the most remote regions. For example, remote sensing is used to count Little auks (*Alle alle*) on Northumbria Island, Greenland (Egevang et al., 2003), and computer-based analysis was applied to count Macaroni penguins in colour aerial photographs on Bird Island, South Georgia (Trathan, 2004). However, because seabirds are generally difficult to reach and new methods are expensive, large uncertainty in population estimates remain. Total uncertainty associated with type and digestion of food is 16 % (see Section 3.4.2).

Climate can change a great deal over short distances. For instance, GSOD data measured on Ascension Island are only 1 km from the field site (Table 7.3), yet data are still different between the two locations. Despite this, the database used in this study is the best available description of the climate at each site, and uncertainty associated with local-scale change in climate is spatially heterogeneous and if quantified, may be misleading.

The inclusion of four climate factors to the emission calculations substantially affects the size of the estimated NH_3 emission. Output from the model shows that, even though temperature is the strongest factor it is not the sole driver of NH_3 emission. Precipitation has a negative correlation with NH_3 emission, and the effect on NH_3 emission is equal to temperature. Precipitation and relative humidity increases the rate of urea hydrolysis to NH_3. Increases in wind speed increase the rate of emission from the ground, but it does not significantly change the amount of NH_3 produced but can affect the partitioning of produced NH_3 between volatilization and run off. Combining the sources of error provides a global best estimate of NH_3 emission from seabird colonies of 82 [37 - 127] Gg NH_3 $year^{-1}$.

8. General discussion

This thesis has presented a number of findings that further our understanding of global NH_3 emissions from seabird colonies. The results vary from direct estimates of colony NH_3 emissions (Chapter 5) to the first global maps of NH_3 emissions from seabird colonies (Chapters 3 and 7). The maps and climate driven model of emissions allow future scenarios to be made of seabird mediated marine-terrestrial N transfers and their subsequent volatilisation to the atmosphere as NH_3. Furthermore, the mapped emissions are calculated using a climate dependent process based model that has the potential for a broader application for other sources of NH_3 emissions.

8.1 Summary of findings

8.1.1 NH_3 emissions at seabird colonies

Results of the near-source NH_3 measurement campaigns at seabird colonies in a range of climates (Chapter 5) show that NH_3 emissions can be of a considerable magnitude, at a local scale, when compared to other emission sources. The lowest average seabird NH_3 emission of 5.3 μg m^{-2} s^{-1} was measured at the Atlantic puffin colony on the Isle of May, Scotland, and the largest average seabird NH_3 emission of 21.8 μg m^{-2} s^{-1} was measured at the mixed tern and noddy colony on Michaelmas Cay, Australia.

The magnitudes of these emissions indicate that seabird colonies represent appreciable NH_3 sources compared with the better known agricultural sources of NH_3 emissions. For example, a poultry installation of similar daily NH_3 emission as Michaelmas Cay would house 70,000 birds, with each bird emitting NH_3 at 0.1 kg NH_3 $bird^{-1}$ $year^{-1}$ (Sutton et al., 2011). This is similar to the daily emission from a cattle feedlot of over 650 animals emitting ~10.4 kg NH_3 $animal^{-1}$ $year^{-1}$ (Sutton et al., 2011).

Wilson et al. (2004) reported that UK seabird colonies in remote regions are significant local sources of NH_3 where other emission sources are scarce. This thesis shows that, globally, seabird colonies are even more removed from anthropogenic nitrogen sources and in many locations could be considered the only significant local atmospheric nitrogen deposition source for the terrestrial

ecosystem. The isolation of seabird NH_3 emissions from anthropogenic sources can be put into context by comparison with the spatial estimates of NH_3 emissions from other sources in the EDGAR database (EC-JRC/PBL, 2010). When the 0.1 x 0.1 degree NH_3 emissions in the EDGAR database are co-located with the seabird NH_3 emissions database at same scale, contributions of NH_3 from seabirds often account for more than 99.9 % of NH_3 emissions from all sources within the 0.1 x 0.1 degree cell where this occurs, as shown in Figure 8.1.

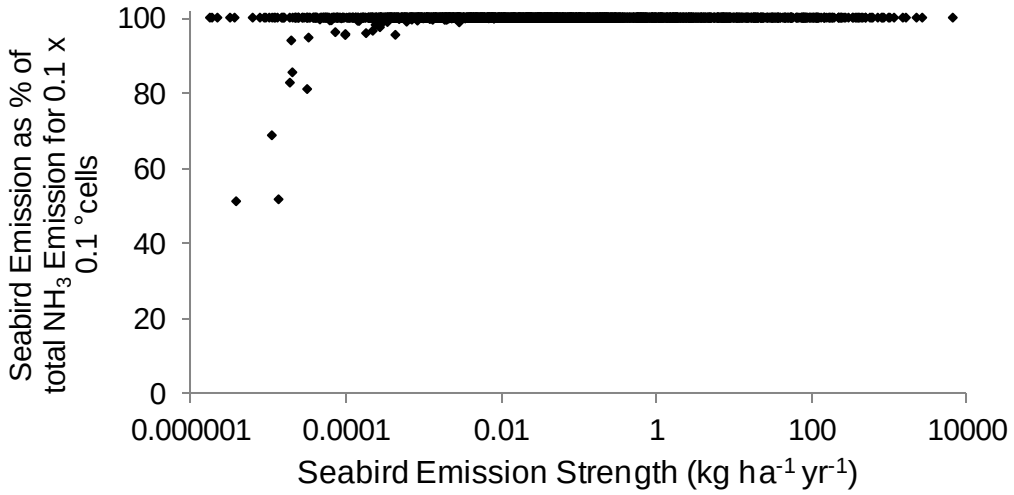

Figure 8.1 Contribution of seabird NH_3 emissions as estimated here as a percentage of total NH_3 emissions from seabirds and other sources (estimated by the EDGAR database (version 4.1) of EC-JRC, 2010).

8.1.2 Climate-specific NH_3 emission rates from seabirds

For all active sampling measurement campaigns, NH_3 emissions showed a diurnal pattern, with higher emissions during the day and lower emissions at night. Measurements made in warm climates with larger temperature values showed a more defined diurnal pattern than those in colder climates. Similar diurnal patterns in NH_3 emission have been reported from measurements made in agricultural environments, such as grazed pasture land (Loubet et al., 2001), wheat stubble (Nemtiz et al., 2000) and from naturally ventilated farm buildings (Sutton et al., 2009). These studies suggest that temperature is the main driver of NH_3 emissions because the diurnal pattern in emissions co-occurring with the daily temperature pattern.

However, emissions from the parameter based GUANO model simulate that temperature is not the sole driver of NH_3 emission and that the rate of NH_3 emission depends on the combined effects of temperature, relative humidity, precipitation and wind speed. The largest recorded 15 minute emission of NH_3 was observed at the Sooty tern colony on Ascension Island was 377 $\mu g\ NH_3\ m^2\ s^{-1}$ (Section 5.3.3). This is the result of combined climate effects: water evaporates quickly on Ascension, and nitrogen excreted by the birds cannot hydrolyse and remains on the surface. Only when water is supplied by a rain event, does the accumulated uric acid rapidly converts to NH_3, which is emitted in large quantities as the surface dries. The highest NH_3 emission measured in non-tropical climate for this thesis, at the Big Mac colony on Bird Island, was 52 $\mu g\ NH_3\ m^2\ s^{-1}$. In colder climates, microbial evolution of uric acid to NH_3 is rate-limited by temperature as is its partitioning to gas phase according to Henry's Law so that higher NH_3 emission occurs in tandem with higher ground temperature. Ground temperature is much lower on Bird Island, therefore NH_3 emissions are smaller than under tropical conditions. This allows a larger fraction of the excreted nitrogen to be lost by the competing processes of run-off

Even though studies have reported the individual effect of climate variables on NH_3 emission, e.g. the exponential relationship between temperature and NH_3 emission (Zhu et al., 2011), this is the first known study to report the response of NH_3 emission from excreted nitrogen to a range of climate variables. Of the climate variables investigated in this thesis, precipitation effects are the least well quantified and in particular, the estimation of run-off from the colony. Measurement of NH_3 emission over the course of a year would help to quantify the amount of nitrogen lost during precipitation events, which is a particularly difficult parameter to quantify in such environments. Given the highly complex topography of many seabird colonies, there may never be a universal solution for parameterising run-off and simple approximations may remain the best suited.

8.1.3 Assessment of measurement techniques

Both passive and active sampling methods were successfully deployed to measure NH_3 emissions at seabird colonies in a range of climates. Passive sampling is useful as a low-cost solution that can be used to sample NH_3 concentrations in air

in remote locations by non-instrument specialists, but has weaknesses including low time-resolution, and birds can physically damage/remove samplers. Active sampling is advantageous in producing data that can show variation in NH_3 concentration over high-resolution time-series. However, active sampling has drawbacks in that it presents considerable logistical challenges. The fundamental requirement of the active campaign is power and the success of the campaign depends on the reliable supply of electricity in remote and ecologically sensitive environments. As such, active and passive sampling methods are both valuable tools to be applied flexibly depending on local conditions.

The use of a backward Lagrangian stochastic dispersion model (WindTrax) provides a versatile method for calculating NH_3 emissions from measured NH_3 concentration data. The main advantage of WindTrax is its user-friendly interface that allows input from a range of parameters to calculate NH_3 emission estimates for an area source. The most difficult aspect of using WindTrax is ensuring the input values are correctly parameterized, since incorrect assignment of values (especially Monin-Obukhov length) can result in uncertainty of up to ± 70 %. WindTrax requires that the area to be modelled is aerodynamically flat, the source is less than 1 km from the detector and the roughness length is less than 15 cm. All fieldwork sites in this project were chosen to provide conditions as suitable as possible for the requirements of WindTrax.

Despite choosing the best available site, the natural landscape of the seabird colonies used are not perfectly flat and possibly the mechanical turbulence, caused by aerodynamic obstructions, could be underestimated and result in the underestimation of NH_3 emission. However, the roughness length was measured by a sonic anemometer, where available, and for the sites where this data was not available the associated uncertainty was calculated. One suggested improvement for WindTrax would be to incorporate relief into the landscape, to allow emission estimates be calculated at sites with complex aerodynamics, such as from cliffs or with tall vegetation. Another improvement would be increasing the range over which WindTrax can calculate emissions. Currently, the maximum distance between source and detector is 1km, however some seabird emission sources can be larger than that.

The calculation of NH_3 emissions using land-based NH_3 concentration measurements in WindTrax has overcome many of the challenges presented to previous NH_3 measurement campaigns at seabird colonies. Blackall et al., (2004) reported good agreement between NH_3 emission calculated by tracer ratio and inverse dispersion methods from more distant boat based measurements (> 1 km). However, these NH_3 concentration measurements were limited by the low frequency of suitable conditions for the boat when campaigns could be undertaken. The methods presented in this thesis are not constrained by these considerations and with adequate petrol to supply a small generator and working instruments, measurement can be made indefinitely.

The average NH_3 emission estimates made by the passive and active sampling methods on both Ascension Island and the Isle of May agreed well and differed by only 5 % (Section 5.4.2). However, the uncertainty of the passive sampling was higher (between 38 and 74 %) compared to the uncertainty in the active sampling emission (12 %). However, the use of passive sampling was justified and beneficial in locations where data could not be collected by active means. Furthermore, it is likely that in less harsh environments passive sampling provides a highly cost effective method for determining ammonia emissions (Theobald et al., 2006).

To improve the understanding of NH_3 emission at seabird colonies, longer term measurements over the period of a year or longer would identify the lag-time between excretion and emission as the birds arrive at the colony and the duration of residual NH_3 emission after the birds leave the colony. A large uncertainty in our understanding of seabird colony N dynamics is the magnitude of surface run-off from colony to sea after the breeding season, and longer temporal data sets of NH_3 downwind of colonies may provide some insight into these surface processes.

8.1.4 Assessment of modelling techniques

This study presents a range of models used to calculate NH_3 emissions from seabird excreted N. Chapter 3 describes the three scenarios using the Wilson et al. (2004) bioenergetics model of temperature independence (Scenario 1), theoretical temperature dependence (Scenario 2) and a mid-estimate between Scenario 1 and

Scenario 2 that accounts for non-linear interactions with water availability and surface infiltration (Scenario 3). When compared to measured values, Scenario 1 overestimated NH_3 emissions at polar sites and underestimated NH_3 emissions at tropical sites. The inclusion of temperature dependence to the bioenergetics model (TABE model; Chapter 3 - Scenario 2) improved the agreement of NH_3 emission estimates to measurements in a range of climates, but this model does not consider the effects of precipitation and relative humidity. Scenario 3 was thought to be the "best estimate" because it considered that the effects of limited water availability that may counteract the temperature effects in tropical climates. However, when compared to measured emissions Scenario 3 overestimated NH_3 emissions at polar sites.

The refined GUANO model provides a method for calculating NH_3 emission from a range of climates. The processes that describe the ammonification of excreted nitrogen and subsequent volatilization used in the GUANO model are validated against measurements in a range of climates (Chapter 6). A major asset of the refined GUANO model is its relative simplicity, and it was easily adapted to model NH_3 emissions for all colonies globally (Chapter 7).

The simplicity of the GUANO model imposes limitations. The model uses basic expressions to calculate vertical air movement at the colony. Also, the model is only validated with NH_3 emissions from colonies with simple aerodynamic properties. To ascertain if complex topography has a large affect on NH_3 emission, the model should be validated with NH_3 emissions from colonies with more complex aerodynamics.

Many seabird colonies are low lying (e.g., Michaelmas Cay is only 3.5 m above sea-level) and the potentially volatilizable nitrogen may be washed away by storms washing over the land. Until now, wash-off by storm action has been omitted from the GUANO model. However, the effect of storms could be modelled with the inclusion of colony height above sea level and a relationship between wind speed and wave height. This would require detailed high-resolution digital elevation data for colonies, as some sites are at risk in their entirety, whereas only the lower parts of steeper sloping sites or cliffs would be at increased risk from storms. The slope would also be a key parameter for

calculating wash-off by rain during and between breeding seasons. However, the spatial resolution of the global seabird database (Section 3.2.1) is currently insufficient for all parts of the globe, with data from some countries not being available at the individual colony level. However, in general, the colonies with the poorest spatial resolution are the smallest colonies with smaller contribution to the total seabird NH_3 emission.

While it is acknowledged that the refined GUANO model still has weaknesses in the representation of run-off and wash-off by precipitation and storms, it reproduces measured NH_3 emissions at the study sites well (Chapter 6). The further refinements suggested above would help to gain better understanding of NH_3 emissions, particularly in regions with high precipitation and storm frequency.

8.2 Implications of the research

8.2.1 Comparison of global emissions with other estimates

The global NH_3 emission estimates by the refined GUANO model of 82 Gg NH_3 $year^{-1}$ is lower than previous estimates. Blackall et al. (2007) estimated a global NH_3 emission from seabirds of 242 Gg N $year^{-1}$ with 54 % emissions coming from the Antarctic region. Blackall et al. (2007)'s estimate was based on field measurements, where the fraction of excreted nitrogen available for volatilization (F_{Nv}) was estimated at 0.16 for vegetation/burrow nesters and 0.36 from rock nesters. F_{Nv} was used as a single value to incorporate the effects of climate and nesting. Blackall et al. (2007) argued that any change in volatilization rate caused by thermodynamic effects would be offset by the restriction of urea hydrolysis in the tropics and a reduction in surface absorption in frozen conditions.

Measurements of this study show that Blackall et al. (2007) overestimates the global NH_3 emission from seabirds because volatilization rates in polar regions are limited by cold temperatures (e.g. this thesis estimates F_{Nv} for Macaroni penguins on Bird Island is 0.08). A major consequence of the lower NH_3 emission calculated in this thesis is the change this makes to understanding nitrogen pathways at the colony. Lindeboom (1984) estimated that the percentage of excreted nitrogen that volatilizes (P_v) could be 80 % at a Macaroni colony on

Marion Island (47 °S, 38 °E). By contrast, a value of 8 % P_v is estimated for the Macaroni penguin colonies on Bird Island (54 °S, 38 °W) in this thesis (Section 5.4.5). This large difference in P_v cannot be explained by taking into account the 2 °C higher average temperature during the breeding season at Marion Island (NCDC, 2011). Lindeboom (1984) estimated P_v by comparing nitrogen and phosphorus ratios in fresh excreta to older excreta at the colony, assuming that nitrogen was only lost by volatilization. Lindeboom did not consider nitrogen loss by run-off which could explain their over-estimation in P_v for Marion Island Macaroni penguins. In contrast to the low P_v value of this study for penguins, 66 % of the excreted nitrogen volatilizes to form NH_3 at the seabird colony on Michaelmas Cay (Section 5.4.5).

8.2.2 Effects of seabirds on local environment

Chapter 1 describes potential effects of both NH_3 emission and nitrogen enriched run-off, where both pathways have been shown to result in growth of primary producers. NH_3 emissions are associated with an increase in above surface vegetation growth. For instance, Lindeboom (1984) observed that plants downwind of the penguin colony on Marion Island were larger and grew more vigorously than in other parts of the island. Nitrogen rich run-off is also associated with increased growth of primary producers in marine ecosystems near seabird colonies. Bosman and Hockey (1988), for example, observed an increase in the growth rate of algae at inter-tidal ecosystems near seabird colonies on islands off the coast of southern Africa.

The impact that nitrogen from seabird colonies has on a surrounding ecosystem partly depends on the species and habitats present in this vicinity. In naturally low-nitrogen ecosystems, small inputs of nitrogen from seabirds have been shown to cause increases in plant productivity that would not have normally been observed in nutrient rich environments (Ellis, 2005). Vigorous plant growth near seabird colonies in naturally low-nutrient environments has also been observed on hot, arid islands in the Gulf of California, Mexico (Sanchez- Piñero and Polis, 2000) and in low temperature ecosystems on the Spitsbergen Archipelago, Norway (Summerhayes and Elton, 1926).

At some seabird colonies, high concentrations of NH_3 can become toxic to plants (Posthumus, 1988). A long-term critical level for NH_3 (CLE_{NH3}) of 1 $\mu g\ NH_3\ m^{-3}$ was suggested as the maximum limit of NH_3 concentration to protect the biodiversity of the most sensitive ecosystems (Cape et al., 2009). The average NH_3 concentration measured by this project at the Sooty tern colony on Ascension Island ranged from 26 $\mu g\ m^{-3}$ at the edge of the colony to 2 $\mu g\ m^{-3}$ 450 m away from the colony. This suggests that when the Sooty terns are present at the colony, the ecosystem up to and beyond 450 m from the colony may be affected by NH_3 emissions. In remote locations with low background nitrogen and large bird populations, effects of NH_3 emission over larger distances may be expected.

8.2.3 Seabirds as a model for global emissions

This project aimed to gain a better understanding of the role of natural NH_3 sources, including the sensitivity to environmental conditions relevant for developing a global perspective. Seabirds represent a "model system" and can be compared with other sources of NH_3 emission. Many sources of NH_3, especially in agriculture, are complicated by different management practices, whereas seabird emissions are a natural system for studying climate dependence of NH_3 emission. This “simple” scenario, where nitrogen from seabird excreta directly deposited to a natural surface evolves to form NH_3 by chemical and physical processes, means that relationships between NH_3 emissions and climate can be identified without complications from external anthropogenic factors.

This project may help current thinking of NH_3 emissions and could change how global NH_3 emissions are calculated. At present, NH_3 emissions, such as those presented in the EDGAR database, are calculated using emission factors with empirically derived temperature dependence based on findings of Bouwman et al. (2002) (EC-JRC/PBL, 2010). Emissions from synthetic fertilizers contribute 48% of the total anthropogenic NH_3 emissions and animal manure contributes 21 % (EC-JRC/PBL, 2010). NH_3 emissions from synthetic fertilizers are calculated using an estimated percentage loss of NH_3 of 7% in industrialized countries and 18% in developing countries. The estimated percentage loss of NH_3 from animal manure is 21% in industrialized and 26% in developing countries (Bouwman et al., 2002). These estimated percentage loss estimates are estimated based on

temperature and farm management methods. However, the results presented in this study present a much larger range in NH_3 emission in response to climate differences than suggested by Bouwman et al. (2002).

This thesis shows that NH_3 emissions from seabird nitrogen are highly climate dependent, ranging from average species P_v of 0.4 % from Emperor penguins to 70.6 % for the Rock shag found in South America. It is acknowledged that there are differences in emission processes between seabird excreta and animal manure. However the GUANO model could be adapted for different types of excreta (such as manure and slurry) or mineral fertilisers. These adapted models could be used to investigate the climate dependence of NH_3 emissions from manure, fertiliser application and livestock grazing. A parameter based model similar to the GUANO model could be further developed to investigate regional differences in farm management.

Table 8.1 Average percentage of nitrogen that volatilizes (P_v) for a range of species.

Species	Average P_v (%)	Change in P_v 2010 to 2099 (%)	Average temperature during breeding (°C)
Emperor Penguin	0.4	0.2	-15.9
Adelie Penguin	2.7	0.6	-10.2
Atlantic Puffin	3.1	4.7	9.1
Macaroni Penguin	4.4	-1.2	1.1
Brown Noddy	25.8	21.6	27.1
Sooty Tern	40.7	20.1	27.1

8.2.4 Climate change and seabird nitrogen

Chapter 7 reported spatial changes in the percentage of nitrogen that volatilizes as a result of global climate change as described by the Intergovernmental Panel on Climate Change (IPCC) (Section 7.3.4). At seabird colonies where the largest temperatures are predicted (e.g. Tristan da Cunha, South Atlantic and Midway Atoll, Pacific Ocean), it is likely that P_v will increase (Section 7.3.4). Higher P_v leads to an increase in NH_3 volatilized, and may result in increased plant growth and decreased biodiversity by eliminating nitrogen sensitive plant species (Lindeboom, 1984; Ellis, 2005). However, at seabird colonies where precipitation is also predicted to increase, run-off will also increase offsetting the increase in temperature. The net result is the expectation of negligible changes to P_v, e.g. on Willis Island and Isles Kerguelen in the Southern Ocean) (Figure 7.9).

By taking average values of the change in simulated P_v from 2010 to 2099 as calculated by the GUANO model, average P_v values for seabird species in hot climates are predicted to increase by more than 20 %, such as the Sooty tern and the Common noddy (Table 8.1). Average P_v values for seabird in temperate climates, such as the Atlantic puffin, are estimated to increase by nearly 5 %. For seabird in the cold regions P_v values are predicted to increase by small amounts or decrease, e.g. a decrease in average P_v of 1.2 % for Macaroni penguins.

The GUANO model predictions for 2099 only take climate change into account, while assuming that seabird populations will remain stable at their colonies. However, seabird populations, and hence NH_3 emissions, are also expected to be affected by the changing climate. Predicting future population changes in seabirds in response to anticipated climate change was beyond the scope of this project, but should also be considered in future scenario development.

Some of the global changes expected to affect seabird colonies are sea-level rise (0.23 – 0.51 m for the A2 scenario), an increased frequency of extreme weather events, increased frequency in the El Niño Southern Oscillation and increased sea surface temperatures (IPCC, 2007). As well as changes to temperature, wind speed, precipitation and relative humidity (already considered by the spatial changes to *Pv*).

Sooty terns nesting on low lying atolls in the Pacific Ocean provide an example of how sea-level rise and an increase in the frequency of extreme weather events may affect breeding grounds of seabirds. Michaelmas Cay is currently 3.5 m above sea-level, but with the change in sea-level and more extreme weather events, this land may not be a viable nesting site in the future. 120 days are required between egg-laying and fledging for the species at this site, and changing climate may limit the number of consecutive days the island is above water.

An example of the effect of El Niño is the change to the Guanay cormorant populations on the west coast of South America. The El Niño Southern Oscillation occurs when warm water appears off the coast of Peru and results in lower primary production of the oceans (Wyrtki, 1975). Past El Niño events coupled with overfishing have had a large impact on the food chain and resulted

in a decrease of the Guanay Cormorant population in Peru from 20 million in the 1950s (Santander, 1981) to 3 million in 2009 (Birdlife International, 2009).

Existing changes in populations of penguins may also reflect the impact of changing sea surface temperature. Higher sea surface temperatures have already reduced sea ice, leading to a reduction in Antarctic krill, a vital food source for penguins in the Antarctic region (Brierly, 2008). Failure in krill recruitment may lead to a decline in penguin populations (Trathan et al., 2007). Adelie penguin populations have decreased over the past 25 years because of a reduction in their food supply (Forcada et al., 2006). However, with the climate becoming milder at these latitudes, the environment is more suited to Gentoo penguins (*Pygoscelis papua*), which have increased in numbers (Forcada et al., 2006). These examples illustrate the complexity of forecasting overall changes in NH_3 emission in future scenarios, if both the direct and indirect effects of climate change on bird populations are to be taken into account in a model system.

It is clear, however, that changes in seabird populations would result in changes to the nitrogen dynamics of the surrounding ecosystems. This especially true for environments where naturally occurring nutrients are scarce, such as in polar or arid tropical climates, where small changes to the amount of seabird-mediated marine nutrients imported to terrestrial ecosystems could result in substantial changes to plant productivity.

8.3 Suggestions for future research

The global NH_3 emission estimate from seabirds presented in this thesis represents the most comprehensive and up-to-date assessment available. Further work could be directed at reducing the uncertainty of the NH_3 estimates and investigating the ecological implications of the findings of this study. As such, suggestions for further research are detailed below.

1. Improve the method for calculating ground temperature because it is one of the largest uncertainties used as input to the GUANO model.

2. Validate the GUANO model at the seabird colonies with the largest NH_3 emission, especially the Guanay cormorant colonies on the west coast of South

America to investigate the simulated high percentage of excreted N that volatilizes (c.70 %) as calculated by the GUANO model.

3. Conduct field measurements for a complete year to investigate: build up of NH_3 emissions as the birds arrive, peak emissions during the hottest part of the year and residual decay of emissions after the birds leave the colony. This will also assess the parameterization for loss of nitrogen from the colony caused by N run-off during rain events, a parameter used in the GUANO model.

4. Extend the GUANO model to investigate NH_3 emissions from other nitrogen excreta. Seals have been shown to emit NH_3 at their breeding locations (e.g. Theobald et al. 2006 in Namibia), and the model could be adapted and used to estimate NH_3 emissions for locations where seals and seabirds are the only major NH_3 sources.

5. Investigate the effects of NH_3 emissions at seabird colonies on plant community structure, and changes in relation to seabird nesting proximity, plant utilisation of seabird derived N (direct input and NH_3 deposition). Such impact studies could be extended to assess the effects of seabirds on soils and related fluxes of GHG's such as N_2O, N_2, NO, CH_4 and CO_2.

8.4 Summary

- This study updates previous seabird estimates of the global seabird population from 110 million (Blackall et al., 2007) to 261 million breeding pairs; total number of free-living individual seabirds (including pre-breeding adults & chicks) of 1,180 million.
- Habitat fractional release parameter, F_{hab}, values are revised from previous studies by measuring NH_3 emissions from seabird guano on range of nesting substrates in a controlled environment. The new values of F_{hab} are: Rock = 1.00, Sand = 0.68, Soil = 0.41, Vegetation = 0.27, Burrow = 0.00 and Nest = 0.27. These values are similar to those reported by Wilson et al. (2004) and also estimate soil and sand values for the first time.
- NH_3 emissions were measured at five seabird colonies across a climate gradient ranging from sub-polar to tropical conditions.

- Measured NH_3 emissions at seabird colonies range from 5.39 μg m^{-2} s^{-1} for a UK Atlantic puffin colony to 18.40 μg m^{-2} s^{-1} for a Sooty tern colony on Ascension Island.
- In the Sub-Antarctic, penguin colonies are large sources of NH_3 emission (11.8 μg m^{-2} s^{-1} for a Macaroni penguin colony on Bird Island), however only 3 - 8 % of the nitrogen excreted by the birds volatilises to the atmosphere as NH_3 gas.
- Tropical seabird colonies, such as Michaelmas Cay and Ascension Island, are large sources of NH_3 emission, despite smaller amounts of nitrogen excretion than at penguin colonies, because a large percentage (30 – 60 %) of the excreted nitrogen volatilises as NH_3.

- The NH_3 emission estimates made by the active and passive measurement methods agreed on average, with the main differences being the uncertainty of the emission estimate (passive measurement uncertainty was greater by a least 23 %) and the temporal resolution of the emissions (passive sampling 1-2 weeks; active sampling 15 minutes).
  - The passive campaigns provide excellent data and can be deployed by non-instrument specialists.
  - The active sampling campaigns produce detailed NH_3 concentration data, which allowed comparisons with high-resolution modelling using met data and thereby increased understanding of NH_3 emission processes. However, active sampling uses larger, heavier instruments which require electricity and maintenance during sampling, and are therefore less suited for extremely remote locations or use by non-experts. .
- GUANO model, first created by Blackall (2004) to investigate NH_3 emissions from seabird colonies in the UK, is adapted to represent processes by which seabird nitrogen forms NH_3 under different climates. The GUANO model is refined by adding a water budget increasing the relative humidity factor during rain events, using new habitat correction factors (F_{hab}) and using ground temperatures instead of air temperature. With the use of ground temperature and the water budget having the largest impact on NH_3 emission.

- The GUANO model can be used to calculate hourly NH_3 emissions for individual seabird colonies in a range of climates, using temperature, wind speed, relative humidity and precipitation. When compared to measured emission from colonies, the percentage of nitrogen volatilized, as calculated by the revised GUANO model, describes the measured percentage of nitrogen volatilized with R^2 of 0.91.

  The model simulates the following effects:

  - A greater percentage of nitrogen excreted by seabirds is emitted as NH_3 in hot climates when compared to cold climates.
  - Water availability limits NH_3 production from uric acid, so periods of no rain in a hot climate (30 °C) result in low emissions and accumulation of guano deposits. However, rain events were also observed to remove available nitrogen by wash-off and therefore reduce the N available for NH_3 volatilisation.
  - An increase in wind speed increases the percentage nitrogen volatilized by reducing R_a and R_b.
  - An increase in relative humidity increases NH_3 emission in the model because it increases the arte that uric acid is converted to TAN.

- The GUANO model estimates a total global NH_3 emission from seabird colonies of 82 Gg NH_3 per year with an overall uncertainty range of [37 - 127].
  - At low temperatures and high rainfall colonies, the volatilisation rate (P_v) is relatively small. For example, P_v is estimated at 4% on Bird Island.
  - At colonies in hot temperatures, P_v is much higher. For example, P_v is estimated at 44% for Baker Island in the Pacific Ocean .

- The GUANO Model was used to simulate changes to ammonia emissions from seabirds under IPCC climate change scenarios, excluding potential changes to seabird populations. Emissions are simulated to increase by between 26 and 39 %, mainly due to increased temperatures, but mediated by increased precipitation in the southern Ocean. As calculated by the GUANO model, the total NH_3 emission estimate from seabird colonies in 2099, using the following

climate change scenarios would be 104, 112 and 114 Gg NH_3 $year^{-1}$ for the B1, A1B and A2 scenarios, respectively.

References

Aarnink, A. J. A. and Elzing, A. (1998) Dynamic model for ammonia volatilization in housing with partially slatted floors, for fattening pigs. Livestock Production Science, 53, 153-169.

Anderson, W. B. and Polis, G. A. (1999) Nutrient fluxes from water to land: seabirds affect plant nutrient status on Gulf of California islands. Oecologia, 118, 324-332.

Asman, W. A. H., Harrison, R. M. and Ottey, C. J. (1994) Estimation of the net air-sea flux of ammonia over the southern bight of the North Sea. Atmospheric Environment, 28, 3647-3654.

Asman, W. A. H., Sutton, M. A. and Schjoerring, J. K. (1998) Ammonia: emission, atmospheric transport and deposition. New Phytologist, 27 - 48.

BAS (2007) Signy Research Station, British Antarctic Survey. Accessed June 2011. URL was correct at a given date. http://www.antarctica.ac.uk/.

Berden, G., Peeters, R. and Meijer, G. (2000) Cavity ring-down spectroscopy: Experimental schemes and applications. International Reviews in Physical Chemistry, 19, 565-607.

Bjorneberg, D. L., Leytem, A. B., Westermann, D. T., Griffiths, P. R., Shao, L. and Pollard, M. J. (2009) Measurement of atmospheric ammonia, methane and nitrous oxide at a concentrated diary production facility in southern Idaho using open path FTIR spectrometry. Transactions of the ASABE, 52, 1749-1756.

Blackall, T. D. (2004) The emission of ammonia from seabird colonies. PhD thesis, University of Leeds.

Blackall, T. D., Theobald, M. R., Milford, C., Hargreaves, K. J., Nemitz, E., Wilson, L. J., Bull, J., Bacon, P. J., Hamer, K. C., Wanless, S. and Sutton, M. A. (2004) Application of tracer ratio and inverse dispersion methods with boat-based plume measurements to estimate ammonia emissions from seabird colonies. Water, Air, & Soil Pollution: Focus, 4, 279-285.

Blackall, T. D., Wilson, L. J., Bull, J., Theobald, M. R., Bacon, P. J., Hamer, K. C., Wanless, S. and Sutton, M. A. (2008) Temporal variation in atmospheric ammonia concentrations above seabird colonies. Atmospheric Environment, 42, 6942-6950.

Blackall, T. D., Wilson, L. J., Theobald, M. R., Milford, C., Nemitz, E., Bull, J., Bacon, P. J., Hamer, K. C., Wanless, S. and Sutton, M. A. (2007) Ammonia emissions from seabird colonies. Geophysical Research Letters, 34, 5-17.

Bobbink, R., Hornung, M. and Roelofs, J. G. M. (1998) The effects of air-borne nitrogen pollutants on species diversity in natural and semi-natural European vegetation. Journal of Ecology, 86, 717-738.

Bogstad, B., Hauge, K. H. and Ulltang, O. (1997) MULTSPEC: A multi-species model for fish and marine mammals in the Barents Sea. Journal of Northwest Atlantic Fishery Science, 317-341.

Bosman, A. L. and Hockey, P. A. R. (1988) The influence of seabird guano on the biological structure of rocky intertidal communities on islands off the west coast of southern Africa. South African Journal of Marine Science, 7, 61-68.

Böttcher, U. (1996) Estimating ammonia excretion by seabirds: the example of the Northern Gannet Sula bassana on the Bass Rock, Scotland. ITE Edinburgh. MSc Thesis Technical University Braunschweig, Germany, pp. 67.

Bouwman, A. F., Lee, D. S., Asman, W. A. H., Dentener, F. J., Vanderhoek, K. W. and Olivier, J. G. J. (1997) A global high-resolution emission inventory for ammonia. Global Biogeochemical Cycles, 11, 561-587.

Bouwman, A. F., Boumans, L. J. M. and Batjes, N.H. (2002) Estimation of global NH_3 volatilization loss from synthetic fertilizers and animal manure applied to arable lands and grasslands. Global biogeochemical cycles, 16, 14 pp.

Brierley, A. S. (2008) Antarctic Ecosystem: Are deep krill ecologicla outliers or portents of a paradigm shift? Current Biology, 18, 252-254.

Brooke, M. D. (2004) The food consumption of the world's seabirds. Proceedings of the Royal Society of London Series B-Biological Sciences, 271, S246-S248.

Bryant, D. M. and Furness, R. W. (1995) Basal metabolic rates of North-Atlantic seabirds. Ibis, 137, 219-226.

Businger, J. A., Wyngaard, C. J. and Izumi, Y. (1971) Flux profile relationships in the atmospheric surface layer. Journal Atmosheric Science, 28, 181-189.

Cape, J. N., van der Eerden, L. J., Sheppard, L. J., Leith, I. D. and Sutton, M. A. (2009) Evidence for changing the Critical Level for ammonia. Environmental Pollution, 157, 1033-1037.

Chantigny, M. H., Rochette, P., Angers, D. A., Massé, D. and Côté, D. (2004) Ammonia volatilization and selected soil characteristics following application of anaerobically digested pig slurry. Soil Science Society America Journal, 68, 306-213.

Coates, T., Mcginn, S. M. and Bauer, J. (2004) Application of open-path TDL analysers for determination of methane and ammonia emissions from livestock facilities. 26th Conference on Ag. & Forest Meteorology, Vancouver.

Cortus, E. L., Lemay, S. P. and Barber, E. M. (2009) Dynamic simulation of ammonia concentration and emission within swine barns: Part I. Model development. Transactions of the Asabe, 53, 911-923.

Cortus, E. L., Lemay, S. P., Barber, E. M., Hill, G. A. and Godbout, S. (2008) A dynamic model of ammonia emission from urine puddles. Biosystems Engineering, 99, 390-402.

Cowen, K., Summer, A. L., Dindal, A., Riggs, K., Willienberg, Z., Hatfield, J. L., Pfeffer, R. and Scoggin, K. (2004) Environmental Technology

Verification Report. Pranalytica, Inc. Nitrolux 1000 Ambient NH_3 Analyser. ETV, pp.57.

Cramp, S. and Simmons, K. L. E. (1983) The birds of the Western Palearctic. Handbook of the Birds of Europe, the Middle East and North Africa, vols. I, III, IV., Oxford, U.K., Oxford Univ. Press.

Cramp, S. and Simmons, K. L. E. (1985) The birds of the Western Palearctic. Handbook of the Birds of Europe, the Middle East and North Africa, vols. I, III, IV., Oxford, U.K., Oxford Univ. Press.

Croxall, J. P. (1987) Seabirds: feeding ecology and role in marine ecosystems, Cambridge Univ. Press.

Croxall, J. P. and Davis, R. W. (1990) Metabolic rate and foraging behavior of Pygoscelis and Eudyptes penguins at sea. In Davis, L. S. and Darby, J. T. (Eds.) Penguin Biology. San Diego, Academic Press.

Croxall, J. P., Evans, P. G. H. & Schreiber, R. W. (1984) *Status and Conservation of the World's Seabirds*, Cambridge, UK, ICBP Publication.

Croxall, J. P., Silk, J. R. D., Phillips, R. A., Afanasyev, V. and Briggs, D. R. (2005) Global circumnavigations: Tracking year-round ranges of nonbreeding albatrosses. Science, 307, 249-250.

Croxall, J. P., Trathan, P. N. and Murphy, E. J. (2002) Environmental change and Antarctic seabird populations. Science, 297, 1510-1514.

DEFRA (2010) UK Eutrophying and Acidifying Atmospheric Pollutants: Annual Report A http://uk-air.defra.gov.uk/reports/cat13/1105130856_ UKEAP_ report_ 2010_Final.pdf. URL was correct at a given date.

Demmers, T. G. M., Burgess, L. R., Short, J. L., Phillips, V. R., Clark, J. A. and Wathes, C. M. (1998) First experiences with methods to measure ammonia emissions from naturally ventilated cattle buildings in the UK. Atmospheric Environment, 32, 285-293.

Denmead, O. (2008) Approaches to measuring fluxes of methane and nitrous oxide between landscapes and the atmosphere. Plant and Soil, 309, 5-24.

Denmead, O. T., Chen, D., Griffith, D. W. T., Loh, Z. M., Bai, M. and Naylor, T. (2008) Emissions of the indirect greenhouse gases NH3 and NOx from Australian beef cattle feedlots. Australian Journal of Experimental Agriculture, 48, 2130218.

Denvil, S. (2005) Intergovernmental Panel on Climate Change - Data Distribution Center. Accessed January 2012. URL was correct at a given date. http://www.ipcc-data.org/.

Drent, R. H. and Daan, S. (1980) The prudent parent - energetic adjustments in avian breeding. Ardea, 68, 225-252.

EC-JRC/PBL (2010) Emission Database for Global Atmospheric Research (EDGAR), release version 4.1. Accessed December 2011., European Commission, Joint Research Centre (JRC) / Netherlands Environmental Assessment Agency (PBL).

ECN (2003) AiRRmonia - Automated Ammonia Analyzer. Energy Research Foundation of the Netherlands. Petten, NL. pp.57.

Egevang, C., Stenhouse, I. J., Phillips, R. A., Petersen, A., Fox, J. W. and Silk, J. R. D. (2010) Tracking of Arctic terns Sterna paradisaea reveals longest animal migration. Proceedings of the National Academy of Sciences of the United States of America, 107, 2078-2081.

Elliott, H. A. and Collins, N. E. (1982) Factors affecting ammonia release in broiler houses. Transactions of the Asae, 25, 413-418.

Ellis, J. C. (2005) Marine birds on land: a review of plant biomass, species richness, and community composition in seabird colonies. Plant Ecology, 181, 227-241.

Elzing, A. and Monteny, G. J. (1997) Ammonia Emissions in a Scale Model of a Dairy-cow House. Transactions of the ASAE, 40, 713-720.

Erisman, J. W., Sutton, M. A., Galloway, J., Klimont, Z. and Winiwarter, W. (2008) How a century of ammonia synthesis changed the world. Nature Geoscience, 1, 636-639.

Evans, P. G. H. (1981) Ecology and behavior of the Little auk *Alle alle* in West Greenland. Ibis, 123, 1-18.

Flechard, C. R., Fowler, D., Sutton, M. A. and Cape, J. N. (1999) A dynamic chemical model of bi-directional ammonia exchange between semi-natural vegetation and the atmosphere. Quarterly Journal of the Royal Meteorological Society, 125, 2611-2641.

Flesch, T. K., Wilson, J. D., Harper, L. A. and Crenna, B. P. (2005) Estimating gas emission from a farm using an inverse-dispersion technique. Atmospheric Environment, 39, 4863-4874.

Flesch, T. K., Wilson, J. D., Harper, L. A., Crenna, B. P. and Sharpe, R. R. (2004) Deducing ground-air emissions from observed trace gas concentrations: A field trial. Journal of Applied Meteorology, 43, 487-502.

Flesch, T. K., Wilson, J. D. and Yee, E. (1995) Backward-time Lagrangian stochastic dispersion models, and their application to estimate gaseous emissions. Journal of Applied Meteorology, 34, 1320-1332.

Forcada, J., Trathan, P. N., Reid, K., Murphy, E. J. and Croxall, J. P. (2006) Contrasting population changes in sympatric penguin species in association with climate warming. Global Change Biology, 12, 411-423.

Fowler, D., Smith, R. I., Coyle, M., Sutton, M. A., Campbell, G., Downing, C. and Vincent, K. (1997) Rural air pollution in the UK. In Davison, G. and Hewitt, C. N. (Eds.) Air Pollution in the United Kingdom. Cambridge, Royal Society of Chemistry.

Fowler, D., Sutton, M. A., Smith, R. I., Pitcairn, C. E. R., Coyle, M., Campbell, G. and Stedman, J. (1998) Regional mass budgets of oxidized and reduced nitrogen and their relative contribution to the N inputs of sensitive ecosystems. Environmental Pollutution (Nitrogen Conference Special Issue), 102, 337-342.

Furness, R. W. (1991) The occurrence of burrow-nesting among birds and its influence on soil fertility and stability. Symposia of the Zoological Society of London, 63, 53-67.

Gales, R. and Green, B. (1990) The annual energetics cycle of Little penguins (*Eudyptula minor*). Ecology, 71, 2297-2312.

Galloway, J. N., Dentener, F. J., Capone, D. G., Boyer, E. W., Howarth, R. W., Seitzinger, S. P., Asner, G. P., Cleveland, C. C., Green, P. A., Holland, E. A., Karl, D. M., Michaels, A. F., Porter, J. H., Townsend, A. R. and Vorosmarty, C. J. (2004) Nitrogen cycles: past, present, and future. Biogeochemistry, 70, 153-226.

Galloway, J. N., Schlesinger, W. H., Levy, H., Michaels, A. and Schnoor, J. L. (1995) Nitrogen-fixation - Anthropogenic enhancement- Environmental response. Global Biogeochemical Cycles, 9, 235-252.

Galloway, J. N., Townsend, A. R., Erisman, J. W., Bekunda, M., Cai, Z. C., Freney, J. R., Martinelli, L. A., Seitzinger, S. P. and Sutton, M. A. (2008) Transformation of the nitrogen cycle: Recent trends, questions, and potential solutions. Science, 320, 889-892.

Gao, Z., Desjardins, R. L. and Flesch, T. K. (2009) Comparison of a simplified micrometeorological mass difference technique and an inverse dispersion technique for estimating methane emissions from small area sources. Agricultural and Forest Meteorology, 149, 891-898.

Gao, Z., Desjardins, R. L. and Flesch, T. K. (2010) Assessment of the uncertainty of using an inverse-dispersion technique to measure methane emissions from animals in a barn and in a small pen. Atmospheric Environment, 44, 3128-3134.

Garcia, L. V., Maranon, T., Ojeda, F., Clemente, L. and Redondo, R. (2002) Seagull influence on soil properties, chenopod shrub distribution, and leaf nutrient status in semi-arid Mediterranean islands. Oikos, 98, 75-86.

Garland, J. A. (1977) Dry deposition of sulfur-dioxide to land and water surfaces. Proceedings of the Royal Society of London Series a-Mathematical Physical and Engineering Sciences, 354, 245-268.

Garratt, J. R. (1994) An introduction to boundary layer meteorology, Cambridge University Press.

Génermont, S. and Cellier, P. (1997) A mechanistic model for estimating ammonia volatilization from slurry applied to bare soil. Agricultural and Forest Meteorology, 88, 145-167.

Gradko (2011) Gradko Environmental - Diffusion tubes. Accessed November 2012. URL was correct at a given date. http://www.gradko.co.uk.

Gras, J. L. (1983) Ammonia and Ammonium Concentrations in the Antarctic Atmosphere. Atmospheric Environment, 17, 815-818.

Green, J. A., Boyd, I. L., Woakes, A. J., Green, C. J. and Butler, P. J. (2007) Feeding, fasting and foraging success during chick rearing in macaroni penguins. Marine Ecology-Progress Series, 346, 299-312.

Green, K., Williams, R. and Green, M. G. (1998) Foraging ecology and diving behaviour of Macaroni Penguins Eudyptes chrysolophus at Heard Island. Marine Ornithology, 26, 27-34.

Groot Koerkamp, P. W. G. (1998) Ammonia emission from aviary housing systems for laying hens -inventory, characteristics and solutions. PhD Thesis, Wageningen University, Wageningen, The Netherlands.

Groot Koerkamp, P. W. G., Metz, J. H. M., Uenk, G. H., Phillips, V. R., Holden, M. R., Sneath, R. W., Short, J., L., White, R. P., Hartung, J., Seedorf, J., Schroder, M., Linkert, K. H., Pedersen, S., Takai, H., Johnsen, J. O. and Wathes, C. M. (1998) Concentrations and emissions of ammonia in livestock buildings in Northern Europe. Journal of Agricultural Engineering Research, 70, 79-95.

Hafkenscheid, T., Fromage-Mariette, A., Goelen, E., Hangartner, M., Pfeffer, U., Plaisance, H., de Santis, F., Saunders, K. Swaans, W., Tang, Y.S., Targa, J., van Hoek, C. and Gerboles, M. (2009) Review of the application of diffusive samplers in the European Union for the monitoring of nitrogen dioxide in ambient air. Joint Research Centre, Institute for Environment and Sustainability. Scientific and technical reports. pp. 80.

Hansell, M. (2000) Bird Nests and Construction Behaviour, Cambridge University Press.

Hargreaves, K. J. and Atkins, D. H. F. (1987) The measurement of ammonia in the outdoor environment using passive diffusion tube samplers. Report AERE-R-12568, Harwell Laboratory, Didcot, Oxon, UK.

Harper, L. A., Flesch, T. K., Powell, J. M., Coblentz, W. K., Jokela, W. E. and Martin, N. P. (2009) Ammonia emissions from dairy production in Wisconsin. Journal of Dairy Science, 92, 2326-2337.

Harper, L. A., Flesch, T. K. and Wilson, J. D. (2010) Ammonia emissions from broiler production in the San Joaquin Valley. Poultry Science, 889, 1802-1814.

Harris, I. (2007) Climatic Research Unit (CRU) at the University of East Anglia. High-resolution Gridded Datasets. Accessed June 2011. URL was correct at a given date. http://www.cru.uea.ac.uk/cru/data/hrg/.

Hensen, A., Nemitz, E., Flynn, M. J., Blatter, A., Jones, S. K., Sorensen, L. L., Hensen, B., Pryor, S. C., Jensen, B., Otjes, R. P., Cobussen, J., Loubet, B., Erisman, J. W., Gallagher, M. W., Neftel, A. and Sutton, M. A. (2009) Inter-comparison of ammonia fluxes obtained using the Relaxed Eddy Accumulation technique. Biogeosciences, 6, 2575-2588.

Hensen, A. and Scharff, H. (2001) Methane Emission Estimates from Landfills Obtained with Dynamic Plume Measurements. Water, Air and Soil Pollution: Focus, 1, 455-464.

Hicks, B. B., Baldocchi, D. D., Meyers, T. P., Hosker, R. P. and Matt, D. R. (1987) A preliminary multiple resistance routine for deriving dry deposition velocities from measured quantities. Water Air and Soil Pollution, 36, 311-330.

Hodum, P. J. (2002) Breeding biology of high-latitude Antarctic fulmarine petrels (Procellariidae). Journal of Zoology, 256, 139-149.

Hodum, P. J. and Wainstein, M. (2002) Biology and Conservation of the Juan Fernández Archipelago Seabird Community. CONCAF Report 2002.

International, B. (2009) Birdlife International. Accessed June 2011. URL was correct at a given date. http://www.birdlife.org.

Jahncke, J., Checkley, D. M. and Hunt, G. L. (2004) Trends in carbon flux to seabirds in the Peruvian upwelling system: effects of wind and fisheries on population regulation. Fisheries Oceanography, 13, 208-223.

JNCC (2011) Joint National Conservation Committee - Seabird 2000. Accessed June 2011. URL was correct at a given date. http://www.jncc.gov.uk/page-4460.

Johnson, M. T. (2004) The air-sea flux of ammonia. PhD Thesis, University of East Anglia, Norwich, UK,.

Kampp, K., Falk, K. and Pedersen, C. E. (2000) Breeding density and population of little auks (Alle alle) in a Northwest Greenland colony. Polar Biology, 23, 517-521.

Karpouzi, V. S., Watson, R. and Pauly, D. (2007) Modelling and mapping resource overlap between seabirds and fisheries on a global scale: a preliminary assessment. Marine Ecology-Progress Series, 343, 87-99.

Kildaw, S. D., Irons, D. B., Nysewander, D. R. and Buck, C. L. (2005) Formation and growth of new seabird colonies: The significance of habitat quality. Marine Ornithology, 33, 49-58.

Kim, W. K. and Patterson, P. H. (2003) Effect of minerals on activity of microbial uricase to reduce ammonia volatilization in poultry manure. Poultry Science, 82, 223-231.

Klemperer, F. (1945) Enzymatic oxidation of Uric acid. Federation Proceedings, 4, 94-95.

Kljun, N., Calanca, P., Rotachhi, M. W. and Schmid, H. P. (2004) A simple parameterisation for flux footprint predictions. Boundary-Layer Meteorology, 112, 503-523.

Ko, M. K. W., Sze, N.D., Wang, W.C., Shia, G., Goldman, A., Murcray, F.J., Murcray, D.G. & Rinsland, C.P. (1993) Atmospheric sulfur hexafluoride: sources, sinks and greenhouse warming. *Journal of Geophysical Research* 98, 10499-10507.

Kooyman, G. L., Siniff, D. B., Stirling, I. and Bengtson, J. L. (2004) Moult habitat, pre- and post-moult diet and post-moult travel of Ross Sea emperor penguins. Marine Ecology-Progress Series, 267, 281-290.

Krupa, S. V. (2003) Effects of atmospheric ammonia (NH3) on terrestrial vegetation: a review. Environmental Pollution, 124, 179-221.

Larsson, L., Ferm, M., Kasimir-Klemedtsson, A. and Klemedtsson, L. (1998) Ammonia and nitrous oxide emissions from grass and alfalfa mulches. Nutrient Cycling in Agroecosystems, 51, 41-46.

Laubach, J. (2010) Testing of a Lagrangian model of dispersion in the surface layer with cattle methane emissions. Agricultural and Forest Meteorology 150, 1428-1442.

Laubach, J. and Kelliher, F. M. (2005) Measuring methane emission rates of a dairy cow herd (II): results from a backward-Lagrangian stochastic model. Agricultural and Forest Meteorology, 129, 137-150.

Laubach, J., Kelliher, F. M., Knight, T. W., Clark, H., Molano, G. and Cavanagh, A. (2008) Methane emissions from beef cattle - a comparison of paddock- and animal-scale measurements. Australian Journal of Experimental Agriculture, 48, 132-137.

Legrand, M., Ducroz, F., Wagenbach, D., Mulvaney, R. and Hall, J. (1998) Ammonium in coastal Antarctic aerosol and snow: Role of polar ocean and penguin emissions. Journal of Geophysical Research-Atmospheres, 103, 11043-11056.

Lewis, S., Wanless, S., Wright, P. J., Harris, M. P., Bull, J. and Elston, D. A. (2001) Diet and breeding performance of black-legged kittiwakes Rissa tridactyla at a North Sea colony. Marine Ecology-Progress Series, 221, 277-284.

Leytem, A. B., Dungan, R. S., Bjorneberg, D. L. and Koehn, A. C. (2010) Emissions of ammonia, methane, carbon dioxide, and nitrous oxide from dairy cattle housing and manure management systems. Journal of Environmental Quality, 40, 1383-1394.

Lindeboom, H. J. (1984) The nitrogen pathway in a penguin rookery. Ecology, 65, 269-277.

Loder, T. C., Ganning, B. and Love, J. A. (1996) Ammonia nitrogen dynamics in coastal rockpools affected by gull guano. Journal of Experimental Marine Biology and Ecology, 196, 113-129.

Loh, Z., Leuning, R., Zegelin, S., Etheridge, D., Bai, M., Naylor, T. and Griffith, D. (2009) Testing Lagrangian atmospheric dispersion modeling to monitor CO2 and CH4 leakage from geosequestration. Atmospheric Environment, 43, 2602-2611.

Loubet, B., Milford, C., Sutton, M. A. and Cellier, P. (2001) Investigation of the interaction between sources and sinks of atmospheric ammonia in an upland landscape using a simplified dispersion-exchange model. Journal of Geophysical Research-Atmospheres, 106, 24183-24195.

Loubet, B., Decuq, C., Personne, E., Massad, R. S., Flechard, C., Fanucci, O., Mascher, N., Gueudet, J.-C., Masson, S., Durand, B., Génermont, S., Fauvel, Y. and Cellier, P. (2011) Investigating the stomatal, cuticular and soil ammonia fluxes over a growing critical crop under high acidic loads. Biogeosciences Discussion, 8, 10317-10350.

Maiss, M. and Brenninkmeijer, C. A. M. (1998) Atmospheric SF6: Trends, sources, and prospects. Environmental Science & Technology, 32, 3077-3086.

Mann, M. E. and Kump, L. R. (2008) Dire predictions: understanding global warming, DK Publishing.

McGinn, S. M., Beauchemin, K. A., Flesch, T. K. and Coates, T. (2009) Performance of a dispersion model to estimate methane loss from cattle in pens. Journal of Environmental Quality, 38, 1796-1802.

McGinn, S. M., Coates, T., Flesch, T. K. and Crenna, B. P. (2008) Ammonia emissions from dairy cow manure stored in a lagoon over summer. Canadian Journal of Soil Science, 88, 611-615.

Milford, C., Theobald, M. R., Nemitz, E., Hargreaves, K. J., Horvath, L., Raso, J., Dämmgen, U., Neftel, A., Jones, S. K., Hensen, A., Loubet, B., Cellier, P. and Sutton, M. A. (2009) Ammonia fluxes in relation to cutting and fertilization of an intensively managed grassland derived from an inter-comparison of gradient measurements. Biogeosciences, 6, 819-834.

Misselbrook, T. H., Nicholson, F. A. and Chambers, B. J. (2005) Predicting ammonia losses following the application of livestock manure to land. Bioresource Technology, 96, 159-168.

Misselbrook, T. H., Van Der Weerden, T. J., Pain, B. F., Jarvis, S. C., Chambers, B. J., Smith, K. A., Phillips, V. R. and Demmers, T. G. M. (2000) Ammonia emission factors for UK agriculture. Atmospheric Environment, 34, 871-880.

Mizutani, H., Kabaya, Y. and Wada, E. (1985) Ammonia volatilization and high 15n/14n ratio in a penguin rookery in Antarctica. Geochemical Journal, 19, 323-327.

Mizutani, H. and Wada, E. (1988) Nitrogen and carbon isotope ratios in seabird rookeries and their ecological implications. Ecology, 69, 340-349.

Monteith, J. L. (1973) Principles of Environmental Physics, London.

Namiesnik, J., Zabiegala, B., Kot-Wasik, A., Partyka, M. and Wasik, A. (2005) Passive sampling and/or extraction techniques in environmental analysis: a review. Analytical and Bioanalytical Chemistry, 381, 279-301.

NCDC (2011) National Climatic Data Center, Integrated Surface Hourly (ISH) database. http://www.ncdc.noaa.gov/oa/climate/surfaceinventories.html Downloaded Monday, 19-Dec-2011 04:44:15 EST. Accessed December 2011. URL was correct at a given date.

NCEP (2011) National Centres for Environmental Protection / National Center for Atmospheric Research NCEP/NCAR Reanalysis project. Accessed November 2011. URL was correct at a given date. http://www.esrl.noaa.gov/psd/data/reanalysis/reanalysis.shtml.

Nemitz, E., Milford, C. and Sutton, M. A. (2001) A two-layer canopy compensation point model for describing bi-directional biosphere-

atmosphere exchange of ammonia. Quarterly Journal of the Royal Meteorological Society, 127, 815-833.

Nemitz, E., Sutton, M. A., Schjoerring, J. K., Husted, S. and Wyers, G. P. (2000) Resistance modelling of ammonia exchange over oilseed rape. Agricultural and Forest Meteorology, 105, 405-425.

Ni, J. Q. (1999) Mechanistic models of ammonia release from liquid manure: a review. Journal of Agricultural Engineering Research, 72, 1-17.

Ni, J. Q., Heber, A. J., Diehl, C. A. and Lim, T. T. (2000) Ammonia, hydrogen sulphide and carbon dioxide release from pig manure in under-floor deep pits. Journal of Agricultural Engineering Research, 77, 53-66.

NOAA (2010) National Oceanic and Atmospheric Administration - METAR Data Access. Accessed November 2011. URL was correct at a given date. http://weather.noaa.gov/

Norman, M., Spirig, C., Wolff, V., Trebs, I., Flechard, C., Wisthaler, A., Schnitzhofer, R., Hansel, A. and Neftel, A. (2009) Intercomparison of ammonia measurement techniques at an intensively managed grassland site (Oensingen, Switzerland). Atmospheric Chemistry, 9, 2635-2645.

Nunn, G. B. and Stanley, S. E. (2000) Body size effects and rates of cytochrome-b evolution in tube-nosed seabirds. Molecular Biology and Evolution, 17, 1774-1774.

Parton, W. J. and Logan, J. A. (1981) A model for diurnal variation in soil and air temperature. Agricultural and Forest Meteorology, 23, 205-216.

Pasquill, F. (1974) Limitations and prospects in estimation of dispersion of pollution on a regional scale. Transactions-American Geophysical Union, 55, 144-144.

Paulson, C. A. (1970) The mathematical representation of wind speed and temperature profiles in the unstable atmospheric surface layer. Journal of Applied Meteorology, 9, 857–861.

Pearson, J. and Stewart, G. R. (1993) The deposition of atmospheric ammonia and its effects on plants. New Phytologist, 125, 283-305.

Pfeffer, M. A., Rietmeijer, F. J. M., Brearley, A. J. and Fischer, T. P. (2006) Electron microbeam analyses of aerosol particles from the plume of Poa´s Volcano, Costa Rica and comparison with equilibrium plume chemistry modeling. Journal of Volcanology and Geothermal Research, 152, 174-188.

Phillips, R. A., Phalan, B. and Forster, I. P. (2004) Diet and long-term changes in population size and productivity of brown skuas at Bird Island, South Georgia. Polar Biology, 27, 555-561.

Phillips, R. A., Thompson, D. R. and Hamer, K. C. (1999) The impact of great skua predation on seabird populations at St Kilda: a bioenergetics model. Journal of Applied Ecology, 36, 218-232.

Pinder, R. W., Pekney, N. J., Davidson, C. I. and Adams, P. J. (2004) A process-based model of ammonia emissions from dairy cows: improved temporal and spatial resolution. Atmospheric Environment, 38, 1357-1365.

Pogany, A., Mohacsi, A., Varga, A., Bozoki, Z., Galbacs, Z., Horvath, L. and Szabo, G. (2009) A compact NH3 detector with sub-ppb accuracy using near-infrared photoacoustic spectroscopy and preconcentration sampling. Environmental Science & Technology, 43, 826-830.

Posthumus, A. C. (1988) Critical levels for effects of ammonia and ammonium. Proceedings of the Bad Harzburg Workshop. UBA, Berlin, pp. 117-127.

Priddel, D., Carlile, N. and Wheeler, R. (2008) Population size, breeding success and provenance of a mainland colony of Little Penguins (Eudyptula minor). Emu, 108, 35-41.

Purves, W., Sadava, D., Orians, G. and Heller, C. (2003) Life: The Science of Biology, 7th Edition, Sinauer Associates and W. H. Freeman.

Quintana, R. D., Cirelli, V. and Orgeira, J. L. (2000) Abundance and spatial distribution of bird populations at Cierva Point, Antarctic Peninsula. Marine Ornithology, 28, 21-27.

Ramanathan, V., Callis, L., Cess, R., Hansen, J., Isaksen, I., Kuhn, W., Lacis, A., Luther, F., Mahlman, J., Reck, R. and Schlesinger, M. (1987) Climate-chemical interactions and effects of changing atmospheric trace gases. Reviews of Geophysics, 25, 1441-1482.

Raven, J. A. (1988) Acquisition of nitrogen by the shoots of land plants - its occurrence and implications for acid-base regulation. New Phytologist, 109, 1-20.

Ravishankara, A. R., Solomon, S., Turnipseed, A.A. & Warren, R.F. (1993) Atmospheric lifetimes of long-lived halogenated species. Science, 259, 194-199.

Sanchez-Piñero F. and Polis G. A. (2000) Bottom-up dynamics of allochthonous input: direct and indirect effects of seabirds on islands. Ecology 81: 3117–3132.

Santander, H. (1981) Patterns of distribution and spawning fluctuations of anchovy and sardines. Boletin del Instituto del Mar de Peru, Vol. extraordinario**,** 180-192.

Schmidt, S., Mackintosh, K., Gillett, R., Pudmenzky, A., Allen, D. E., Rennenberg, H. and Mueller, J. F. (2010) Atmospheric concentrations of ammonia and nitrogen dioxide at a tropical coral cay with high seabird density. Journal of Environmental Monitoring, 12, 460-465.

Schreiber, E. A. and Burger, J. (2001) Biology of Marine Birds, Boca Raton, FL, CRC Press.

Seinfeld, J. H. and Pandis, S. N. (2006) Atmospheric Chemistry and Physics: From Air Pollution to Climate Change London, John Wiley & Sons.

Sheppard, L. J., Leith, I. D., Crossley, A., Van Dijk, N., Fowler, D., Sutton, M. A. and Woods, C. (2008) Stress responses of Calluna vulgaris to reduced and

oxidised N applied under 'real world conditions'. Environmental Pollution, 154, 404-413.

Shuttleworth, W. J. (2007) Putting the 'vap' into evaporation. Hydrology and Earth System Sciences, 11, 210-244.

Simas, F. N. B., Schaefer, C. E. G. R., Melo, V. F., Albuquerquefilho, M. R., Michel, R. F., Pereira, V. V. and Gomes, M. R. M. (2007) Ornithogenic Cryosols from maritime Antarctica: phosphatization as a soil forming process. Geoderma, 138, 191-203.

Solomon, S., Qin, D., Manning, M., Chen, Z., Marquis, M., Averyt, K. B., Tignor, M. and Miller, H. L. (2007) Contribution of Working Group I to the Fourth Assessment Report of the Intergovernmental Panel on Climate Change, Cambridge, UK, Cambridge University Press.

Sommer, S. G., Mcginn, S. M. and Flesch, T. K. (2005) Simple use of the backwards Lagrangian stochastic dispersion technique for measuring emissions from small field plots. European Journal of Agronomy, 23, 1-7.

Sommer, S. G. and Olesen, J. E. (2000) Modelling ammonia volatilization from animal slurry applied with trail hoses to cereals. Atmospheric Environment, 34, 2361-2372.

Sommer, S. G., Olesen, J. E. and Christensen, B. T. (1991) Effects of temperature, wind-speed and air humidity on ammonia volatilization from surface applied cattle slurry. Journal of Agricultural Science, 117, 91-100.

Steele, J. H. (2010) Marine Biology: A derivative of the Encyclopedia of Ocean Sciences, Academic Press.

Stevens, R. J., Laughlin, R. J. and Kilpatrick, D. J. (1989) Soil properties related to the dynamics of ammonia volatilization from urea applied to the surface of acidic soils. Fertility Research, 20, 1-9.

Stonehouse, B. (1952) Breeding behaviour of the Emperor penguin. Nature, 169, 760-760.

Stulen, I., Perez-Soba, M., De Kok, L. J. and Van Der Eerden, L. (1998) Impact of gaseous nitrogen deposition on plant functioning. New Phytologist, 139, 61-70.

Stull, R. B. (1988) An introduction to boundary layer meteorology, Springer.

Summerhayes, V. S. and Elton, C. S. (1928) Further contributions to the ecology of Spitzbergen. Journal of Ecology, 16, 193–268.

Sun, L. G., Zhu, R. B., Yin, X. B., Liu, X. D., Xie, Z. Q. and Wang, Y. H. (2004) A geochemical method for the reconstruction of the occupation history of a penguin colony in the maritime Antarctic. Polar Biology, 27, 670-678.

Sutton, M. A., Asman, W. A. H., Ellermann, T., Van Jaarsveld, J. A., Acker, K., Aneja, V., Duyzer, J., Horvath, L., Paramonov, S., Mitosinkova, M., Tang, Y. S., Achermann, B., Gauger, T., Bartniki, J., Neftel, A. and Erisman, J. W. (2003) Establishing the link between ammonia emission control and measurements of reduced nitrogen concentrations and deposition. Environmental Monitoring and Assessment, 82, 149-185.

Sutton, M. A., Dragosits, U., Tang, Y. S. and Fowler, D. (2000a) Ammonia emissions from non-agricultural sources in the UK. Atmospheric Environment, 34, 855-869.

Sutton, M. A., Erisman J. W., Dentener F. & Möller D. (2008) Ammonia in the environment: From ancient times to the present. Environmental Pollution, 156, 583-604.

Sutton, M. A., Fowler, D., Burkhardt, J. K. and Milford, C. (1995a) Vegetation atmosphere exchange of ammonia: Canopy cycling and the impacts of elevated nitrogen inputs. Water Air and Soil Pollution, 85, 2057-2063.

Sutton, M. A., Fowler, D. and Moncrieff, J. B. (1993a) The exchange of atmospheric ammonia with vegetated surfaces .1. Unfertilized vegetation. Quarterly Journal of the Royal Meteorological Society, 119, 1023-1045.

Sutton, M. A., Fowler, D., Moncrieff, J. B. and Storetonwest, R. L. (1993b) The exchange of atmospheric ammonia with vegetated surfaces .2. Fertilized vegetation. Quarterly Journal of the Royal Meteorological Society, 119, 1047-1070.

Sutton, M. A., Howard, C. M. and Erisman, J. W. (Eds.) (2011) The European Nitrogen Assessment: Sources, Effects and Policy Perspectives, Cambridge University Press.

Sutton, M. A., Nemitz, E., Milford, C., Fowler, D., Moreno, J., San Jose, R., Wyers, G. P., Otjes, R. P., Harrison, R., Husted, S. and Schjoerring, J. K. (2000b) Micrometeorological measurements of net ammonia fluxes over oilseed rape during two vegetation periods. Agricultural and Forest Meteorology, 105, 351-369.

Sutton, M. A., Place, C. J., Eager, M., Fowler, D. and Smith, R. I. (1995b) Assessment of the magnitude of ammonia emissions in the United Kingdom. Atmospheric Environment, 29, 1393-1411.

Tang, Y. S., Cape, J. N. and Sutton, M. A. (2001) Development and types of passive samplers for NH3 and NOx. In Proceedings of the International Symposium on Passive Sampling of Gaseous Pollutants in Ecological Research. The Scientific World, 1, 513-529.

Tatur, A. and Myrcha, A. (2002) Ornithogenic ecosystems in the maritime Antarctic: formation, development and disintigration. Ecological Studies, 161-184.

Theobald, M. (2009) Sampling strategy for input and verification data of the NitroScape model, NitroEurope IP - Component 4 (Landscape Analysis). Accessed June 2011. URL was correct at a given date. http://www.nitroeurope.eu/.

Theobald, M. R., Crittenden, P. D., Hunt, A. P., Tang, Y. S., Dragosits, U. and Sutton, M. A. (2006) Ammonia emissions from a Cape fur seal colony, Cape Cross, Namibia. Geophysical Research Letters, 33, L03812.

Trathan, P. N., Forcada, J. and Murphy, E. J. (2007) Environmental forcing and Southern Ocean marine predator populations: effects of climate change

and variability. Philosophical Transactions of the Royal Society B-Biological Sciences, 362, 2351-2365.

Trottier, S., Gunter, W. D., Kadatz, B., Olson, M. and Perkins, E. H. (2009) Atmospheric monitoring for the Pembina Cardium CO2 Monitoring Project using open path laser technology. Energy Procedia, 1, 2307-2314.

Tsunogai, S. (1971) Ammonia in the oceanic atmosphere and the cycle of nitrogen compounds through the atmopshere and hydrosphere. Geochemical Journal, 5, 57- 67.

Turner, D. A., Edis, R. B., Chen, D., Freney, J. R., Denmead, O. T. and Christie, R. (2010) Determination and mitigation of ammonia loss from urea applied to winter wheat with N-(n-butyl) thiophosphorictriamide. Agriculture, Ecosystems & Environment, 137, 261-266.

Twigg, M. (2005) High resolution measurement of NH3 and HNO3 fluxes between grasslands and the atmosphere using TDL spectroscopy. PhD Thesis, University of Edinburgh.

Twigg, M., Famulari, D., Fowler, D., Gallagher, M., Nemitz, E., Sutton, M. A., Whitehead, J. and Rippey, B. (2005) Principles and development of tunable laser diode absorption spectroscopy for measuring fluxes of ammonia and nitric acid. Proceedings of the First ACCENT Symposium, Urbino, 3, 12-16.

Twigg, M. M., House, E., Thomas, R., Whitehead, J., Phillips, G. J., Famulari, D., Fowler, D., Gallagher, M. W., Cape, J. N., Sutton, M. A. and Nemitz, E. (2011) Surface/atmosphere exchange and chemical interactions of reactive nitrogen compounds above a manured grassland. Agricultural and Forest Meteorology, 151, 1488-1503.

Uematsu, M., Toratani, M., Kajino, M., Narita, Y., Senga, Y. and Kimoto, T. (2004) Enhancement of primary productivity in the western North Pacific caused by the eruption of the Miyake-jima Volcano. Geophysical Research Letters 31, L06106.

Veitch, C. R. and Harper, G. (1998) Breeding season of Kermadee Petrels (Pterodroma neglecta neglecta) at Meyer Islands, Kermadec Group, New Zealand. Notornis, 45, 67-69.

Venkatesan, R., Mathiyarasu, R. and Somayaji, K. M. (2002) A study of atmospheric dispersion of radionuclides at a coastal site using a modified Gaussian model and a mesoscale sea breeze model. Atmospheric Environment, 18, 2933-2942.

Visek, W. J. (1984) Ammonia: its effects on biological systems, metabolic hormones, and reproduction. Journal Dairy Science, 67, 481-498.

Volkman, N. J. and Trivelpiece, W. (1981) Nest-site selection among Adelie, Chinstrap and Gentoo penguins in mixed species rookeries. Wilson Bulletin, 93, 243-248.

Von Bobrutzki, K., Braban, C. F., Famulari, D., Jones, S. K., Blackall, T., Smith, T. E. L., Blom, M., Coe, H., Gallagher, M., Ghalaieny, M., Mcgillen, M. R., Percival, C. J., Whitehead, J. D., Ellis, R., Murphy, J., Mohacsi, A.,

Pogany, A., Junninen, H., Rantanen, S., Sutton, M. A. and Nemitz, E. (2010) Field inter-comparison of eleven atmospheric ammonia measurement techniques. Atmospheric Measurement Techniques, 3, 91-112.

Weathers, W. W. (1992) Scaling nestling energy-requirements. Ibis, 134, 142-153.

Webb, E. K. (1970) Profile relationships: the log-linear range and extension to strong stability. Quarterly Journal Royal Meteorolgy Society, 96, 67-90.

Whitehead, J. D., Twigg, M., Famulari, D., Nemitz, E., Sutton, M. A., Gallagher, M. W. and Fowler, D. (2008) Evaluation of Laser Absorption Spectroscopic Techniques for Eddy Covariance Flux Measurements of NH3. Environmental Science Technology, 42, 2041-2046.

Willems, J. J. H. and Adema, E. H. (1992) In Development of analytical techniques for air pollution measurement. ed. I. Allegrini, CEC, Brussels, pp. 159-170.

Williams, A. J. (1981) The clutch size of Macaroni and Rockhopper penguins. Emu, 81, 87-90.

Williams, T. D. and Rodwell, S. (1992) Annual variation in return rate, mate and nest-site fidelity in breeding Gentoo and Macaroni penguins. Condor, 94, 636-645.

Wilson, J. D. and Sawford, B. L. (1995) Review of Lagrangian Stochastic Models for Trajectories in the Turbulent Atmosphere. Boundary-Layer Meteorology, 78, 191-210.

Wilson, L. J., Bacon, P. J., Bull, J., Dragosits, U., Blackall, T. D., Dunn, T. E., Hamer, K. C., Sutton, M. A. and Wanless, S. (2004) Modelling the spatial distribution of ammonia emissions from seabirds in the UK. Environmental Pollution, 131, 173-185.

Wing, M. G., Eklund, A. and Kellogg, L. D. (2005) Consumer grade global positioning system (GPS) accuracy and reliability. Journal of Forestry, 103, 169-173.

Woehler, E. J. (1993) The distribution and abundance of Antarctic and Subantarctic penguins. Cambridge, Scientific Committee on Antarctic Research (SCAR) Bird Biology Subcommittee.

Wright, P. A. (1995) Nitrogen excretion - 3 end-products, many physiological roles. Journal of Experimental Biology, 198, 273-281.

Wyers, G. P., Oties, R. P. and Slanina, J. (1993) A continuous-flow denuder for the measurement of ambient concentrations and surface-exchange fluxes of ammonia. Atmospheric Environment Part a-General Topics, 27, 2085-2090.

Wyrtki, K. (1975) El-Niño - Dynamic response of equatorial Pacific Ocean to atmospheric forcing. Journal of Physical Oceanography, 5, 572-584.

Yorio, P., Frere, E., Gandini, P. and Conway, W. (1999) Status and conservation of seabirds breeding in Argentina. Bird Conservation International, 9, 299-314.

Zhang, R. H., Day, D. L., Christianson, L. L. and Jepson, W. P. (1994) A computer model for predicting ammonia release from swine manure pits. Journal of Agricultural Engineering Research 58, 223-229.

Zhu, R., Sun, J., Liu, Y., Gong, Z. and Sun, L. (2011) Potential ammonia emissions from penguin guano, ornithogenic soils and seal colony soils in coastal Antarctica: effects of freezing-thawing cycles and selected environmental variables. Antarctic Science, 23, 78-92.

Appendix 1 Bird species data

Entries in bold are where species specific data was unavailable, the data used was taken from similar species identified using Birdlife International. References are available from the author.

F: Family

Family values: Alicdae(A), Chionididae (Ch), Diomedeidae (D), Fregatidae (F), Hydrobatidae (H), Laridae (L), Phalacrocoracidae (P), Pelecanidae (Pe), Phaethontidae (Ph), Procellariidae (Pr), Sternidae (S), Spheniscidae (Sp), Stercorariidae (St), Sulidae (Su)

M: Adult Mass (g)

D: Number of days attendance per year at the colony

T: Fraction of time spent at the colony when in attendance

P: Productivity per pair

FM: Fledging Mass (g)

AS: Adult Substrate

CS: Chick Substrate

ND: Nest Density (nests m^{-2})

Substrate value: Rock (R), Sand (S), Soil (So), Vegetation (V), Burrow (B) & Nest (N)

Species	F	M	D	T	P	FM	AS	CS	ND
Crested Auklet	A	260	122	0.6	0.50	240	R	R	1.3
Least Auklet	A	80	122	0.6	0.50	80	R	R	0.5
Whiskered Auklet	A	110	122	0.6	0.50	100	R	R	1.5
Razorbill	A	670	152	0.6	0.60	250	R	R	20

Species	F	M	D	T	P	FM	AS	CS	ND
Little Auk	A	150	122	0.6	0.50	100	R	R	1.3
Kittlitz's Murrelet	A	220	120	0.6	0.20	100	R	R	4
Marbled Murrelet	A	200	183	0.6	0.50	160	V	V	0.8
Long-billed Murrelet	A	290	122	0.6	0.50	220	V	V	0.8
Spectacled Guillemot	A	680	122	0.3	1.03	620	R	B	1
Pigeon Guillemot	A	460	122	0.3	0.82	400	R	B	1
Black Guillemot	A	380	152	0.3	1.10	370	R	B	0.2
Rhinoceros Auklet	A	480	152	0.3	0.90	320	So	B	0.8
Parakeet Auklet	A	260	122	0.3	0.50	200	R	B	1.5
Atlantic Puffin	A	410	152	0.3	0.71	290	V	B	1.27
Tufted Puffin	A	780	120	0.3	0.55	500	V	B	0.6
Horned Puffin	A	570	152	0.3	0.68	370	So	B	2.1
Cassin's Auklet	A	170	152	0.3	0.60	160	B	B	0.6
Ancient Murrelet	A	190	91	0.3	1.54	20	So	B	0.1
Craveri's Murrelet	A	150	122	0.3	1.00	20	R	B	0.2
Xantus's Murrelet	A	160	122	0.3	0.72	20	R	B	0.2
Japanese Murrelet	A	180	120	0.6	0.36	25	R	R	0.2
Common Guillemot	A	970	152	0.6	0.71	210	R	R	20
Thick-billed Murre	A	960	122	0.6	0.80	220	R	R	20
Snowy Sheathbill	Ch	640	365	0.6	0.50	600	R	R	0.0001
Black-faced Sheathbill	**Ch**	**640**	**365**	**0.6**	**0.50**	**600**	**R**	**R**	0.0001
Brown-headed Gull	L	310	152	0.6	0.90	250	V	V	0.01
Black-billed Gull	L	300	152	0.6	1.10	270	V	V	1
Brown-hooded Gull	L	300	150	0.6	1.00	250	R	R	0.015
Bonaparte's Gull	L	200	152	0.6	1.00	160	V	V	0.01
Red-billed Gull	L	300	152	0.6	1.10	270	V	V	1

Species	F	M	D	T	P	FM	AS	CS	ND
Andean Gull	L	400	152	0.6	0.90	350	V	V	0.2
Swallow-tailed Gull	L	700	150	0.6	0.35	650	R	R	0.1
Franklin's Gull	L	280	150	0.6	1.00	250	V	V	0.05
Herring Gull	L	980	152	0.6	0.89	750	R	R	0.026
Olrog's Gull	L	930	152	0.6	0.90	770	V	V	1
Laughing Gull	L	290	152	0.6	1.00	250	V	V	0.1
Audouin's Gull	L	770	152	0.6	0.90	640	V	V	1
Belcher's Gull	L	600	150	0.6	1.00	600	S	S	1
Yellow-legged Gull	L	1080	152	0.6	0.80	900	V	V	0.01
California Gull	L	200	122	0.6	1.00	200	V	V	0.5
Common Gull	L	410	152	0.6	0.82	340	V	V	0.1
Grey-headed Gull	L	310	152	0.6	0.90	250	V	V	1
Black-tailed Gull	L	530	152	0.6	0.80	450	V	V	1.67
Ring-billed Gull	L	420	152	0.6	1.00	400	V	V	0.5
Kelp Gull	L	1000	152	0.6	1.10	830	V	V	0.001
Lesser Black-backed Gull	L	810	152	0.6	0.61	720	V	V	1
Slender-billed Gull	L	270	152	0.6	1.00	220	V	V	3
Glaucous-winged Gull	L	1600	152	0.6	1.10	920	V	V	0.1
Iceland Gull	L	770	152	0.6	1.10	650	V	V	1
King Gull	L	300	152	0.6	1.00	240	V	V	0.15
Heermann's Gull	L	500	152	0.6	0.70	420	R	R	0.7
Sooty Gull	L	350	152	0.6	1.00	280	R	R	0.01
Glaucous Gull	L	1590	122	0.6	1.00	1320	V	V	0.01
Pallas's Gull	L	1500	152	0.6	1.40	1300	V	V	1
White-eyed Gull	L	350	152	0.6	1.00	280	R	R	1
Yellow-footed Gull	L	1000	150	0.6	0.50	1000	S	S	0.01

Species	F	M	D	T	P	FM	AS	CS	ND
Great Black-backed Gull	L	1620	152	0.6	1.29	1380	R	R	0.01
Mediterranean Gull	L	300	122	0.6	0.90	250	V	V	1
Little Gull	L	100	152	0.6	1.60	70	V	V	0.03
Gray Gull	L	350	150	0.6	1.80	300	S	S	0.011
Silver Gull	L	350	152	0.6	0.80	250	V	V	0.3
Western Gull	L	1200	152	0.6	0.60	1000	V	V	0.01
Pacific Gull	L	1000	152	0.6	1.00	850	V	V	1
Relict Gull	L	260	152	0.6	1.00	220	V	V	0.35
Black-headed Gull	L	260	152	0.6	0.90	220	V	V	0.15
Slaty-backed Gull	L	1400	152	0.6	1.00	1100	R	R	0.01
Thayer's Gull	L	1100	152	0.6	1.00	1000	V	V	10
Lava Gull	L	300	150	0.6	1.50	100	S	S	0.01
Dolphin Gull	L	500	150	0.6	0.86	450	V	V	1
Ivory Gull	L	530	122	0.6	1.00	430	R	R	0.01
Ross's Gull	L	200	150	0.6	1.00	175	V	V	0.0001
Red-legged Kittiwake	L	390	183	0.6	0.25	370	R	N	2
Black-legged Kittiwake	L	390	152	0.6	0.78	320	R	N	2
Saunders's Gull	L	260	152	0.6	0.90	220	V	V	0.15
Sabines Gull	L	190	152	0.6	0.41	140	V	V	1
Southern Skua	St	2100	150	0.6	1.20	1900	V	V	0.00025
Brown Skua	St	2100	150	0.6	1.20	1900	V	V	0.00013
South Polar Skua	St	1750	150	0.6	0.50	1200	V	V	0.00025
Great Skua	St	1430	150	0.6	0.78	1150	V	V	0.0001
Chilean Skua	St	1300	150	0.6	1.00	1000	V	V	0.0001
Long-tailed Skua	St	350	150	0.6	0.25	250	V	V	0.0001

Species	F	M	D	T	P	FM	AS	CS	ND
Parasitic Skua	St	460	150	0.6	0.49	460	V	V	0.0001
Pomarine Skua	St	1430	150	0.6	0.78	1150	V	V	0.0001
Black Noddy	S	120	122	0.6	0.50	100	V	V	0.4
Brown Noddy	S	200	122	0.6	0.50	150	V	V	1.7
Lesser Noddy	S	100	122	0.6	0.56	90	V	V	2.15
Whiskered Tern	S	90	122	0.6	0.92	80	V	V	0.03
White-winged Tern	**S**	**90**	**122**	**0.6**	**0.92**	**80**	**V**	**V**	0.001
Black Tern	S	60	122	0.6	0.90	60	V	V	3
Common White Tern	S	120	122	0.6	0.56	100	V	V	1
Little White Tern	S	100	122	0.6	0.56	100	S	S	1
Inca Tern	S	180	120	0.6	0.40	150	R	R	1
Large-billed Tern	S	250	120	0.6	0.60	200	S	S	0.002
Blue Noddy	S	40	122	0.6	0.50	40	R	R	1
Black-bellied Tern	S	90	122	0.6	0.92	80	V	V	1
Little Tern	S	40	122	0.6	1.90	30	S	S	0.5
Aleutian Tern	S	120	122	0.6	0.85	100	S	S	0.0084
Bridled Tern	S	140	122	0.6	0.81	130	S	S	0.001
Least Tern	S	40	122	0.6	0.65	40	S	S	0.1
River Tern	S	250	120	0.6	0.35	200	S	S	1
Damara Tern	S	40	122	0.6	0.56	40	S	S	0.0001
Lesser Crested Tern	S	220	122	0.6	0.80	190	S	S	12
Greater Crested Tern	S	350	122	0.6	0.35	310	S	S	1
Caspian Tern	S	660	122	0.6	0.80	520	S	S	10
Roseate Tern	S	110	91	0.6	1.49	100	S	S	1.8
Elegant tern	S	250	122	0.6	0.56	230	S	S	10
Forster's Tern	S	150	122	0.6	0.70	140	S	S	0.1

Species	F	M	D	T	P	FM	AS	CS	ND
Sooty Tern	S	190	122	0.6	0.50	170	S	S	0.5
South American Tern	S	190	122	0.6	0.35	180	S	S	5
Common Tern	S	120	122	0.6	1.25	120	S	S	0.1
Grey-backed Tern	S	140	91	0.6	0.50	120	S	S	0.1
Royal Tern	S	470	122	0.6	0.56	340	S	S	10
Fairy Tern	S	70	122	0.6	0.20	50	S	S	0.5
Gull-billed tern	S	170	122	0.6	1.48	150	S	S	1
Arctic Tern	S	100	122	0.6	0.80	90	V	V	0.1
White-cheeked Tern	S	120	122	0.6	0.92	110	S	S	1
Sandwich Tern	S	240	122	0.6	1.01	210	S	S	10
Saunders's Tern	S	40	122	0.6	0.85	40	S	S	0.001
White-fronted Tern	S	190	122	0.6	0.80	170	S	S	1
Black-naped Tern	S	100	122	0.6	0.20	90	S	S	0.5
Yellow-billed Tern	S	50	120	0.6	0.66	45	S	S	0.41
Snowy-crowned Tern	S	150	120	0.6	0.60	130	V	V	0.15
Kerguelen Tern	S	130	122	0.6	0.24	110	R	R	1
Antarctic Tern	S	140	122	0.6	0.56	130	S	S	1
Black-fronted Tern	S	100	120	0.6	0.28	100	S	S	0.03
Peruvian Tern	S	50	120	0.6	0.40	45	S	S	0.0006
Chinese Crested Tern	S	350	122	0.6	0.35	310	S	S	1
Christmas Island Frigatebird	**F**	**1310**	**243**	**0.6**	**0.20**	**1310**	**V**	**N**	1
Ascension Frigatebird	**F**	**1470**	**243**	**0.6**	**0.17**	**1470**	**V**	**N**	0.9
Lesser Frigatebird	F	840	213	0.6	0.20	840	V	N	0.7
Magnificent Frigatebird	F	1470	243	0.6	0.20	1470	V	N	0.9
Great Frigatebird	F	1310	213	0.6	0.35	1310	V	N	1.3
Brown Pelican	Pe	3750	270	0.6	1.20	3500	V	N	3

Species	F	M	D	T	P	FM	AS	CS	ND
Reed Cormorant	P	500	200	0.6	0.30	450	V	N	0.02
European shag	P	1760	243	0.6	1.34	1520	R	R	0.02
Imperial Shag	P	1930	243	0.6	1.40	1520	R	N	1.8
Double-crested Cormorant	P	2350	213	0.6	1.46	2060	V	N	0.44
Guanay Cormorant	P	2100	213	0.6	2.40	1800	R	N	1
Neotropic Cormorant	P	1300	122	0.6	1.65	1000	V	N	0.5
Campbell Island Shag	P	1500	200	0.6	0.40	1500	R	N	1
Cape Cormorant	P	1200	213	0.6	1.35	1100	R	N	2
Japanese Cormorant	P	2800	213	0.6	2.40	2720	R	N	0.02
Great Cormorant	P	2300	152	0.6	2.16	2220	R	R	0.02
King Shag	P	2500	200	0.6	0.50	2500	R	N	1
Stewart Island Shag	P	3000	200	0.6	0.40	3000	R	N	2
Auckland Shag	P	1500	200	0.6	0.40	1500	R	N	1
Crowned Cormorant	P	700	213	0.6	1.35	610	V	N	0.02
Pitt Cormorant	P	2000	200	0.6	0.40	1500	R	N	2
Black-faced Shag	P	1510	183	0.6	1.35	1330	R	N	0.02
Indian Cormorant	P	400	200	0.6	2.50	400	V	N	0.02
Red-legged Cormorant	P	1300	213	0.6	2.40	1140	R	N	0.02
Flightless Cormorant	P	4000	365	0.6	2.50	4000	R	N	1
Rock Shag	P	1500	300	0.6	2.00	1250	R	V	1
Little Pied Cormorant	P	720	243	0.6	1.80	630	V	N	0.02
Bank Cormorant	P	1800	213	0.6	1.50	1580	R	N	0.02
Little Cormorant	P	400	200	0.6	2.50	400	V	N	0.02
Socotra Cormorant	P	2270	213	0.6	1.35	2000	R	N	0.02
Chatham Island Shag	P	2500	200	0.6	1.00	2000	R	N	1
Pelagic Cormorant	P	1910	213	0.6	2.20	1800	R	N	0.5

Species	F	M	D	T	P	FM	AS	CS	ND
Brandt's Cormorant	P	2110	213	0.6	1.90	1900	R	N	1
Spotted Shag	P	1200	274	0.6	2.05	1070	R	N	2
Pygmy Cormorant	P	450	152	0.6	3.20	400	V	N	0.02
Bounty Islands Shag	P	2500	200	0.6	1.50	2000	R	N	1
Little Black Shag	P	450	152	0.6	1.84	400	R	N	0.02
Red-faced Cormorant	P	1940	213	0.6	1.25	1700	R	N	0.5
Greater Pied Cormorant	P	2050	213	0.6	1.34	1800	R	N	0.02
Kerguelen Shag	P	1930	243	0.6	1.40	1520	R	N	0.02
Northern Gannet	Su	3010	243	0.6	0.73	3900	R	R	2.3
Cape Gannet	Su	2800	243	0.6	0.76	3000	R	R	3.5
Australasian Gannet	Su	2350	183	0.6	0.63	2900	R	R	2.5
Abbott's Booby	Su	1550	274	0.6	0.20	1550	V	V	0.0005
Masked Booby	Su	2000	274	0.6	0.51	2230	S	S	0.03
Nazca Booby	Su	1000	200	0.6	0.50	1100	S	S	0.33
Brown Booby	Su	1150	243	0.6	0.80	1250	S	S	0.01
Blue-footed Booby	Su	1500	274	0.6	0.45	1750	R	R	0.33
Red-footed Booby	Su	1000	243	0.6	0.40	920	V	V	0.06
Peruvian booby	Su	1410	213	0.6	0.45	1500	R	R	0.03
Red-billed Tropicbird	Ph	420	213	0.6	0.46	430	R	N	0.04
White-tailed Tropicbird	Ph	320	243	0.6	0.43	320	R	N	0.04
Red-tailed Tropicbird	Ph	670	183	0.6	0.48	680	R	N	0.4
Short-tailed Albatross	D	3910	243	0.6	0.51	3710	V	N	0.002
Amsterdam Albatross	D	6000	240	0.6	0.70	5500	V	V	0.0022
Antipodean Albatross	D	10000	240	0.6	0.20	9000	V	V	0.0022
Tristan Albatross	D	8390	152	0.6	0.33	8390	V	N	0.0022
Wandering Albatross	D	10200	152	0.6	0.33	9500	V	N	0.0022

Species	F	M	D	T	P	FM	AS	CS	ND
Northern Royal Albatross	D	6500	300	0.6	0.31	6000	V	N	0.002
Southern Royal Albatross	D	6500	240	0.6	0.62	6000	V	N	0.002
Shy Albatross	D	3910	243	0.6	0.51	3710	V	N	1.5
Laysan Albatross	D	3040	274	0.6	0.48	2310	S	N	0.01
Waved Albatross	D	3390	274	0.6	0.25	3700	V	N	0.003
Black-footed Albatross	D	3010	274	0.6	0.50	2310	S	S	0.016
Sooty Albatross	D	2470	122	0.6	0.22	2250	R	R	0.03
Light-mantled Albatross	D	3150	274	0.6	0.63	2310	So	N	0.03
Indian Yellow-nosed Albatross	D	2500	243	0.6	0.24	2200	V	N	0.0005
Atlantic Yellow-nosed Albatross	D	2320	243	0.6	0.70	2200	V	N	0.0005
Grey-headed Albatross	D	3750	122	0.6	0.50	3500	V	N	0.0005
Chatham Albatross	D	4500	240	0.6	0.80	4000	R	N	0.0005
Campbell Albatross	D	3000	240	0.6	0.50	2500	V	N	0.0005
Black-browed Albatross	D	3530	274	0.6	0.51	3250	V	N	0.0005
Salvin's Albatross	D	3910	243	0.6	0.51	3710	R	N	0.0005
Buller's Albatross	D	2700	240	0.6	0.58	2500	V	N	0.0005
White-capped Albatross	D	4000	243	0.6	0.50	3500	R	N	0.0005
White-bellied Storm-petrel	H	50	117	0.1	0.50	50	R	B	0.0001
Black-bellied Storm-petrel	H	50	117	0.1	0.50	50	R	B	0.0001
Grey-backed Storm-petrel	H	30	90	0.1	0.50	30	B	B	0.0001
Least Storm Petrel	H	20	122	0.1	0.50	20	V	B	0.0001
European Storm-petrel	H	20	150	0.1	0.50	30	R	B	0.0003
White-throated Storm-petrel	H	60	160	0.1	0.50	60	S	B	0.05
White-vented Storm-petrel	H	50	120	0.1	0.45	50	R	B	0.0001
New Zealand Storm-petrel	H	50	120	0.1	0.45	50	V	B	0.0001
Wilson's Storm-petrel	H	40	160	0.1	0.40	40	R	B	0.07

Species	F	M	D	T	P	FM	AS	CS	ND
Madeiran Storm-petrel	H	40	180	0.1	0.40	50	S	B	0.003
Fork Tailed Storm-Petrel	H	40	122	0.1	0.70	40	V	B	0.07
Ashy Storm-Petrel	H	40	200	0.1	0.60	40	R	B	0.01
Hornby's Storm-petrel	H	50	100	0.1	0.45	50	R	B	0.01
Leach's Storm-petrel	H	40	150	0.1	0.50	60	R	B	1.5
Markham's Storm-petrel	H	50	200	0.1	0.45	50	R	B	0.01
Matsudaira's Storm-petrel	H	40	122	0.1	0.45	50	V	B	0.01
Black Storm-Petrel	H	40	150	0.1	0.60	50	So	B	0.01
Swinhoe's Storm-petrel	H	40	160	0.1	0.60	40	So	B	2
Monteiro's Storm-petrel	H	40	180	0.1	0.40	50	S	B	0.003
Wedge-rumped Storm-petrel	H	30	100	0.1	0.40	30	V	B	0.002
Tristram’s Storm-Petrel	H	40	122	0.1	0.45	50	S	B	0.05
White-faced Storm-petrel	H	50	122	0.1	0.60	40	R	B	0.38
South Georgia Diving-petrel	H	120	122	0.3	0.70	120	S	B	3
Common Diving-petrel	H	140	110	0.3	0.80	120	So	B	3
Bulwer’s Petrel	Pr	90	150	0.6	0.44	90	S	N	0.003
Jouanin's Petrel	Pr	400	120	0.3	0.45	400	R	B	0.03
Cory's Shearwater	Pr	730	240	0.3	0.50	700	B	B	0.1
Cape Verde Shearwater	**Pr**	**730**	**240**	**0.3**	**0.50**	**700**	**B**	**B**	0.1
Streaked Shearwater	Pr	500	180	0.3	0.40	500	V	B	0.04
Cape Petrel	Pr	470	94	0.6	0.50	400	R	R	0.02
Snares Cape Pigeon	Pr	470	94	0.6	0.50	400	R	R	0.2
Northern Fulmar	Pr	750	183	0.6	0.57	800	R	R	0.02
Southern Fulmar	Pr	850	99	0.6	0.57	930	R	R	0.02
Blue Petrel	Pr	190	105	0.3	0.50	170	V	B	0.0077

Species	F	M	D	T	P	FM	AS	CS	ND
Kerguelen Petrel	Pr	80	122	0.3	1.00	60	So	B	0.0007
Southern Giant-petrel	Pr	3890	200	0.6	0.88	3400	So	V	0.0005
Northern Giant-petrel	Pr	4500	122	0.6	0.90	4000	V	V	0.0005
Slender-billed Prion	Pr	150	122	0.3	0.38	150	V	B	0.6
Antarctic Prion	Pr	130	122	0.3	0.50	130	V	B	0.02
Medium-billed Prion	Pr	150	122	0.3	0.50	150	So	B	0.0065
Fairy Prion	Pr	130	122	0.3	0.50	150	V	B	1
Broad-billed Prion	Pr	190	122	0.3	0.50	180	R	B	0.31
Fulmar Prion	Pr	130	122	0.3	0.50	150	R	B	0.6
Snow Petrel	Pr	260	90	0.6	0.50	250	R	R	0.0003
White-chinned Petrel	Pr	1280	122	0.3	0.49	1100	So	B	0.001
Grey Petrel	Pr	1000	122	0.3	0.70	900	V	B	0.0003
Spectacled Petrel	Pr	200	180	0.3	0.45	200	V	B	0.01
Parkinson's Petrel	Pr	700	120	0.3	0.45	700	V	B	0.005
Westland Petrel	Pr	800	180	0.3	0.45	750	V	B	0.005
Tahiti Petrel	Pr	150	122	0.3	0.50	140	B	B	0.001
Mascarene Petrel	Pr	100	120	0.3	0.45	100	R	B	0.003
Beck's Petrel	Pr	120	120	0.3	0.45	120	V	B	0.001
Fiji Petrel	Pr	120	120	0.3	0.45	100	V	B	0.05
Phoenix Petrel	**Pr**	**150**	**122**	**0.3**	**0.50**	**140**	**B**	**B**	0.001
Trindade Petrel	Pr	450	122	0.6	0.45	420	R	R	0.03
Henderson Petrel	**Pr**	**450**	**122**	**0.6**	**0.20**	**420**	**V**	**N**	0.03
Barau's Petrel	Pr	430	180	0.3	0.20	360	So	B	0.62
Collared Petrel	Pr	210	122	0.3	0.20	200	V	B	0.03
Bermuda Petrel	Pr	240	180	0.6	0.25	220	R	N	0.03
Fea's Petrel	Pr	310	122	0.3	0.20	300	So	B	0.03

Species	F	M	D	T	P	FM	AS	CS	ND
Herald Petrel	Pr	450	90	0.3	0.30	420	R	B	0.03
Bonin Petrel	Pr	160	122	0.3	0.25	180	V	B	0.1
Atlantic Petrel	Pr	520	122	0.3	0.20	500	So	B	0.0018
Mottled Petrel	Pr	310	170	0.3	0.65	220	So	B	0.03
White-headed Petrel	Pr	690	220	0.3	0.15	200	So	B	0.03
Great-winged Petrel	Pr	500	122	0.3	0.20	610	So	B	0.0018
Soft-plumaged Petrel	Pr	310	122	0.3	0.40	350	V	B	0.0018
Kermadec Petrel	Pr	500	122	0.6	0.10	500	R	N	0.03
Hawaiian Petrel	Pr	430	320	0.3	0.50	600	R	B	0.038
Murphy's Petrel	Pr	420	122	0.6	0.15	450	R	N	0.03
Chatham Petrel	Pr	185	240	0.3	0.45	175	V	B	0.31
Cook's Petrel	Pr	200	120	0.3	0.40	200	V	B	0.038
De Filippi's Petrel	Pr	200	120	0.3	0.45	200	R	B	0.038
Juan Fernandez Petrel	Pr	450	180	0.3	0.25	450	V	B	0.038
Black-capped Petrel	Pr	300	120	0.3	0.45	300	V	B	0.03
Gould's Petrel	Pr	200	120	0.3	0.45	200	V	B	0.03
Stejneger's Petrel	Pr	150	180	0.3	0.50	150	V	B	0.038
Magenta Petrel	Pr	150	122	0.3	0.45	140	V	B	0.0018
Kermadec Petrel	Pr	500	180	0.6	0.40	500	V	V	0.03
Black-winged Petrel	Pr	185	240	0.3	0.75	175	V	B	0.0006
Galapagos Petrel	Pr	400	120	0.3	0.24	400	R	B	0.038
Pycroft's Petrel	Pr	200	120	0.3	0.50	200	V	B	0.038
Providence Petrel	Pr	420	122	0.3	0.35	450	R	B	0.003
Little Shearwater	Pr	220	180	0.1	0.45	150	V	B	0.05
Newell’s Shearwater	Pr	270	180	0.1	0.45	240	V	B	0.075
Flesh-footed Shearwater	Pr	560	280	0.1	0.47	500	V	B	0.15

Species	F	M	D	T	P	FM	AS	CS	ND
Fluttering Shearwater	Pr	320	200	0.1	0.45	300	V	B	0.1
Great Shearwater	Pr	840	300	0.1	0.66	800	V	B	0.5
Sooty Shearwater	Pr	780	122	0.1	0.55	600	V	B	0.001
Audubon's Shearwater	Pr	160	150	0.1	0.59	160	So	B	0.05
Christmas Shearwater	Pr	350	122	0.6	0.45	340	R	R	0.05
Black-vented Shearwater	Pr	270	180	0.1	0.45	250	S	B	0.05
Wedge-tailed Shearwater	Pr	380	122	0.1	0.45	450	V	B	0.036
Manx Shearwater	Pr	410	122	0.1	0.70	450	V	B	0.036
Yelkouan Shearwater	Pr	400	122	0.1	0.67	390	V	B	0.05
Townsend's Shearwater	Pr	270	180	0.1	0.45	250	V	B	0.09
Buller's Shearwater	Pr	400	122	0.1	0.40	400	V	B	0.05
Pink-footed shearwater	Pr	700	180	0.1	0.50	750	V	B	0.001
Heinroth's Shearwater	Pr	160	150	0.1	0.59	160	So	B	0.15
Hutton's Shearwater	Pr	350	180	0.1	0.40	350	V	B	0.5
Balearic Shearwater	Pr	780	122	0.1	0.55	600	V	B	0.001
Short-tailed Shearwater	Pr	500	200	0.6	0.60	450	V	V	0.76
Antarctic Petrel	Pr	690	96	0.6	0.50	600	R	R	2.8
Emperor Penguin	Sp	39000	330	0.6	0.61	10560	Ice	Ice	1.69
King Penguin	Sp	12000	243	0.6	0.39	10000	R	R	0.55
Rockhopper Penguin	Sp	3060	213	0.6	0.43	2300	R	R	0.85
Macaroni Penguin	Sp	4680	213	0.6	0.44	3270	R	R	0.01
Fiordland Penguin	Sp	3500	300	0.6	1.00	3000	R	R	0.85
Royal Penguin	Sp	6000	213	0.6	0.44	5400	R	R	0.05
Erect-crested Penguin	Sp	3900	274	0.6	0.64	3000	R	R	0.01
Snares Penguin	Sp	3500	274	0.6	0.64	3000	R	R	0.01
Little Penguin	Sp	1080	340	0.3	0.35	940	So	B	0.0003

Species	F	M	D	T	P	FM	AS	CS	ND
Yellow-eyed Penguin	Sp	4800	250	0.6	0.80	4000	V	V	0.63
Adelie Penguin	Sp	4200	243	0.6	1.02	3000	R	R	0.5
Chinstrap Penguin	Sp	4150	274	0.6	1.20	2900	R	R	0.25
Gentoo Penguin	Sp	5500	213	0.6	1.00	5100	R	R	0.87
African Penguin	Sp	3170	300	0.3	0.61	2950	V	B	0.87
Humboldt penguin	Sp	4100	340	0.3	0.70	3000	V	B	0.87
Magellanic Penguin	Sp	3500	243	0.3	0.56	2500	So	B	0.87
Galapagos Penguin	Sp	2500	180	0.6	1.50	2000	R	R	0.87